Development of a Pressurized Low-Temperature Tablet Press for a Carbon Dioxide Flash Frozen Ice Confection

by

David M. Lopez

S.B. in Mechanical Engineering
Massachusetts Institute of Technology, 2007

Submitted to the Department of Mechanical Engineering
in Partial Fulfillment of the Requirements for the Degree of

Master of Science in Mechanical Engineering

at the

Massachusetts Institute of Technology

September 2009

Signature of Author:_____
Department of Mechanical Engineering
August 19th, 2009

Certified by:_____
John G. Brisson II
Professor of Mechanical Engineering
Thesis Supervisor

Accepted by:_____
David Hardt
Chairman, Department Committee on Graduate Students

Development of a Pressurized Low-Temperature Tablet Press for a Carbon Dioxide Flash Frozen Ice Confection

by

David M. Lopez

Submitted to the Department of Mechanical Engineering
on August 19th, 2009 in Partial Fulfillment of the
Requirements for the Degree of Master of Science in
Mechanical Engineering

Abstract

This document details the conception, design, and testing of a series of prototype powder-pelletizing devices for use with an ice confection powder produced using a CO_2 spray freezing process. The device must function at a temperature of 233 K and at pressures of up to 12 bar(a) and must produce at least 500 pellets for use in consumer testing. Design considerations include stress analysis for critical parts, minimization of powder flow path length, formulation of requirements of thermal management system, implementation of the powder compression methods, examination of various agitation methods, and the testing of the prototype apparatus. Trials proved the concept sound as several dozen pellets could be produced using the final prototype. However, ensuring sufficient powder flow for the consistent and continuous production of full-sized pellets is the key difficulty in the implementation of this device. As such, further work should be devoted toward understanding and quantifying the flow properties of the CO_2 flash freezing powder.

Thesis Supervisor: John G. Brisson II

Title: Professor of Mechanical Engineering

Acknowledgements

I would like to thank Professor John G. Brisson and Professor Joseph L. Smith Jr. for providing me the opportunity to work on this project as well as for their generous assistance and guidance along the way. I would also like to thank Teresa Baker Peters for her explanations of the CO_2 flash freezing process and equipment as well as for acting as a sounding board for ideas along the way.

I would like to extend my gratitude to the entire staff of Nestlé PTC Beauvais for being so extraordinarily welcoming and encouraging during my stay in France. I would especially like to recognize Anthony Pizzagalli, María Fernanda Villacís, Rémi Thomas, Joumana Saïkali, Hans Wille, Max Puaud, Robert Mazurek, Philippe Valour, Jean Judam, Francis Verdin, and Julien Minot for the help they provided and for all the time and effort they put in to this project.

Finally, I am extremely grateful for the support I received from my friends and family throughout this effort. I could not have done this without you.

Table of Contents

List of Figures

List of Tables

List of Symbols

Symbol	Meaning	Unit
α	Coefficient of Thermal Expansion | Thermal Diffusivity	- | $m^2 s^{-1}$
d	Diameter	mm
δ	Deflection	mm
E	Young's Modulus	Pa
f	Friction Factor	-
F_{crit}	Critical Load for Buckling	N
g	Gravitational Constant (9.81)	$m s^{-2}$
I	Area Moment of Inertia	m^4
l	Length	mm
m	Mass	kg
$\dot{m}$	Mass Flow	$kg s^{-1}$
$\dot{M}'$	Momentum Flux	$kg m s^{-2}$
μ	Dynamic Viscosity	Pa s
$\mu_{d\text{-}ss}$	Coefficient of Friction between Delrin and Stainless Steel	-
v	Poisson's Ratio | Kinematic Viscosity	- | $m^2 s^{-1}$
P	Pressure (absolute unless otherwise noted)	bar
ρ	Density	$kg m^{-3}$
s	Stroke	mm
σ	Stress|Stefan-Boltzmann Constant (5.67×10^{-8})	Pa|$W m^{-2} K^{-4}$
T	Temperature	K
t	Time|Thickness	s|mm
$\dot{V}$	Volumetric Flow	$m^3 s^{-1}$
x	Quality of a Fluid Flow, defined as the Mass Fraction of Vapor	-

List of Subscripts

Note: Multiple subscripts can be assigned to a single symbol. In these cases, the subscripts are separated by a comma.

Subscript	Meaning
a	Pertaining to Ambient Conditions
act	Actuator
air	Pertaining to Air
axial	In the Axial Direction
base	Pertaining to the Base of a Component
bridge	Pertaining to the Location of Bridged Powder
circ	In the Circumferential Direction
CO2/CO_2	Carbon Dioxide
COM	Center of Mass
comp	Compression
i	Inner
ICT	Ice Confection Tank
ID	Inner Diameter
ins	Insulation
max	Maximum
o	Outer
OD	Outer Diameter
pellet	Pellet
pr	Piston Rod of the Actuator
sat	Saturation
t	Pertaining to a Tip Load
t-t	Tip-to-Tip

total	Total
tube	Pertaining to a Tube, e.g. Thermal Isolation Tube
uniform	Uniformly Experienced by a Part
w	Pertaining to a Component Weight
y	Yield

Chapter 1: Introduction

This thesis describes a device designed to compress the powder created by the CO_2 flash freezing process into pellets for use in consumer testing. The compression process is to occur as powder is being formed, with the goal of having a continuous process producing homogenous product. This first chapter provides background information on the CO_2 flash freezing process and on the goals of this specific part of the project. Chapter 2 presents the initial concept of this form of pelletizing machinery. In Chapter 3, details of the alpha prototype are discussed, including its form, trial results, and conclusions drawn from this device. Chapter 4 is about the beta prototype, touching on its design, trial results, and conclusions. Chapter 5 summarizes the conclusions reached in Chapter 4 and presents the most relevant aspects of the CO_2 flash freezing process that should be focused on in further work.

1.1.Purpose

The Nestlé/MIT CO_2 Flash Freezing collaboration is meant to produce an ice confection that fizzes as it is consumed. The production process creates very fine, snow-like powder, which can then be compressed into a pellet for consumption. A diagram of the current production equipment is shown in Figure 1-1, which will be a useful reference during the following description of the process. Liquid mix is injected through a pressure swirl nozzle into liquid CO_2 in the Emulsion Chamber. This chamber typically experiences temperatures between 283 K and 293 K (10°C to 20°C) and has a chamber pressure of approximately 50 bar. This liquid emulsion is then sprayed through a pressure-swirl nozzle, atomizing the mixture as it enters the Ice Confection Tank (ICT). The ICT is held at a pressure of approximately 10 bar, which is low enough to cause the liquid CO_2 in the mixture to vaporize. Liquid carbon dioxide vaporizes, lowering the temperature of the ICT and the mix to boiling point temperature of the CO_2, equal to 233 K at the tank's 10 bar pressure. At this combination of pressure and temperature, the water and CO_2 form a phase called a carbon dioxide clathrate hydrate, in which molecules of CO_2 gas are trapped within cages of water molecules. The release of the CO_2 from these structures upon consumption is what gives the product its characteristic fizziness.

Development of the CO_2 flash freezing process has been ongoing since 2006. To further develop this product, between 250 and 500 pellets are required for a consumer testing panel. Individual pellets have made by manually compressing powder in a piston-cylinder apparatus held in a freezer or cold room. Unfortunately, this method results in large pellet-to-pellet and batch-to-batch variations in key product characteristics, such as CO_2 concentration, texture, and density.

The goal of this project is to develop a continuous production method of pellets that will substantially reduce the variability of the product and allow the rapid production of the required number of pellets. Continuous production should result in a homogeneous product by limiting the effect of transients during initial powder production. The device must produce at least 500 homogenous pellets while working with the existing equipment. In addition to the requirements

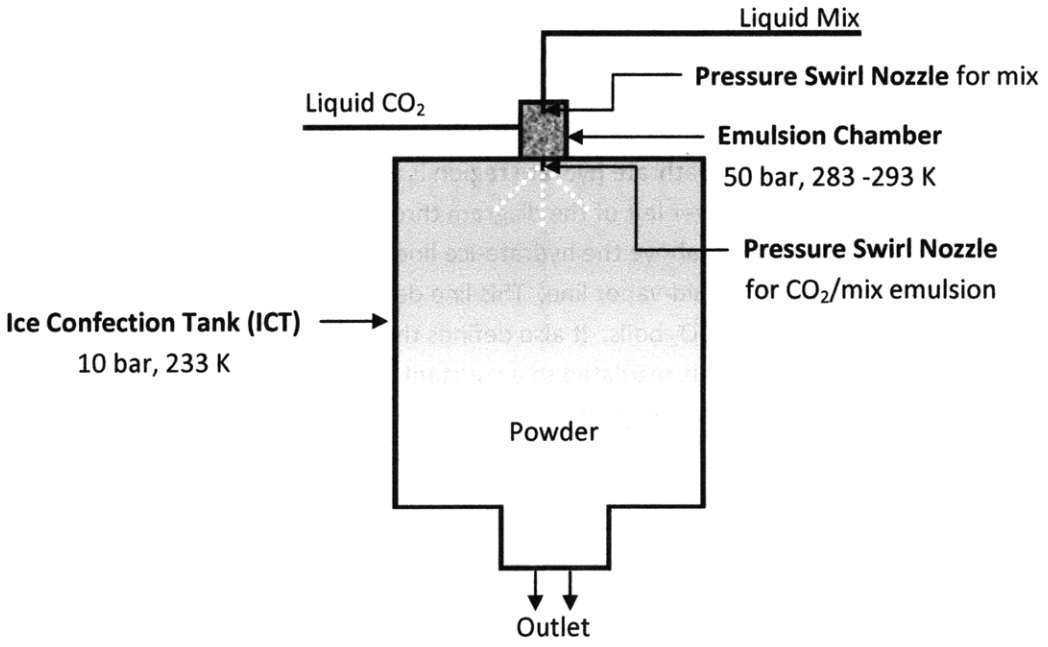

Figure 1-1: Diagram of Ice Confection Production Equipment

focused on the production of pellets for the consumer trials, the design should include plans for scaling up the device to match its throughput to that of a large production line.

Since the packaging for this product has not yet been finalized, the production device will be designed to deliver pellets to the operator so that they can be manually inserted into their containers. Thus, the device must serve as both a compressor and extractor. Compression refers to the formation of the pellet through forcible compaction of the powder. Extraction refers to the removal of the product, either powder or pellets, from the high pressure environment of the production equipment. The extraction operation could occur before or after that of compression; the order of operation choice is described in Chapter 2.

1.2.Constraints

The design of an extraction and compression device for use with the CO_2 Spray Freezing product is subject to several constraints. In the following sections, the most important of these constraints will be described.

1.2.1. Pressure and Temperature

Two of the most important constraints are the operating pressure and temperature of the production equipment. Any extraction device will need to withstand both the high pressures and low temperatures required to produce desired characteristics of this product. The CO_2 spray frozen ice confection relies on the cooling effects of flashing carbon dioxide to freeze the liquid mix and maintain the temperature in the Ice Confection Tank, so production must occur at a pressure and temperature combination at which CO_2 can exist as a gas. Its fizziness, however, is dependent on the presence of clathrate hydrates in the powder produced, so conditions must also be amenable for the presence of this phase. Examination of the CO_2-H_2O mixture phase diagram, presented in Figure 1-2, provides guidelines for the pressure and temperature requirements of the process.

Both CO_2 and H_2O exist in their usual solid, liquid, and gaseous forms at various points on the phase diagram. However, they can also combine to form the carbon dioxide clathrate hydrate phase at certain pressures and temperatures. The region in which this phase exists is shaded in blue in Figure 1-2. The lower boundary of the CO_2 clathrate hydrate region is the water hydrate-ice line, which runs from the point labeled {LW} in the lower left of the diagram through the points labeled {SL}, and {SI} in the upper right of the graph. Directly above the hydrate-ice line and to the left of the triple point of CO_2 (217 K, 5.3 bar) is carbon dioxide's liquid-vapor line. This line defines the relationship between pressure and the temperature at which liquid CO_2 boils. It also defines the operating temperature of the Ice Confection Tank. The tank's pressure is regulated to a constant value and enough excess liquid CO_2 is vaporized during production to pull the temperature down to its liquid-vapor equilibrium value. The CO_2 liquid-vapor line is well within the clathrate hydrate region of the phase diagram, thus ensuring the formation of clathrate hydrates within the product.

As mentioned above, the process relies on the evaporation of liquid CO_2 to cool the chamber. Current production methods call for a flow of CO_2 three to four times that of the mix, far greater than the 0.2 to 0.3 ratio required to provide sufficient CO_2 to stabilize the clathrates in the powder (Pizzagalli, 2008, *Guide d'utilisation...*). As a result, the extra CO_2 provides the required cooling effect to stabilize the temperature of the Ice Confection Tank at the value on the CO_2 liquid-vapor line for the selected pressure. Thus, the operating pressure of the system determines its temperature. Transient conditions can arise where the operating pressure does not determine its temperature, most notably during the very start of powder production and after sudden perturbations to either pressure or temperature.

Higher pressures, and thus higher temperatures, allow for greater operating efficiency of the equipment and also assist in the formation of clathrates (Baker, 2006). Therefore, it is desirable to run at the highest pressure that can be obtained. However, from an equipment design point of view, low temperatures are easier to design for than high pressures. It was decided that the process would run between 10 bar and 11 bar as a compromise between efficiency and simplicity of design, corresponding to temperatures of 238 K (-35°C) and 233 K (-40°C) on the liquid-vapor CO_2 line. In Figure 1-2, the thick, horizontal dotted line marks the range between 10 and 11 bar pressure, and the vertical dotted lines denote 238 K (-35°C) and 233 K (-40°C). The red rectangle in Figure 1-2 shows the approximate operating range of the process. The extremes of this operating range provide the design pressures and temperatures of the device.

There is a possibility of running the compression and extraction device slightly warmer than the conditions inside of the tank if the above design temperature cannot be easily achieved. According to a compilation of data done by Baker from literature on clathrate hydrate formation, the equation for the H_2O hydrate-ice line, shown as the bottom border of the clathrate hydrate region of Figure 1-2, is given by (Baker, 2009):

$$\ln(P) = 0.0432\,T - 9.3826 \qquad (1)$$

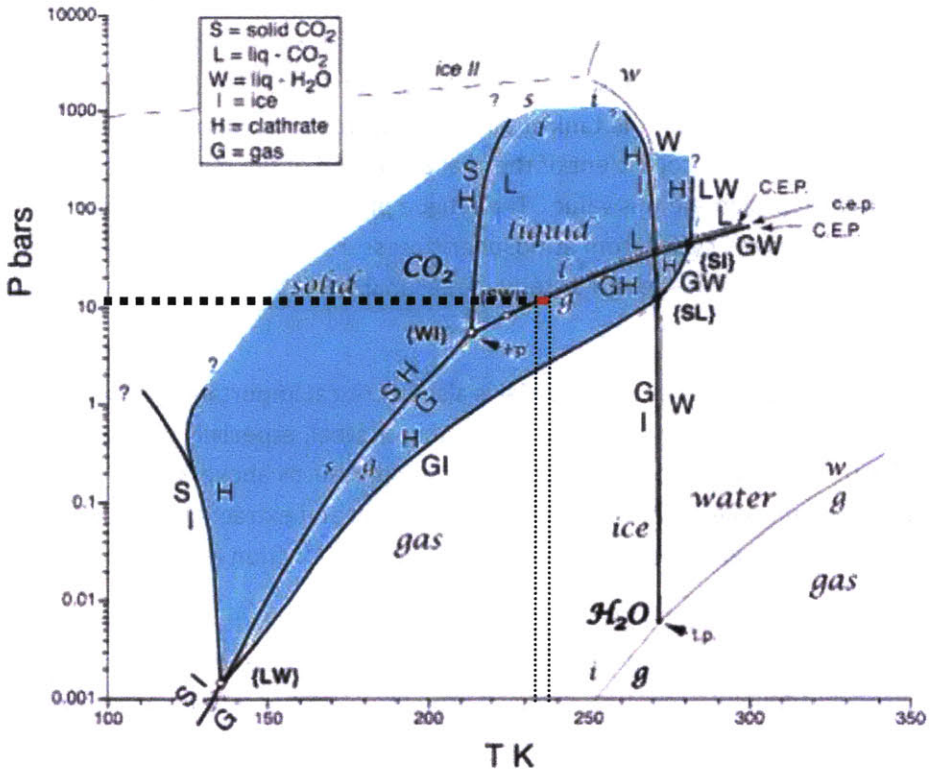

Figure 1-2: CO_2-H_2O Phase Diagram

Adapted from Longhi, 2005. The horizontal dotted line denotes the operating pressure of the CO_2 spray freezing equipment, while the vertical dotted lines show the maximum and minimum operating temperatures of this equipment. The intersection of these ranges is shown by the red rectangle.

In Equation *(1)*, *P* is in units of bar and *T* is in units of Kelvin. According to this relation, at the 10 bar design pressure the maximum temperature for clathrate stability is 270 K (-3°C). Any powder- handling device could theoretically be run at this temperature without much degradation of the product. In order to ensure that the powder is never exposed to elevated temperatures, however, the more conservative design temperature limit of 253 K (-20°C) is assumed, providing a larger margin for localized heating effects and other temperature perturbations.

These devices will have to occasionally deal with even more extreme conditions, especially regarding temperature. During the venting process, when the pressure of the tank is returned from its operating value to ambient, temperatures often fall to approximately 213 K (-60°C). Though this venting process will be a rare occurrence during a continuously operating production run, care was taken to ensure that the new device was designed so as to not incur any damage when exposed to temperatures at these levels.

1.2.2. Material and Geometry

Closely related to the constraints of pressure and temperature is that of material used in the construction of the device. The production tank is made of AISI Type 316L (1-4404) stainless steel, which has a coefficient of thermal expansion of roughly 16.0 μm/(m*K) (AK Steel). In order to ensure that the extractor is compatible with the tank at all temperatures so as to form a good seal to hold the operating pressure constant, the coefficient of thermal expansion of the material used to construct the new apparatus should approximate this value. The fatigue properties of the material must also allow the extractor to undergo many cycles from atmospheric pressure to operating pressure and back again while allowing the geometry of the design to remain reasonable. Finally, the material must be approved for usage with food.

The surface finish of the selected material is also of critical importance. It was experimentally shown that the powder is very likely to stick to bare stainless steel, especially during and after pellet compression. This tendency was most pronounced for temperatures above 233 K (-40°C). This makes surface finish an important factor in the design of compression and extraction equipment, where temperatures will likely be slightly higher than they are in the production tank.

Experiments carried out at 253 K (-20°C) showed the powder to have a strong tendency to stick to stainless steel at this temperature even when loose. When compressed, the product adhered to the stainless steel strongly enough to resist a dislodging pressure of 15 bar on a compressed 16-mm-diameter by 20-mm-length cylindrical pellet stuck in the compression cylinder. The pellet also stuck to a stainless steel piston face with enough tenacity that removal resulted in the separation of a layer of compressed powder from the pellet's face, which remained firmly attached to the piston. This separation left the end of the pellet rough and unevenly textured. This is less desirable to the consumer than the smooth, flat surface finish left after a successful ejection, and thus is unacceptable from a marketing point of view.

Fortunately, this penchant for sticking was nearly eliminated through the use of non-stick coatings, such as Accoat's Accolan Silver fluoroplastic coating (the properties of which are described in detail in the technical data sheet for Accolan Silver by Accoat A/S), or by the utilization of low-friction plastics in these critical areas. Powder compression in a plastic sleeve or with a plastic piston, in contrast, does not result in jamming or sticking. Care was taken to ensure that the thermal contraction of adjacent parts made of these differing materials did not cause any interference.

In order to meet the goal of continuous production, the pellet forming device must collect the powder produced in the Ice Confection Tank as it is being produced. The easiest way to enable this collection is to attach the device to the bottom of the ICT. As shown in Figure 1-3, the bottom of this tank is a hinged door with an inner diameter of 300 mm, and at the center of this door is a 150 mm inner diameter outlet port with a standard 150 mm quick clamp fitting at its end. During operation, the hinged door is held in place by eight clamps arranged around the circumference of the device. A device could be constructed so that it either attaches to the 150 mm quick clamp fitting or replaces the

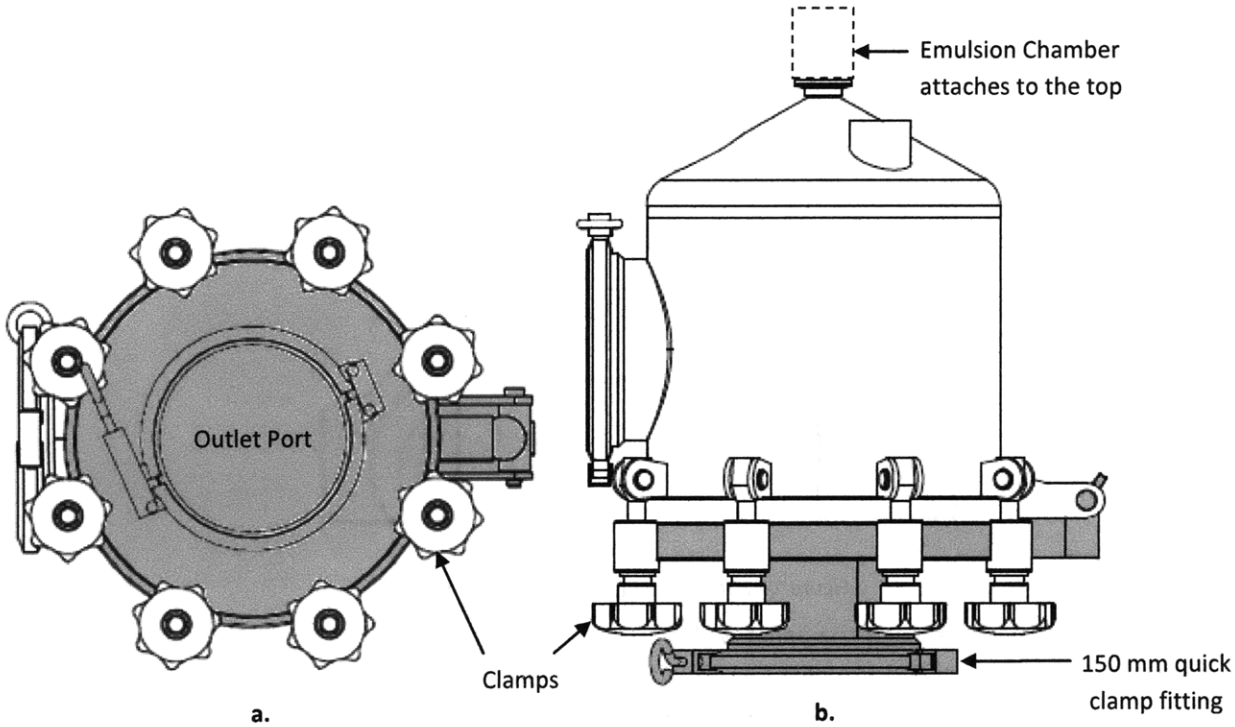

Figure 1-3: Drawings of the a.) Bottom and b.) Side Views of the Ice Confection Tank
In both figures, the hinged door of the tank and everything attached to it are shaded gray for clarity. Adapted from a drawing provided by ERI-EST (Guichard).

hinged door entirely. Replacing the hinged door would require recertification of the Ice Confection Tank (ICT) with the device attached in order to bring it into compliance with French law regarding pressure-holding vessels, so initial prototypes were constructed to take advantage of the standardized fitting at the bottom of the ICT.

1.2.3. Product

The final category of design constraints deals with the finished product itself. The product is meant to be a fizzy ice cream, so it is important that the powder does not lose its fizziness before it is compacted into a pellet and packaged. Experimental data have shown that CO_2 clathrate hydrates have a dissociation time constant of 24 minutes in fresh powder at atmospheric pressure and 253 K (-20°C) (Pizzagalli, 2008). Thus, it is imperative that the time the powder is exposed to atmospheric pressure, especially at higher temperatures, does not exceed more than a few minutes. As a consequence, a time of one minute has been chosen as the maximum time that the powder should be allowed to remain at atmospheric pressure.

Product size and shape is another key element of device design. It was initially decided that the final product be a cylindrical pellet measuring 18 mm in diameter and 10 mm in height. This pellet is to be formed by compressing loose powder into a volume roughly one-fifth its initial size, giving a compression ratio of five-to-one. It was experimentally determined that the pressure required on the flat face of a pellet to achieve this level of compression is approximately 15 bar.

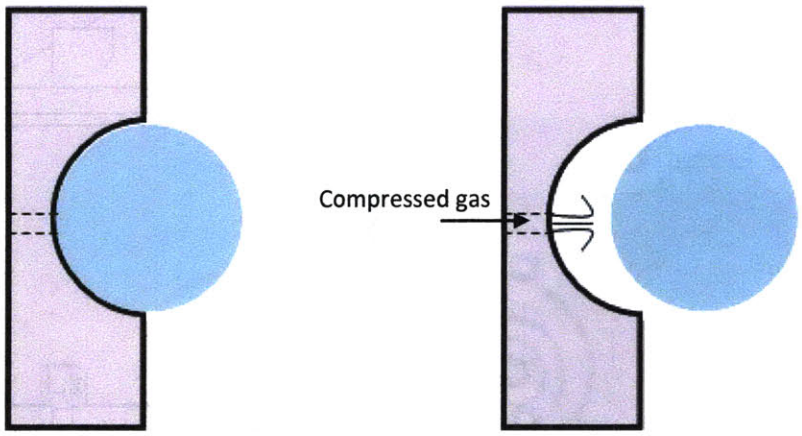

Figure 1-4: Gas-aided Ejection of a Shaped Pellet

Physical appearance of the pellet is also an important parameter. Although the initial requirements call for a cylindrical pellet, more attractive pellet forms are currently under consideration. The most popular of these alternative forms are spherical or oblate spheroid shapes (such as Mars' M&Ms or Nestlé's Smarties), which require that special attention be paid to the surface finish of the compression molds so as to avoid sticking and entrapment after the compression process. Experiments have also shown that an ejection mechanism is also needed for hemispherical molds regardless of the surface finish; compressed gas injected through a hole in the mold behind the pellet, as depicted in Figure 1-4, has shown promise in dislodging a stuck, spherically formed piece. It is important that the design of the pellet forming device considers possible moves from a cylindrical pellet to a spherical or oblate spheroid geometries.

1.2.4. Future Implementation

Any device designed should also take the future expansion of the production line into consideration. Current estimations put production rate at five to ten million 100 mL packages output per year at roughly 20 g of product per package, creating a need for approximately 100 to 200 million grams of powder a year. The current production rate of approximately 1.2 g/sec results in a total yearly production rate of 20.4 million grams of powder, if the device is operating for 54% of the 8760 hours in a year. Thus, the production rate of this process will have to be expanded to roughly five to ten times its current value in order to supply the necessary amount of powder. If a machine has its compression and extraction capabilities strained to simply keep up with the current production rate, then it will require much more time, effort, and money to adapt to the increased flow of a final production line. It is desirable, then, that any device created has excess extraction capacity or has the ability to be easily modified to add additional capacity.

1.2.5. Summary

In summary, a device meant to interact with and/or extract the powder from its production tank must be able to withstand an operating pressure and temperature of 11 bar and 233 K (-40°C), respectively. Any prototype equipment produced should be compatible the 150 mm diameter clamp fitting on the outlet port of the tank for ease of installation and maintenance. It should be made of

stainless steel to meet sanitary guidelines for food equipment. Every valve, seal, coating, and material used in any device that contacts the product needs to be approved for use with food, further supporting the use of stainless steel. The temperatures of the powder and pellets should never rise above 253 K (-20°C), and the time that it remains at atmospheric pressure should be limited to one minute or less.

The purpose of the device is to produce 250 to 500 homogenous pellets for consumer trials. This machine should be able to form cylindrical pellets with a diameter of approximately 18 mm, a height of approximately 10 mm, while utilizing a compression ratio of 5:1. Attaining this level of compression was found to require a pressure of approximately 15 bar, so the compressor should be capable of providing at least this amount of force. The apparatus should be designed with some degree of shape flexibility for the pellet. While cylindrical pellets are acceptable, 18 mm diameter spherical pellets are preferred, and other shapes may also be suggested in the future. A full-scale production line will also feature a maximum production rate of approximately ten times that of the current prototype, so the throughput of the compression and extraction mechanisms should be easily expanded to handle this increase.

Chapter 2: Initial Concept

The first design choice made was that of the working order of the compression and extraction device. As explained in Chapter 1, the device must function as both a compressor and an extractor. The order in which these processes occur can be set by the designer. Initial ideas mirrored the current batch process, in which the powder is extracted from the tank and then manually compressed at atmospheric pressure. This extraction-compression method has been generally successful when utilized with the manual batch process, but it does have some drawbacks. During depressurization of the Ice Confection Tank, a large piece of dry ice can form at the bottom of the tank. This mass of dry ice, formed once every few trials, clogs the outlet of this tank and prevents powder flow when the tank is opened. During a production run with a pellet forming device in place, the formation of this chunk of dry ice during a depressurization cycle would require the cessation of the trial until it is removed from the system. This is not only time consuming, but also prevents continuous production.

Another problem with the extraction-compression method is the behavior of the powder under atmospheric pressure. The powder tends to sinter and clump once at atmospheric pressure, making it more difficult to load into the piston-cylinder apparatus used for compression. During manual compression, the powder is stirred as it is loaded into the compression cylinder and large, sintered chunks are discarded. This problem not only results in excessive waste in the form of the rejected chunks of powder, but it also requires there to be a reliable method in sorting these chunks from the powder so that they do not clog the compression cylinder.

A method in which the powder is compressed while under pressure and then the pellets are extracted from the pressurized environment was also examined. With the compression-extraction method, the powder is maintained at the ICT pressure and temperature. It is hoped that this will prevent excessive dry ice formation as well as the flow issues caused by powder sintering and clumping. The pellets are also much less sensitive to the temperature and pressure changes experienced during depressurization due to their greater density, cohesiveness, and lower surface to volume ratio when compared to the loose powder. The much greater density of pellets compared to powder also means that fewer depressurization cycles will be required for the production of a given number of pellets, decreasing the likelihood of dry ice formation occurring and disrupting a trial and limiting the effects of pressure fluctuations due to depressurization on the process itself.

The compression-extraction method does have its own limitations, however. Several powder agitation and compression components move to perform their functions. This means that the pressurized volume of the device must either be large enough to contain these parts and their actuators, increasing the size and weight of the machine, or dynamic seals must be found that can withstand the operating conditions of the device. Observation of powder flow and pellet formation, both of which occur under pressure, will also be greatly inhibited by the pressure-holding walls of the device. This will make it more difficult to troubleshoot any issues the device may have, since it will be very difficult to determine where, when, and how any problems crop up.

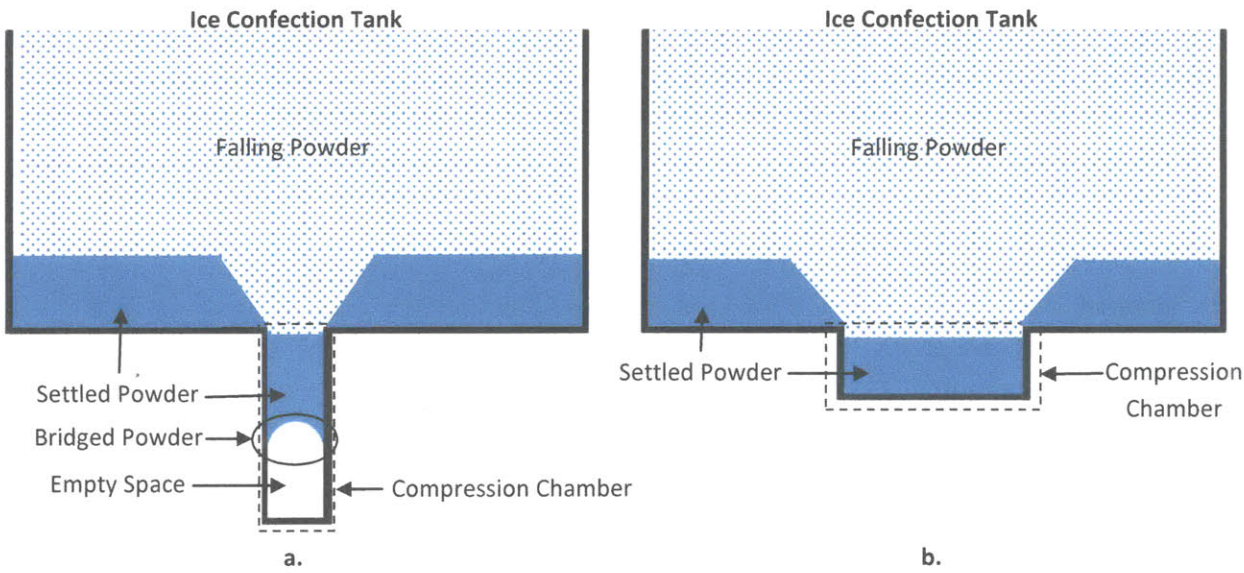

Figure 2-1: Cross Sections of a.) a Vertical Compression Scheme; b.) a Horizontal Compression Scheme
The compression chambers are encircled by dashed-line rectangles for clarity.

After careful consideration of the two methods, it was decided that the compression-extraction method was the better of the two options. Experience with dry ice formation and powder behavior seen with the current batch production method suggests that powder flow will be a troublesome issue with the extraction-compression method. The compression-extraction method does not expose powder to changes in temperature or pressure until after it has been compressed into a pellet, at which point it is much less sensitive to these variations. It also limits the number of depressurizations required for the production of a set number of pellets, avoiding possible complications caused by either dry ice formation or pressure fluctuations.

Several prototype pellet formation devices based on the compression-extraction mode of operation were examined during the initial stages of this project. In all of these devices, powder flowed vertically down a cylindrical tube into a compression chamber as shown in Figure 2-1a, where it was then compressed into a pellet. All such devices were found to experience severe problems with powder flow during the loading processes. Specifically, the powder would flow a short distance down the cylinders and then bridge, blocking the passage and preventing powder from filling these volumes to create pellets of the desired size and texture. Attempts to experimentally quantify this distance-to-bridging were foiled by the sintering and clumping behavior of the powder as described above. Coating the walls of the cylindrical passageways with a Teflon-like coating had a beneficial effect on powder flow, especially when the powder was being manually agitated, but it did not solve these issues.

In an attempt to alleviate the bridging problem, powder flow path geometry was reexamined. Rather than having powder flow down a long, thin vertical compression chamber, it made more sense to have powder flow down through the side of a horizontal tube, as shown in Figure 2-1b. This decreases the distance the powder has to flow, thus increasing the chance that it completely fills the chamber. Though a horizontal compression layout should be advantageous regarding powder flow, it is not without drawbacks. Pellet ejection is no longer assisted by gravity, which may make it more difficult to

dislodge pellets that stick to the compression surfaces without the use of additional ejection mechanisms. The device will also be longer than a machine with a vertical layout, which means that care must be taken to ensure that the designed equipment will fit underneath the existing production apparatus.

2.1. Horizontal Loading Single Piston Compression Device

The initial concept of a horizontal loading compression device was one in which a piston compressed powder against a movable wall. See Figure 2-2 below for a pictorial description of its actuation cycle. These actions take place subjected to tank pressure, 10-12 bar, and under temperatures ranging from 233 K to 243 K (-40°C to-30°C).

The cycle starts with the filling step, in which the piston is held retracted as powder drifts down from the ICT and collects in front of the piston in the filling chamber. Once this filling chamber is full, the piston moves to the right, pushing the powder to the right and compacting it against the wall at the end of the compartment. The wall descends for the final ejection step, thus allowing the piston to continue its forward motion and push the pellet out of the compression chamber so it can fall to the

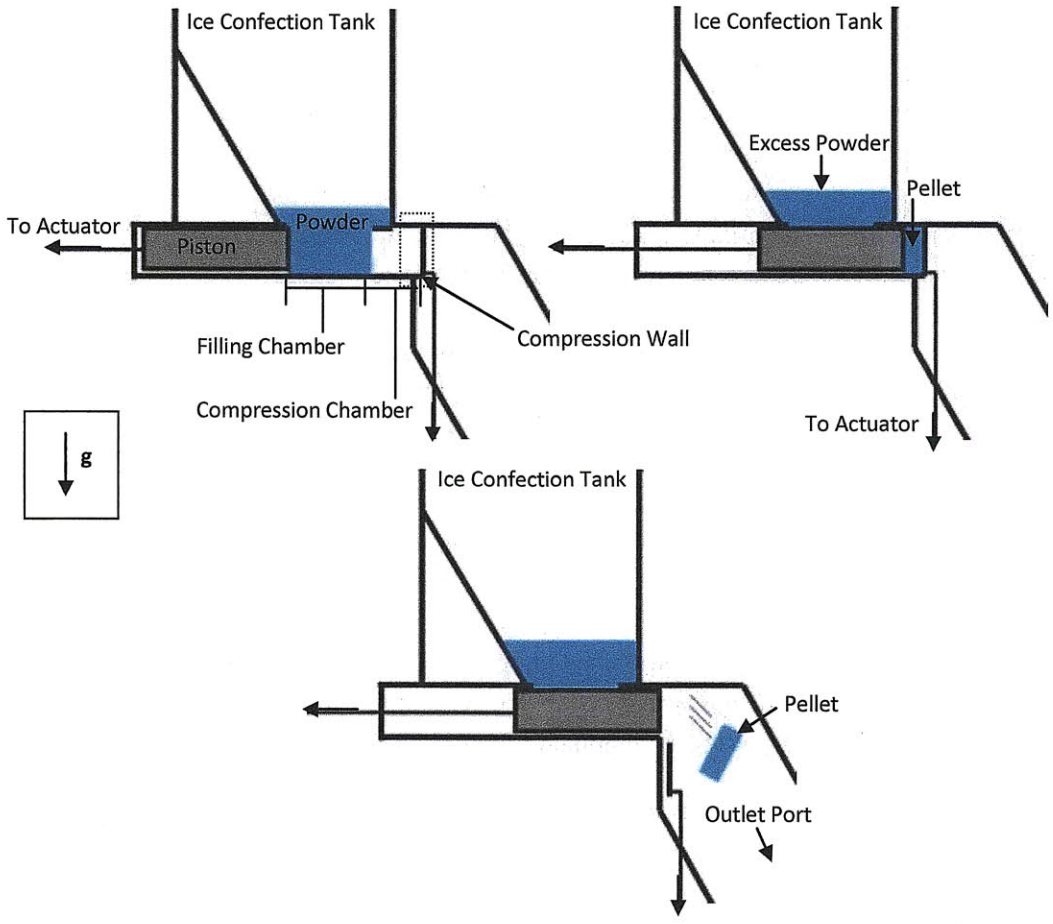

Figure 2-2: Horizontal Loading Single Piston Compression Device, Conceptual Drawings
Clockwise from Upper Left: Filling, Compression, Ejection. An airlock is attached below, its location denoted by the arrow. The dotted square in the first figure highlights the portion of the device seen from above in Figure 2-3.

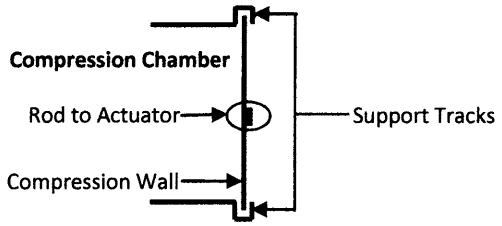

Figure 2-3: Top View of the Compression Wall
Shows the supporting track the wall rides in, providing support during compression events.

airlock below. In order to avoid excess wear at the wall-track interface, the force exerted by the piston's actuator may need to be decreased while the wall is moved.

The compression wall is an integral part of this concept and presents a few design challenges. It must be stiff enough to withstand the force of the piston as it compresses the powder, and must also be able to move vertically to allow for the ejection of a pellet. One way in which this could be assured is to have the wall move in a track that constrains it in the horizontal direction, as shown in Figure 2-3.

This track has several constraints placed upon it. It must be strong enough that it does not deform under load, and it must be made of a food-grade material. There must also be little friction between the compression wall and its track so that the wall can be easily retracted after the pellet is formed without damaging the wall, the track, or the pellet. Stainless steel coated with a low friction material, such as Teflon, would likely be satisfactory, as would several kinds of structural polymers such as Delrin. Since the track will be constructed of or coated with a low-friction material, it is expected that any powder trapped in the track will be easily dislodged by the motion of the wall and will not threaten to jam the equipment.

A sliding wall limits the shape of a pellet to something with a flat side, as forming this wall into some other shape would make it extraordinarily difficult to prevent pellet damage as it is retracted. If the pellet sticks to the wall-mold as the wall is pulled downwards by its actuator, it will be damaged due to the constraints imposed by the walls of the compression chamber, which will not allow the newly formed pellet to follow the wall on its downward journey. In order to allow for more flexibility in product shape, a rotating wall was proposed, as shown in Figure 2-4.

The actuation cycle remains the same, with the only difference being that the wall now rotates out of place rather than sliding out of place. This rotation is achieved through the combination of a hinge at the top of the wall and an actuating mechanism that can drive rotational movement. The wall's rotation should break the pellet loose if it becomes stuck to the wall during compression. If the pellet becomes stuck to the piston, it can be successfully ejected through use of an ejection mechanism on the wall itself that pushes the pellet downwards when the piston is fully extended.

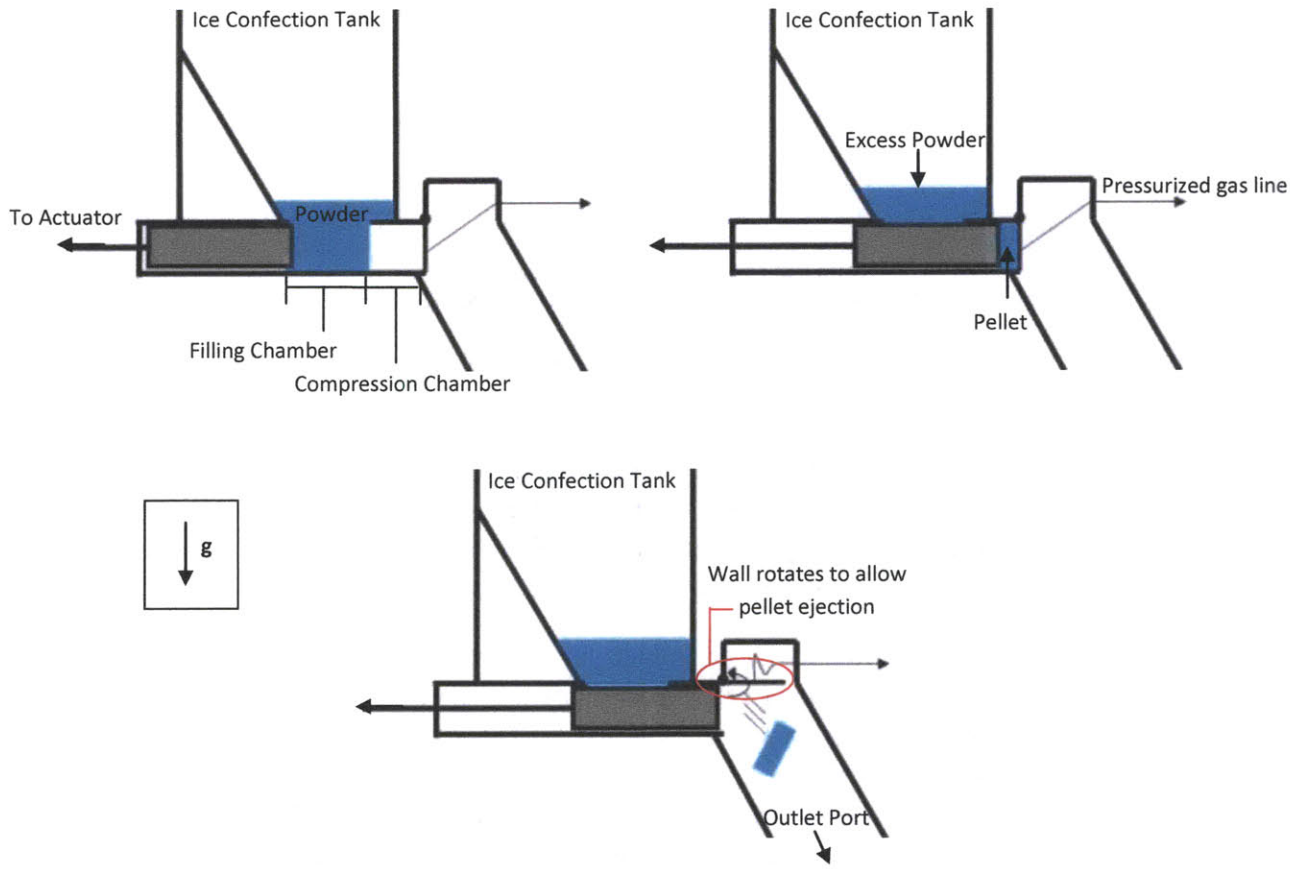

Figure 2-4: Rotating Compression Wall, Conceptual Drawings
Clockwise from Upper Left: Filling, Compression, Ejection. Pressurized gas ejection mechanism shown. The outlet is denoted by a downwards-pointing arrow.

Two possible ejection mechanisms were considered for this concept. One was mechanical, consisting of a piston located in the center of the wall that could be actuated after the wall has rotated. The other was a stream of pressurized CO_2 gas as it is already available in the system and will not contaminate the product with other materials. This stream would be directed at the top of the pellet, dislodging it from the piston and pushing it downwards out the outlet port.

The hinge, however, has a few questions associated with it. It is unknown how a hinge will hold up to the high pressures and low temperatures found in the tank, especially if abrasive dry ice is formed during the process. An actuator must be found that can rapidly open and close the rotating wall and be strong enough to hold the wall shut during the compression process. If the wall is to hold against tank pressure, the actuator will need to be strong enough to provide adequate sealing force and withstand the combination of the pressure and compression forces. Regardless of the actuation method of the compression wall, the core of the horizontal loading single piston compression device will look the same. In Figure 2-5, a rough schematic of such a machine is shown, giving a feel for the size and layout of this sort of apparatus.

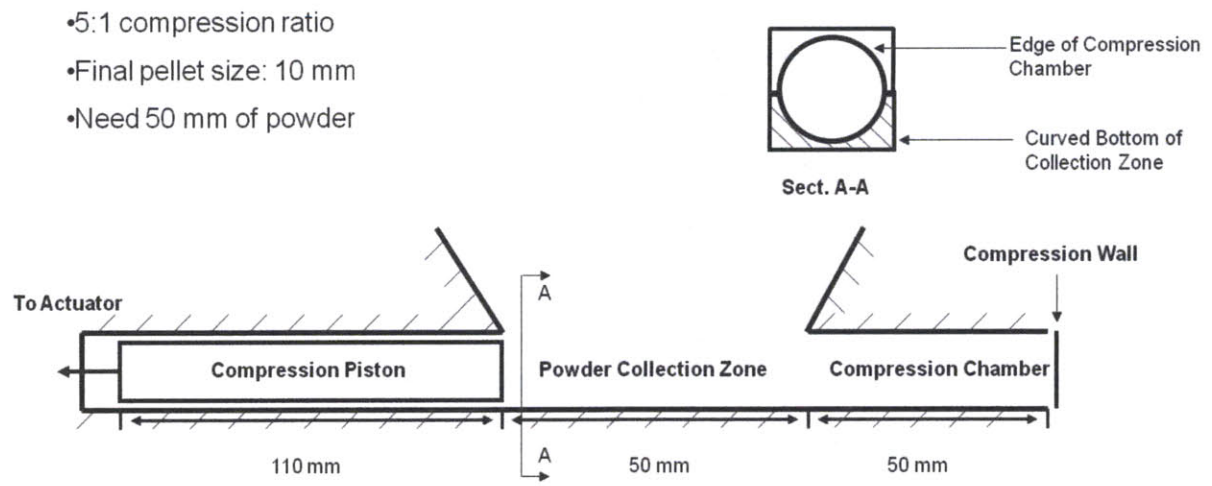

Figure 2-5: Schematic of Single Piston Device

2.2.Horizontal Loading Dual Piston Compression Device

Another concept of a horizontal loading compression device was called the dual piston compression device. In this machine, one piston compresses the product against the surface of a second piston, which can then move to allow for ejection. Figure 2-6 below depicts this actuation cycle. As with the single piston design, these actions take place under tank conditions, corresponding to pressures between 10 and 12 bar, and under temperatures of 233 K (-40°C) to 243 K (-30°C).

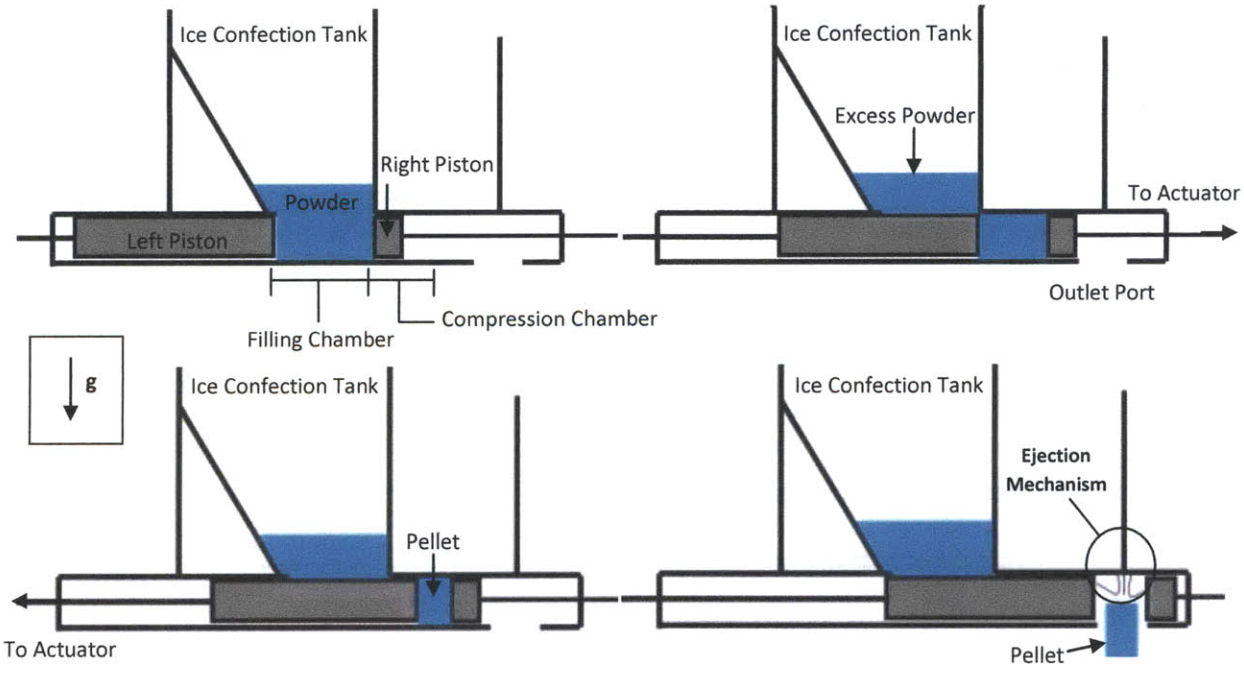

Figure 2-6: Horizontal Loading Dual Piston Compression Device, Conceptual Drawings
Left to Right, Top to Bottom: Filling, Compression, Ejection. A Pressurized Gas Ejection Mechanism is depicted in this figure.

The cycle starts with the piston retracted as powder flows down from the Ice Confection Tank and collects in the filling chamber. After the filling chamber is full, both the left and right pistons move to the right, pushing the powder into the compression chamber and separating it from the powder remaining in the ICT. Once all of the powder in that load is in the compression chamber, the right piston stops and the left piston continues its forward motion, compacting the powder against the front surface of the stationary right piston. The right piston then moves to the right, allowing the left piston to continue its forward motion and push the pellet over the outlet port on the bottom of the device, where it falls to an airlock below. Should the pellet stick to one of the piston faces, an ejection mechanism, such as an additional piston or a blast of pressurized CO_2 gas, can be located above this outlet port to push or agitate the pellet to assist it in exiting of the compression device.

This dual piston layout could also act as an airlock between the Ice Confection Tank and an unpressurized outlet port through the use of ring seals on the pistons themselves, which would preclude the use of a separate airlock to perform this function. The pellets would still be created under pressure, but when the right piston moves past the outlet port during the ejection step the pellet would be depressurized. This method of sealing would require careful synchronization of the two pistons to ensure that there is never an open gas path from the tank to the outside environment, but could reduce the overall complexity of the powder processing equipment. These seals must be able to deal with the dynamic motion of the pistons, the high pressures and low temperatures of the ICT, and the possible presence of abrasive dry ice without losing their effectiveness.

As with the single piston compression machine, a schematic showing the layout of the device and giving estimated dimensions is shown in Figure 2-7. The estimated length of the dual piston apparatus is 260 mm, slightly greater than the 210 mm of the single piston machine. The locations of the right pistons are labeled 1, 2, and 3, with 1 being its location during the filling step, 2 its location during pellet compression, and 3 its location during ejection.

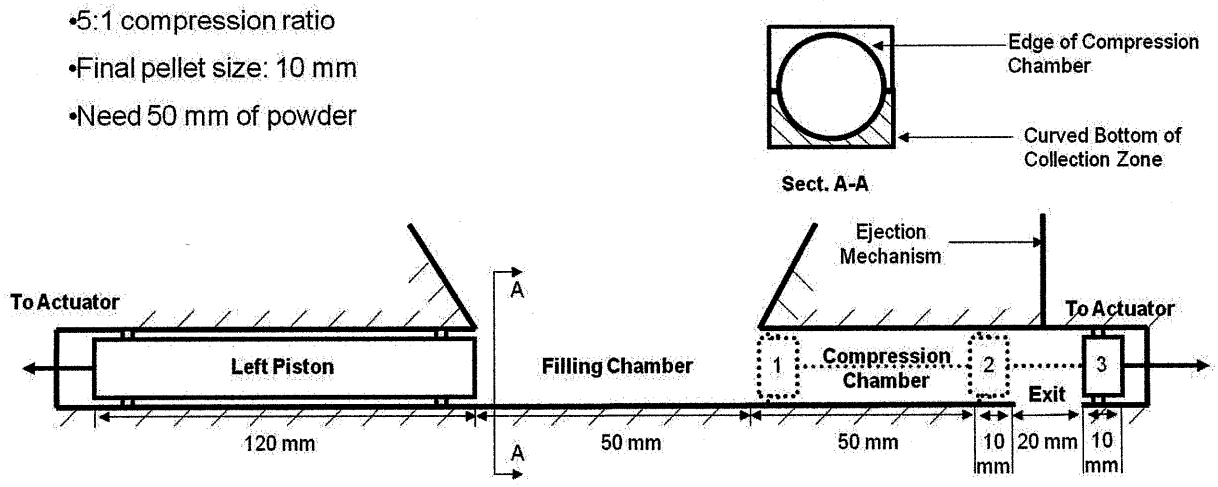

Figure 2-7: Schematic of Dual Piston Device

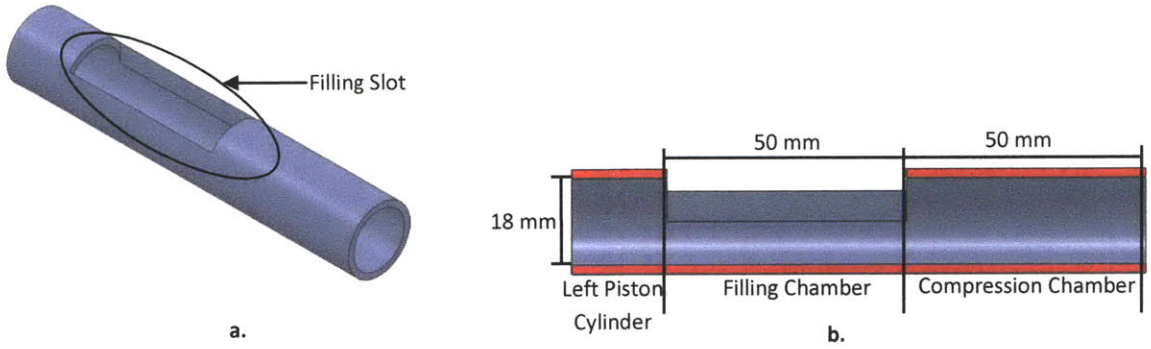

Figure 2-8: a.) Isometric and b.) Midline Cross-Sectional Views of the Proposed Sleeve

The dual piston apparatus has several inherent advantages over the single piston concept. In a dual piston machine, all motion and actuator-induced forces are along the axis of the loading and compression chambers, which greatly reduces the friction load and potential for wear of these parts when compared to a sliding wall setup. A dual piston compressor also has fewer independent critical features than a single piston and wall apparatus. With a piston and wall setup, two separate problems need to be solved – that of moving and sealing a piston, and that of moving and sealing a wall. With the dual piston setup, only one of these problems needs to be addressed in order to produce a functional device.

The dual piston design does have a few problems, however. The largest one of these is its requirement that the right piston have three set positions, as shown in Figure 2-6 and Figure 2-7. Though this is easily handled with the implementation of a mechanical piston actuation system, the planned use of readily-available pneumatic actuators required the addition of a mechanical stop, which raised safety concerns. The device is also longer than the single piston design, which makes it slightly harder to handle during mounting, dismounting, and device transportation situations.

Another option for the dual piston concept would obviate the need for a separate compression chamber, thus eliminating the intermediate position of the right piston and alleviating the subsequent safety concerns. Rather than pushing the powder into the smooth compression chamber, the chamber can be formed around the powder through the use of a mobile cylindrical sleeve. This sleeve has a filling slot cut through its upper surface to allow the filling chamber to be open to the Ice Confection Tank above. The sleeve slides over to enclose the powder that fell into it during the filling process, at which point compression and ejection are carried out as before. An isometric and a cross-sectional view of a model sleeve are shown Figure 2-8. It should be noted that this model does not include any considerations of the attachment of an actuator needed to move the sleeve back and forth. It simply illustrates the concept in a clear way.

Figure 2-9 shows the actuation cycle of this proposed device. In order to keep the drawing neat and clear, the sleeve has been represented schematically as a series of lines corresponding to cross-section view shown in Figure 2-8b.

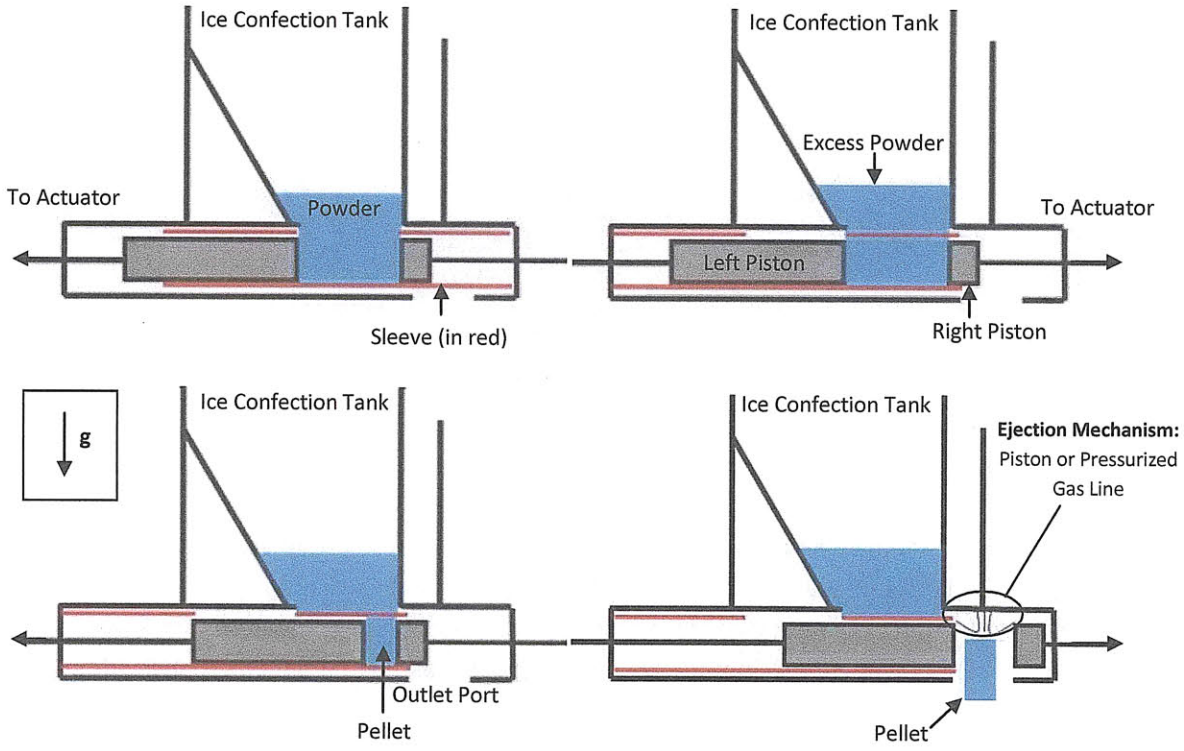

Figure 2-9: Horizontal Loading Sleeved Dual Piston Compression Device, Conceptual Drawings
Left-to-right, starting on top: Filling, Sequestration, Compression, Ejection. The sleeve is colored red for clarity. Note that the sleeve slides over during the sequestration step to fully enclose the powder. A Pressurized Gas Ejection Mechanism is depicted in this figure.

This cycle begins with powder falling from the Ice Confection Tank above through the hole cut into the upper surface of the sleeve and into the filling chamber. Once this chamber is full, the sleeve is pushed to the side, sliding its upper hole away from the filling chamber and thus sequestering that

- 5:1 compression ratio
- Final pellet size: 10 mm
- Need 50 mm of powder

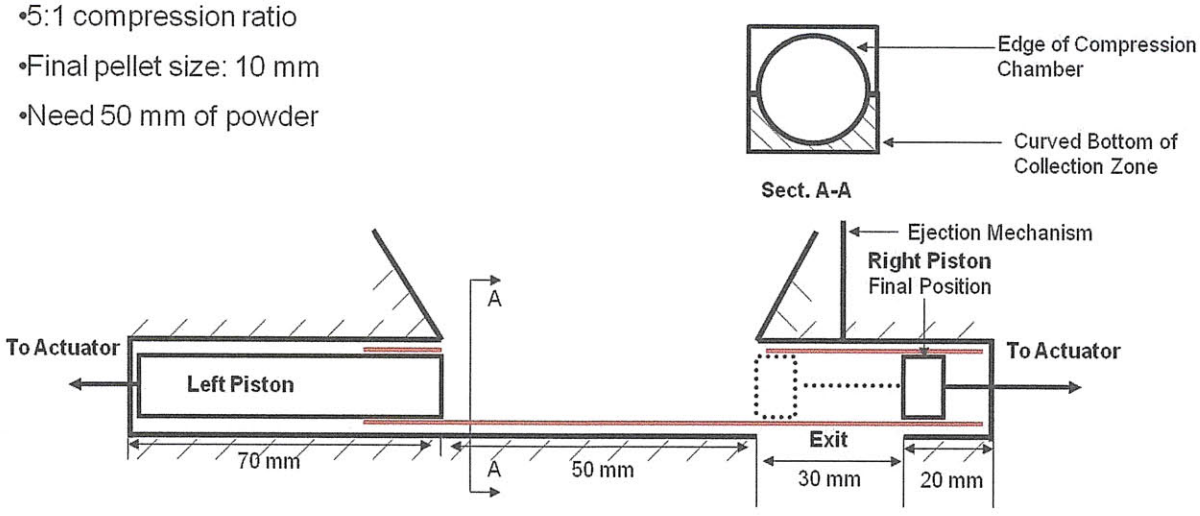

Figure 2-10: Schematic of the Sleeved Dual Piston Device
The sleeve is colored red for clarity and is shown in the loading position in this diagram.

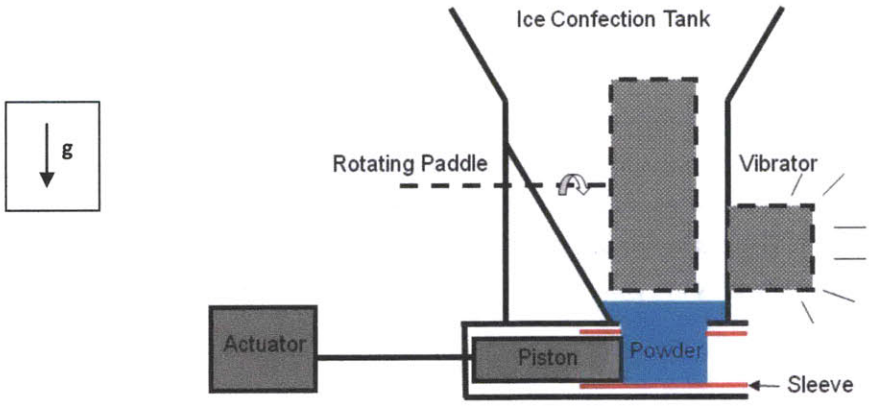

Figure 2-11: Originally Envisioned Agitation Options

powder from both the ICT and the outlet of the device. The left piston then moves to the right, compressing the powder against the stationary face of the right piston and forming a pellet. The right piston moves to the right to eject the pellet, allowing the left piston to extend further and push the pellet out of the sleeve. The pellet then falls through the outlet of the machine and into the airlock waiting below. Also as before, an ejection mechanism can be located above this outlet port to push or agitate the pellet to assist it in exiting of the compression device should the pellet stick to the face of one of the pistons. A simple schematic of the concept is presented in Figure 2-10.

This layout allows for the elimination of the separate compression chamber of the previous designs. This eliminates the length of the compression chamber and the length and stroke of both pistons, since neither piston needs to traverse a separate compression chamber. This limits device length to approximately 170 mm, compared to the 260 mm of the dual piston concept and the 210 mm of the single piston one. The advantages of this design do come at a price, however. The powder flow path length is increased marginally, which could make the device more prone to bridging. The design of the concept is also more complicated with the addition of the sleeve, the extra actuators required to move this part, and the additional seals required by the presence of the new part. Given its advantages, the more complex design of the sleeved dual piston is acceptable, and the slight increase in powder flow path is not expected to be problematic. Thus, it was chosen as the one to pursue further.

There are several additional issues that must be considered in order to more fully evaluate the potential of such a design. The most important of these issues are powder agitation, equipment cooling, and consideration for future expansion to a full-scale industrial line. In Figure 2-11, two different methods of agitating the powder to keep it flowing into the pellet forming device are displayed. The first of these is an industrial vibrator, which could be strapped to the exterior of the Ice Confection Tank or the pellet forming device. It would constantly shake the entirety of the apparatus to prevent the powder from settling down and sticking to the walls of the equipment or to itself. Another option is a mechanical paddle, operated by a shaft passing through a hole in the wall of the funneling section directly above the powder collection zone. This paddle wheel would continually rotate during the production process, stirring the powder and keeping it from bridging over the entrance to the pellet

forming device's filling chamber. One or both of these methods of agitation could be implemented if necessary.

The temperature of the pellet forming device should be held between temperatures of 233 K (-40°C) and 253 K (-20°C). Experience has shown that the powder tends to sinter and bridge more effectively with increasing temperatures, so the device must be kept below 253 K. If the temperature of the apparatus is too low, the CO_2 gas in the device can liquefy (233 K) or even solidify (218 K), compromising the quality of the product and possibly preventing the production of pellets.

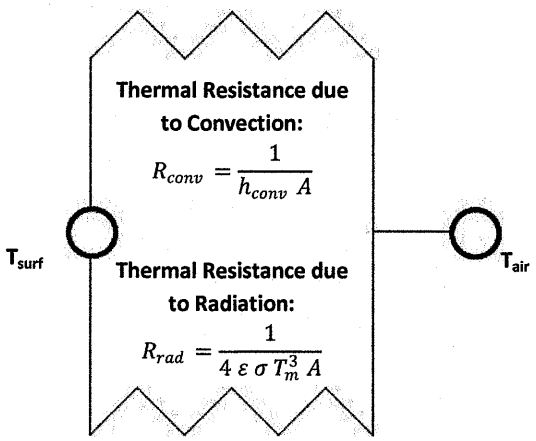

Figure 2-12: Thermal Resistance Model for Convection and Radiation off of a Surface

A simple model can be used in order to obtain an estimate of the cooling load placed on this system. The heat load placed on this device will be due to natural convection and radiation. Since the device temperature will be close to that of its environment, the thermal resistance model will be valid for both of these modes of heat transfer. In the equations given below, h_{conv} is the convective heat transfer coefficient, A is the external area of the device, ε is the emissivity of the device, σ is the Stefan-Boltzmann constant (5.67×10^{-8} W m^{-2} K^{-4}), and T_m is the average temperature of the surface of the device (T_{surf}) and the air (T_{air}).

$$\dot{Q} = \left(R_{conv}^{-1} + R_{rad}^{-1}\right)\left(T_{surf} - T_{air}\right) \qquad (2)$$

Several assumptions have been made in order to use Equation *(2)* to determine the rate of heat flow into the device. It is assumed that the device is wrapped in adequate insulation to obtain a surface temperature of 280 K, thus avoiding condensation. The convective heat transfer coefficient is taken to be 10 W m^{-2} K^{-1} in the case of natural convection and 2000 W m^{-2} K^{-1} when condensation is present. The apparatus is modeled as a black body, giving it an emissivity of one. In order to calculate the area, the device is assumed to be a rectangular bar with an external height and width of 60 mm. For this calculation, it is assumed that the device is built as a 260 mm long dual piston apparatus. The top of the device is partially covered by the 150 mm outlet port of the Ice Confection Tank. The device

temperature is assumed to be 233 K. Given these assumptions, the rate of heat flow into the device is calculated as 38 W assuming natural convection and 5400 W assuming condensation.

Both of the calculated cooling loads are well within the range of large commercially available refrigeration units. However, it is desired to use a lab-scale circulator during initial development, since they are more portable than larger designs and several are already on-hand. Most commercially available lab-scale units have maximum cooling capacities of a few hundred Watts, making them unsuitable for cooling the apparatus while condensation is forming on its surface. The device could be insulated to avoid condensation and allow for the use of these smaller refrigeration units. If expanded polystyrene (EPS) is used as an insulating material, approximately 8 mm of insulation will be required to bring the temperature of the device/air interface to 280 K. This temperature is high enough that it should avoid condensation in the climate-controlled plant where the device will be installed. Further calculations will be performed to determine insulation and cooling capacity requirements once the geometry of the device has been finalized and the machine is proven ready for trials requiring the implementation of the cooling circuit.

There are several acceptable refrigeration units commercially available that can provide coolant flow to a device-mounted heat exchanger. This heat exchanger can be designed as a separate, externally-mounted part of the pellet forming device. The lower surfaces of the sleeved dual piston device should be open and free from protruding features, which would make this the most effective place to attach a modular heat exchanger plate. The upper surfaces of the pellet forming device could also be cooled, but care must be taken to ensure that the cooling plate is designed to fit around the connection between the compressing device and the ICT above. Figure 2-13 below shows an illustration of the described coolant plate mounting scheme.

Figure 2-14 illustrates a proposed design of the heat exchanger plate itself. This plate would span the width of the device and would cover most of the lower portion of the apparatus. A refrigerant, such as propylene glycol or 2-propanol, is pumped in on the inlet side of the compression device. The coolant then passes through the sinuous pathway in the heat exchanger, in contact with the bottom of the pellet forming device at all times, and then exits the coolant plate. Upon exiting the heat exchanger, the coolant returns to the external refrigeration unit to shed its heat before it is pumped back to the coolant plate inlet. This design is simple and should be able to be built on-site, saving time and resources compared to sending the plans to an outside supplier for construction. More detailed analysis of the heat exchanger design is presented during the description of its implementation with the beta prototype.

The transition to mass production will see the production rate of this product increase to approximately ten times its current value, as described in the Constraints section above. Therefore, compression device throughput must also increase in order to match the increased rate if production of the CO_2 spray freezer. This increase of flow rate of product through the compression device while keeping pellet properties constant can be accomplished by either increasing the cycle rate of the device or by increasing the number of devices attached to a single production tank.

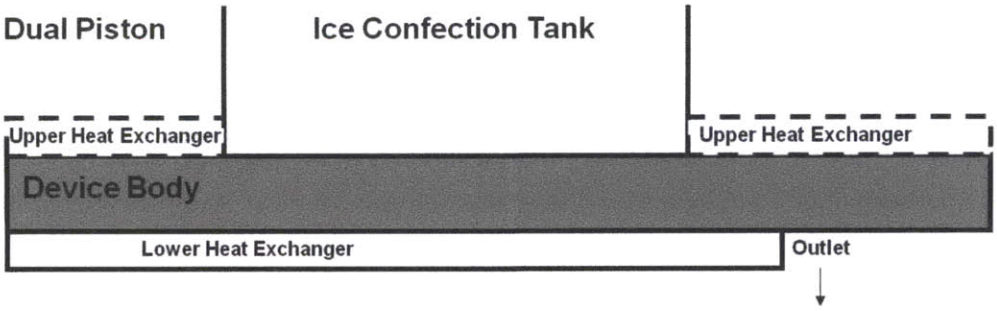

Figure 2-13: Cooling Circuit Plate Mounting Scheme
The cooling plates are mounting to the exterior of the pellet forming machine, leaving room for the pellets to exit the device.

The increase of cycle rate will be limited by the cycling speed of the actuators and the rate at which powder will flow from the ICT into the powder collection zone of the device. Mechanical or pneumatic actuators can physically be cycled multiple times per second, given the appropriate control scheme to ensure they are properly synchronized and adequate thermal control to prevent frictional heating of the apparatus beyond the powder's limit.

Powder's flow rate, however, is not as easily modified. After the compression piston retracts, the powder must accelerate from rest and fall into the just-vacated powder collection zone below. An initially inert particle in free fall will take 0.06 seconds to fall the 0.75 inches to the bottom of the chamber under the influence of gravity. If the compression and ejection processes are assumed to take

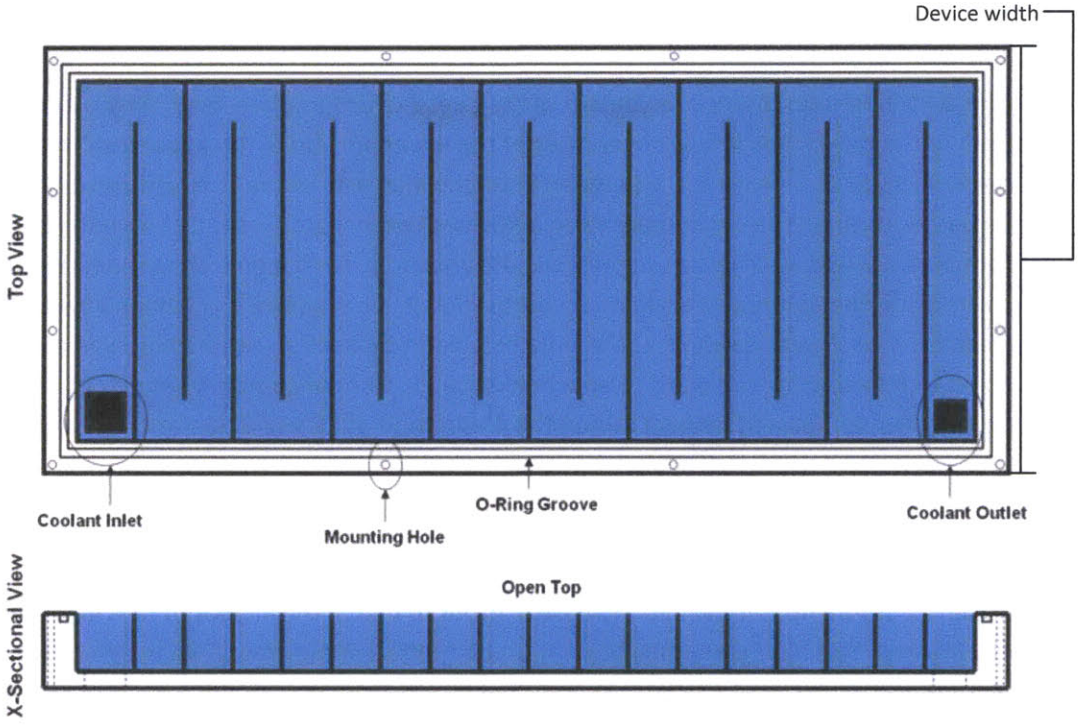

Figure 2-14: Example Cooling Circuit Plate

the same amount of time, equivalent to a cam mechanism spinning at approximately 500 rpm to account for the filling, compression, and ejection times, the maximum production rate is eight pellets per second. However, the powder often requires some form of agitation to move after sitting still, as it sticks to itself and the walls of its container and bridges. This increases the filling time from the free fall time, suggesting that the powder's flow rate into the device will be the limiting factor of cycle rate augmentation.

Trials performed with conceptual models of this equipment suggest that a production rate of one pellet per second can be reasonably expected. Each 18 mm diameter, 10 mm long cylindrical pellet contains approximately 1.2 g of powder, so a production rate of a single pellet per second will be able to just match the current 1.2 g per second powder production rate of the current equipment. Therefore, it is unlikely that solely improving the cycling rate will provide the required throughput boost.

Once the maximum cycle rate has been reached, the only way to further increase throughput is to add multiple devices working in parallel. The addition of these devices will be limited by the space available at the bottom of the Ice Confection Tank. The inlet of each compression apparatus must be afforded an unobstructed path to the powder above in order for successful powder loading. There must also be space left for the pistons and actuators off to either side of the inlets. One space-efficient way to implement a multiple device solution is shown in Figure 2-15.

In Figure 2-15, the devices arranged vertically lie above the horizontally arranged devices, leaving space for all the machines present. Figure 2-16 below shows a cross sectional view of the layout displayed in Figure 2-15, illustrating the method of stacking the compression modules in the bottom of the Ice Confection Tank in such a way as to provide each device with a clear, open filling chamber. Multiple layers of the tablet presses can lie in each orientation to increase the throughput of the overall system. The design illustrated in Figure 2-16 shows a setup with two layers of pelletizing mechanisms in each orientation, allowing a maximum of 54 modules to be implemented in such a layout if the full diameter of the ICT is available. However, since the increase in powder production rate is expected to

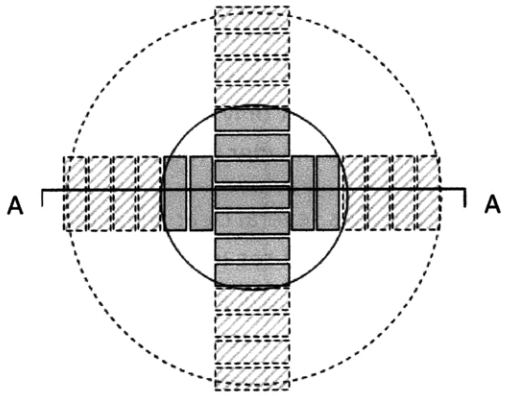

Figure 2-15: Expansion Options for the Horizontal Loading Piston Compression Devices
This view is taken from the top down. The gray boxes show the filling chamber of each apparatus. The solid lines show what is possible given the current dimensions of the current ICT outlet, while the dotted lines show what could be possible if the ICT outlet spanned the entire diameter of the tank.

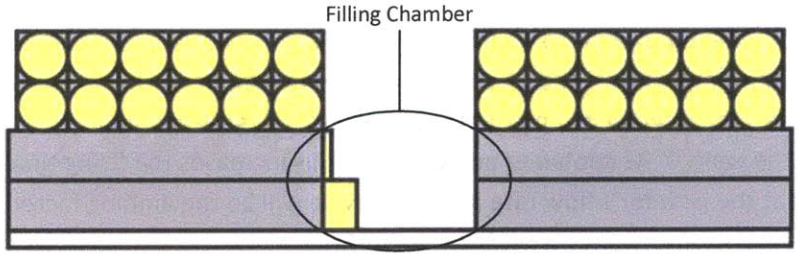

Figure 2-16: Module Stacking as a Method of Increasing Throughput
Section A-A of Figure 2-15, showing the possible stacking of modules. The light gray boxes are the compression chambers and body of each device, while the yellow rectangles and circles represent the cylindrical compression pistons as seen from the side and from the front, respectively.

reach a maximum of ten times its current value, it is likely that a single layer 11 devices inside the current diameter of the ICT outlet will be sufficient for any future production needs. Figure 2-16 simply shows what is possible with this methodology, should production demands rise above current expectations.

In order to save space, multiple pistons can be driven off a common, larger actuator. As already noted, the operating pressure of the Ice Confection Tank (P_{ICT}) is 10 bar, while the pressure required to compress the powder into a pellet is 15 bar. Thus, the maximum total pressure at the end of a piston during the compression process is 25 bar. For an 18 mm diameter piston, the size required to produce an 18 mm diameter pellet, this pressure is equivalent to a force of 636 N. A system driving multiple pistons must proportionally increase the amount of force that it is able to exert. For example, if pneumatic actuators running off the 5 bar pressurized air source near the equipment are used to actuate the pistons, a single actuator driving a single piston will need to have a working area of 1272 mm^2, equivalent to a 40 mm diameter actuator. If a single actuator is to drive five pistons, the working area requirement increases to 6362 mm^2, equivalent to a 90 mm diameter actuator.

2.3.Summary

Both horizontal compression devices have significant advantages over their vertical compression counterparts in terms of assuring powder flow. The powder must flow a significantly shorter distance to completely fill the filling chamber of these devices. Experience has shown that this generally decreases the chances of it bridging and leaving the chamber only partially filled, though attempts to quantify this were thwarted due to variations in the physics powder produced by the equipment.

The sleeved dual piston apparatus has several clear advantages over the single and dual piston designs discussed. The sleeved dual piston should see less friction and less wear than the single piston apparatus due to the application of all forces on moving parts along their axes of motion. The pistons and sleeve all move in a reciprocating motion in this device, leading to design work being variations on a single theme. The single piston apparatus, however, contains both a reciprocating piston and a rotating or sliding wall, resulting in two separate design features that need to be perfected independently. The sleeved dual piston machine eliminates the need for the right piston of the apparatus to stop in an intermediate position, difficult to accomplish safely with basic pneumatic actuations with no positioning control. It is also more compact than the standard dual piston apparatus, making it easier to handle.

The sleeved dual piston design's advantages outweigh the disadvantages presented by its more complex design and slightly longer powder flow path, so it has been chosen as the design to pursue further. Before a prototype was built, thought was given to its ability to ensure powder flow, controlling its temperature, and its potential to handle increased production rates of mass production. To guarantee powder flow, the powder could be physically agitated by a spinning paddle or an industrial vibrator. Cooling calculations place the rate of heat leakage at 9 W, well within the capabilities of commercially available refrigerating units, and a possible design of a device-side heat exchanger was developed. Future increases in powder production can be handled through the arrangement of multiple devices at the bottom of the Ice Confection Tank. The full scale production rate is expected to be ten times its current level, so approximately ten modules will be necessary for continuous production. These ten modules will fit to the current outlet on the bottom of the ICT, so it is possible for a sleeved dual piston design to operate on a full scale production line.

Chapter 3: Alpha Prototype

The alpha prototype was the implementation of the sleeved dual piston horizontal compression concept. This device was designed with help from ERI-EST of Sainte-Marie-Aux-Chênes, France, who also constructed the machine. All parts are made of STAVAX Supreme stainless steel, a modified version of AISI 420 stainless steel. This material has a coefficient of thermal expansion of approximately 10.2 $\mu m\ m^{-1}\ K^{-1}$, 36% lower than that of tank's 316L stainless steel (AK Steel 420 Datasheet, AK Steel 316 Datasheet). The two metals will be separated by a polyurethane gasket, so this difference, though significant, should not cause any issues related to thermal expansion or contraction when the devices are warmed or cooled. This prototype was tested during a series of trials taking place in Beauvais, France during August and September of 2008, giving a clear idea of the strengths and weaknesses of its design features. The device and these trials are described in more detail in the following sections of this chapter.

3.1. Description

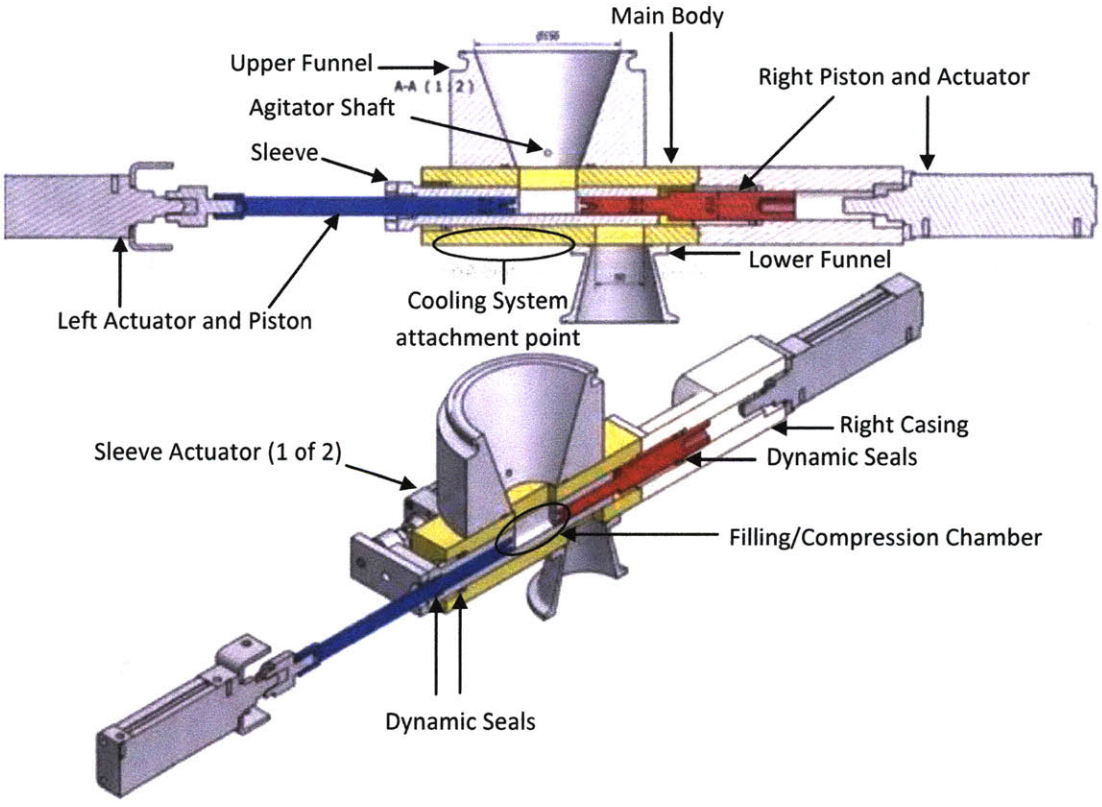

Figure 3-1: Alpha Prototype – Sleeved Dual Piston
2-D cross sectional and 3-D isometric cross sectional views. Adapted from a drawing provided by ERI-EST (Guichard).

The alpha prototype consists of a single combination compression and extraction module. As described in Chapter 2, the device takes in powder from the Ice Confection Tank, compresses it into a pellet, and then ejects the pellet out of a port cut into the bottom of the prototype. Figure 3-2 shows the four main steps of this process: Filling, Sequestration, Compression, and Ejection.

All of the parts of the alpha prototype are shown in Figure 3-1. At the top of the device is the Upper Funnel, the diameter of which is sized to fit the 150 mm diameter clamp fitting of the tank outlet and whose height allows the rest of the device to sit underneath the insulating shell of the Ice Confection Tank. The agitator shaft pokes through the side of the Upper Funnel, near the bottom of that part. A paddle is attached to this shaft and will rotate and stir the powder sitting in the bottom of the Upper Funnel. This action should prevent the powder from bridging or jamming at the narrowest point of the inlet path.

Below the Upper Funnel is the Main Body of the alpha prototype, shown in yellow in Figure 3-1. This is the solid core of the device; all other parts of this device are mounted to it. During the powder filling step, powder descends from the tank, flows through the Upper Funnel, and enters the Main Body (Figure 3-2a), with a little help from the rotating agitator if needed. Once the powder passes into the Main Body, the next part that it interacts with is the Sleeve, so named because it wraps around the powder to form the outer shell of the filling and compression chamber. The Sleeve has a hole in its top to allow the flow of powder into this chamber. During powder sequestration, the Sleeve is pushed to the left by its two parallel actuators, sealing the powder in a smooth chamber suitable for pellet manufacturing (Figure 3-2b).

To the left and right of the Sleeve are the left and right pneumatically-actuated compression pistons, which provide the compressive force necessary for forming a pellet. These pistons have end caps made of polyaryletheretherketone (PEEK), an FDA-approved plastic that resists adhesion of the powder formed during the production process. The caps screw into the end of the piston and so can be easily replaced should they break or should a different pellet shape be desired. The left piston is driven to the right by its pneumatic actuator during the compression step, thus compressing the loose powder into a pellet against the face of the stationary right piston (Figure 3-2c).

Surrounding and to the right of the right piston is the Right Casing, a structure that both provides a mount for the right piston and contains the seal for the right piston. It is detachable from the Main Body for ease of maintenance and cleaning purposes. The final part of the assembly is the Lower Funnel, which is attached to the Main Body of the alpha prototype and provides an outlet pathway for formed pellets released during the ejection step. In this process, the right piston is retracted, allowing the left piston to continue its rightward motion and push the newly-minted pellet out of the compression chamber. From here, it then falls through the Lower Funnel to be collected below (Figure 3-2d). If the device is not set up to form a seal between the ICT and the outlet on its own, an airlock can be attached to the end of this funnel, thus ensuring that tank pressure will be held for the duration of a trial.

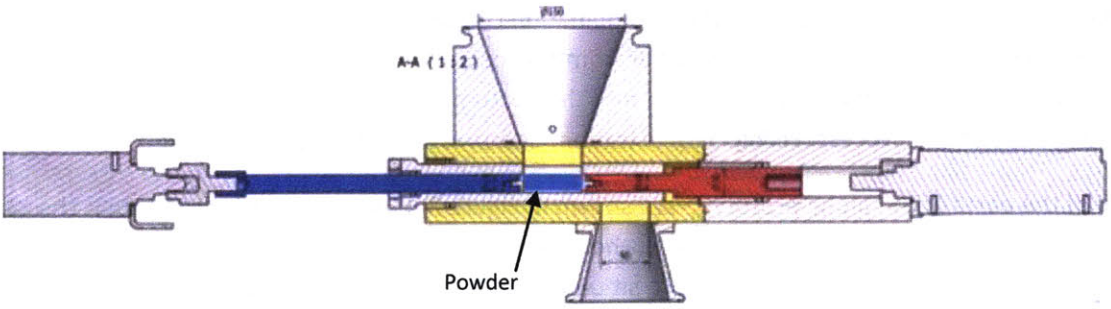

a: Powder Filling

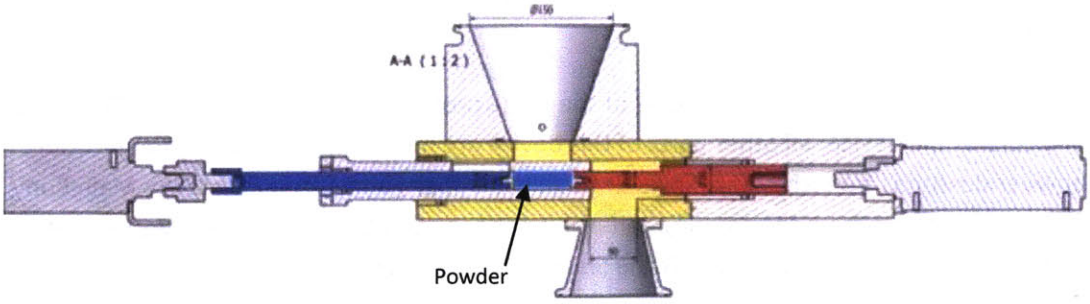

b: Powder Sequestration – Compression Chamber Closed

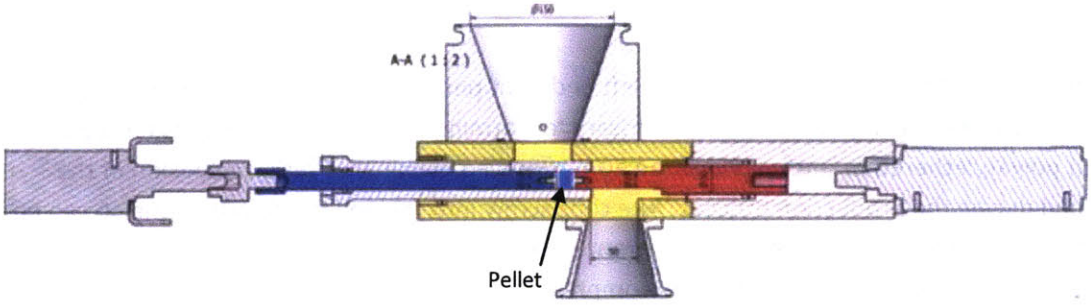

c: Powder Compression

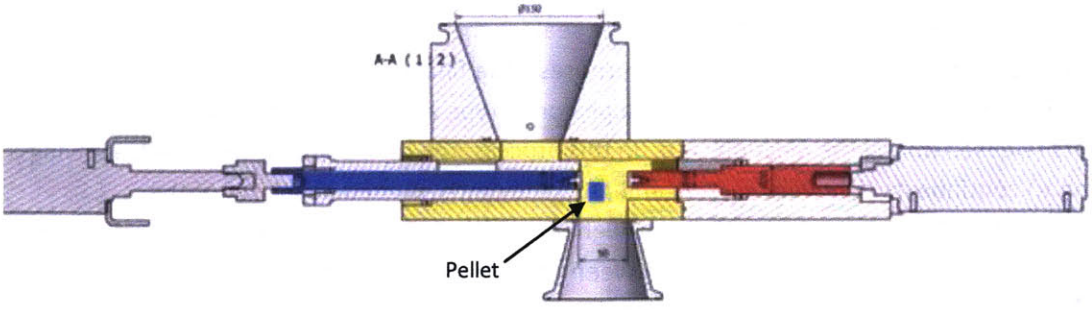

d: Pellet Ejection

Figure 3-2a. - d.: Alpha Prototype - Operation
Adapted from a drawing provided by ERI-EST (Guichard).

The dynamic seals of this device are formed with either white ethylene propylene diene monomer rubber (EPDM) or red polyurethane o-rings (Guichard). These seals encircle both the left and right pistons as well as the Sleeve, preventing leakage around the periphery of these parts while allowing their reciprocating motion during pellet production. The seals are meant to form a seal strong enough to withstand an internal pressure no less than the 10 bar required for powder production while also withstanding the 233 K (-40°C) operating temperature of the prototype. It was hoped that one of the two materials given above will prove able to meet these criteria.

Cooling for the device will be provided by a cooling system attached on the flat underside of the Main Body next to the Lower Funnel, as shown in Figure 3-1. A portable refrigeration unit pumping either propylene glycol, appropriate for temperatures to 253 K (-20°C), or 2-propanol, appropriate for temperatures to 193 K (-80°C), through a heat exchanger bolted on to the Main Body should be sufficient for trial runs with this prototype (Haouet). Due to its large heat capacity, the device was precooled before trials in a 243 K (-30°C) cold room, the coldest freezer large enough to hold the assembled prototype in PTC Beauvais. Initial trials did not make use of the refrigeration loop in order to speed the trial process, as there would have been significant lead-time regarding the procurement and set-up of such a refrigeration system.

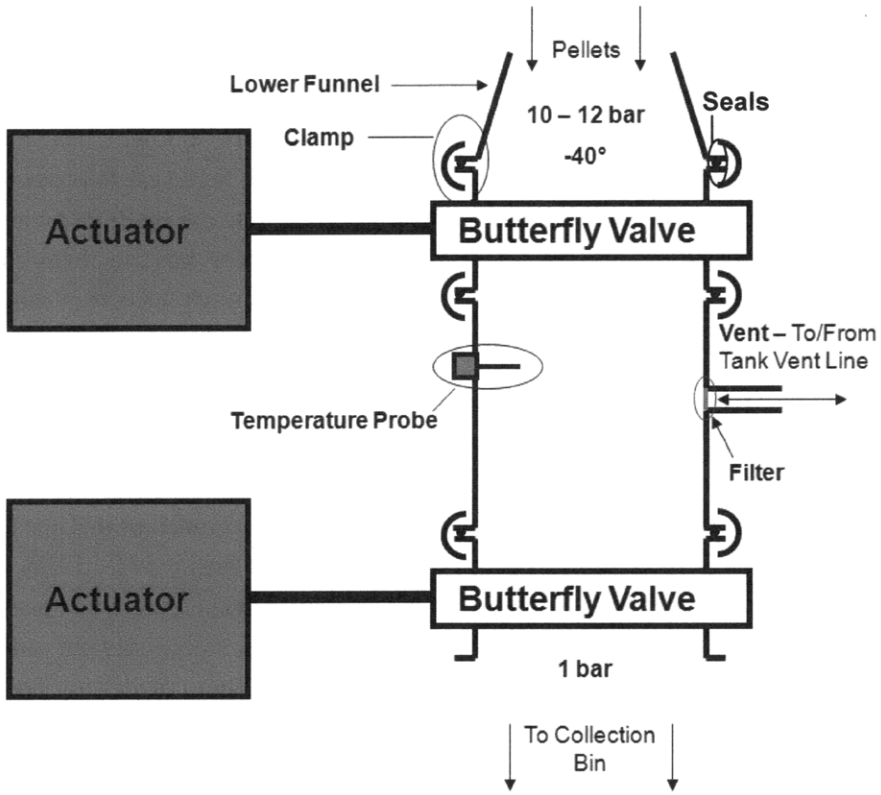

Figure 3-3: Airlock Schematic

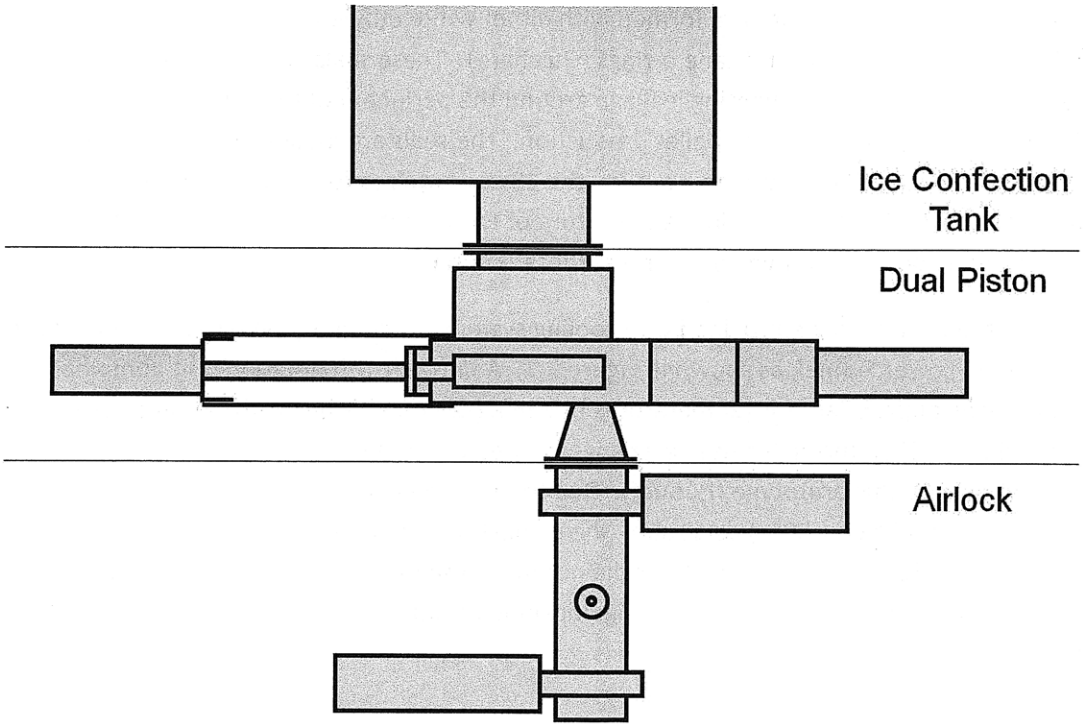

Figure 3-4: Mounting Schematic of the Alpha Prototype and Airlock
Cart supporting the weight of the alpha prototype and airlock not shown.

It is envisioned that the final version of a dual piston apparatus will be able to use seals attached to its pistons to prevent the flow of gas from the ICT to the outside environment. However, in the interest of simplicity, this alpha prototype does not incorporate such features. In order to form a seal and prevent excessive gas leakage from its outlet, the alpha prototype made use of an airlock clamped on to its Lower Funnel. This airlock, itself a prototype extraction device, has the ability to extract pellets after they are made and remove them from the pressurized internal environment of the production equipment. A schematic of the airlock is shown above in Figure 3-3.

The airlock consists of two butterfly valves surrounding a cylindrical body. A temperature probe protruding through a port on the side of the airlock body allows the monitoring of that property of the gas in the airlock. A line connected to the tank's vent line allows the airlock to be pressurized directly from the tank without opening the top butterfly valve, while another branch of this line open to the atmosphere allows the airlock to be depressurized independently of the lower butterfly valve. The airlock is mounted to the Lower Funnel of the prototype, as depicted in Figure 3-4. Pellets are formed in the alpha prototype and drop down to the airlock below. The airlock then cycles pressure and releases them to a collection bin sitting below the device while disrupting neither powder nor pellet production above.

3.2. Trials and Discussion

When assembled with the EPDM seals, the alpha prototype held pressure remarkably well, showing no leakage from any of its seals up to a pressure of 11 bar, the maximum tested. However,

initial trials with powder were performed in a cold room held at 243 K (-30°C). Since the machine was not attached to the ice cream tank, the powder's reaction to the various steps of the procedure was observed throughout the process to pinpoint any potential problems. Powder was extracted from the ice cream tank and loaded into the inlet of the dual piston mechanism. Then, the device was actuated properly in order to create a pellet.

Tests with powder showed that the dual piston device can form pellets. However, during the actuation of the device, the seals of the right piston, made of white EPDM, were pushed out of their seats and into the compression and ejection areas of the machine. The seals then blocked both the powder and pellet from moving through these areas, thus preventing further testing of the device during that trial. Several of the seals disintegrated into pieces during the trial, pieces of which were later found in the formed pellet. Seal failure was a common occurrence with this device; seals rarely lasted more than ten cycles before failing, even when not under pressure. Figure 3-5 and Figure 3-6 below show the results of two trials occurring on separate days showing the failure of the seals around the left piston. The seals around the Sleeve and the right piston also failed in a similar manner.

It was then discovered that these EPDM seals are known to be problematic at temperatures higher than 253 K (-20°C), leading to the trials being held in a temperature-controlled 243 K (-30°C) cold room (Guichard). Temperature readings of the device taken just before this trial commenced showed that the parts of the prototype were at temperatures between 256 K and 258 K (-17°C and -15°C), as was the front portion of the cold room itself. Unfortunately, the device could not be moved to the rear of the cold room, where temperatures were held at 243 K (-30°C), because it could not fit between the rows of storage shelves in that area. Previous tests in this temperature range, in which the machine was actuated without any powder, exposed no problems with the seals, so it was believed that they would function correctly and reliably. However, this was not the case during the actual trial itself. It is unknown as to whether the seal failure was due to a small rise in the temperature of the cold room, seal wear due to the several previous actuators, or due to the presence of powder in the system.

These tests were repeated with the red polyurethane seals. The pistons moved freely and easily upon actuation with no signs of seal failure at room temperature and at 256 K (-17°C). However, when connected to the Ice Confection Tank, the equipment was only able to attain a maximum pressure of 2.9 bar before leakage from the alpha prototype prevented the further build of pressure. This is far below the minimum of 10 bar required to successfully create carbon dioxide clathrate hydrate saturated powder, thus preventing the use of the polyurethane sealed prototype with the production equipment during powder production.

Another problem that appeared during testing was the right piston's propensity to jam in its bore in the Right Casing. Both the piston and the bore showed signs of galling on their surfaces upon closer examination, leading to the conclusion that the tolerances between the piston and bore were too tight for the materials used. Machining the piston or the bore of the Right Casing was a complicated task, as the stainless steel used was heat treated and thus difficult to machine while the two surfaces needed to be very smooth in order to keep the friction between them to a minimum. Pistons made

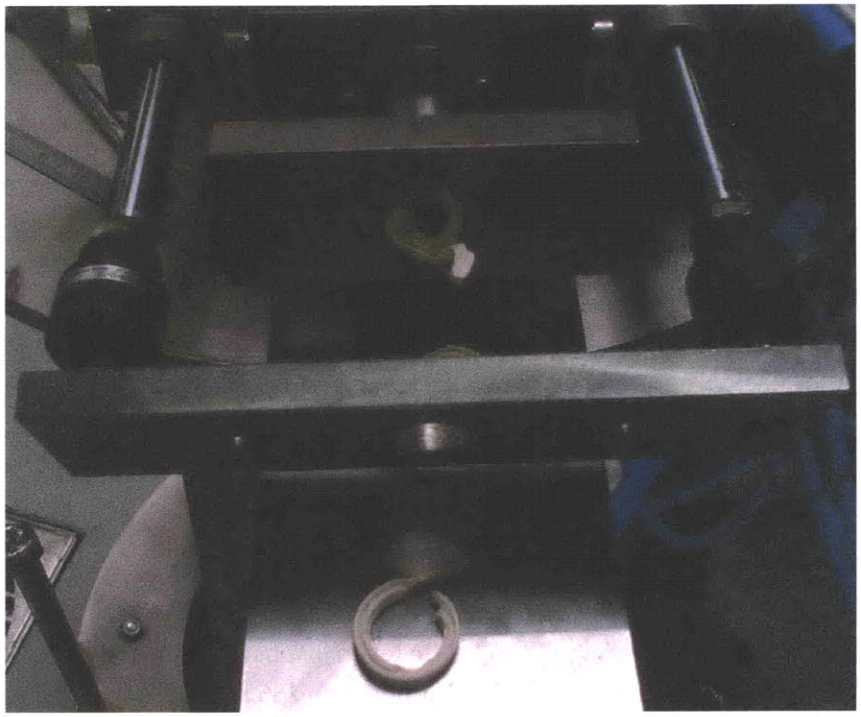

Figure 3-5: Seal Failure during a Trial on August 7th, 2008

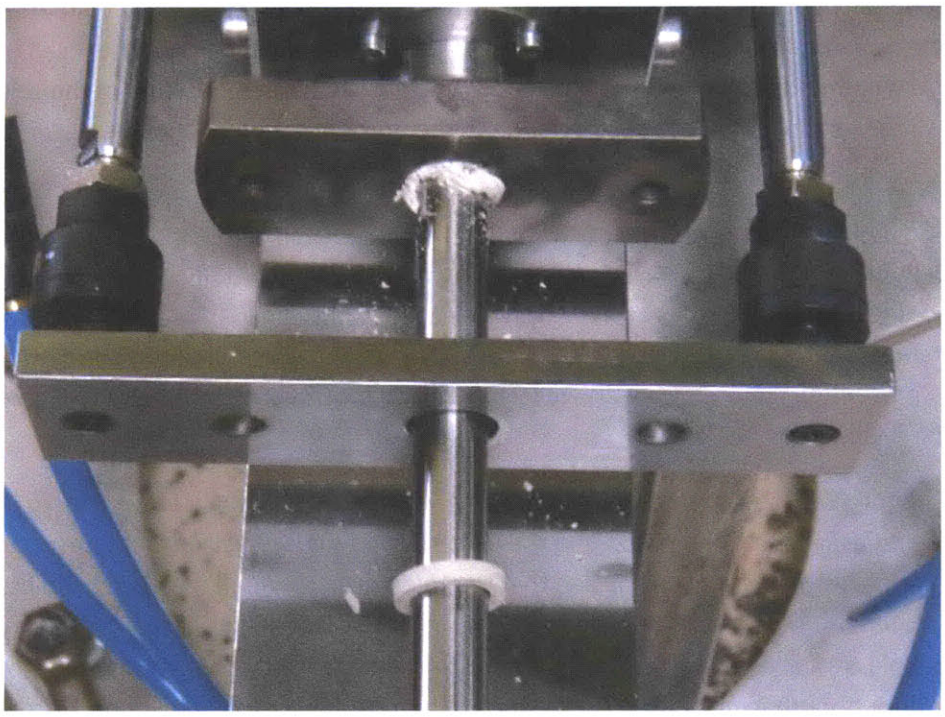

Figure 3-6: Seal Failure during a Trial on August 11, 2008

entirely of PEEK were also tried, but they were brittle, prone to cracking, and had a rougher surface finish than the stainless steel did, further accelerating dynamic seal wear. This galling problem was never successfully solved in the alpha prototype. (Thomas, Haouet)

Due to the limited production runs during trials caused by seal failure, it was not possible to analyze powder flow characteristics. However, due to past experiences with the product, it appears likely that the combined thicknesses of the Main Body and Sleeve taken along with the narrow width of the filling chamber will likely lead to bridging. The Agitator cannot reach past the bottom of the top of the Sleeve without interfering with the sliding motion of that part and thus cannot clear any bridging that happens directly above the filling chamber. This leaves the hole in the Sleeve as a prime area for a powder bridge to form if this interference is to be avoided at all times, which is desired by the Health and Safety group at Nestlé due to safety concerns.

Previous powder compression experience with manually operated piston and cylinder apparatus has also showed that the powder has a strong tendency to stick to the walls of its compression chamber as well as the face of the piston after being compressed. Once stuck, it can take several times the force of compression to dislodge the pellet. In order to avoid this jamming, a special nonstick coating was applied to the compression chamber walls and the piston face of the previous compression device. No coatings were applied to the chamber walls of the alpha prototype in order to save time, but the piston face was made of PEEK to avoid this phenomenon. Jamming or sticking did not appear to be an issue, as the pellet created was easily ejected with no apparent straining of the machine. The surface of the pellet was also physically undamaged, further evidence that it did not stick to a surface and then break loose. Thus, the use of an uncoated bore and plastic piston appears to be a successful combination for the creation of undamaged pellets.

The cooling system used on this device proved inadequate to cool it down to less than 253 K (-20°C) during trails held by Haouet and Thomas. As shown in Figure 3-1, the heat exchanger for this system is attached to the flat bottom of the prototype below the Upper Funnel. It was thought that this location would best allow the refrigeration of the critical powder flow path through the apparatus. However, this flat spot was too far away from the Upper Funnel for conduction through the stainless steel of the alpha prototype to allow for adequate heat flow from this part. It was found to be impossible to keep the Upper Funnel cooled during tests of this cooling system, and as a result powder flow from the ICT through the Upper Funnel could not be guaranteed. (Haouet, Thomas)

One of the device's biggest non-performance related drawbacks was its sheer mass. The alpha prototype has a mass of approximately 50 kg not including the roughly 10 kg airlock, making it difficult for a single person to handle on his or her own. This weight is also enough that Nestlé's safety regulations call for a specially designed supporting cart to be used to move the device around and hold its weight while it is attached to the bottom of the ICT. This cart is made of stainless steel to be appropriate for use in Nestlé's Pilot Plant. Its base, shown below in Figure 3-7 has four wheels to allow the cart to slide the prototype into and out of position and has three heavy screws to allow the cart and prototype to be lifted so that it could be connected to the ICT. The cart stayed in position throughout the trial.

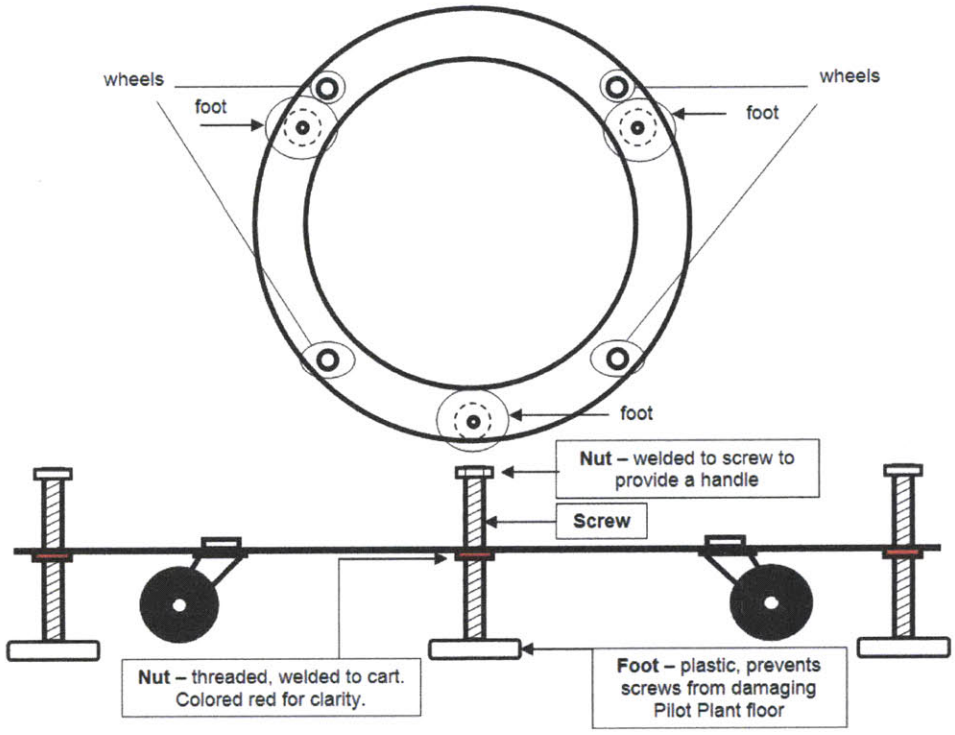

Figure 3-7: Base of the Supporting Cart for the Alpha Prototype

The implementation of the cart had several shortcomings that could not be easily solved. Its mass was approximately 25 kg, so the total mass being lifted is about 75 kg if it is assumed that the airlock is attached after the raising process. This is enough force to cause the screws to slowly wear down, making the raising and lowering process difficult over time. Attaining proper alignment with the flange on the bottom of the ICT is also troublesome, since the screws must all be manually set to the same heights to keep the device level and accurately sliding 75 kg of mass without the benefits of wheels is a non-trivial problem.

3.3. Summary

The Dual Piston was shown to be capable of statically handling tank pressures of up to 11 bar and tank temperatures down to 233 K (-40°C) when equipped with EPDM seals. It was also able to successfully create pellets during testing in a cold room, though a seal failure prevented detailed analysis of its production rate and its performance over multiple production cycles. The successful production of pellets suggests that the basic concept has merit. However, the prototype has several significant flaws that must be addressed before it is known if it is able to produce pellets in the numbers desired.

Reliable dynamic seals must be found before the device can be run attached to the ICT during powder production. So far, no material has been found that can withstand the constraints imposed by the motion, the temperature, and the pressure experienced by these seals. The implementation of these seals must be rethought in order to eliminate at least one of these constraints. An improved seal

design would ideally allow the usage of a material in the construction of the pistons that resists galling when sliding along stainless steel, a lasting issue with the alpha prototype.

Powder flow characteristics through the device were not examined. The truncated nature of the trials due to repeated seal failures meant that very little powder flowed through the prototype, leaving its ability to consistently fill the filling chamber and then be ejected as a pellet as an unknown variable. However, previous trials with this powder have shown the powder's strong inclination toward bridging when flowing through a constrained passage, especially if left undisturbed for any amount of time. Decreasing the length of the powder flow path and allowing the Agitator to agitate powder throughout this entire length are two measures that could be undertaken to help alleviate some of these concerns.

During trials of the device held by Haouet and Thomas, the cooling system used on this device could not adequately cool the powder flow path through the prototype. In order to maintain powder flow through the device, this flow path must be held between temperatures of 253 K (-20°C) and 233 K (-40°C). This is especially true for the Upper Funnel, where powder sits quiescent during compression strokes. Greater attention should be paid to the cooling requirements of the device, and the Upper Funnel will likely require its own dedicated cooling loop to ensure that its temperature is maintained within appropriate bounds. (Haouet, Thomas)

The prototype's mass of roughly 50 kg makes it difficult to handle and requires an almost equally weighty and unwieldy cart to satisfy Nestlé's safety inspectors. Though some of this bulk is necessary to create a machine that can safely handle the forces the machine will experience during a typical operation, significant weight can likely be removed through a focused redesign of several of the individual components, most notably the Upper Funnel, Main Body, and Right Casing. If the mass of the prototype could be lowered to the point where the device can be easily handled by one or two technicians, the process of running a trial with this device would be significantly simplified as the machine could be cleaned, assembled, and mounted with much less. The elimination of the cart, required to protect the technicians from possible heavy lifting or repetitive stress injuries due the handling of this device during the mounting and dismounting process, would also greatly decrease the amount of time and effort required to operate prototype. A lighter design would allow trials to be run in quicker succession, increasing the amount of data on the prototype that can be gathered in a given amount of time.

Chapter 4: Beta Prototype

The new design, developed and built at MIT during the fall of 2008, retained the Dual Piston name and many of its basic characteristics. However, this beta prototype was a much-improved design, drawing heavily on the lessons learned from the alpha prototype built by ERI-EST in France during the spring and summer of 2008. Technical drawings of the custom components of this device are provided at the end of this paper in Appendix A.

It was originally desired to have this device operational by the beginning of December 2008 to produce pellets for consumer testing to be held during the middle of that month. This need left approximately two months for design, manufacture, and initial testing of the beta prototype. Thus, many design choices were made to ease and speed the procurement and manufacturing processes, rather than focusing on optimal performance. These choices will be expanded upon in the descriptions of the individual parts.

The beta Prototype was built in the United States for installation in a facility in Europe. In order to save time, the prototype was built using imperial-sized dimensions, fasteners, and o-rings. Care was taken to limit the number of sizes of fasteners used wherever possible to make maintenance easier for the European technicians, who may have some difficulty finding an easy supply of appropriately sized parts. O-ring grooves on all custom parts built specifically for the beta Prototype were designed to be equal in volume to that of the o-rings that were to be used. This ensures a good seal and good alignment between mating surfaces. Standard-sized o-rings were chosen to speed acquisition, and it was attempted to limit the number of individual o-ring sizes used to further ease procurement and support requirements. As before, these considerations were important not only to speed the development and building process, but also to make servicing and part procurement easier while the device is in metric-dominated Europe.

4.1.Description

All food contact parts of the Dual Piston compression device are made of 304 Stainless Steel unless otherwise noted. Cooling components are constructed of copper due to its advantageous thermal properties, ready availability, and formability. The material, surface finish, solder type, and welding methods used in constructing this machine were all chosen due to their compliance with FDA guidelines pertaining to the hygienic design of food processing equipment (FDA, 2005). The device, as a prototype in the early stages of development, was not built with clean-in-place (CIP) operations in mind. Later iterations of the machine will implement these sanitation methods, should it be put to use in an industrial setting.

Figure 4-1 and Figure 4-2 show frontal views of the beta prototype. The parts off to the left and right sides of the Main Body as displayed in these figures, including the Pistons, Actuators, Actuator Flanges, Thermal Isolation Tubes, and CO_2 Flush Flanges, are collectively referred to as side components. In order to ease notation and reduce confusion throughout this section, the labels "small" and "large"

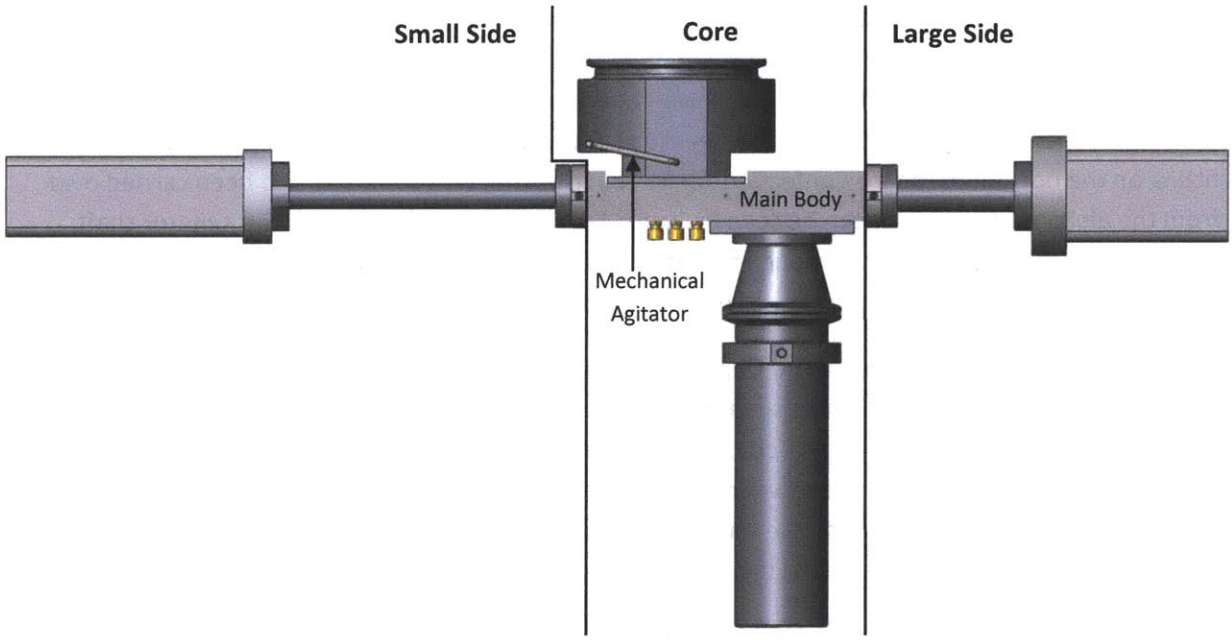

Figure 4-1: Beta Prototype - Dual Piston, Front View

have been adopted to refer to the parts shown on the left and right sides, respectively, of the Main Body in Figure 4-1 and Figure 4-2. These labels refer to the relative size of the diameters of these components. In those figures, for example, the small Piston, small Actuator, small Actuator Flange, small Thermal Isolation Tube, and small and CO_2 Flush Flange are all displayed directly to the left of the Main Body. The Upper Funnel, Upper Funnel Anchor Plate, Agitators, Main Body, Lower Funnel Anchor Plate, Lower Funnel, and Collection Container are collectively referred to as the core components of the beta Prototype. These notations have been adopted by the remainder of this document and are illustrated in Figure 4-1.

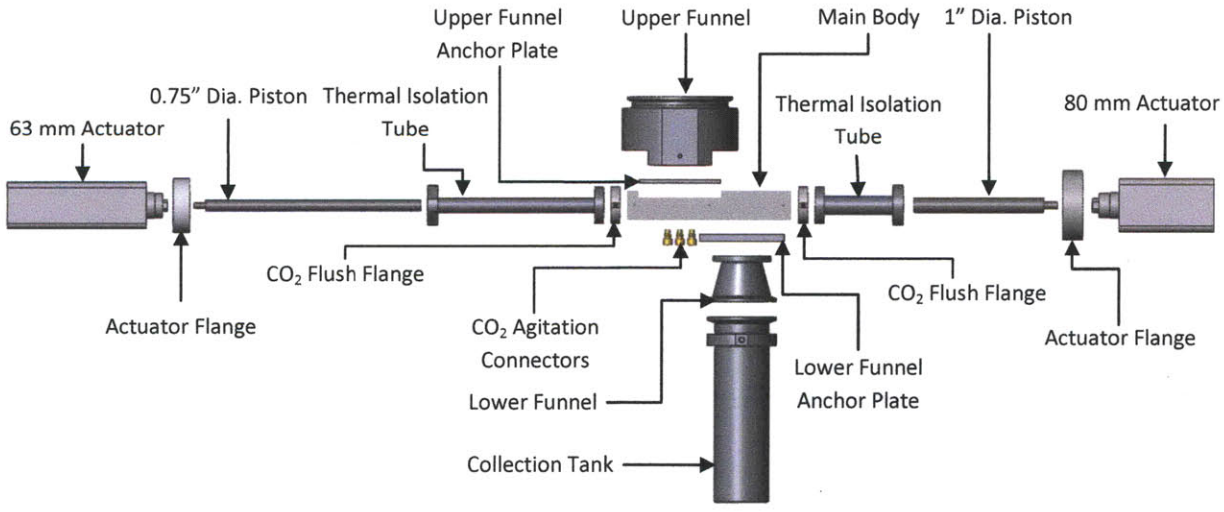

Figure 4-2: Beta Prototype – Dual Piston, Exploded Front View

Figure 4-2 shows an exploded view of the solid model of the beta prototype. All parts of the device are shown and labeled, with the exception of the mechanical agitator. At the top of the device is the Upper Funnel, slightly modified from its use in the alpha prototype to fit the new geometry of the beta prototype. As before, the Upper Funnel allows the prototype to be mounted to the 150 mm clamp fitting on the bottom of the Ice Confection Tank. The mechanical agitator has also been carried over from the alpha prototype and can be seen in Figure 4-1. A paddle is attached to the agitator shaft, which passes through a port cut through the Upper Funnel. The agitator will be rotated to prevent powder bridging or jamming in the lower reaches of the Upper Funnel.

Below the Upper Funnel is the Upper Funnel Anchor Plate, an adapter flange that allows the Upper Funnel, with its four-bolt-hole square bolt pattern with 80 mm (3.15") bolt hole separation, to be attached to the 50.8 (2") wide Main Body. As with the alpha prototype, the Main Body is the core of this machine. It is in this part that the powder collects, is compressed, and then is ejected into the Collection Tank below. The Main Body is also the foundation of the prototype, supporting the Collection Container, Actuators, and the various flanges that allow the mounting of these parts.

To the left and right sides of the Main Body are the CO_2 Flush Flanges, Thermal Isolation Tubes, Pistons, Actuator Flanges, and Actuators. The Actuators move the Pistons through the compression cycle to produce a pellet, while the CO_2 Flush Flanges allow a flow of carbon dioxide to clear the gap between the Pistons and the inner wall of the Main Body of any accumulated powder. The Actuator Flanges allow the attachment of the Actuator to the Thermal Isolation Tubes that suspend these components away from the Main Body. These tubes allow the Actuator seals, as well as those between the Actuators, Actuator Flanges, and outer ends of the Thermal Isolation Tubes, to be held at room temperature while the parts of the device that interact with powder are chilled to 233 K to 253 K (-40°C to -20°C). This gives more flexibility in the design of the seals as they no longer have to cope with low temperatures or abrasive product.

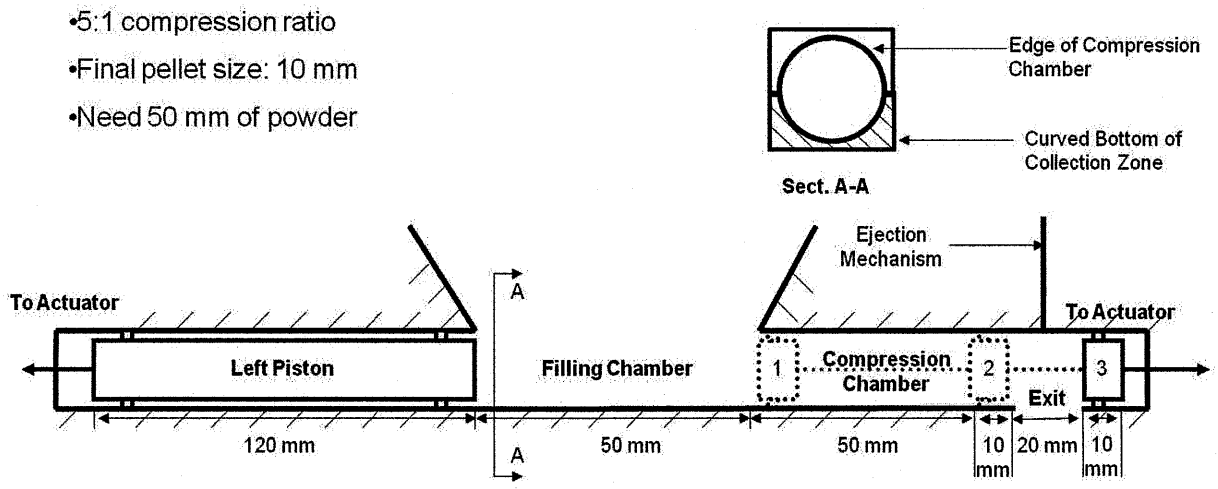

Reproduction of Figure 2-7: Schematic of Dual Piston Device

Attached to the Main Body is the Lower Funnel Anchor Plate. Like the Upper Funnel Anchor Plate, this piece is an intermediate flange that allows a funnel with a bolt circle exceeding the 50.8 mm (2") width of the Main Body to be used with this prototype. The Lower Funnel's six bolt holes are arranged in a 90 mm (3.54") diameter circle and are used to mount this part onto the anchor plate. The Lower Funnel adds a 100 mm diameter clamp fitting to the bottom of the Main Body, allowing for quick mounting and dismounting of the Collection Container. This container collects pellets as they are formed, allowing them to be easily extracted at the end of a trial. It is able to hold the roughly 500 pellets required for consumer testing, allowing the entire production run to be completed in a single trial.

The operational steps of the beta prototype are a modified version of the cycle shown in Figure 2-6. As it may be remembered, the shortcoming of that cycle was the requirement of the right piston to move to three different positions, as shown and labeled in the reproduction of Figure 2-7. The beta prototype avoids this requirement by eliminating position 1 of the right, large piston. Instead, as depicted in Figure 4-4, this piston only moves between a modified position 2 and position 3 during the process. Rather than entering the compression chamber, shown as position 2 in Figure 2-7, the large piston presses up against the wall of the compression chamber when fully extended.

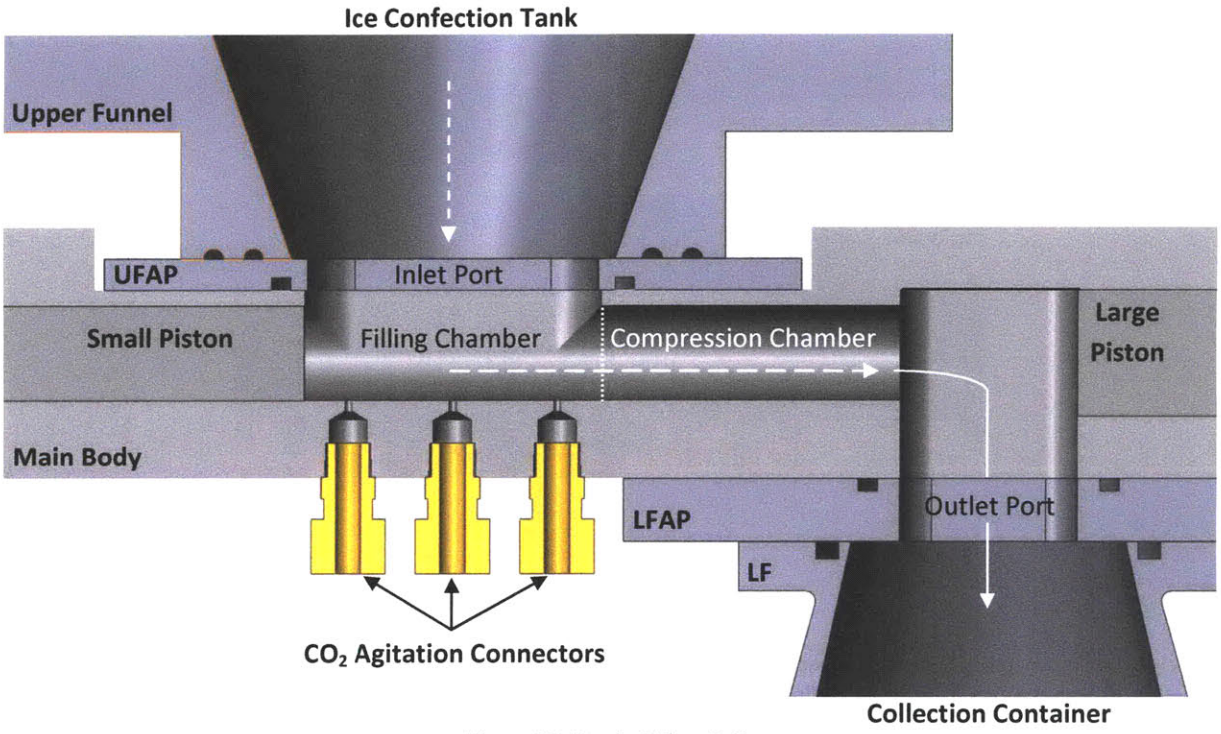

Figure 4-3: Product Flow Path

The dashed lines represent powder flow, while the solid line represents the formed pellet's path. The pistons are both in their retracted positions in this drawing to more clearly show the path of the product through this device. UFAP stands for Upper Funnel Anchor Plate, LFAP stands for Lower Funnel Anchor Plate, and LF Stands for Lower Funnel.

a.

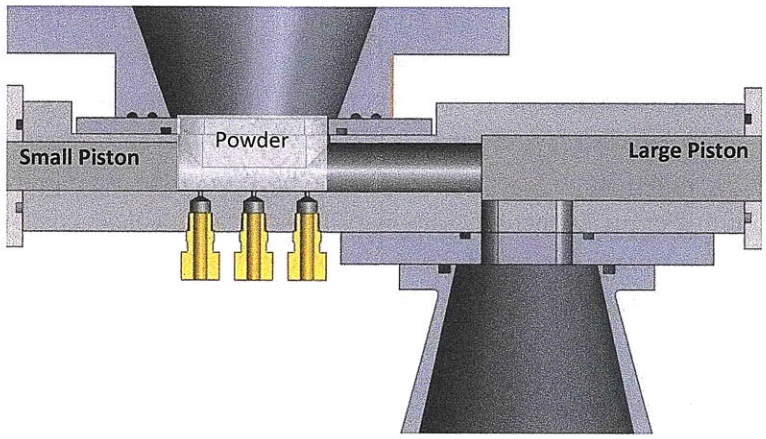

b.

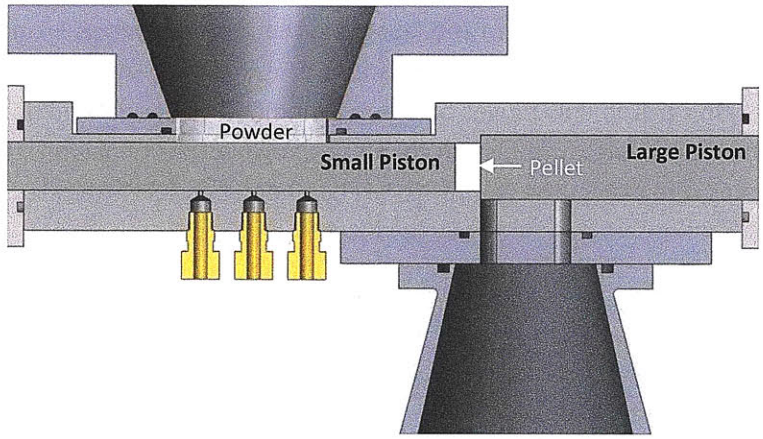

c.

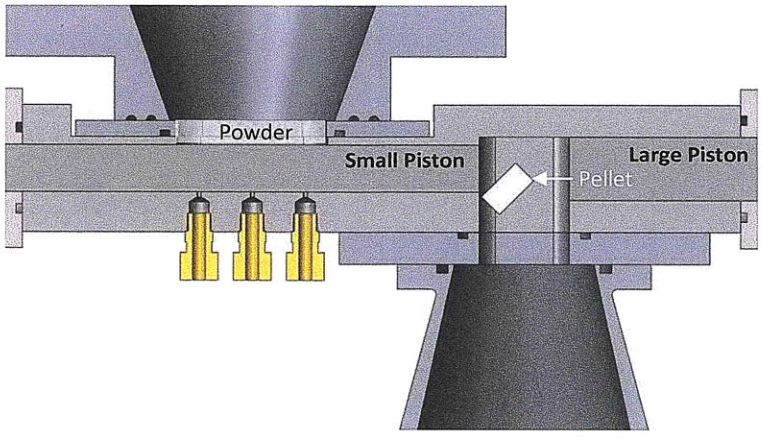

Figure 4-4a, b, and c: Beta Prototype - Operation
Filling, Compression, and Ejection, respectively.

The various parts of the beta prototype and the locations within its interior referenced below in the description of its operation are labeled in Figure 4-3. The prototype's operation can be split into three distinct steps, shown below in Figure 4-4a, b, and c. The first of these steps, shown in Figure 4-4a, is the filling step, in which the powder flows through the inlet port from the Ice Confection Tank above and settles in the filling chamber. During this step, the small piston is fully retracted, sitting clear of the filling chamber, while the large piston is fully extended, sealing off the compression chamber and

blocking the exit path to the Collection Container. Then, the small piston is extended, compressing the powder against the large piston and forming a pellet, as shown in Figure 4-4b. Finally, Figure 4-4c shows the large piston retracting and the small piston, which is still under actuating pressure, extending further. The newly created pellet is thus pushed out of the compression chamber and into the Collection Container.

4.1.1. Core Components

The core components of the beta prototype include the Main Body and every component attached to its upper or lower surfaces. These include the Upper and Lower Funnels, Agitators, Upper and Lower Funnel Anchor Plates, Main Body, and Collection Container. These are the parts that will be described in this section.

The Upper Funnel, along with the Lower Funnel, is one of two pieces reused from the alpha prototype. As such, it was designed and built by ERI-EST of Sainte-Marie-Aux-Chênes, France. The Upper Funnel is meant to provide a smooth transition between the 150 mm inner diameter of the port at the bottom of the ice confection tank and the oval inlet to the filling chamber of the Dual Piston machine. This part is made of STAVAX Supreme stainless steel, a modified version of AISI 420 stainless steel. Its top is machined to provide a matching 150 mm clamp fitting for the outlet port of the ICT, which, in conjunction with a silicone gasket and a clamp ring, will allow a gas-tight, pressure-holding seal to be formed between the two pieces of equipment. This clamp fitting will also be used to support the weight of the Dual Piston during a trial. Figure 4-5 and Figure 4-6 provide different views of this part to show more detail and are described below.

Figure 4-5 shows a midplane cross-sectional view of the Upper Funnel. The outline of the clamp fitting and its o-ring groove are clearly visible at the top of the part. Two concentric o-ring grooves on the bottom of the part provide space for o-ring seals between the Upper Funnel and the anchor plate that it sits on. In the beta prototype only the inner o-ring groove is used. An agitator port is drilled through the thick steel wall of the funnel to allow the insertion of a mechanical agitation device, such as

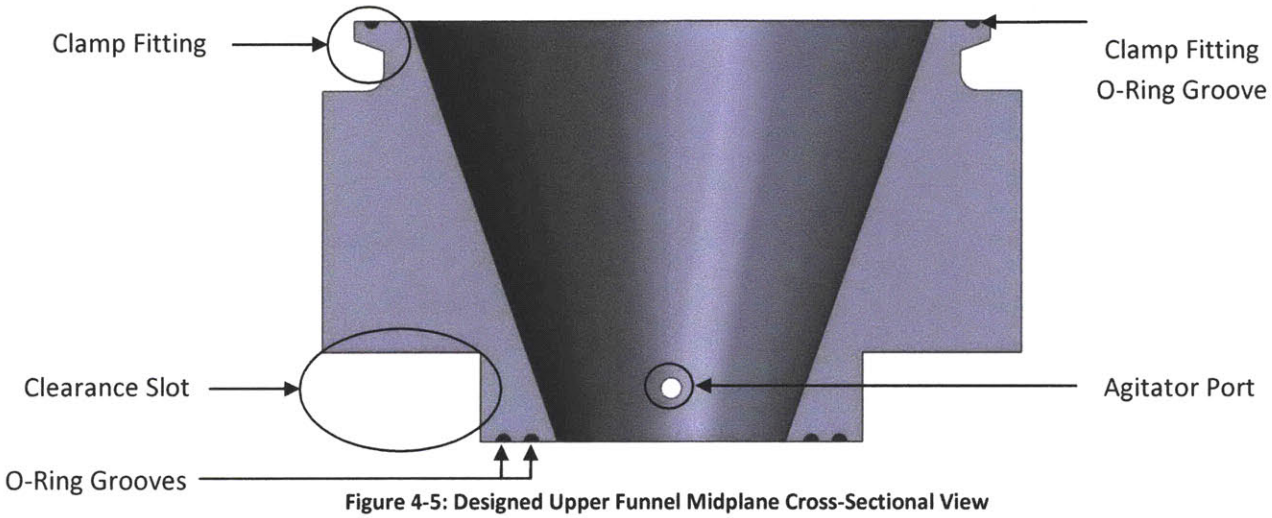

Figure 4-5: Designed Upper Funnel Midplane Cross-Sectional View

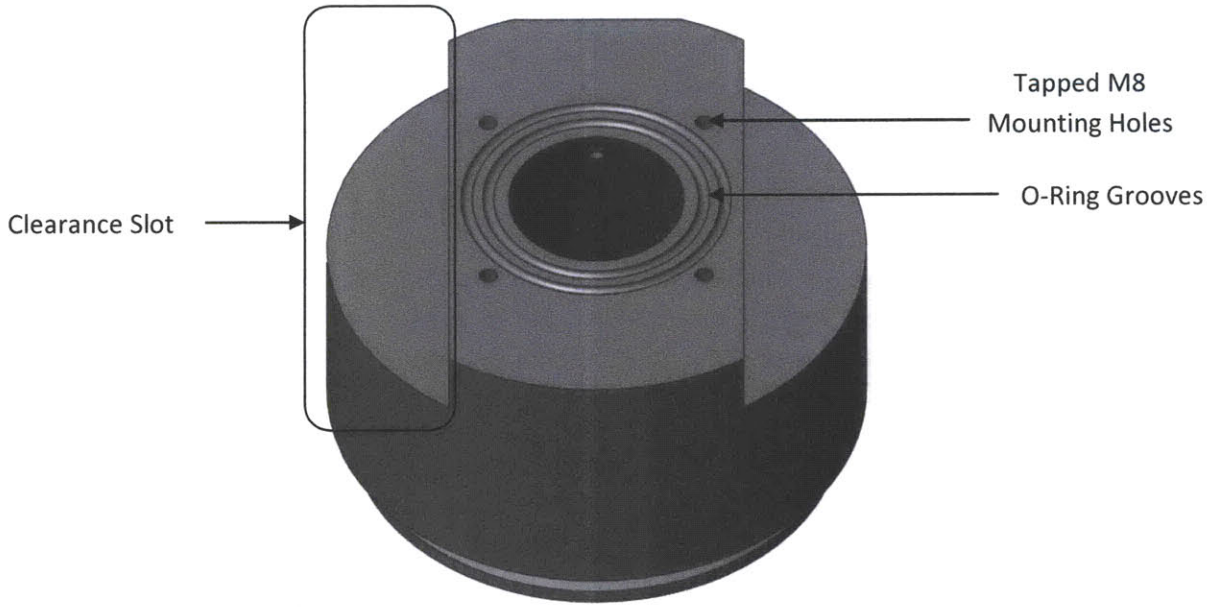

Figure 4-6: Designed Upper Funnel, Angled Bottom View

a rotating paddle. Two parallel grooves are cut into the bottom of the funnel to provide clearance over some of the features of the Main Body of the device that the Upper Funnel sits on. These features are described in more detail below during the discussion of the Main Body. Figure 4-6 shows a more detailed view of the bottom of the Upper Funnel, clearly showing the geometry of these clearance slots.

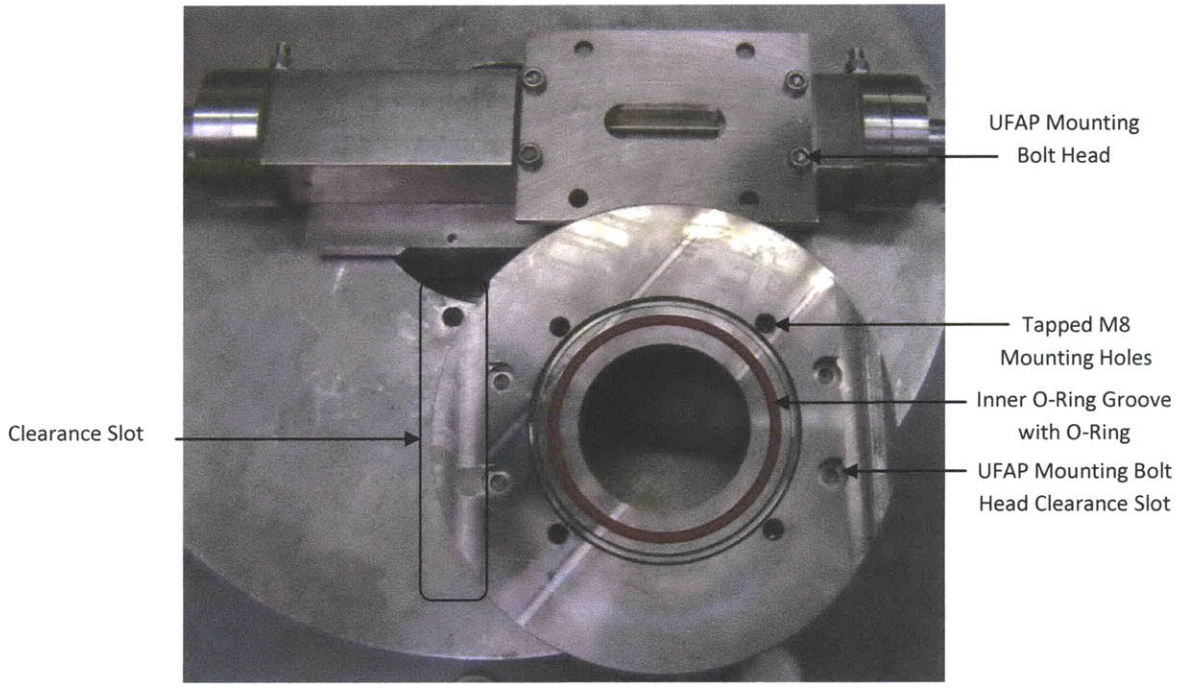

Figure 4-7: Constructed Upper Funnel During Assembly, Bottom View

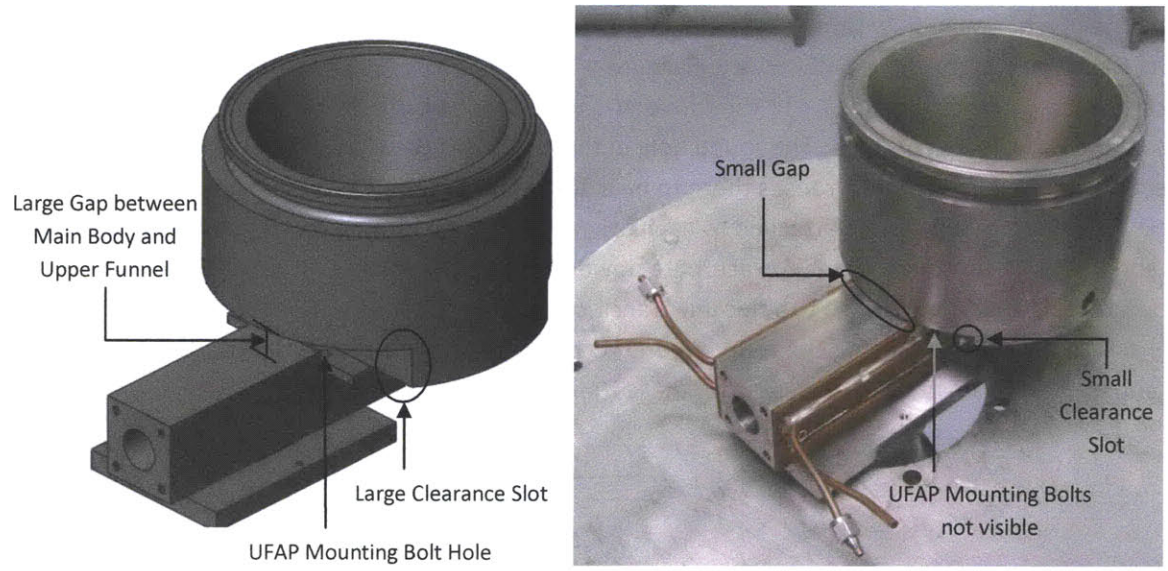

Figure 4-8: Comparison of Designed and Constructed Upper Funnels when Mounted.

Due to time constraints, it was decided that, rather than mill out the clearance slots to the degree shown in Figure 4-6, it would be less time-intensive to cut the clearance slots just broad and deep enough to allow the Upper Funnel to clear the flow-path-shortening slot cut into the Main Body (see Figure 4-21). Four separate slots were then milled into the lower surface of the Upper Funnel to provide clearance for the heads of the bolts that hold the Upper Funnel Anchor Plate (UFAP) to the Main Body, as shown in Figure 4-7. Figure 4-8 shows isometric views of both the modeled and actual Upper Funnels mounted to the UFAP and Main Body, helping to illustrate the difference in clearance slot geometry.

Figure 4-9: Upper Funnel and Upper Funnel Anchor Plate - Top View

The powder must flow through the Upper Funnel and the Upper Funnel Anchor Plate on its way into the Main Body of the device, illustrated in Figure 4-3 above. The circular opening of the bottom of the Upper Funnel does not match up to the rounded-end rectangular slot in the UFAP, as shown in Figure 4-9. The mismatch between the round hole in the bottom of the Upper Funnel and the rounded-end rectangular hole in the UFAP causes there to be a horizontal flat shelf at the bottom of the Upper Funnel when these two parts are attached to each other. During operation, powder will build up on this shelf, and this build-up could cause or exacerbate powder bridging problems. In order to mitigate these effects, internal funnels were used to smoothly transition from the circular cross section of the Upper Funnel and Ice Confection Tank to the rounded-end rectangular cross section of the passage through the UFAP and into the Main Body. The designs of these funnels are presented below.

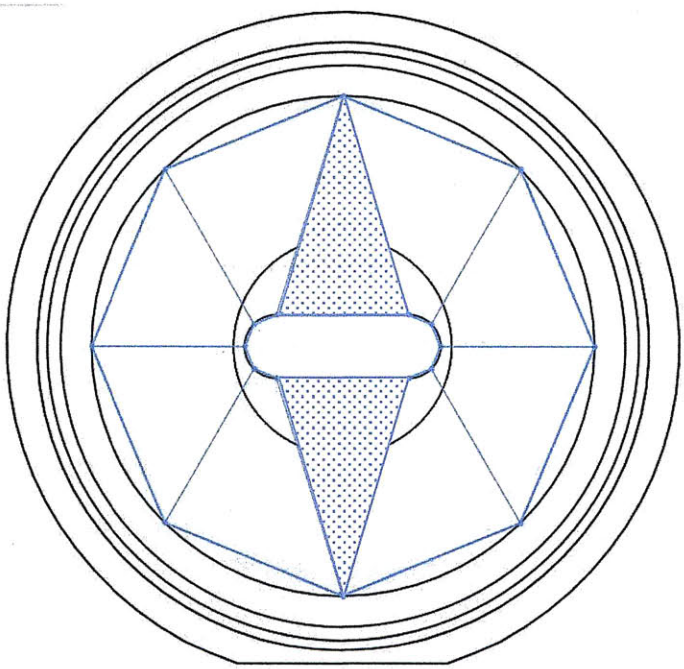

Figure 4-10: Sketch from Above of a Funnel Made of Folded Delrin Sheet
This funnel is made of two overlapping halves formed from two separate sheets of Delrin. The shaded areas represent the overlapping sections of these two halves.

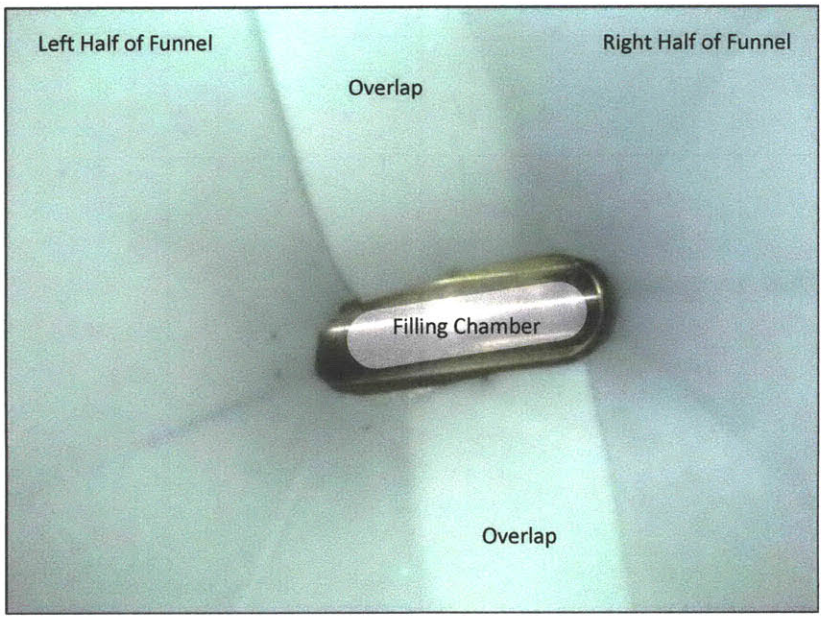

Figure 4-11: View from Above of an Internal Funnel Made of Folded Delrin Sheet and the Filling Chamber

The first design considered was a funnel formed of two identical, overlapping folded sheets of food-grade Delrin, which was chosen for its non-stick properties and food-grade certification. These folded sheets are joined together to form the final funnel. This design consists of an inscribed regular octagon in the 150 mm inner diameter circular cross section of the top of the Upper Funnel and an inscribed irregular decagon in the 19 mm (0.75") wide, 19 mm (0.75") inner diameter rounded-end rectangular cross section of the Upper Funnel Anchor Plate and the Main Body, as shown in light blue in Figure 4-10. Four sections of the decagon are inscribed into each of the half-circular rounded ends of the rectangular slot, which are then connected by two straight sections. These straight sections are where the two half-funnels overlap, allowing the funnel to be tied together with stainless steel wire, as epoxies and other adhesives have difficulty adhering to Delrin. DuPont, the makers of Delrin, recommend a laser welding process, which could be used on an end-stage device (DuPont). A dimensioned drawing of one of the halves of the funnel is shown below in Figure 4-12 (Smith). This funnel half is shown laying flat after it has been cut to shape but before it has been folded.

A second design extended the funnel up to the top of the 150 mm inner diameter outlet port of the ICT. The funnel is made of polystyrene, which allows the part to be made on three-dimensional printing machines available at PTC Beauvais. In order to conform to the size restraints of the printing machines, the funnel utilizes a three-piece design, in which three concentric parts are stacked vertically in one another as shown in Figure 4-13. Each of the pieces will overlap by approximately 23 mm to keep the three parts of the funnel firmly attached during the operation of the powder production equipment. The ability to manufacture the funnel in-house allows testing to take place approximately a week sooner than if it had been built by an outside supplier (Haouet).

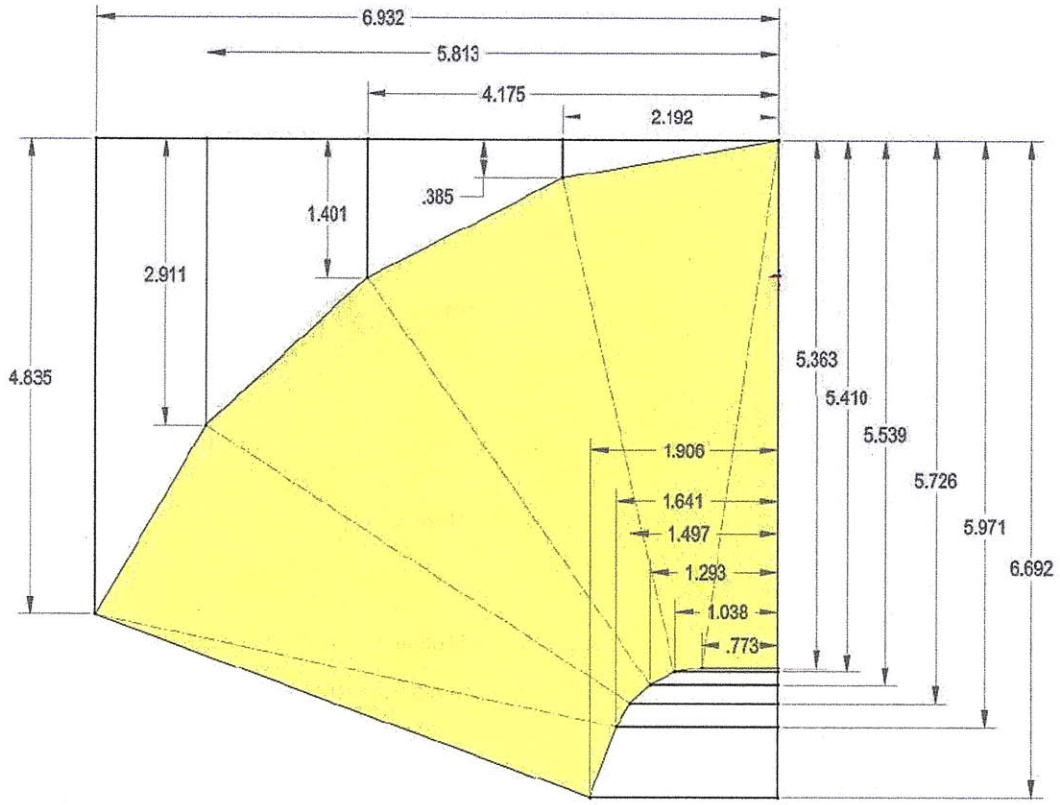

Figure 4-12: Drawing for a Planar Section of One-Half of the Folded Delrin Sheet Funnel
Provided by Joseph Smith, Jr (Smith).

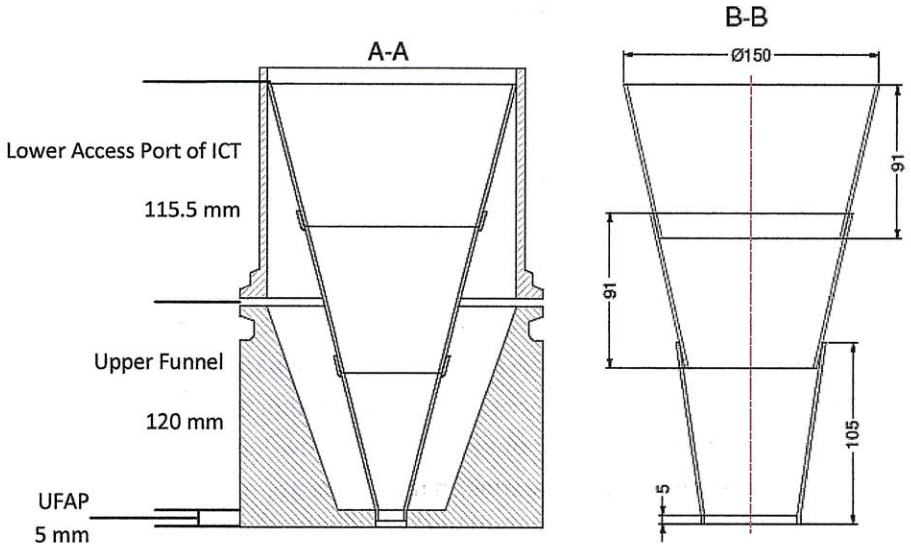

Figure 4-13: Nestlé Thermoformed Inner Funnel
From Saïkali et al, 2009.

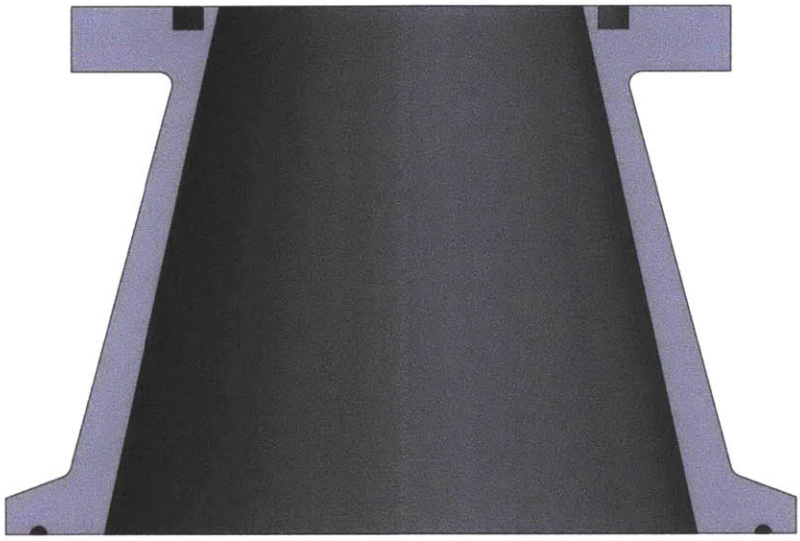

Figure 4-14: Cross Sectional View of the Lower Funnel

The Lower Funnel of the alpha prototype is used in the beta prototype without any alteration. The Lower Funnel's purpose is to add a 100 mm inner diameter clamp flange to the Main Body to allow for quick and easy mounting and dismounting of the Collection Container before and after trials. This clamp flange could be machined on or welded to the Main Body, but this adds significant complication to the manufacturing process and greatly increases the potential for delay should the machining or welding operations go awry. Thus, it was decided to incorporate the already-machined Lower Funnel into this design, as it met all performance and form requirements for such a piece.

The powder produced using the CO_2 flash freezing process has difficulty flowing through an enclosed flow path due to a tendency to bridge. In order to ensure uninterrupted flow of powder into the filling chamber during every stroke, a means of preventing bridging had to be developed. Several concepts were considered, including vibration, powder entrainment in gas flow through the device, mechanical agitation via a rotating mechanical paddle or screw, and agitation through gas injection.

Industrial vibrators are commonly used to promote powder flow and prevent binding, sintering, and/or bridging of such a product. With the ice confection powder produced by the CO_2 flash freezing process, experience has shown that shaking a container will assist powder motion. However, this shaking must be fairly vigorous, with an amplitude on the order of millimeters and a frequency of several hertz. The current flash freezing equipment is rigidly mounted to its supporting framework and cannot be easily modified to accept several millimeters of play. Therefore, this method has been relegated to backup status until other, more easily implemented techniques have been tried.

Under current operating conditions, in which excess CO_2 is injected into the ICT with the mix in order to maintain thermal control of the system, a steady stream of CO_2 gas is vented from the

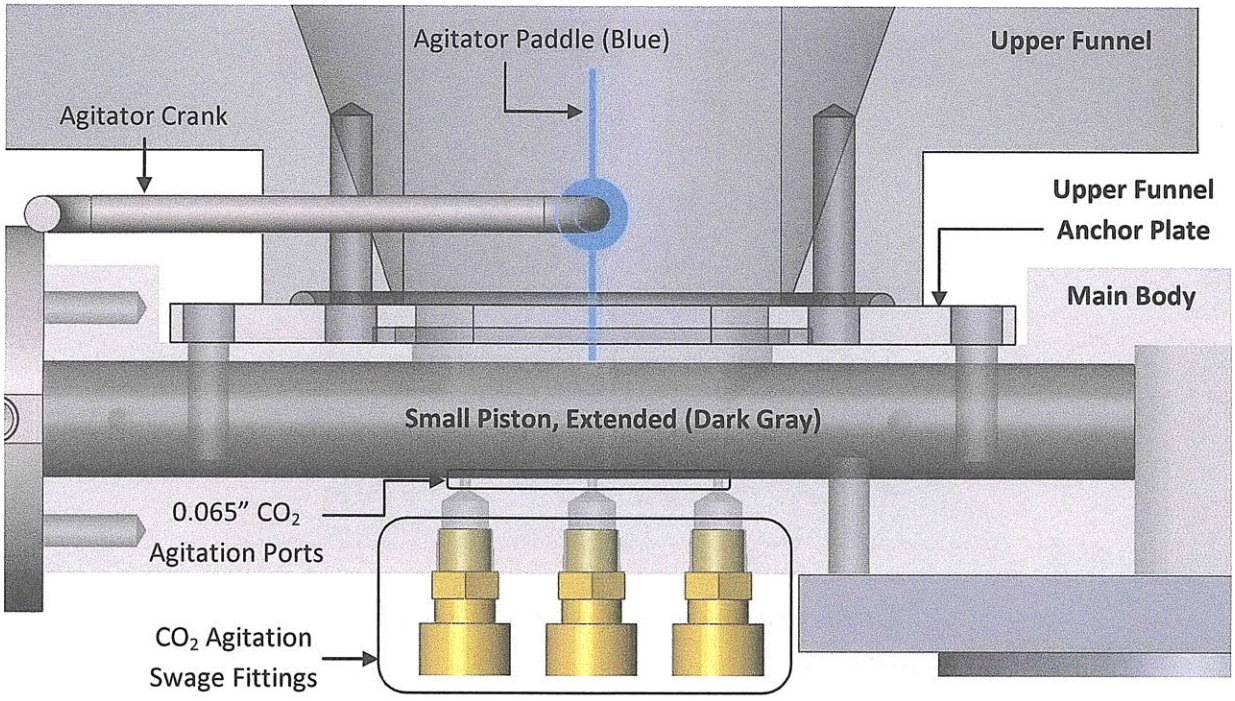

Figure 4-15: Mechanical and CO_2 Agitators, Front View

apparatus through a line in the top of the ICT. This venting gas could instead be released through a vent line off the Collection Container, forcing a steady flow of gas through the apparatus. Powder could become entrained in this gas flow, breaking up any bridging that occurs when the powder is sitting stationary during pellet compression (as in Figure 4-4b. and c.).

The potential velocities achieved using this technique can be estimated using current operating conditions of 10 bar and 233 K (-40°C). Under these conditions, gaseous CO_2 has a density of 26 kg/m^3 (ρ_{CO2}) (NIST). Assuming a CO_2/mix mass flow ratio of 3.5:1 and a mix flow rate of 0.001 kg/s, approximately 0.003 kg/s of CO_2 ($\dot{m}_{CO2}$) is vented from the tank during operation. The powder has been proven to bridge in the interior of the Upper Funnel, which contracts from a diameter of 150 mm to 65 mm along its height. Assuming the smaller diameter as the bridge diameter (d_{bridge}) and incompressible flow, gas velocity and momentum flux ($\dot{M}''_{CO2}$) at the site of a powder bridge can be given by the following equations:

$$v_{CO2} = \frac{\dot{m}_{CO2}}{\rho_{CO2} * \frac{\pi d_{bridge}}{4}} \qquad (3)$$

$$\dot{M}''_{CO2} = \rho_{CO2} v_{CO2}^2 \frac{\pi d_{bridge}}{4} \qquad (4)$$

As defined above, gas velocity through the potential bridging section will be 0.0003 m s^{-1} and its momentum flux will be 1.04 x 10^{-6} kg m s^{-2}. These values can be compared to those seen during trials of

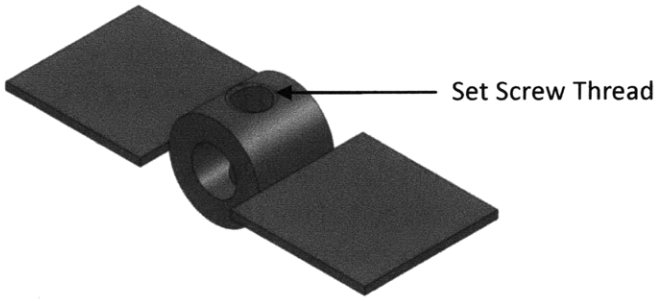

Figure 4-16: Initial Agitator Paddle

the CO_2 Agitation concept, in which pressurized CO_2 gas is injected upwards through ports below the Main Body's Inlet Port. In these trials, velocities were on the order of 100 m s^{-1}, and the momentum flux was on the order of 0.1 kg m s^{-2}, several orders of magnitude greater than the values expected from the vented gas. Thus, the mass flow of CO_2 is not expected to be sufficient to dislodge and break up bridged powder present in the Upper Funnel on its own, given current knowledge of powder flow and bridging characteristics. Therefore, vented CO_2 gas is not appropriate for use as a primary means of powder agitation.

A mechanical agitator was used in initial trials of the beta prototype. Transferred largely intact from the alpha prototype, the mechanical agitator consists of a paddle mounted on a six-millimeter stainless steel rod using two set screws. This rod protrudes through the agitator port drilled through the wall of the Upper Funnel. The paddle utilized in most of the trials is the simple, small paddle shown in both Figure 4-16 and Figure 4-17. This small paddle allows for 360° of rotation, though its span is limited to 48 mm as a result. In order to sweep more volume in the Upper Funnel and extend the reach of the paddle, other paddle forms have been tried and will be discussed later in this chapter.

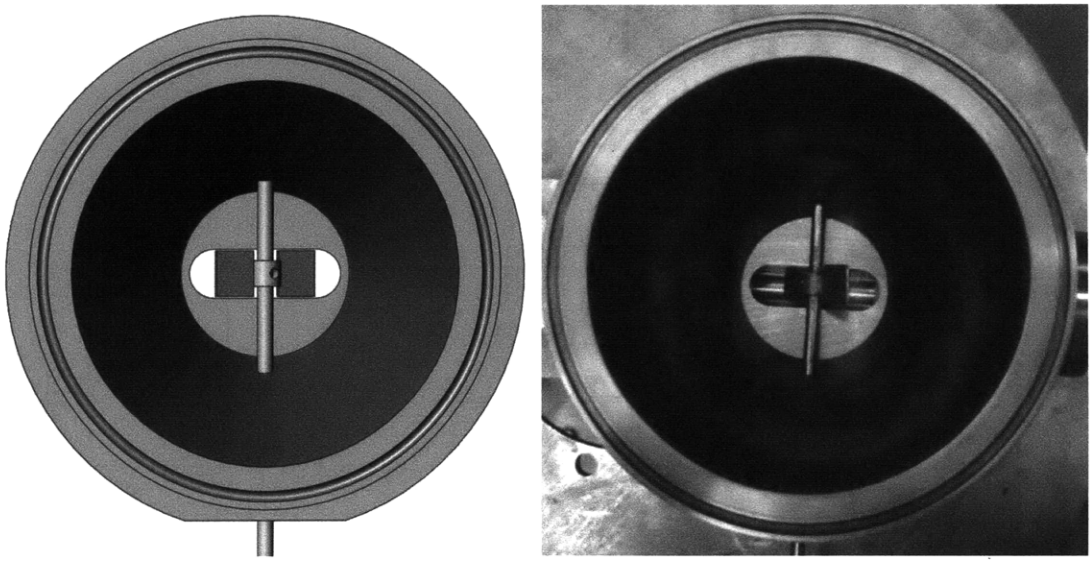

a. b.

Figure 4-17a. and b.: Two Top Views of the Installed Mechanical Agitator Shaft and Paddle

Another bridging prevention concept was that of gas injection. This agitation method involves the injection of high pressure CO_2 gas through three 1.7 mm (0.065") vertical holes drilled in the bottom of the filling chamber of the Main Body. As shown in Figure 4-18, one of these holes was centered underneath the middle of the rounded-end-rectangle-shaped inlet port, while the other two were placed beneath the circular ends of the slot, one under the center of the arc on either side. These jets are directed upwards through the inlet port of the Main Body, where they will interact with the powder building up in the Upper Funnel and presumably keep it moving. Swage fittings are used to connect the CO_2 supply lines to the holes in the Main Body. This concept was tested, as described below in the CO_2 Agitation Trials section of the Trials subheading below, but was never implemented due to time constraints.

When designing the beta prototype, an effort was made to keep the number of parts to a minimum with the goal of decreasing device complexity and eliminating possible leakage sources at the seals between each part. However, in order to produce this device within the allotted time, some compromises had to be made to this end. In order to avoid long lead times, the decision was made to use readily available 51 mm x 51 mm x 305 mm (2" x 2" x 12") 304 stainless steel stock for the Main Body to speed its manufacture while still allowing the use of the already-made Upper and Lower Funnels.

The Upper Funnel's bolt holes are arranged in a square pattern with each bolt hole 80 mm (3.15") from its two closest neighbors. However, the Main Body is only 50.8 mm (2") wide and so cannot support the Upper Funnel's bolt pattern on its own. Obtaining a piece of appropriate stainless steel wide enough to allow the Main Body to take this bolt pattern would take at least two to three weeks, and with only six weeks available for the design and manufacture of this device, this lead time was unacceptable. Thus, the Upper Funnel Anchor Plate (UFAP), shown in Figure 4-19, was designed to allow the wide Upper Funnel to be connected to the narrow Main Body.

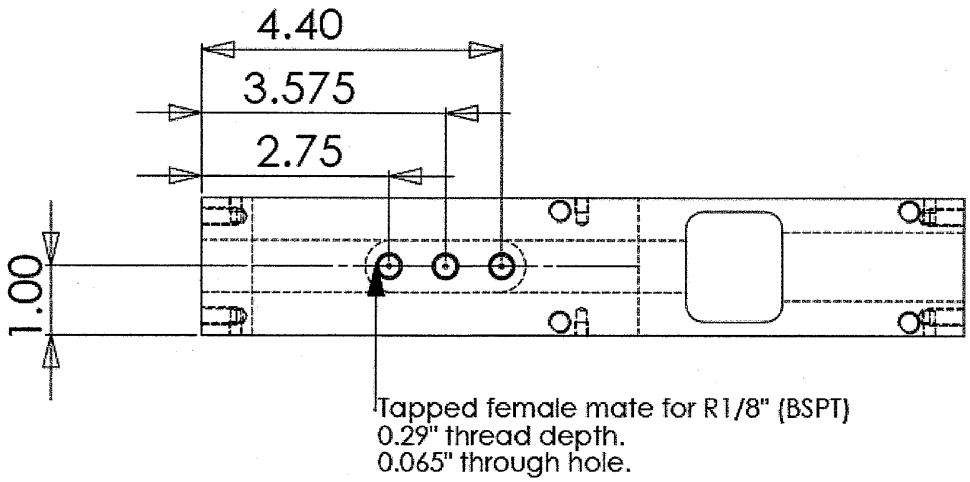

Figure 4-18: Location and Sizing of the CO_2 Agitation Ports on the Main Body
Note: Dimensions are in inches.

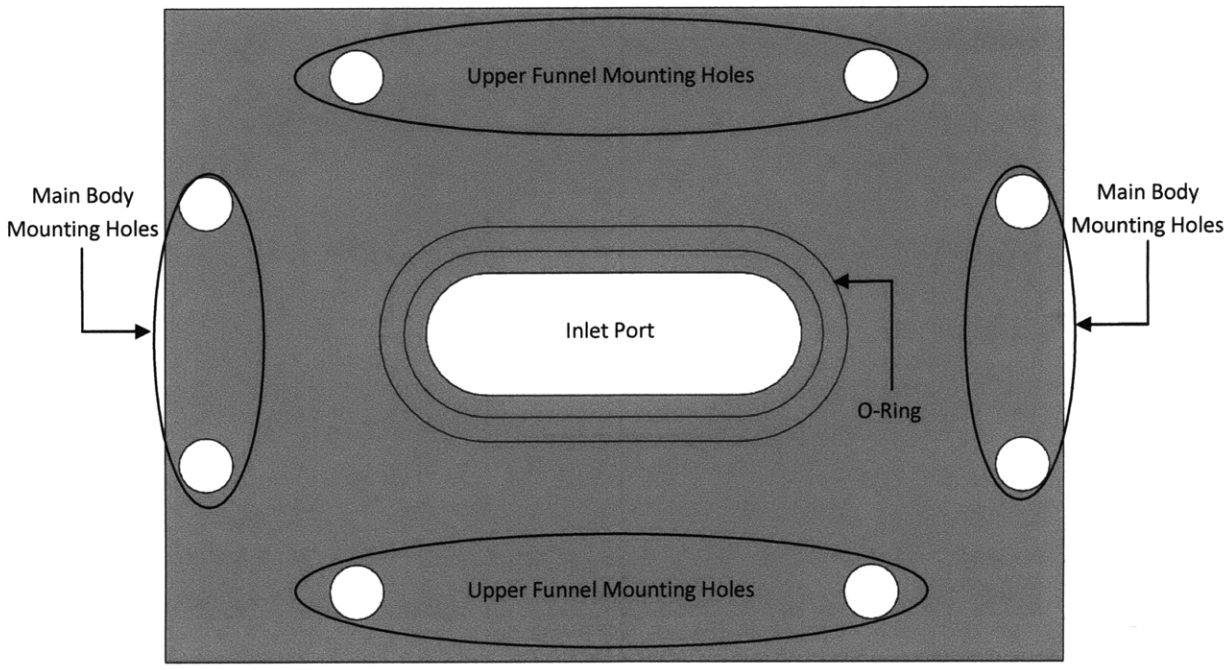

Figure 4-19: Upper Funnel Anchor Plate with O-Ring - Bottom View

The Upper Funnel Anchor Plate is an intermediate piece that is attached to both the Main Body and the Upper Funnel. Powder passes through the hole in its center on its way from the Upper Funnel to the filling chamber in the Main Body, so its thickness was kept as small as possible. However, it supports the entire weight of the device when the prototype is hanging from the tank, so it had to be thick enough to take this load without fracturing or fatiguing. A thickness of 6.4 mm (0.25") was chosen as a very conservative, readily available size that did not overly extend the powder flow path. The rest of the part simply provides a base for the mounting holes. These holes are clearance holes; the Upper Funnel and the Main Body contain the threaded holes for the mounting bolts. A simple square profile was the easiest and fastest to create and so was chosen for this part.

As with the Upper Funnel Anchor Plate, the Lower Funnel Anchor Plate (LFAP), shown in Figure 4-20, is an adapter plate between the Lower Funnel and its six bolt, 90 mm (3.54") diameter bolt circle with the 51 mm (2") wide Main Body of the beta prototype. Once pellets are made in the Main Body, they are ejected from the compression chamber and fall through the outlet port of the LFAP on their way to the Collection Container below. Bridging, sintering, and other flow-disrupting phenomena are not expected to be issues with pellets, so minimization of the thickness of the LFAP is not as critical to successful operation of the device as that of the UFAP. The holes of the Lower Funnel bolt circle drilled into the LFAP will be threaded to allow for the mounting of the Lower Funnel, so the LFAP has been designed as 13 mm (0.5") thick. This will allow for a maximum of 2.5 diameters of thread depth for the Lower Funnel's M5 mounting bolts, which should be sufficient to support the Lower Funnel and the Collection Container that hang below when the device is pressurized. As with the UFAP, a simple rectangular profile was chosen as the optimal geometry for this part as it is the easiest and quickest to fabricate.

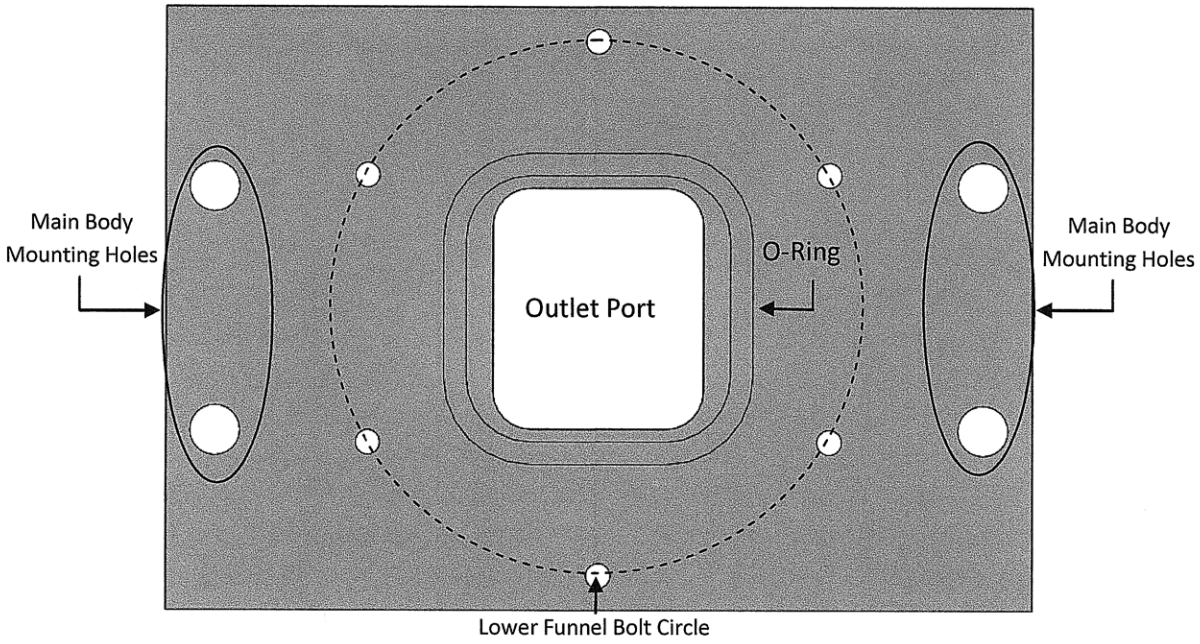

Figure 4-20: Lower Funnel Anchor Plate - Bottom View

Figure 4-21 and Figure 4-22 are of the Main Body, the heart of the beta prototype. The powder is collected and compressed within the walls of this piece, and it forms the structural foundation of this device where all other pieces connect and interact. As such, the Main Body was designed to be physically compatible with the other parts of the prototype. However, it was also designed to be produced as quickly and simply as possible, leading to a few compromises. As mentioned previously, obtaining a piece of appropriate stainless steel for the Main Body to allow it to support the 80 mm bolt separation of the Upper Funnel or the 90 mm bolt circle of the Lower Funnel would take a minimum of two to three weeks. This time represented an unacceptably large fraction of the six weeks allocated to the design and manufacture of the beta prototype. Thus, the anchor plates were added to the design, allowing the Main Body to be built from a 51 mm x 51 mm x 305 mm (2" x 2" x 12") rectangular bar stock that could be procured in only a single day. It was also decided to add removable, screw-mounted coolant plates rather than drill or weld coolant passages in the part itself, thus avoiding possible machining and welding errors.

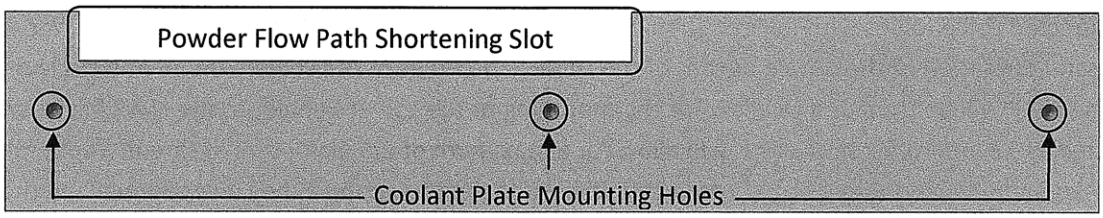

Figure 4-21: Main Body - Profile View

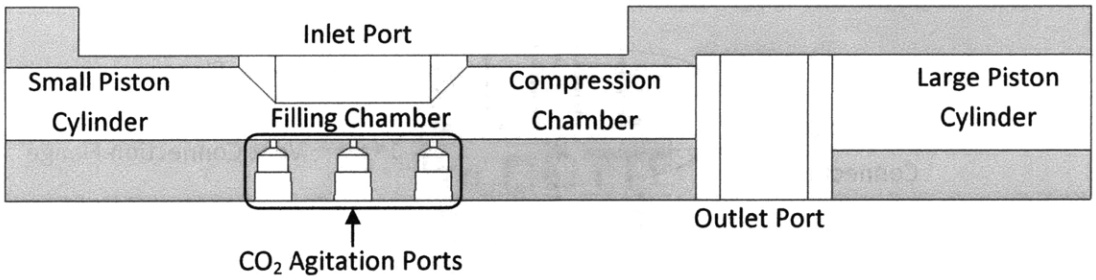

Figure 4-22: Main Body - Labeled Cross-Section

One of the main considerations in designing the Main Body was the optimization of the product flow path through the part. One of the most visible of these optimizations is the slot milled into the upper surface of the Main Body, as shown in Figure 4-21. The alpha prototype, with its funnel, body, and movable sleeve laying between the powder in the ICT and its filling chamber, experienced powder flow difficulties even with its mechanical agitator in place. The slot in the Main Body of the beta prototype allows the bottom of the Upper Funnel to sit closer to the Filling Chamber than it would otherwise. This shortens the powder flow path from the ICT to the filling chamber, making it less likely that the powder will bridge.

The small and large piston cylinders were designed to both guide and support the small and large pistons. At 61.0 mm (2.40") and 67.3 mm (2.65"), respectively, the cylinder lengths are 3.2 and 2.65 times their respective piston diameters. This should be sufficiently long to guide the pistons, meeting the general rule of thumb of length-to-diameter ratio greater than 1.6:1 for proper shaft guidance (Slocum).

The Collection Container is the final piece of the beta prototype and is displayed in Figure 4-23. Freshly made pellets fall from the Main Body through the Lower Funnel Anchor Plate and the Lower Funnel to land in the Collection Container, where they are held until the end of the trial. This container is attached to the Lower Funnel using a clamp fitting; its upper lip is a standard 100 mm clamp flange. Below this clamp flange is a thick, rectangular annulus with a tapped 1/8" NPT hole. This is the vent connection flange, and the hole is the vent connection.

This vent connection is for the attachment of a line or a valve at this location lets the Collection Container be vented separately from the main vent line of the ICT, allowing gas to be released from the container in the case of a blockage upstream of this part. This prevents the accidental release of pressure upon removing the clamp holding the Collection Container to the Lower Funnel. The vent connection flange provides enough material to allow for a full-depth NPT-tapped hole, ensuring that the connection is leak-free and strong enough to withstand the required operational pressures. The full annulus is not needed, but was kept intact to speed the manufacturing of this part and to allow for a second vent connection hole to be drilled and tapped in case appropriate male NPT fittings could not be found once the machine was in France.

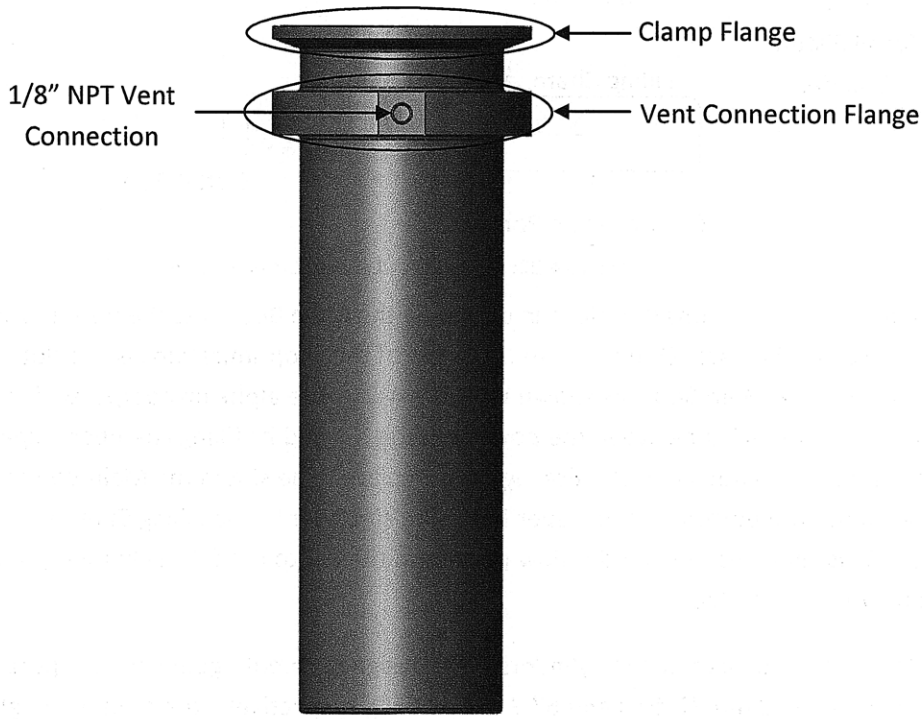

Figure 4-23: Collection Container

4.1.2. Side Components

The side components of the beta prototype consist of all of the parts attached to either the left or right sides of the Main Body, including the Pistons, Actuators, Actuator Flanges, Thermal Isolation Tubes, and CO_2 Flush Flanges. These components are described below in more detail.

The actuators used in the beta prototype were both off-the-shelf pneumatically operated units made by Festo, Inc. They were chosen due to their customizability regarding stroke lengths, their availability in sizes closely approximating what was needed for the proper functioning of this prototype, Nestlé's acceptance and familiarity with actuators of this type, and their short lead-time of only a few days. Hygienic actuators were also available and would be preferred, but choosing these actuators would have increased time to delivery by at least four weeks, which was unacceptable in the case of this project.

Figure 4-25 shows a cross section of the pneumatic actuator. The internal piston of the actuator is colored red, while the pressurized gas held inside actuator is colored blue. The pressurized gas enters the actuator's cylinder body through one of the two ports in its side while, in most cases, the other port is opened to the atmosphere. In Figure 4-25, the gas has entered through the left port, so the force it imparts on the internal piston pushes both the piston and piston rod to the right. This force is simply the product gauge pressure of the inflowing gas and the area of the piston. Rather than specify the area of the cylindrical internal piston, most manufacturers specify the diameter of this part. This specified diameter can then be used to calculate the internal piston's area.

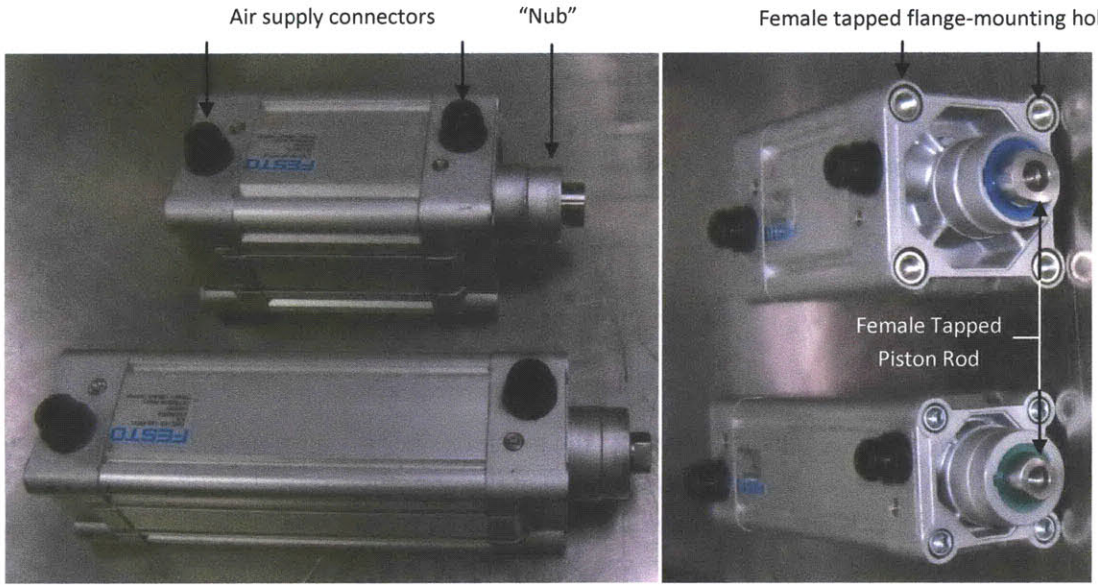

Figure 4-24: The Pneumatic Actuators
The 80 mm large actuator is on top, while the 63 mm small actuator is on the bottom in these pictures.

Part geometry and operating conditions were both considered when determining the specifications of the actuators. The strokes of the actuators were determined by the geometry of the Main Body. The stroke of the small actuator is equal to the lengths of the Filling Chamber and the Compression Chamber combined, where "length" refers to the distance down the axis of the through hole through the Main Body. This comes to a total of 119.4 mm (4.7"). Since Festo's actuators are defined in whole metric units, the final stroke for the small actuator came to 120 mm. The stroke of the large actuator was simply the length of the outlet port, or 35.6 mm (1.4"). As before, this number was rounded up to an even 36 mm when specifying the actuator.

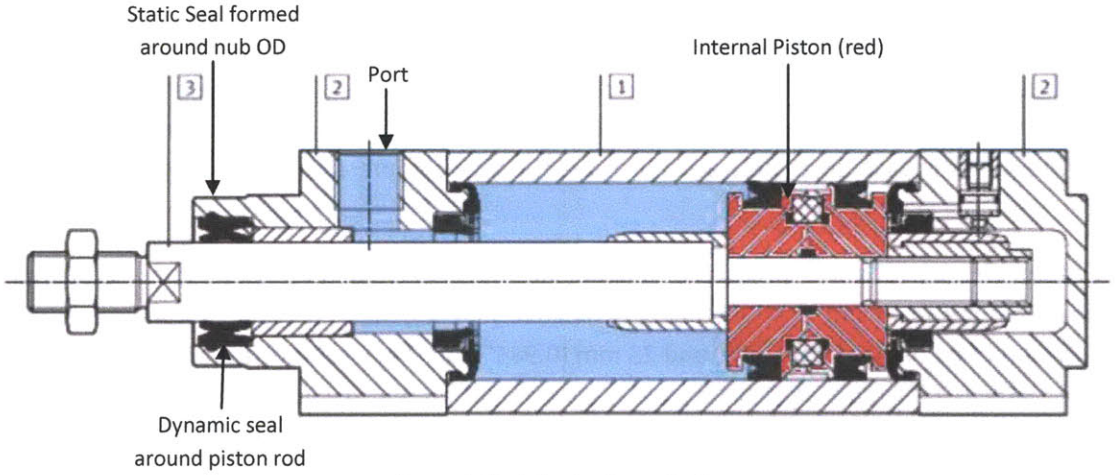

Figure 4-25: Actuator Cross Section
Modified from Festo, Inc. A male threaded piston rod version is shown, but the female threaded piston rod is similar. 1: Cylinder Body; 2: Bearing and End Caps; 3: Piston Rod. The internal piston of the actuator has been colored red for clarity.

In order to successfully produce the specified pellets, the actuators need to provide enough force to overcome the roughly 10 bar internal pressure of the ICT and prototype while also providing the approximately 15 bar pressure needed to adequately compress the powder into a pellet. The compressed air system in the Pilot Plant in PTC Beauvais operates at a pressure of approximately five bar. The minimum diameter of a given actuator's internal piston was determined using the following equation:

$$d_{act} = \sqrt{\frac{P_{ICT} * d_{pr}^2 + P_{comp} * d_{pellet}^2}{P_{act}}} \qquad (5)$$

where d_{act} is the minimum required diameter of the actuator's internal piston, P_{ICT} is the pressure in the ice confection tank, also equal to the pressure inside of the prototype, d_{pr} is the diameter of the piston rod of the actuator, P_{comp} is the pressure required to compress the pellet to its desired density, d_{pellet} is the diameter of the pellet, and P_{act} is the pressure of the gas used to control the actuator.

In determining the values of the above variables, worst-case scenarios were considered to ensure adequate operation under any reasonable combination of operating conditions. P_{ICT} was set to 12 bar, reflecting the fact that there was some discussion on raising the operating pressure due to favorable experimental results. P_{act} was set to 4 bar, reflecting the fact that the pressure of the shop air is not always stable at 5 bar but can sometimes fall below this level. The equation above gave a diameter requirement 45.3 mm for the small actuator and one of 65.5 mm for the large actuator.

The final criterion for choosing the actuator's internal piston diameter was the piston rod diameter associated with that size actuator. It was desired to keep the piston rod diameter as close as possible to the piston diameter in order to minimize the volume of gas displaced around the piston rod or piston as the actuator extended and retracted the piston rod. This would minimize gas flow in the thermal isolation tubes, making them more effective at separating the warm and cold ends of the device as well as reducing the chance of powder being pulled into and subsequently clogging the tubes. The diameter would have to be at least equal to the diameter given by the equation above in order to assure that adequate compression would be possible under all reasonable operating conditions, and would preferably be larger in case it was desired to increase the final compression pressure past its projected value.

After referring to Festo's product catalogue, internal piston diameters of 63 mm and 80 mm were chosen for the small and large actuators, respectively (Festo, Inc.). These actuators had respective piston rod diameters of 20 mm (0.787") and 25 mm (0.984"), which closely correspond to their respective 19.05 (0.75") and 25.4 (1.0") diameter pistons. When the small piston is in the fully extended position, the piston rod will displace an extra 3.5×10^{-6} m^3 of gas in the thermal isolation tube, or 11.7% more when compared to when the piston is in the fully retracted position. When the large piston is in the fully extended position, the piston rod will displace 5.7×10^{-7} fewer cubic meters of gas in its tube, or 2.9% less when compared to its fully retracted position. These gas flows are the best values that can be

Actuator	Delrin Piston Diameter [mm]	Specified Internal Piston Diameter [mm]	Specified Stroke [mm]
Small	19.05	63	120
Large	25.4	80	36

Table 1: Actuator Specifications

obtained using standard sized piston rods, and the actuator diameters are adequate for compressing the pellet the desired amount, so these actuators are as optimized as possible for this implementation.

Table 1 summarizes the actuator specifications. As previously described, the actuator with the 63 mm diameter internal piston is referred to as the small actuator, while the actuator with the 80 mm diameter internal piston is referred to as the large actuator.

To maintain continuous operation, the beta prototype must produce roughly one pellet every second to match the powder production rate of the flash freezing equipment. The volumetric flow of air required to drive the actuators at this rate can be calculated by recognizing that the production of a single pellet requires two strokes of each actuator. The average volumetric flow of the air into the actuator is therefore:

$$\dot{V} = \frac{\pi d_{act}^2}{4} * \frac{2s}{t} \qquad (6)$$

where $\dot{V}$ is the volumetric flow of the working gas, d_{act} is the actuator's internal piston diameter, s is the actuator stroke, and t is the total cycle time. With a cycle time of one second and actuator geometry as given in Table 1, the volumetric flow of compressed air in its compressed state is 7.9×10^{-4} m^3 s^{-1} for the small actuator and 3.6×10^{-4} m^3 s^{-1} for the large actuator. For initial trials, both actuators will be run at the roughly five bar that can be provided by the shop air system, requiring 1.15×10^{-3} m^3/s of compressed air at the system's pressure. This is well within the capacity of the shop air system, and so the beta prototype will not be limited by constraints on the actuator pressurized gas supply.

One of the alpha prototype's major failings was the issues experienced with its seals. While the static seals of the device offered problem-free, reliable performance, the dynamic seals fitting around the alpha prototype's moving components were neither strong enough to withstand the pressure differential present during operation nor durable enough to hold up after dozens of cycles. Designing and verifying dynamic seals are time-consuming processes that can consume several weeks or even months, especially if multiple iterations are required. In order to address this problem in the time available, the prototype design will incorporate a static seal against the outer diameter of the cylindrical nub on the face of the actuator and will use the dynamic seal built into the actuator that seals off the piston rod. Having been designed by Festo engineers to last the life of the actuator and being located in a room-temperature part of the machine, this dynamic seal should offer reliable performance for the life of the device.

The dynamic seal in the actuator is rated for a 12 bar pressure differential, according to the documentation supplied by the manufacturer (Festo, Inc.). The cross sectional view of the actuator

shown in Figure 4-25 displays the cross section of the dynamic seal, which appears as though it will function as a bi-directional seal. The limits of the seal's bi-drectionality were tested during initial trials with the assembled beta prototype, and it was found to hold with no discernable leakage up to an operating pressure of approximately 11.5 bar, the maximum pressure achieved during these tests.

The Actuator Flange allows the Actuator to be mounted to its Thermal Isolation Tube while also providing a groove for the o-ring seal separating the pressurized tube from the outside environment. As shown in Figure 4-26, the flanges are two metal rings, with the inner diameters of their central holes shaped to provide a snug fit over the front face of their respective actuators. The parts have been made of aluminum, which machines much more easily than stainless steel.

Despite aluminum's advantages over stainless steel during forming processes, the material is not suitable for the chemicals used in Nestlé's standard cleaning cycles. Generally, this makes a part unacceptable for usage in any food processing equipment, but this is not expected to be a problem in the case of the beta prototype for two reasons. The first is that while the device is still in the early testing stages, the parts can be cleaned by hand using a different set of cleansing agents than the standard detergents and solvents commonly used in cleaning and sterilization operations in the Pilot Plant setting. The second is that this aluminum part is in a location where it will not be contacted by product. The narrow gap between the piston and the walls surrounding it is very narrow, making it difficult for powder to travel to the Actuator flange. On top of this, the far end of the thermal isolation tube is held roughly at room temperature, which will quickly melt any powder that is pushed through the thermal isolation tube. The liquid mix will refreeze before it is able to reenter the Main Body, thus preventing any contamination of good product.

The Actuator Flange's position in the beta prototype's assembly is shown in Figure 4-27. The Actuator-Side Flange is bolted onto the Actuator using the four mounting bolts built into the Actuator's

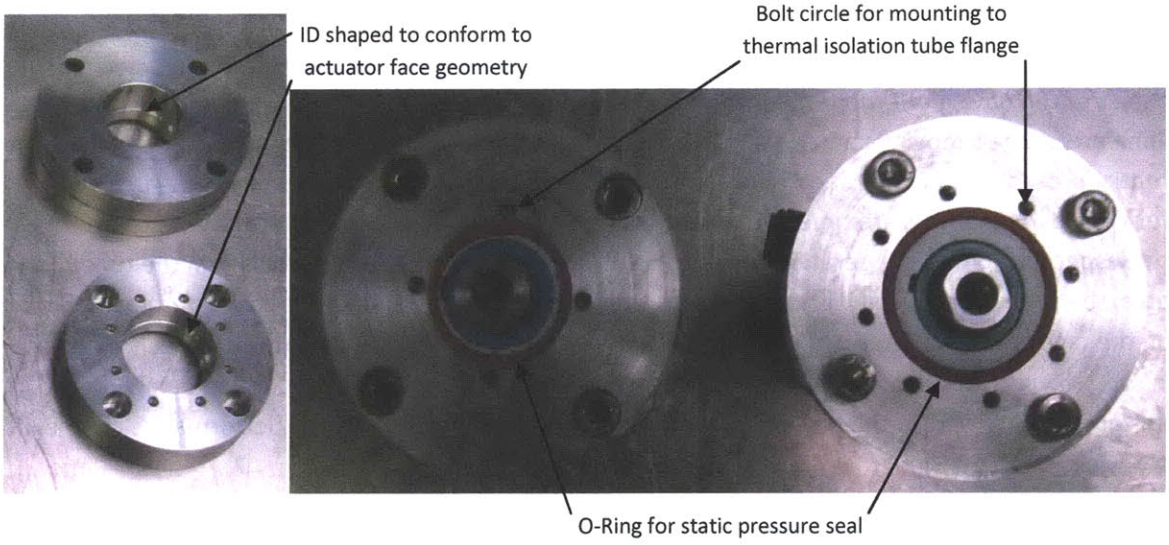

Figure 4-26: Actuator Flanges

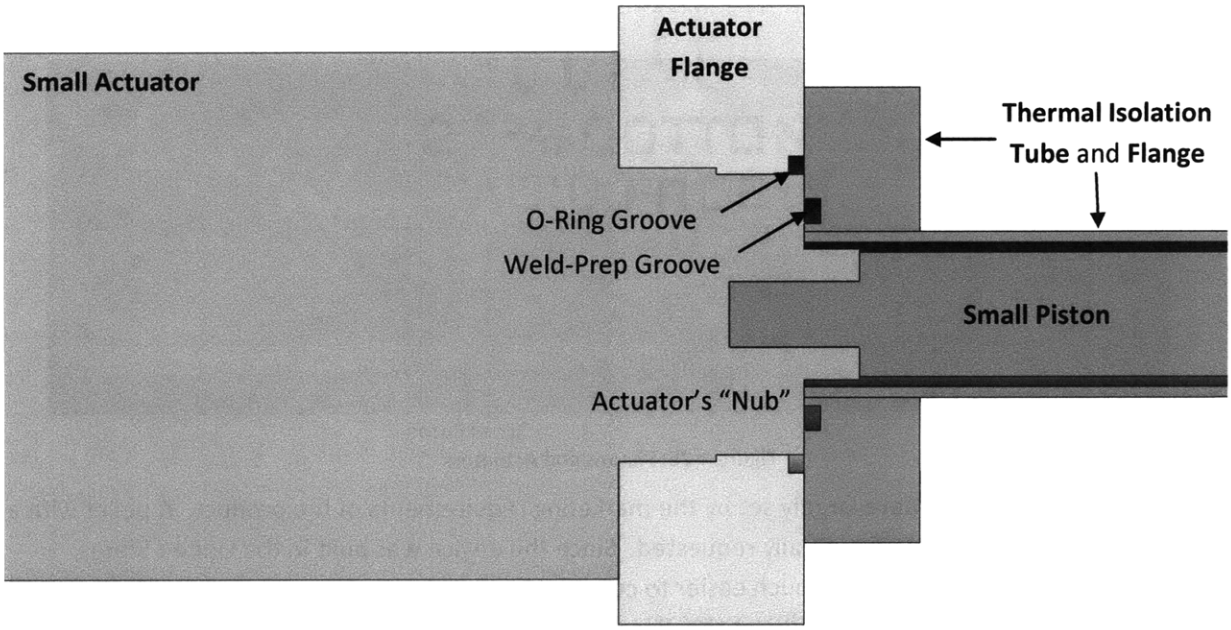

Figure 4-27: Actuator Flange Cross Section, Small Actuator Side

face, shown above in Figure 4-26, with the Actuators' faces shown in Figure 4-24. The Thermal Isolation Tube and its flange are then bolted on to the Actuator Flange, which must be very closely aligned to the axis of the Actuator to allow for proper alignment of the Piston with the Thermal Isolation Tube and its hole in the Main Body. An o-ring is placed into the o-ring groove cut into the inner diameter of the Actuator Flange, which seals against three separate parts – the Actuator, the Actuator Flange, and the Thermal Isolation Tube Flange. Careful alignment is necessary to ensure a reliable seal against these three independent parts. A simpler setup in which the o-ring is placed into the weld preparation groove in the Thermal Isolation Tube Flange was not feasible with these actuators due to the lack of an adequately sized solid, flat surface on the front face of the Actuator's nub. This combination of alignment and sealing requirements necessitates the careful shaping of the inner diameter of the Actuator Flange to allow it to match the geometry of the Actuator's nub.

The pistons of the beta prototype serve to compress the powder into a pellet and push the pellet out of the Main Body. Due to the nature of their contact with the product, their design and material choice had to be carefully considered to ensure reliable, proper functional capabilities. Due to the design geometry of the prototype, the small piston will have the same diameter as the pellet, while the large piston will be somewhat larger to allow it to seal the end of the Compression Chamber as shown in Figure 4-4a. and b. Piston lengths are set by the geometry of the Actuators, Main Body, and Thermal Isolation Tubes and will be fit to their respective cylinders in the Main Body while at room temperature. Analysis has been performed on the pistons to analyze their structural integrity and the effects of the temperature change between room temperature and the 233 K (-40°C) experienced during operation.

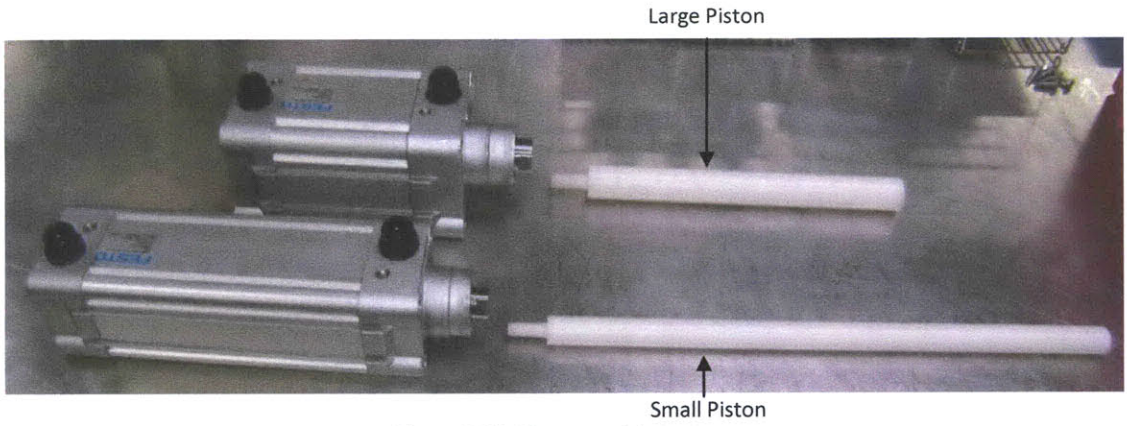

Figure 4-28: Pistons and Actuators

Piston diameters were largely set by the marketing requirements of the product. A pellet with a diameter of around 18 mm was initially requested. Since the device was built in the United States, imperial-dimensioned tooling was much easier to come by than metric tooling, so a size of 19.05 mm (0.75") was chosen for the pellet. This set the diameter of the small piston. The large piston's diameter was then set to 25.4 mm (1.0") so that it would be sufficiently large to completely seal the end of the Compression Chamber without overstressing the piston material, as shown in the analysis below.

The lengths of the pistons were then calculated from the geometry of the Actuators, Thermal Isolation Tubes, Flanges, and Main Body. The small piston should be flush with the end of the Inlet Port of the Main Body when fully retracted, and the large piston should extend slightly past the edge of the Outlet Port when it is fully retracted. In order to meet these criteria, the small piston must be 373 mm (14.69") long and the large piston must be 224 mm (8.83") long.

Material selection was a very important parameter in the design of these pistons. Previous experience with the powder had shown that it is very likely to stick to bare metal, especially when pressed on to that surface during compression. Thus, as with the alpha prototype and its PEEK piston tips, the decision was made to make the powder contact surface out of an FDA-approved plastic. However, experience with the alpha prototype has taught that a stainless steel piston running tight tolerances with a stainless steel bore tends to stick and bind. In order to circumvent these binding problems, the entire piston will be made of FDA-approved Delrin acetal for the beta prototype. This will provide the necessary non-stick requirement for the powder and the bore, be easily machinable if it does stick to the bore, and provide enough strength to make at least 500 pellets.

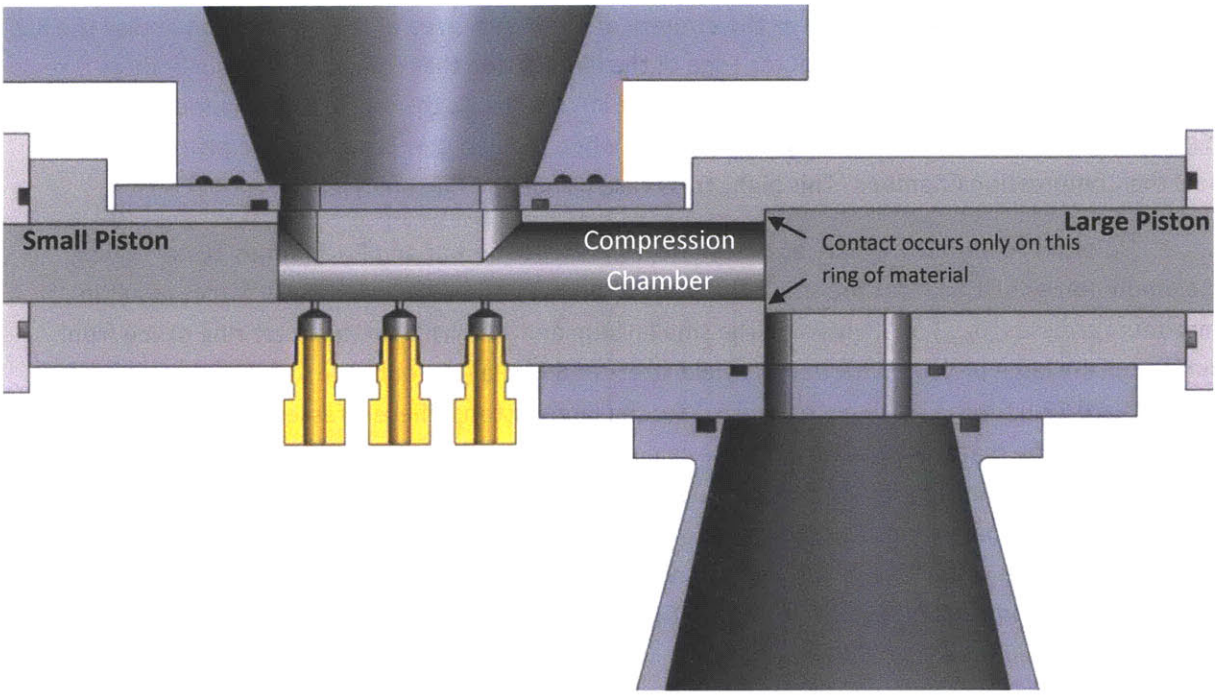

Figure 4-29: Cross Sectional View of Beta Prototype Showing the Pistons in the Loading Position

One of Delrin's advantageous properties is that its linear coefficient of thermal expansion (α_l) of 1.04×10^{-4} K^{-1} is greater than 304 stainless steel's 1.69×10^{-5} K^{-1} (from data sheets by DuPont and AKSteel, respectively). This means that when the prototype is cooled from the room temperature of 293 K (20°C) down to a temperature of 233 K (-40°C), the Delrin will contract more than the stainless steel of the Main Body, opening up a gap between the two parts. Given the assumption that the pistons are perfectly fitted to their bores at room temperature, the small piston will see a 0.051 mm (0.0020") gap open up between its outer diameter and the inner surface of its bore while a 0.066 mm (0.0026") gap will open between the outer diameter of the large piston and its respective passage in the Main Body due to the change in temperature.

Stress on the pistons is easily calculated as the force imparted on them by the actuators per unit area on which the piston is exerting that force. The internal pressure of the device has no direct effect on the pistons because the far end of the piston, screwed into the tapped hole in the end of the actuator's piston rod, is exposed to the same pressure, thus causing no net force. The force exerted by the actuator contributing to piston stress is:

$$F_{net} = P_{act} \frac{\pi\, d_{act}^2}{4} - P_{ICT} \frac{\pi\, d_{pr}^2}{4} \qquad (7)$$

where P_{act} is the actuator working gas pressure, d_{act} is the actuator diameter, P_{ICT} is the pressure in the ice confection tank, and d_{pr} is the diameter of the actuator's piston rod, which is exposed to P_{ICT} on one end but not the other. This force is then distributed over the working area of the piston.

The working area is defined as the entirety of the frontal area of the small piston and as the 3.2 mm (0.125") wide ring around the outer edge of the large piston that contacts the Main Body as it seals the compression chamber. The working area of the large piston is the region that experiences the highest stress during the actuation cycle, occurring when the actuator is pushing the piston forward to seal the Compression Chamber. This high stress case will be the one analyzed.

In order to obtain a worst-case estimate, P_{act} is set to six bar and P_{ICT} is set to 10 bar, giving maximum forces of 1.6 kN for the small piston and 2.5 kN for the large one. These forces result in maximum stresses (σ_{max}) of 5.5 MPa on the small piston and 11.4 MPa on the outer ring of the front surface of the large piston. With Delrin's yield stress of 69 MPa (DuPont), the yield safety factors (σ_{max}/σ_y) are 12.6 for the small piston and 6.1 for the large piston. These stresses well within the capabilities of the material to sustain. These calculations were verified using COSMOSXpress, the results of which are shown in Figure 4-30 below. COSMOSXpress gave realistic maximum stress levels of 5.6 MPa for the small piston and 11.9 MPa for the large piston, only 2.6% and 4.5% greater than the calculations above, respectively. It should be noted that COSMOSXpress automatically scales the deformation of the parts being analyzed, resulting in the slightly tilted look of the large piston in Figure 4-30b.

Figure 4-30a. shows a maximum stress of 7.7 MPa for the small piston at a location near its base. This is an artifact due to the way that COSMOSXpress handles restraining boundary conditions. When a surface is restrained, it is given no degrees of freedom. Thus, a surface under axial stress is not able to expand in any other direction. This Poisson-effect-cancelling restraint locally increases the stress calculated by the solver. However, in real life the piston is only constrained axially, thus avoiding this stress concentration.

Somewhat offsetting the gap-opening effect of the temperature change is the radial expansion of the piston while under the compressive load described above. This expansion is given by the Poisson's ratio of the material through the relation below:

$$\Delta D = D_i * \nu \frac{\sigma_{axial}}{E} \qquad (8)$$

where ΔD is the change in diameter, D_i is the initial, unstressed diameter, ν is the Poisson's ratio of the piston material (0.35 for Delrin), σ_{axial} is the axial stress placed on the piston, and E is the Young's modulus of the piston material (3.1×10^9 Pa for Delrin) (DuPont). Poisson effects account for an

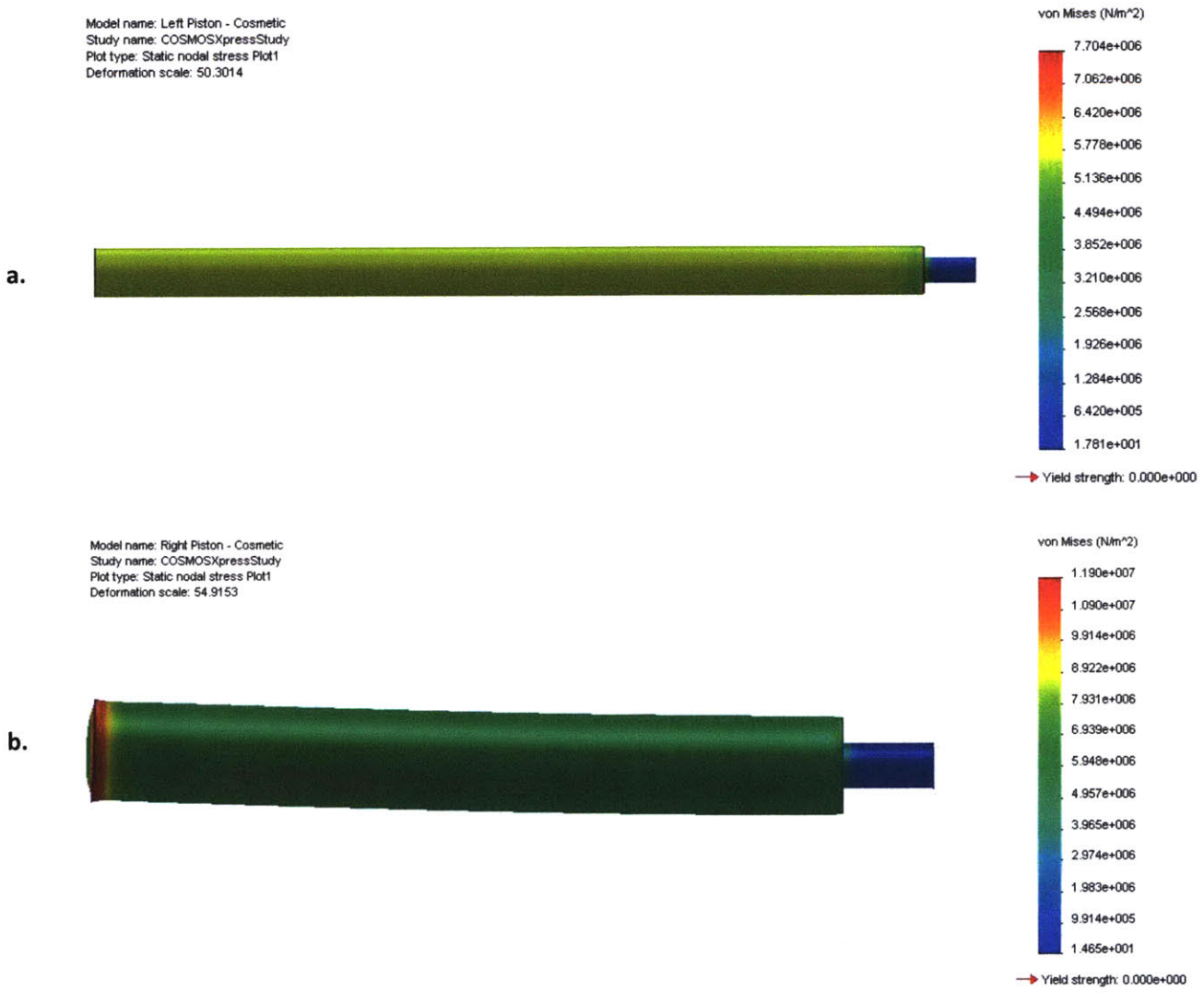

Figure 4-30: a.) Small Piston and b.) Large Piston Stress Distributions, from COSMOSXpress.

increase of 1.1×10^{-5} m (4.6×10^{-3} in) in the diameter of the small piston and one of 1.4×10^{-5} m (5.6×10^{-3} in) of the large piston while under maximum load. The change in the clearance between the piston and bore is equal to half this change in diameter, so the final minimum clearances between the piston outer diameter and the bore inner diameter are 4.4×10^{-5} m (1.7×10^{-3} in) for the small piston and 5.9×10^{-5} m (2.3×10^{-3} in) for the large piston. These minimum clearances assume a perfect fit between the piston and its bore at room temperature, so their size is determined solely by thermal contraction and Poisson expansion effects. The presence of positive clearance between the pistons and their bores suggests that they will not become jammed and/or damaged during operation due to physical interference stemming from thermal- or load-induced strains.

Fatigue life calculation is not as critical for the easily-machined Delrin pistons as it is for the more labor-intensive and pressure-holding stainless steel parts of the machine. If the part breaks, it can be quickly and easily replaced with a new piston machined from Delrin stock. However, this still causes

valuable time to be lost, and with the tight deadlines of this project, it would be beneficial if there were some guideline as to the inspection and replacement timeline for these pistons, so that new pistons could be made and fitted to the prototype proactively rather than reactively. As long as the stress is purely compressive and well under the yield strength of the material, which is the case with these pistons, fatigue will not be an issue for the production of 500 pellets and likely would not be for an implementation on a production line.

Buckling is generally main mode of failure for shafts undergoing compressive stress. It occurs at a critical load (F_{crit}) that is dependent on the manner in which the shaft is constrained on either of its ends. In the case of the pistons of the beta prototype, they can be modeled as either clamped-clamped or free-clamped, depending on how one handles the classifying of the Main Body end of the piston. The actuator-side of the piston can be modeled as a clamped joint for both pistons, since it is securely screwed into the piston rod of the actuator via its threaded end. The Main Body-sides of the pistons can also be modeled as clamped since they are going to be fit to the bore of the Main Body with only a few thousandths of an inch of clearance around their diameters. The equation for critical force is as follows:

$$F_{crit} = \frac{cEI}{L^2}$$

where c is equal to $4\pi^2$ for the clamped-clamped system, E is the Young's Modulus for the material, which is 3.1 x 10^9 Pa for the Delrin used (DuPont), I is the area moment of inertia for the piston, equal to $\frac{\pi r^4}{4}$, and L is the free length of the piston. This length will be taken as the length of piston located outside of the Main Body, where the piston is less constrained, while the pistons are experiencing loading (i.e. while the small piston is extended during pellet compression and the large piston is extended and sealing off the Compression Chamber). The free lengths of the small and large pistons are 0.203 m and 0.121 m, respectively. The critical force for buckling is then 19 kN for the small piston and 169 kN for the large one. When compared to the 1.6 kN and 2.5 kN maximum forces exerted on the pistons, respectively, it is clear that this model does not predict buckling to be an issue.

The pistons are screwed into the Actuator's piston rods during assembly of the device. Each piston has a threaded nub on its Actuator side to match the threaded hole in its respective piston rod. This is expected to be a slightly stronger and more durable design than having the piston have the female thread and the piston rod have the male. As shown in Figure 4-31, the female threaded hole, whether in the plastic piston or the high-alloy steel piston rod, is going to be deeper than its threaded male counterpart is long in order to guarantee good contact between the shoulders of the two parts. This will ensure that the piston's plastic thread does not carry the full compressive load during pellet formation. However, it also means that the female part will be carrying the full load on the thin wall between its threaded inner diameter and its outer diameter. The smaller area presented by this thin wall will amplify the stress experienced by the female part in this region when compared to the stress felt by the part across its solid section away from the threaded hole.

As an example of the above statement on stress concentration, take the possibility of using a male threaded piston rod and a female threaded piston. The small and large actuators used in the beta prototype are available with M16 and M20 male threaded rods, respectively (Festo, Inc.). Tapping an

M16 hole into the end of a 19 mm (0.75") diameter piston would leave a 1.5 mm (0.060") wide ring around the outside of the threaded hole. This thin amount of material would need to support the 1.6 kN maximum force present on this part, equating to a stress of 35.5 MPa . Though this stress is still under the 69 MPa yield stress of Delrin acetal, it is still 6.5 times the stress on the male-threaded piston. Moving this high-stress region to the piston rod was seen as a sensible course of action due to high-alloy steel's greater strength and fatigue resistance when compared to plastic. The two actuators are rated for design pressures of 12 bar, greater than the six bar maximum pressure attainable with the Pilot Plant's compressed air system (Festo, Inc.). Therefore, the piston was given the heavier, sturdier male design, while the piston rod was designed to have the tapped hole.

As previously mentioned, the alpha prototype's major shortcoming was the lack of dynamic seal integrity in the operating temperature range. The seals worked well and held at room temperature, but once they cooled below 253 K (-20°C) they become stiff, brittle, and disintegrated into pieces. This is a common problem in cryogenic equipment, where operating temperatures are often far below the functional temperature range of most reasonable seals. The usual solution is to move the seals from the coldest parts of the machine to a warmer, preferably room temperature location, thereby greatly increasing the options one has for seal materials (Smith).

The path between the seal and the cold, operational part of the machine must have sufficient thermal resistance to minimize the heat leak into the cold side of the device. It must also have sufficient gas flow resistance to ensure that conduction, rather than convection, is the dominant form of heat transfer along the isolation path. These two goals are generally achieved by making the walls and the gas space of the isolation structure as thin as possible (Smith). In this case, a cylindrical tube is the most sensible geometric form for the isolation structure, and Figure 4-33 shows a cross sectional view of the Thermal Isolation Tube mounted to Main Body. The tube has a flange welded to either end to allow for the mounting of this part to the Main Body of the beta prototype and the mounting of the Actuator on the other end of the part. The ends attached to the Main Body will be called the "fixed" ends of the

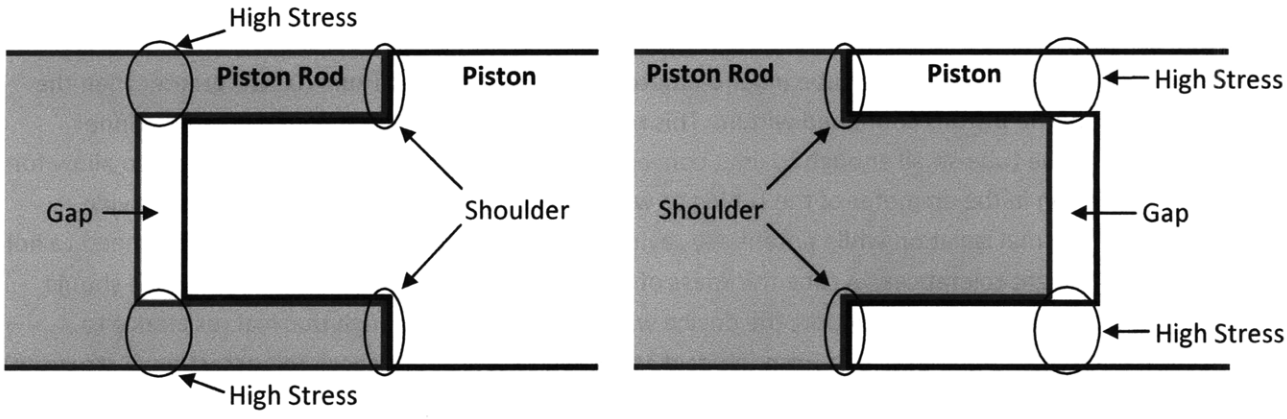

Female Piston Rod Thread

Male Piston Rod Thread

Figure 4-31: Female vs. Male Piston Rod Thread

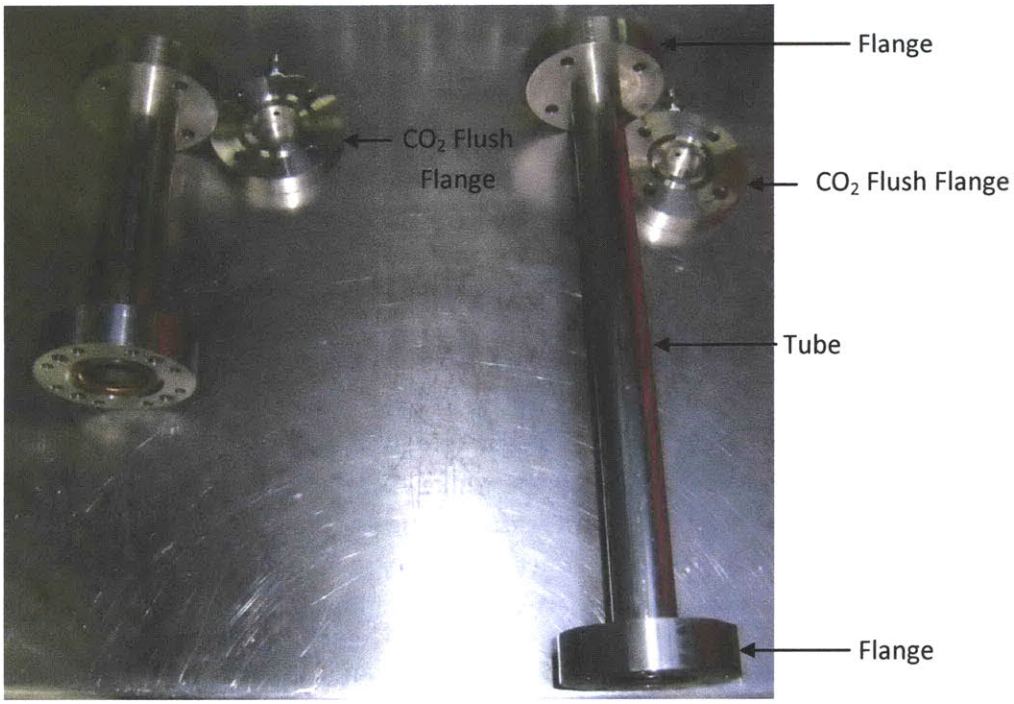

Figure 4-32: Thermal Isolation Tubes
The Large Thermal Isolation Tube is on the left, while the Small Thermal Isolation Tube is on the right. The tubes are named for their diameters, not their lengths. The CO_2 Flush Flanges, described below, are also shown.

tubes, while the ends supporting the Actuators will be denoted the "free" ends of the tubes. The diameters of the two tubes were determined by the size of the piston that runs through the center of the individual tube and structural calculations, while their lengths were determined by heat transfer along the part and the stroke of the piston within. Once the lengths have been set, further structural analysis were run to ensure that any loads placed on the free ends of these tubes do not cause excessive deflection or stresses that could cause component failures.

The Thermal Isolation Tube inner diameters were first set to 3.1 mm (0.12") greater than the diameters of the pistons contained within. This results in a gap between the piston and the inner diameter of the tube small enough to limit convection in this space while still large enough to allow for slight variation in the diameter of the tubing as well as slight misalignments. This should provide adequate thermal isolation while potentially saving machining time, since the parts will not need to hold exceedingly tight tolerances. A tube thickness of 1.7 mm (0.065") was initially assumed, as it should provide enough strength to support the device while still providing enough thermal resistance to properly insulate the warm seals from the cold Main Body. In order to check this assertion, a structural analysis was performed. Stresses that affect the entire tube uniformly were calculated using modified versions of the thin-walled tube stress equation with, in the axial case, additional stress added due to the forces exerted by the actuator during the operational cycle:

$$\sigma_{axial} = \frac{P_{ICT}\, d_{i,tube}}{4\, t_{tube}} + \frac{P_{act}\, \frac{d_{act}^2}{d_{pist}^2}}{2\, \pi\, d_{i,tube}\, t_{tube}} \quad (9a.)$$

$$\sigma_{circ} = \frac{P_{ICT}\, d_{i,tube}}{2\, t_{tube}} \quad (9b.)$$

$$\sigma_{uniform} = \sqrt{\sigma_{axial}^2 + \sigma_{circ}^2} \quad (9c.)$$

In the above equations, σ_{axial}, σ_{circ}, and $\sigma_{uniform}$ refer to the axial, circumferential, and total uniform stresses on the tube, P_{ICT} is the gauge pressure inside the ice confection tank and prototype, $d_{i,tube}$ is the inner diameter of the tube, t_{tube} is the thickness of the tube wall, P_{act} is the gauge pressure of the working gas of the actuator, d_{act} is the working diameter of the actuator, and d_{pist} is the diameter of the piston. Given an Ice Confection Tank pressure of 11 bar(g) and an actuator working gas pressure of 5 bar(g), the value of the total uniform stresses for the large tube is 15.6 times smaller than the 0.2% yield stress (σ_y) of the 304 stainless steel used in the tubes' construction and is 14.3 times smaller than the yield stress for the small tube. According to these initial calculations, plastic deformation is unlikely to occur with the given dimensions due to pressure and compression forces alone.

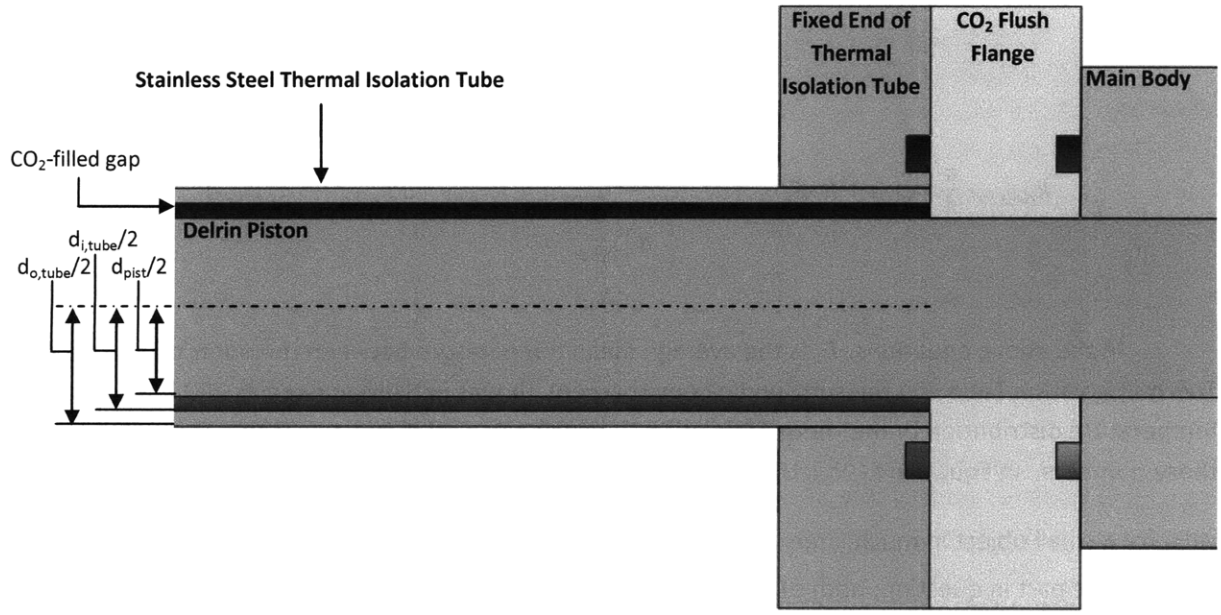

Figure 4-33: Cross-Sectional View of the Thermal Isolation Tube

The lengths of Thermal Isolation Tubes containing reciprocating pistons are generally set as thermal isolation length plus twice the stroke of the piston contained within. This ensures that the cold part of the piston is never withdrawn into the warm part of the isolation tube, limiting shuttle heat transfer into the cold side of the system (Smith). In calculating the thermal isolation length, several assumptions were made. The temperature of the room was assumed to be 293 K with a dew point (T_{sat}) of 277 K, the average dew point at Charles de Gaulle airport, roughly 40 miles southeast of Beauvais, during December and January from 1997 to 2007 (Weather Underground). The minimum device temperature of 233 K (-40°C) was assumed, which should lead to a conservative estimate for the thermal isolation length. Further assumptions are explained below for the sake of clarity.

Due to the geometry of the tubes, it was thought that they could be analyzed thermally as cylindrical fins. In order to check this assumption, the tubes' diametrical Biot numbers were examined. In order for the fin equations to be valid, the Biot number of the tube being examined must be much less than one. These numbers utilize the total heat transfer coefficient (h_{total}), which is defined in Equation *(10b.)* below as the sum of the convective and radiation heat transfer coefficients, as well as an area-averaged conductivity term ($\bar{k}$), defined in Equation *(10c.)*. The conductivity term accounts for the axial conductivities of the Delrin piston, the CO_2-filled gap, and the stainless steel tube by weighting them according to their areas normal to the longitudinal axis of the tube.

$$Bi = \frac{h_{total}\left(d_{o,tube}/4\right)}{\bar{k}} \qquad (10a.)$$

$$h_{total} = h_{conv} + 4\,\varepsilon\,\sigma\,T_m^3 \qquad (10b.)$$

$$\bar{k} = \frac{k_{delrin}\,\frac{\pi}{4}\,d_{pist}^2 + k_{CO2}\,\frac{\pi}{4}\left(d_{i,tube}^2 - d_{pist}^2\right) + k_{ss}\,\frac{\pi}{4}\left(d_{o,tube}^2 - d_{i,tube}^2\right)}{\frac{\pi}{4}\,d_{o,tube}^2} \qquad (10c.)$$

In the above equations, T_m is the average mean temperature between the outer diameter of the Thermal Isolation Tube and the surrounding environment. It was initially guessed as 280 K, and after the temperature distribution of the thermal isolation tube was calculated, its value was recomputed using those numbers. In Equation *(10b.)*, the formulation for the portion of h_{total} due to radiation ($4\,\varepsilon\,\sigma\,T_m^3$) is valid for a small object in much larger isothermal environment and when $\frac{\left(\Delta T/T_m\right)^2}{4}$ is much less than unity for the part in question, both of which are true with the Thermal Isolation Tubes (Lienhard and Leinhard). The tube is assumed to be a black body, making its emissivity (ε) equal to one. Calculations show the heat transfer due to radiation to be equal to roughly half that of natural convection, making radiation a significant source of heat flow in this case.

The convective heat transfer coefficient (h_{conv}) due to natural convection from the air to the tubes (h_{nc}) is assumed constant at 10 W m^{-2} K^{-1}, while the heat transfer coefficient due to condensation of water from the atmosphere to the surface of the tubes (h_c) is assumed constant at 2000 W m^{-2} K^{-1}. The values for these coefficients have been calculated using Equations *(11a.)* and *(12a.)*, and should provide answers that are accurate enough to give a good approximation of the thermal isolation lengths.

$$\overline{Nu}_D = \frac{h_{conv}\ d_{o,tube}}{k_{air}} = 0.36 + \frac{0.518\ Ra_D^{1/4}}{[1 + (0.559/Pr)^{9/16}]^{4/9}} \qquad (11a.)$$

$$Ra_D = \frac{g\ \beta\ \Delta T\ d_{o,tube}^3}{\alpha\ \nu} \qquad (11b.)$$

Equation *(11a.)* gives the formulation for the Nusselt number based on the outer diameter of a horizontal cylinder undergoing convective heat transfer by natural convection. This relation depends on the Prandtl number of the air, the Rayleigh number of the system, the thermal conductivity of the air (k_{air}) , and the outer diameter of the tube ($d_{o,tube}$). The Rayleigh number depends on the acceleration due to gravity (g), the coefficient of thermal expansion of the air (β, equal to $1/T_{air}$ for an ideal gas, which describes air at atmospheric pressure at these temperatures), the temperature difference between the tube outer diameter and the air (ΔT), the outer diameter of the tube, the air's thermal diffusivity (α) and its kinematic viscosity (ν). This Nusselt correlation is good for values of the Rayleigh number based on the outer diameter of the cylinder between 10^{-4} and 10^6, a range which includes the Rayleigh numbers of both the small (23,500) and large (33,000) tubes. (Lienhard and Lienhard)

$$\overline{Nu}_D = \frac{h_c\ d_{o,tube}}{k_{air}} = 0.728\left[\frac{\rho_f\ (\rho_f - \rho_g)\ g\ h_{fg}'\ d_{o,tube}^3}{\mu\ k_{air}\ (T_{sat} - T_{OD})}\right]^{1/4} \qquad (12a.)$$

$$h_{fg}' = h_{fg}\left[1 + 0.68\ \frac{c_p(T_{sat} - T_{OD})}{h_{fg}}\right] \qquad (12b.)$$

Equation *(12a.)* gives the Nusselt number correlation based on the outer diameter of a horizontal cylinder undergoing convective heat transfer by condensation. This relation depends on the densities of both the condensed fluid (ρ_f) and the gas from which it is condensing (ρ_g), gravity, the corrected latent heat of vaporization of the fluid (h_{fg}'), the dynamic viscosity of the air (μ), the thermal conductivity of the air, the saturation temperature of the air (T_{sat}), and the temperature of the outer diameter of the tube (T_{OD}). The corrected latent heat of vaporization, given by Equation *(12b.)*, accounts for subcooling of the liquid film formed on the tube, and it is a function of the latent heat of vaporization of the liquid (h_{fg}), the specific heat of the liquid (c_p), and the temperature difference between the saturation temperature and the temperature of the outer diameter of the tube. (Lienhard and Lienhard)

The Biot numbers for the large and small Thermal Isolation Tubes in the case of natural convection are 0.08 and 0.05, respectively. Both of these are much smaller than 1.0, allowing the tubes to be modeled as fins in this case. However, when the tube's temperature is below the 277 K saturation temperature of the room, condensation will form on its exterior and greatly increase the heat transfer coefficient. This increase in the convective heat transfer coefficient raises the large and small tubes' Biot numbers to 10.7 and 7.1, respectively. Being greater than one, these Biot numbers report that the rate of convective heat transfer from the surface of the tube is high enough that the tube can no longer be assumed to have a constant temperature at each axial cross section along its length. This means that the fin equations will not give accurate results when used to calculate the thermal isolation length.

In this analysis, the thermal isolation length will first be calculated in two ways – once assuming natural convection along the entire length of the tube (the dew point is less than 233 K), and once assuming condensation along the entire length of the tube (the dew point is greater than 293 K). The targeted temperature at the end of the Thermal Isolation Tube will be 290 K to keep tube lengths reasonable. The tip temperature of the tubes asymptotically approaches ambient temperature as tube lengths rise, thus requiring disproportionate lengths of tubing to obtain the last few degrees of temperature rise. As high accuracy is not required using this bracketing methodology, fin equations will be used in both cases even though they are only truly valid for the former case. It is assumed that both of these fins are adiabatic-tipped; their tip temperatures are close to that of ambient, so heat transfer at those points should be minimal.

A mixed-heat-transfer-mode model is also examined. In that model, the thermal isolation tube is split into two separate fins. The first of these fins has a base temperature of 233 K, a tip temperature of 277 K (T_{sat}) , and sees condensation along its entire length. The second of these fins is stacked on top of the first, having a base temperature of 277 K, a tip temperature of 290 K, and seeing only natural convection along its entire length. The first fin will be modeled as an uninsulated-tip fin, while the second will be modeled as an adiabatic tipped fin. This model will be presented along with the two bracketing cases to give a better idea of a possible thermal isolation length.

Before presenting the fin equations, there are two important parameters that need to be defined. The first is the fin constant (m), used in both fin equations given below, while the other is the axial Biot number, utilized only in the uninsulated tip case. Both are dependent on variables that have already been discussed above.

$$m = \sqrt{\frac{h_{total}\ \pi\ d_{o,tube}}{\bar{k}\ \frac{\pi}{4}\ d_{o,tube}^2}}$$

$$Bi_{ax} = \frac{h_{total}\ l_{tube}}{\bar{k}}$$

In both of the following sets of equations, the first gives the temperature profile of the fin as a function of position down its length (x) while the second gives the total amount of heat transfer through the fin. Both equations in each set depend on T_{base}, or the temperature at the base of the fin, as well as the temperature of the medium, in this case air, surrounding the fin (T_{air}) . The first set of equations presented are for the case of an adiabatic tipped fin, which will be used in the natural convection, condensation, and natural convection portion of the mixed-heat-transfer-mode models.

$$T(x) = (T_{base} - T_{air}) \frac{\cosh(m(l_{tube} - x))}{\cosh(m\, l_{tube})} + T_{air} \qquad \textit{(13a.)}$$

$$\dot{Q} = \sqrt{(h_{total}\ \pi\, d_{o,tube}) \left(\bar{k}\ \frac{\pi}{4}\ d_{o,tube}^2\right)}\ \tanh(m\, l_{tube})(T_{base} - T_{air}) \qquad \textit{(13b.)}$$

The second set of equations is for the case of a fin with an uninsulated tip, which will be used in the condensation portion of the mixed model:

$$T(x) = (T_{base} - T_{air}) \frac{\cosh(m(l_{tube} - x)) + (Bi_{ax}/m\, l_{tube})\sinh(m(l_{tube} - x))}{\cosh(m\, l_{tube}) + (Bi_{ax}/m\, l_{tube})\sinh(ml_{tube})} + T_{air} \qquad \textit{(14a.)}$$

$$\dot{Q} = \sqrt{(h_{total}\, \pi\, d_{o,tube}) \left(\bar{k}\ \frac{\pi}{4} d_{o,tube}^2\right)}\ \frac{(Bi_{ax}/m\, l_{fin}) + \tanh(m\, l_{tube})}{1 + (Bi_{ax}/m\, l_{fin})\tanh(m\, l_{tube})}(T_{base} - T_{air}) \qquad \textit{(14b.)}$$

To determine the thermal isolation lengths, tube length was iterated in steps of one millimeter until the tip temperatures of the various fins, calculated using Equations *(13a.)* and *(14a.)*, reached 290 K. The results of these three models are shown by Figure 4-34 and are summarized in Table 2. Table 2 also gives the total length of the tube as calculated by each of the three approaches, which is equal to twice the stroke of each piston added to the calculated thermal isolation length as described above.

The average result from these three models shows that the total tube length should be 322 mm (12.7") for the small tube and 156 mm (6.1") for the large tube. These respective numbers will be rounded down to 305 mm (12") and 152 mm (6"). Choosing a slightly shorter length will fractionally decrease device weight and length, and, more importantly, will decrease the stresses experienced by the tube should force be applied to its free end. According to the models described above, the outputs of which are shown in Figure 4-34, these length decreases will result in less than a degree of difference in temperature at the end of the thermal isolation length. This will slightly increase heat leakage into the Main Body due to shuttle heat transfer, but at an Ice Confection Tank pressure of 10 bar the carbon dioxide clathrate hydrates contained in the powder should be stable up to 270 K according to Equation *(1)* in the Constraints section, so a slight temperature rise should not pose a significant problem.

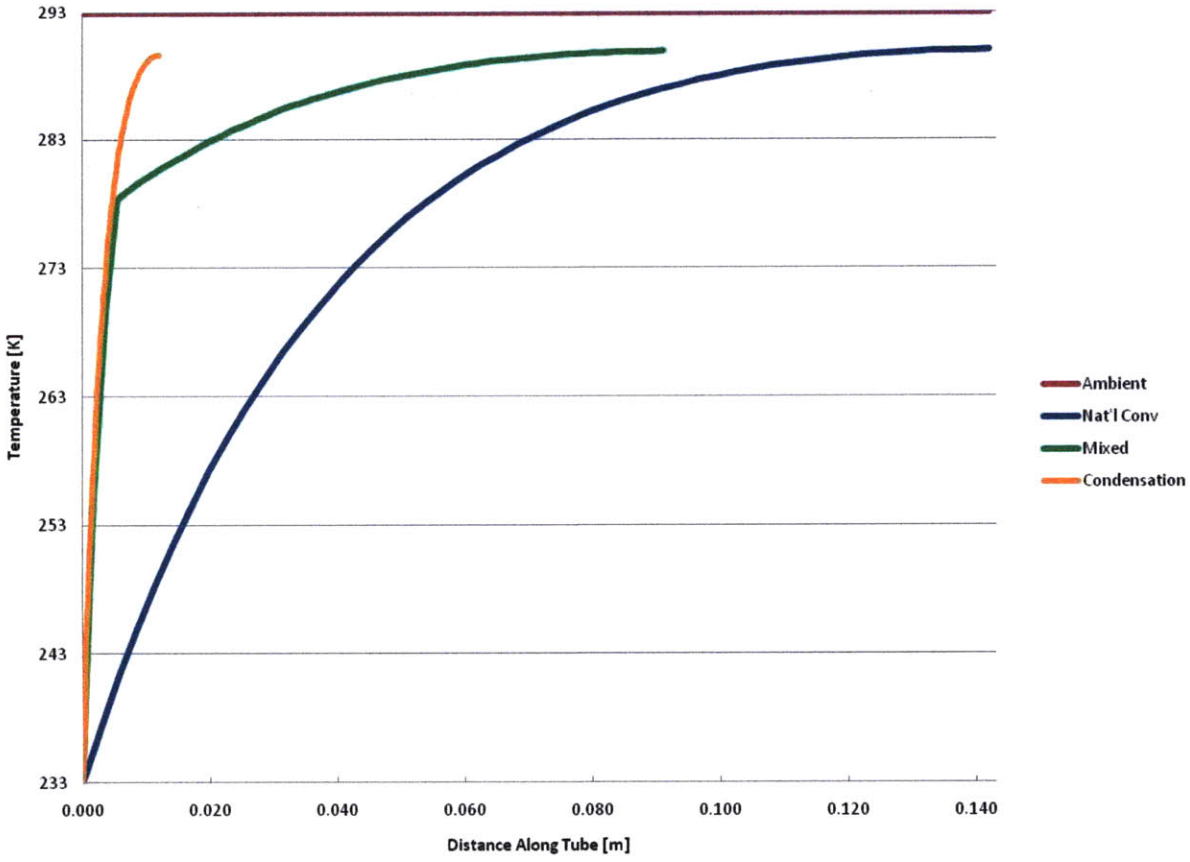

Figure 4-34: Temperature Profile along the Length of the Small Thermal Isolation Tube Given by Three Different Models
Plots from the Large Thermal Isolation Tube are largely similar and so have been omitted.

Now that the lengths of the tubes have been determined, further structural analysis can be performed. These tubes are essentially cantilevered beams supporting both their own weight and that of the Actuator Flange and Actuator mounted on their free ends. These can be analyzed using classical cantilevered beam bending equations. The weight of the tube itself can be modeled as an evenly distributed load along the length of the beam, while the weights of the Thermal Isolation Flange, Actuator Flange, and Actuator can be modeled as tip loads. The cantilevered beam relations have been taken from Crandall, Dahl, and Lardner's *An Introduction to the Mechanics of Solids, Second Edition with SI Units*, as cited in the References section at the end of this paper. Both displacement and stress were

	Small Tube			Large Tube		
	l_{iso} [mm]	l_{tube} [mm]	$\dot{Q}$ [W]	l_{iso} [mm]	l_{tube} [mm]	$\dot{Q}$ [W]
Natural Convection	142	382	2.8	144	216	3.6
Mixed	91	331	24	95	167	36
Condensation	12	252	32	13	85	41
Average	82	322	20	84	156	26

Table 2: Summary of the Results of Thermal Isolation Tube Heat Transfer Models

examined in order to determine the effect of these various loads on piston alignment as well as part strength and longevity as well as. In the equations below, δ_w stands for the downwards displacement of the tip of the tube due to the weight of the tube itself, δ_t is the downwards displacement of the tube's tip due to the mass of the other parts attached there, and δ_{total} is the total downwards displacement of the tip.

$$\delta_w = \frac{m_{tube}\ g\ l_{tube}^3}{8\ E\ I} \tag{15a.}$$

$$\delta_t = \frac{m_t\ g\ l_{tube}^3}{3\ E\ I} \tag{15b.}$$

$$\delta_{total} = \delta_w + \delta_t \tag{15c.}$$

In the above relations, m_{tube} is the mass of the tube, g is the gravitational constant (assumed to be 9.81 m/s^2), m_t is the total mass of the Thermal Isolation Tube Flange, Actuator Flange, and Actuator for the given tube, l_{tube} is the length of the given tube, E is the Young's Modulus of the 304 stainless steel that the tube is made of (193 GPa, from AKSteel), and I is the area moment of inertia of the tube's cross section, given below.

$$I = \frac{\pi\left(r_o^4 - r_i^4\right)}{4} \tag{16}$$

Total downwards displacement was found to be 0.076 mm (0.003") for the large tube and 0.30 mm (0.012") for the small tube. These numbers are small enough, at 0.3% and 1.6% of their respective piston diameters, that they should not pose a problem with piston alignment, especially as the pistons will be machined to fit the Main Body through hole.

The stress equations are presented below in the same manner as the displacement equations are given above. The symbol σ_w gives the stress induced by the weight of the tube, σ_t stands for the stress induced by the weight of the parts attached to the free end of the tube, and σ_{total} gives the total stress.

$$\sigma_w = \frac{m_{tube} * g * y}{2 * I * l_{tube}}(l_{tube} - x)^2 \tag{17a.}$$

$$\sigma_t = \frac{m_{tip} * g * y}{I}(l_{tube} - x) \tag{17b.}$$

$$\sigma_{total} = \sqrt{(\sigma_w + \sigma_t + \sigma_{axial})^2 + \sigma_{circ}^2} \tag{17c.}$$

In the stress equations, y is the distance of the analyzed part of the tube from its bending neutral axis, x is the part's distance along the axis of the tube from the anchored Main Body end, σ_{axial}

and σ_{circ} are given in Equation *(9)* above, and the other variables are as previously described. The highest stressed point on the tube is going to be at a maximized value of *y* and a minimized value of *z*, corresponding to the highest and lowest points on the outer diameter of the tube at its fixed end. At this point, the stress induced by the loads described in Equations *(17a.)* and *(17b.)* are in the axial direction and so will be added to the axial stress induced by the internal pressure of the prototype, as shown in Equation *(17c.)*.

Stress is calculated to be 39.5 MPa (5.7 ksi) for the large Thermal Isolation Tube and 36.6 MPa (5.7 ksi) for the small tube at their points of maximum stress. Type 304 stainless steel has a 0.2% yield stress (σ_y) of 290 MPa (AKSteel), giving a yield safety factor, defined as σ_{total}/σ_y, of 50.5 for the large tube and 19.1 for the small one. These safety factors are sufficiently large that there is no worry of the Thermal Isolation Tubes yielding while under these loads. The values used for the various variables and the displacement and stress results are summarized below in Table 3.

In order to obtain further estimates of the stress distribution and peak stress in these parts, a solid model of the more highly stressed small Thermal Isolation Tube and Flanges was made using SolidWorks and analyzed using its integrated COSMOSXpress software. This software does not have the capability of analyzing assemblies, so the tube and flanges were modeled as a single part, without the weld joints they have in real life. Therefore, these results will not be exact, but should provide an estimate of the stress distribution in this part that does a better job of considering geometry than the simple model described above. The output of this program is given in Figure 4-35 and Figure 4-36

		Small	Large
Thermal Iso. Tube *[kg]*		0.300	0.191
Thermal Iso. Flange *[kg]*		0.395	0.405
Actuator Flange *[kg]*		0.400	0.323
Actuator *[kg]*		2.544	3.466
Prototype Mass Supported *[kg]*		15.958	20.878
ID *[m]*		22.1×10^{-3}	28.5×10^{-3}
OD *[m]*		25.4×10^{-3}	31.8×10^{-3}
L *[m]*		304.8×10^{-3}	152.4×10^{-3}
δ_{total} *[m]*	w/o Prototype Mass	-1.90×10^{-4}	-1.44×10^{-5}
	w/ Prototype Mass	6.88×10^{-4}	5.62×10^{-5}
σ_{total} *[MPa (ksi)]*	w/o Prototype Mass	39.6 (5.7)	39.5 (5.7)
	w/ Prototype Mass	77.1 (11.2)	53.2 (7.7)

Table 3: Simple Stress Model - Input Values and Results

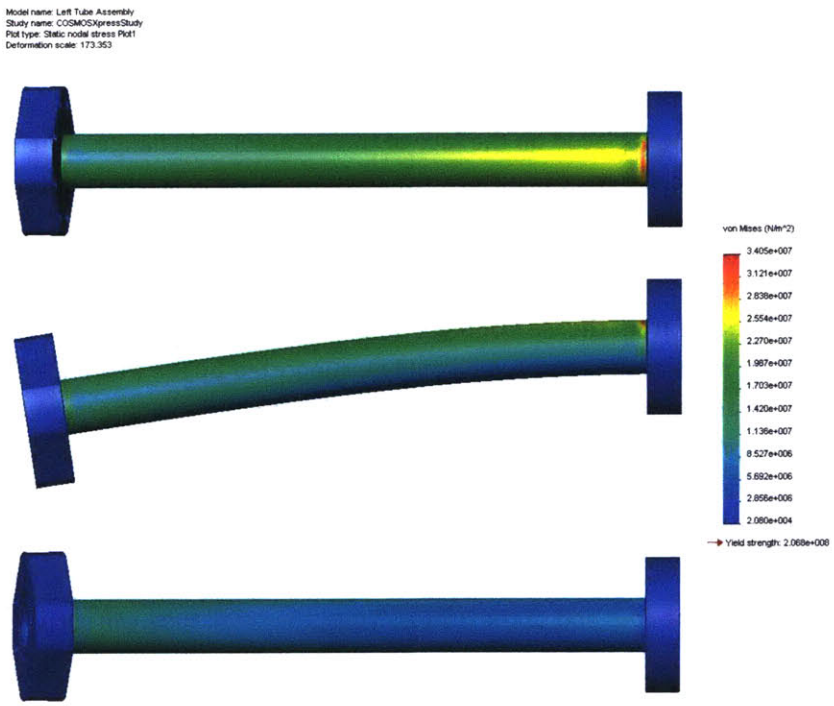

Figure 4-35: From Top to Bottom- Top, Front, and Bottom Views of the Small Thermal Isolation Tube and Flange Assembly Showing Stress Distribution and Exaggerated Deformation

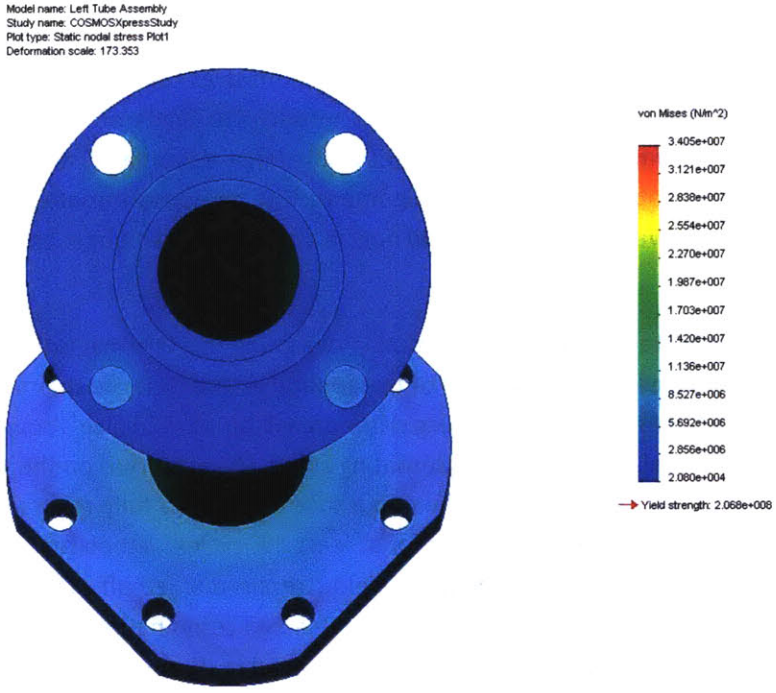

Figure 4-36: Side View of the Small Thermal Isolation Tube and Flange Assembly Showing Stress Distribution and Exaggerated Deformation

The inner surfaces of the bolt holes on the Main Body side of the tube were restrained in this model to give an idea of what stress around these features looks like. A pressure load of 11 bar(g) was put onto the inner surface of the tube, while all other forces, including the axial force on the actuator due to the internal pressure, was placed on the face of the Actuator-side flange. The mesh size was then set to its finest value in order to obtain the most accurate results. The maximum stress calculated for the small tube was 34.1 MPa, or 2.3% lower than the results given by the model above.

The tube may also be subjected to the weight of the entire device during the mounting or dismounting of the prototype from the Ice Confection Tank. In a worst-case scenario, the entire projected 36.7 kg (81 lb) mass of the prototype would be supported by the free ends of the tubes. This could be modeled as an additional tip load in the opposite direction of the others, so that m_{tip} would be the sum of the Actuator, Actuator Flange, and Thermal Isolation Tube Flange weights minus some fraction of the mass of the device given by geometry and the location of the center of mass of the prototype. The solid model of the beta prototype gives the location of its center of mass (l_{COM}) to be 438 mm (17.2") from the free end of the small tube, with a total device length ($l_{t\text{-}t}$) of 772 mm (30.4") from the free end of one tube to the free end of the other. Thus, the small tube will carry $\frac{1+l_{COM}}{l_{t-t}-l_{COM}}$, or 0.433, of the mass of the device if it is being held perfectly horizontally, while the other tube will carry the remainder (0.567).

Adding these loads to the simple displacement and stress models described above gives maximum upwards displacements of 0.051 mm (0.002") and 0.69 mm (0.027") and stresses of 53.2 MPa (7.7 ksi) and 77.1 MPa (11.2 ksi) for the large and small Thermal Isolation Tubes, respectively. COSMOSXpress was used to analyze the solid model of the small Thermal Isolation Tube and Flange as described above after adding this new load. It gave a maximum stress of 77.8 MPa (11.3 ksi), which differs by only 0.8% from the result given by the simple model. The displacements are still small percentages of the piston diameters at 0.2% and 3.6% of the large and small pistons, respectively, and so should not present any problems with piston alignment. The stresses translate to yield safety factors of 5.4 and 3.8, respectively. Verily, yielding should not be a problem even under these severe conditions.

Fatigue life was also taken into consideration in designing the Thermal Isolation Tubes. The tubes are the thinnest, weakest structural parts of the apparatus and thus are the most likely failure points on the device. The conservative Soderberg criterion will be used to give a rough estimate of the fatigue life of this part. For this criterion, the alternating stress (σ_a) is plotted on the y-axis of a chart and the mean stress (σ_m) is plotted on the x-axis. The endurance limit (σ_e), a fully-reversing cyclic stress that a test piece of a material can take without failing for at least 10^8 cycles, is then marked off on the alternating stress axis. On the mean stress axis, the yield stress is marked off. These two points are then connected with a straight line called the Soderberg line. All combinations of mean and alternating stresses that fall on or beneath this line provide infinite fatigue life. (Crandall et al.)

The S-N curve of stainless steel shown in Figure 4-37 does not extend out to 10^8 cycles, making it difficult to obtain an accurate value for the endurance limit. However, one can extrapolate the trend

shown in the current graph to this range, and it is not unreasonable to estimate that the alternating stress causing a failure at 10^8 cycles will be no more than 103 MPa (15 ksi) in magnitude.

The determination of mean and alternating stress is somewhat more precise. This prototype is only meant for one to two production runs of approximately 500 pellets plus initial testing, which is estimated to be about 20 runs of approximately 50 pellets each. The device will thus undergo roughly 2000 pellet creation cycles along with 22 pressure cycles and mounting cycles. In order to obtain a very conservative estimate of fatigue life, the stress range will be set to a value of 77.8 MPa (11.3 ksi) even though most cycles will be far below this number, albeit with a higher mean stress. This gives an alternative stress of 38.6 MPa (5.6 ksi). The mean stress that the piece will experience under these conditions is also 38.6 MPa (5.6 ksi), since the stress will be varying from zero to 77.8 MPa (11.3 ksi) in a cyclic fashion.

When plotted next to the Soderberg Line, it is clear that the current operating point as defined above as a combination of mean and alternating stresses is well within the infinite life range of this criterion. Fatigue is thus not expected to be a problem with this device for any number of cycles, thus clearing it for its expected operational life of 2000 cycles.

Microscopy work performed by Pizzagalli and Baker shows the individual powder particles to have a characteristic length of approximately 5.0×10^{-5} m (2.0×10^{-3} in), roughly equal to the clearance gap size between the pistons and their bores (Pizzagalli, *CO_2 Spray Freezing...* and Baker, Personal Communications). During pellet compression, some particles of powder could be pushed into this gap. A significant amount of powder could build up over several hundred cycles, potentially jamming the device. The CO_2 Flush Flanges are meant to prevent this buildup.

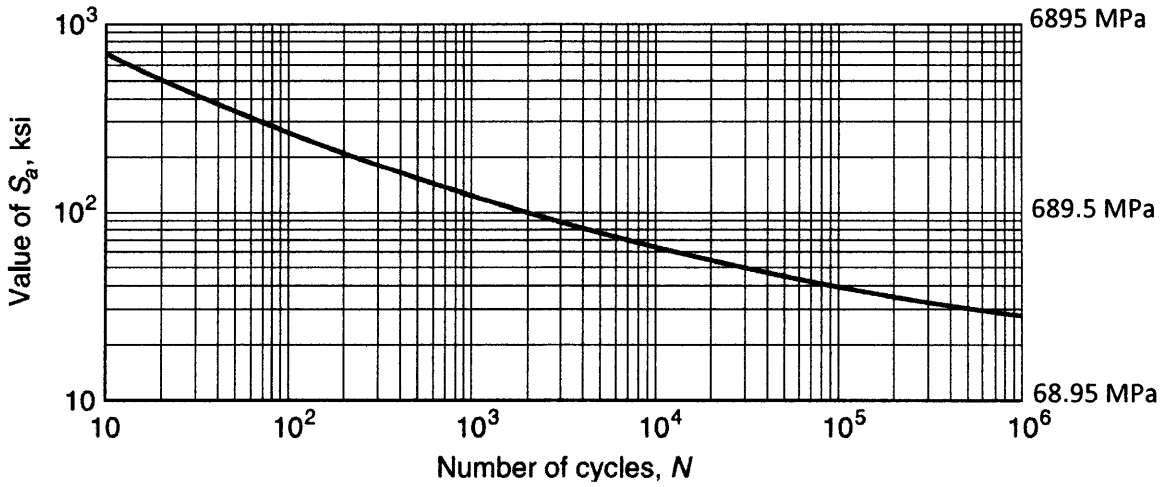

Figure 4-37: S-N Curve for Stainless Steel
Taken from Chattopadhyay. Modified from ASME Boiler and Pressure Vessel Code, ASME, New York.

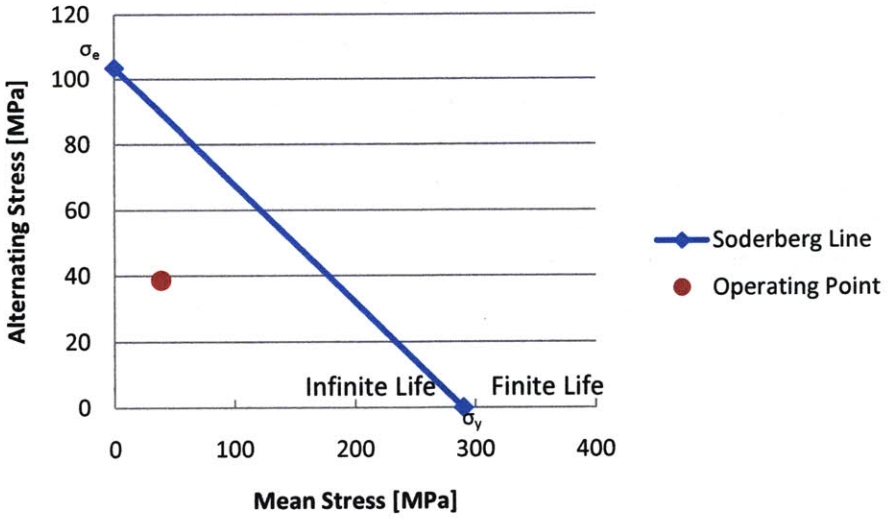

Figure 4-38: Diagram for the Prediction of Fatigue Life

The CO_2 Flush Flanges are mounted between the Thermal Isolation Tubes and the Main Body. Their purpose is to allow the injection of high pressure CO_2 gas into the gap between the piston and bore of the Main Body to flush from this gap any powder that has accumulated. The inclusion of this flushing process into the prototype is meant to be a precautionary measure; at the time of the design and manufacture of these flanges, it was not entirely clear that it would be needed. However, the ability to flush the gaps with CO_2 proved invaluable when powder accumulation proved to be a problem.

The two CO_2 Flush Flanges are shown in Figure 4-39. Each has a hole drilled through its center to allow its piston to pass through them unobstructed. These flanges each have a flush hole drilled radially from their outer to inner diameters to admit the flow of CO_2. The outer end of this hole is tapped to accept a 1/8" NPT fitting, allowing an NPT-to-Swage fitting to be attached to the part to permit the attachment of the necessary CO_2 lines to this part.

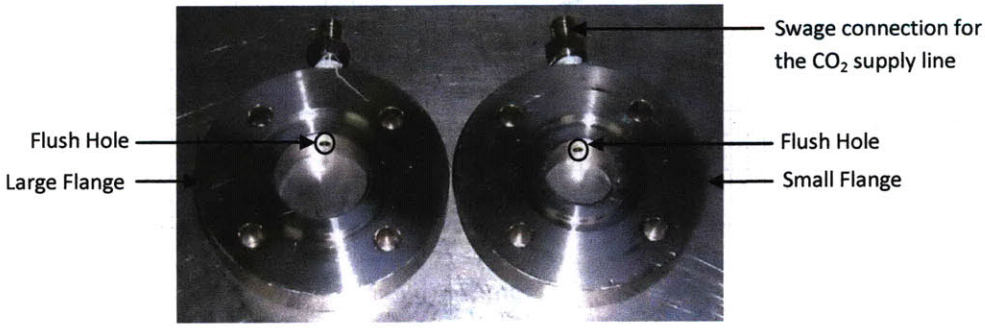

Figure 4-39: CO_2 Flush Flanges

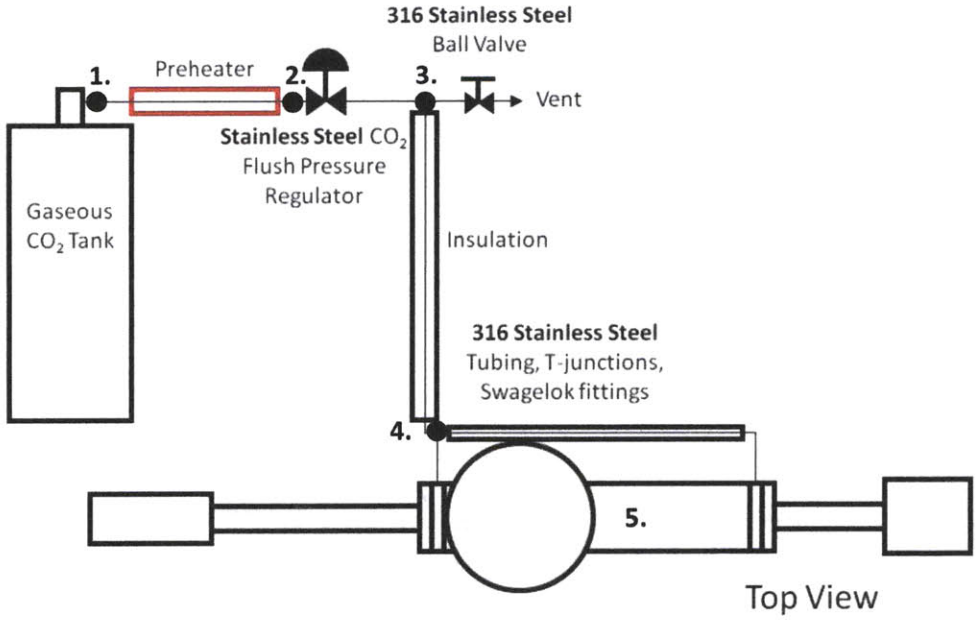

Figure 4-40: Ideal CO_2 Flush Circuit Diagram with Labeled Stations

Ideally, the flush circuit would be set up as shown in Figure 4-40. Gaseous CO_2 would be obtained from a bottle stored at room temperature (293 K) (Station 1). It would leave this tank and pass through a preheater (2), which would warm the CO_2 to a temperature of 302 K (29°C) to ensure that it would remain a vapor when it then passed through a pressure regulator (3). This regulator would drop the pressure of the gas to roughly 0.5 bar above tank pressure, or 10.5 bar in the usual case, to control the flush gas flow rate. The CO_2 gas would flow down a well-insulated tube to a t-junction (4), where the flow would be split between the small and large CO_2 Flush Flanges. At this point, the gas would be injected into the piston-bore gaps and would travel toward the center of the prototype (5), where it would then exit the device through existing vent lines. A valve opening to the atmosphere would be added to the circuit to allow the venting of lines during depressurization of the entire production apparatus. This would prevent situations where the lines remain pressurized due to a blockage in the flush flanges or in the lines themselves, potentially endangering technicians who would be disassembling the device for maintenance and cleaning purposes.

This ideal setup would require the addition of both a second CO_2 circuit and a heating circuit to the current production equipment. Unfortunately, this is something that will take time to implement due to the need to procure both the CO_2 bottle and the heating equipment, which must also pass the sponsor's rigorous safety standards. Therefore, in the interest of both time and in eliminating the additional CO_2 and heating loops in the system, it has been decided to make use of the existing liquid CO_2 source already present.

The diagram in Figure 4-41 shows the flow path of the CO_2 on its way from the tank to the device as implemented at PTC Beauvais. All parts in this line have been made of FDA-approved components with the sole exception of the brass pressure regulator. The carbon dioxide only contacts the regulator for 0.25 seconds, too short a time for harmful contamination to occur (Mazurek).

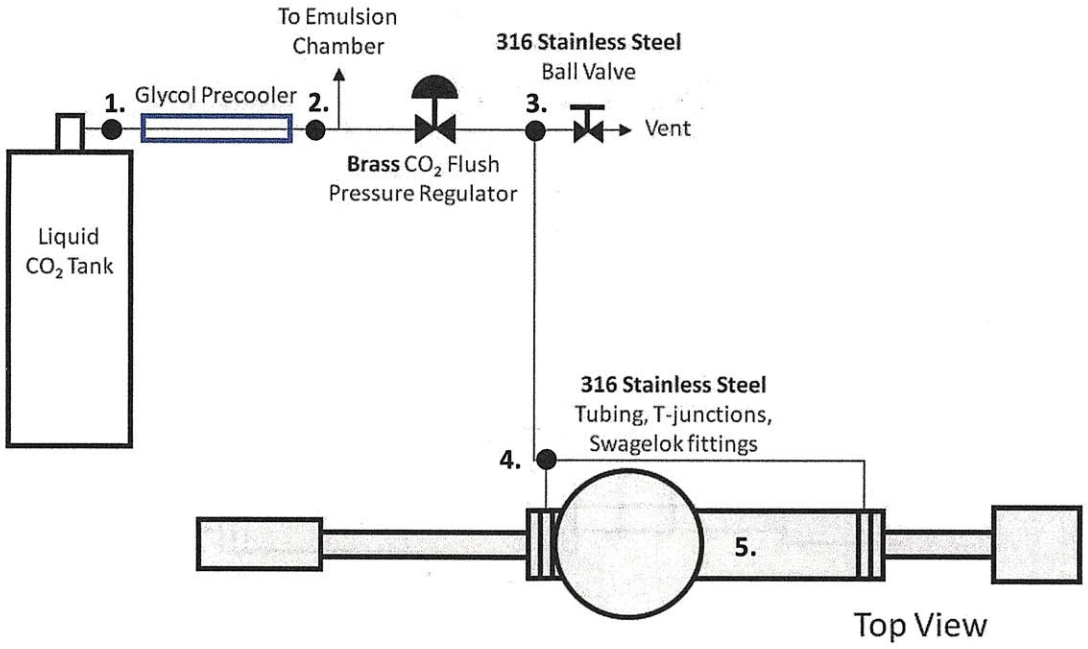

Figure 4-41: Implemented CO_2 Flush Circuit Diagram with Labeled Stations

Liquid CO_2 is taken from a CO_2 tank stored at room temperature (293 K) via a dip tube, so its properties should be those of its saturated state at 57 bar and 293 K (20°C) (Station 1). It then passes through a glycol precooler (2), which lowers the temperature of the CO_2 to approximately 288 K (15°C). After the precooling process, some of the liquid CO_2 is channeled toward the emulsion chamber of the flash freezing apparatus for use in powder production. The remaining CO_2 heads through a pressure regulator (3) and is throttled down to approximately 10.5 bar, or 0.5 bar above the Ice Confection Tank Temperature. The CO_2 then flows down a 6 mm inner diameter stainless steel tube with 1 mm thick walls to a t-junction (4), where its flow is split between the small and large CO_2 Flush Flanges. Once inside the flanges, the CO_2 flows through the gap between their respective pistons and their bores, clearing these gaps of powder (5). The CO_2 then exits the system through one of the existing vent lines.

There was great concern that the carbon dioxide entering the flush flange in this system would be two phase rather than gaseous. It is desired that the bulk of the entering CO_2 be a gas, since it is thought that the presence of liquid CO_2 has a deleterious effect on the process and product, contributing to the formation of excessive amounts of dry ice. Liquid CO_2 may also be less effective than gaseous CO_2 in clearing the gap of accumulated powder. Due to its greater density than the gaseous CO_2 present inside of the device, liquid CO_2 would flow to the bottom of the gap once it enters the flush flange and Main Body. The liquid would likely flush this part of the gap well, but it could leave the top portion clogged with powder.

In order to avoid these potential problems, most of the liquid carbon dioxide obtained from the supply line must then vaporize before it is injected into the gap. The pressure drop through the pressure regulator will vaporize some of the liquid CO_2 despite the use of the precooler, which attempts to ensure that the carbon dioxide remains a liquid through as much of the regulator as possible. There

was some concern as to how the regulator will function when exposed to two-phase flow, but experiments have shown the device to operate satisfactorily under these conditions. More of the CO_2 will vaporize as it flows through the tubing between the regulator and the flush flanges due to inflowing heat, further raising the quality of the flow as it approaches the CO_2 Flush Flanges.

This system was modeled to provide insight on the expected states of the CO_2 as it flowed through the flush line system. Unfortunately, much of the flow through these lines will be two-phase, which is very difficult phenomenon to accurately model. As a result of this difficulty, the outputs of this model were viewed as order-of-magnitude predictions, which should be adequate to determine if flow rates, pressure drop (ΔP), and the quality of the CO_2 (x) are all of reasonable values. Reasonable ranges for these parameters and the methods in which they will be calculated are discussed in more detail below.

The bulk of the heat transfer and phase changing will take place along the approximately 1.5 m stretch between stations 3 and 4, which is uninsulated and fully exposed to the surrounding environment. The 0.08 m and 0.3 m stretches between station 4 and the small and large flush flanges, respectively, will account for a negligible amount of the heat transfer from the environment to the CO_2. Therefore, its thermodynamic state will be relatively unchanged over these lengths. Since this model is only meant to serve as a rough guide, this simplification should still provide enough accuracy to be useful for this purpose.

Although heat transfer past station 4 can be neglected without introducing large errors in the model, flow restrictions cannot be ignored. It is expected that the largest restriction to flow will come from the flow through the clearance gap between the piston and its bore. Therefore, this section must be included in the flow rate and pressure drop models to get accurate estimations of these values.

For two phase flow, the properties of the CO_2 were calculated as the mass weighted average of the liquid and vapor properties of the CO_2. The properties were assumed constant in the tube between stations 3 and 4, calculated at the average quality along this length ($\bar{x} = \frac{x_{initial} + x_{final}}{2}$, where $x_{initial}$ is evaluated at station 3 and x_{final} is evaluated at station 4). Since these properties affect the rate of heat transfer into the system, they affect the final quality and thus affect their own determination. This was handled by iterating through the process until the value of the final quality becomes stable. For the calculation of pressure losses after station 4, the final quality is used to calculate the mass weighted average properties. Though this method is less accurate than one in which the properties are allowed to vary along the flow path, it should be accurate enough to examine the feasibility of this system.

One of the main purposes of the following model was to determine the pressures required to obtain reasonable flush flow rates. In this case, a reasonable flush flow rate would be one that is on the same scale as the 0.003 kg sec^{-1} flow into the Emulsion Chamber during powder production, allowing the use of existing vent lines without any modifications to increase flow capacity. It was hoped that the pressures required to achieve these flow rates was neither too high nor too low. Too high a pressure would require more care to be taken with the tubing and could require bulkier connectors, possibly leading to interference with other parts of the device as well as greatly increasing the risks associated

with part failure. Too low a pressure would make accurate regulation difficult using the manual pressure regulators that are available. A good pressure requirement, then, is somewhere between 0.25 and 5 bar above tank pressure.

The throttling between stations 2 and 3 was assumed to be an isenthalpic process. This is a standard approximation made when analyzing throttled flows, valid because the liquid's residency time in the throttle is not long enough for any significant amount of heat transfer to take place. This assumption allows the calculation of the properties of the flow at station 3. At that point, the flow is 61.7% liquid, 38.3% vapor by mass, and is at a temperature of 234 K. The properties of the fluid at this point ($x_{initial}$) are taken as mass weighted averages of the liquid and vapor properties at the given temperature and pressure state. These values are the initial ones input into the model, used with the calculated final properties to determine the average properties of the carbon dioxide.

The model itself consists of coupled flow and heat transfer models. The mass flow to be examined is set at the beginning of the process, and initial guesses are made as to the value of the final quality (x_{final}) and the regime(s) (laminar or turbulent) of the flow through the tubing and piston-bore gaps. This returns both the rate of heat transfer and the total pressure drop. The rate of heat transfer is used to calculate the final quality, which is then used to calculate the average properties of the flowing CO_2 as described previously. These properties are then input into the pressure loss model to find the Reynolds numbers in the various flow sections, which include the tubing and the gap between the pistons and their respective bores in the Main Body. These Reynolds numbers determine the use of turbulent or laminar friction factor relations in the pipes and piston-bore gaps. The Reynolds numbers are also put back into the heat transfer models, thus changing the calculated value of the final quality and thereby affecting the rest of the calculations. This process is iterated until a stable result is obtained.

The pressure drop model is based on the standard friction factor formulation given in Equation *(18a)*. In that equation, ρ is the density of the flow, which is calculated as a weighted average of gas and liquid densities at the average quality of the flow as described above for calculations between stations 3 and 4, and at the final quality of the flow as calculated at station 4 for press. Velocity is calculated from the mass flow and the density and is used, in conjunction with the averaged properties, in calculating Reynolds numbers. The Reynolds numbers for flow to the large and small pistons after station 4 were calculated separately. Laminar flow was assumed for Reynolds numbers less than 2300, while turbulent flow was assumed for those greater than 4000. For Reynolds numbers between these values, both regimes were examined. In order to calculate these numbers in the piston-bore gap, the width of this gap was assumed as the amount opened by thermal contraction upon cooling the prototype from 293 K (20°C) to 233 K (-40°C) with an additional 0.0254 mm (0.001") added on to account for initial clearance between the piston and the Main Body.

$$\Delta P = f\frac{l}{d}\frac{1}{2}\rho v^2 \qquad (18a.)$$

$$f_{laminar} = \frac{64}{Re_D} \qquad (18b.)$$

$$f_{turbulent} = \left\{-2.0\ log_{10}\left[\frac{\left(\frac{k_s}{d_i}\right)}{3.7} - \frac{4.518}{Re_D}\ log_{10}\left(\left[\frac{\left(\frac{k_s}{d_i}\right)}{3.7}\right]^{1.11} + \frac{6.9}{Re_D}\right)\right]\right\}^{-2} \qquad (18c.)$$

The friction factor given in *(18b)* assumes laminar flow and depends only on the Reynolds number of the flow through the pipe. The one given in *(18c)* assumes turbulent flow and depends on the Reynolds number based on the hydraulic diameter of the pipe and the average roughness of the pipe (k_s). A value of 1.5 μm for this roughness for stainless steel is given in *2.005* by Cravalho et al.

The heat transfer model will first assume that the tubes are uninsulated, which should increase the rate of heat flow into the CO_2 stream. If the model predicts that the liquid CO2 vaporizes quickly and there is a risk of the gas warming excessively before entering the flush flange, then insulation will be added to the tubes between stations 3 and 5 and the model will be updated. Even without insulation, the temperature of the outer diameter of the tube (T_{OD}) should be close to ambient temperature (T_a), allowing radiation to be approximated as linearly dependant on the difference between the two temperatures. This makes it possible to model radiation as a thermal resistance, greatly simplifying the process of determining the rate of heat flow into the CO_2 carried in the pipe. The thermal resistance model for the system is presented in Figure 4-42.

Pressure losses in the large tubes between stations 3 and 4 are expected to be minimal. Since the CO_2 flowing between these is undergoing a phase change at approximately constant pressure, the temperature of the CO_2 (T_{CO2}) is held constant at its boiling point until all of the liquid has boiled off. At a pressure of 10.5 bar, 0.5 bar above the Ice Confection Tank pressure, carbon dioxide boils at 234 K. This sets T_{CO2}, as shown in Figure 4-42.

The heat transfer coefficient between the two phase CO_2 and the inner diameter of the tube (h_{ID}) was calculated using the method developed by Kandlikar as described in Lienhard and Lienhard. In this method, a "liquid only" heat transfer coefficient is calculated using the properties of only the liquid phase, and a correction factor is then applied according to system materials, geometry, and flow and boiling conditions. This method is only recommended for use when qualities are between 0 and 0.8, but has been used for all cases in this analysis. This is not expected to be overly problematic, because the thermal resistance of the system is dominated by the resistance between the outer diameter of the tube and the air. This renders even substantial changes to the heat transfer coefficient between the CO_2 flow and the inner diameter of the tube insignificant.

The Nusselt correlations given in Equation *(19)* were used to determine the "liquid only" heat transfer coefficient. As mentioned, a correction factor is applied to this "liquid only" coefficient to account for the effects of the two phase flow. This correction factor ranges between 11.17 for a mass flow rate of 0.001 kg sec^{-1} and 11.3 for a mass flow rate of 0.005 kg sec^{-1}. The corrected heat transfer coefficient ranges from 360 W m^{-2} K^{-1} at 0.001 kg sec^{-1} to 9100 W m^{-2} K^{-1} for 0.005 kg sec^{-1}. The turbulent flow correlation depends on the friction factor (f) of the pipe, which is given in Equation *(18c)*.

$$\overline{Nu_D} = \frac{h_{ID} l_{tube}}{\bar{k}} = \begin{cases} 3.657 & laminar \\ \dfrac{(f/8)(Re_D - 1000)Pr}{1 + 12.7\,(f/8)^{1/2}(Pr^{2/3} - 1)} & turbulent \end{cases} \qquad (19)$$

The heat transferred from the CO_2 to the inner wall of the tubing is then conducted through the tube wall to the air of the ambient environment. Heat transfer from the outer diameter of the tube to the environment occurs via a combination of condensation and natural convection. Assuming a heat transfer coefficient equal to that given by the condensation relation in Equation *(12a)*, the rate of heat flow into the system is 178.5 W. However, when assuming condensation the temperature of the outer diameter of the tube is calculated as 292 K, significantly higher than the 277 K saturation temperature of the air in the room. The Rayleigh number of the pipes is 735, making Equation *(11a)* an appropriate choice for the calculation of the natural convection heat coefficient. The natural convection relation results in a heat flow of 58.8 W. With this heat transfer coefficient, however, the T_{OD} is calculated to be 253 K, well under T_{sat}. Due to the competing effects of these two modes of heat transfer, it is assumed

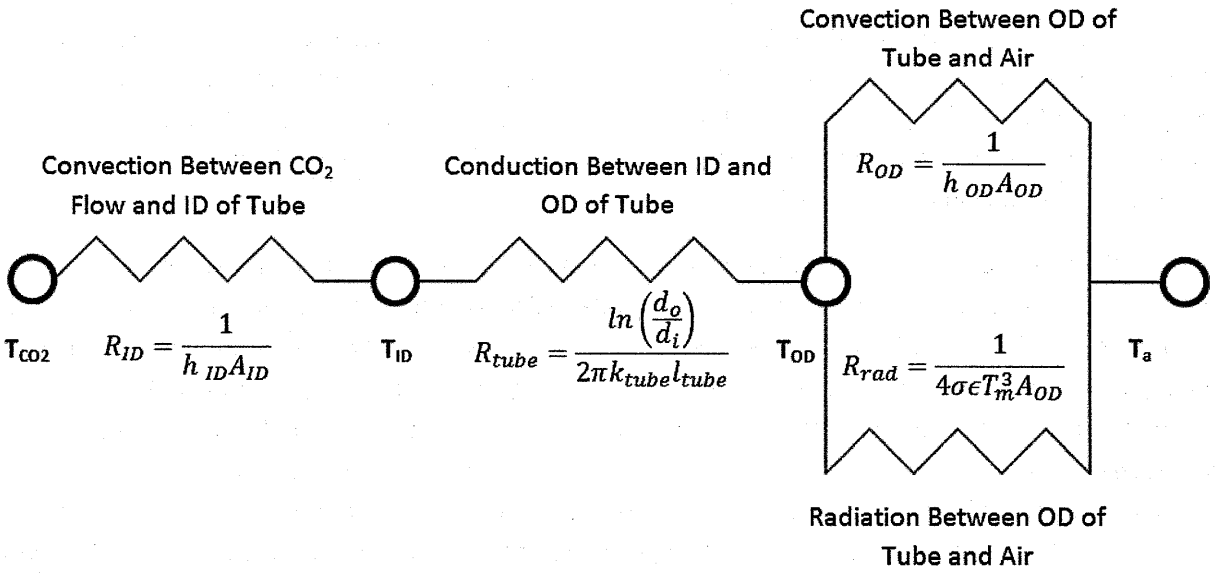

Figure 4-42: Thermal Resistance Model for Heat Transfer between CO_2 Flow in a Cylindrical Tube and the Ambient Environment

that T_{OD} will be held constant at the saturation temperature of the air, as any perturbations from this value will move the system to a heat transfer regime that would return it to that temperature. The heat flow into the system is thus calculated as shown below in Equation *(20)*:

$$\dot{Q} = (R_{ID} + R_{tube})^{-1} (T_{sat} - T_{CO2}) \qquad (20)$$

The model predicts that the CO_2 entering the apparatus will be completely vaporized for all cases examined. In fact, it predicts that a mass flow of 0.033 kg sec^{-1} will be required before the quality of the CO_2 at station 4 will fall below unity, which would require a supply pressure of 153 bar, 143 bar over the 10 bar operating pressure of the tank. This is far beyond the capability of the current CO_2 supply system, which can provide a maximum pressure 50 bar over operating pressure, so it is unlikely that the injection of liquid CO_2 is a problem. As depicted in Figure 4-43, a pressure drop in the range of 0.25 bar to 5 bar provides a mass flow of several grams per second, closely approximating the 0.003 kg sec^{-1} already entering the system as part of the powder production process. Thus, it is unlikely that use of this system would overwhelm the current venting system when in use for any reasonable overpressure. These results showed that the use of a CO_2 flush system to keep the piston-bore gaps free of powder was certainly feasible, leading to its implementation on the beta prototype. This system saw further testing during trials to determine its effectiveness. The results of these tests are described later in this chapter.

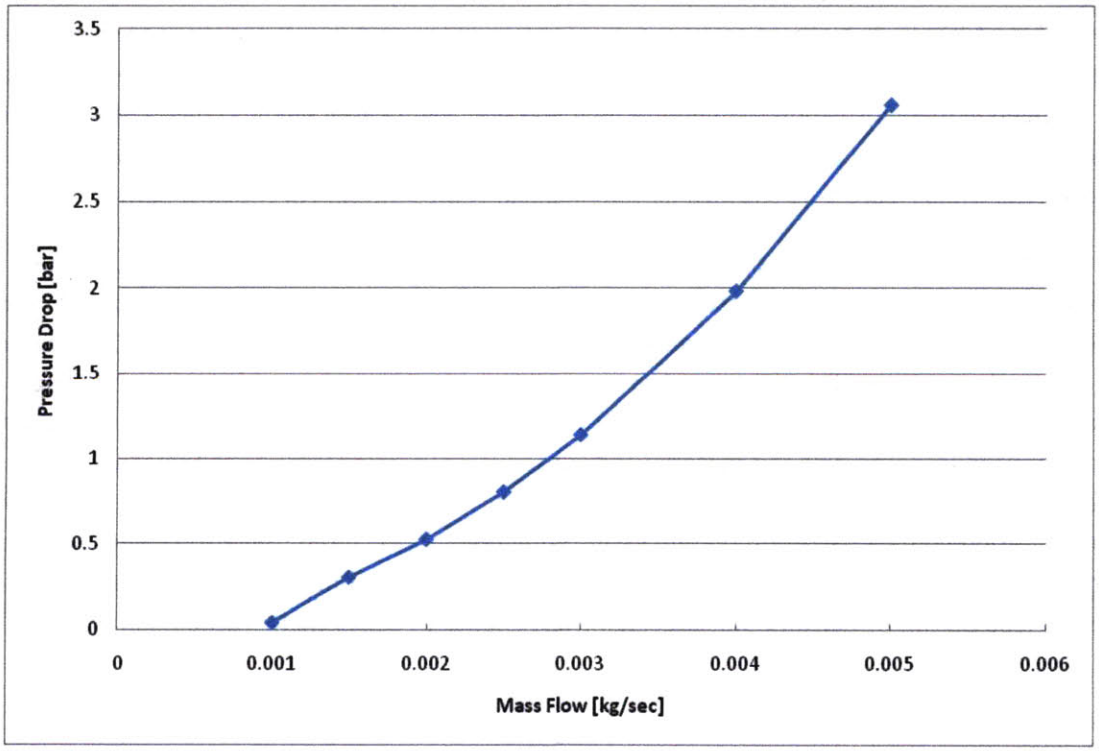

Figure 4-43: Pressure Drop Through the CO_2 Flush Line as a Function of Mass Flow

4.1.3. Thermal Management

The improvement in active thermal management of the beta prototype is one of its most significant advancements compared to the alpha prototype. This device has been designed from the start with thermal management in mind, leading to the development of an integrated system. This system is comprised of two semi-circular copper sheets that fit around the Upper Funnel and two copper plates that sit on either side of the Main Body. The Collection Container, with its large surface area and its exposed location, was also considered as a candidate for a cooling plate, but it was decided to forgo this added complication at this time. The container holds pellets, which can withstand heat shock far better than the powder can and do not experience the flow difficulties at temperatures between 253 K and 273 K (-20°C and 0°C) that the powder does. Therefore, as long as its temperature can be maintained below 273 K for the duration of a trial, the container should be able to perform its function adequately. The container is cooled before the trial starts, and it is wrapped in insulation to limit warming during the trial.

Copper tubes are used to circulate the refrigerant around the device and were soldered onto the copper sheets and plates described above. Copper was chosen for its high coefficient of thermal conductivity, allowing cooling to take place evenly over the covered surfaces of the device despite the refrigerant being constrained in narrow tubes. The copper tubes and sheets around the Upper Funnel conform to the curvature of its outer diameter, while the plates on the sides of the Main Body have been cut to match its features. The two halves of the Upper Funnel loop are held to the funnel by a hose clamp and are connected in series by a u-shaped connector piece. The side loops are attached to the side of the Main Body by three screws each, as shown in Figure 4-21. These loops are connected in series to the Upper Funnel by a plastic tube and to each other by a piece of copper tubing, which has been wrapped in foam insulation to minimize heat leakage. Figure 4-44 below shows a picture of the actual system mounted on the beta prototype, Figure 4-45 shows a schematic of the loops as installed on the device, while Figure 4-46 shows a flattened, linear representation of the flow path.

Despite its advantageous thermal properties, the use of copper does raise potential issues. In the United States, the metal is not recommended for use with foods having a pH under six and is not allowed for use with food products in France, the final destination of the device (FDA, 2005; Mazurek). Since our product is generally acidic, care has been taken to avoid any contact between the copper coolant system and the mix, powder, or pellet. Copper is only utilized on external components, so there is no risk of product contacting this material and subsequently passing through to the consumer. Copper is corrosion resistant, nonabsorbent, and smooth, thus meeting the FDA guidelines for materials used in non-food-contact parts of food processing equipment (FDA, 2005). Silver-tin solder was used to attach the copper tubing to the copper plates rather than the more common lead-tin solder, avoiding any use of lead on this device and thus precluding any chance of heavy-metal contamination of the food.

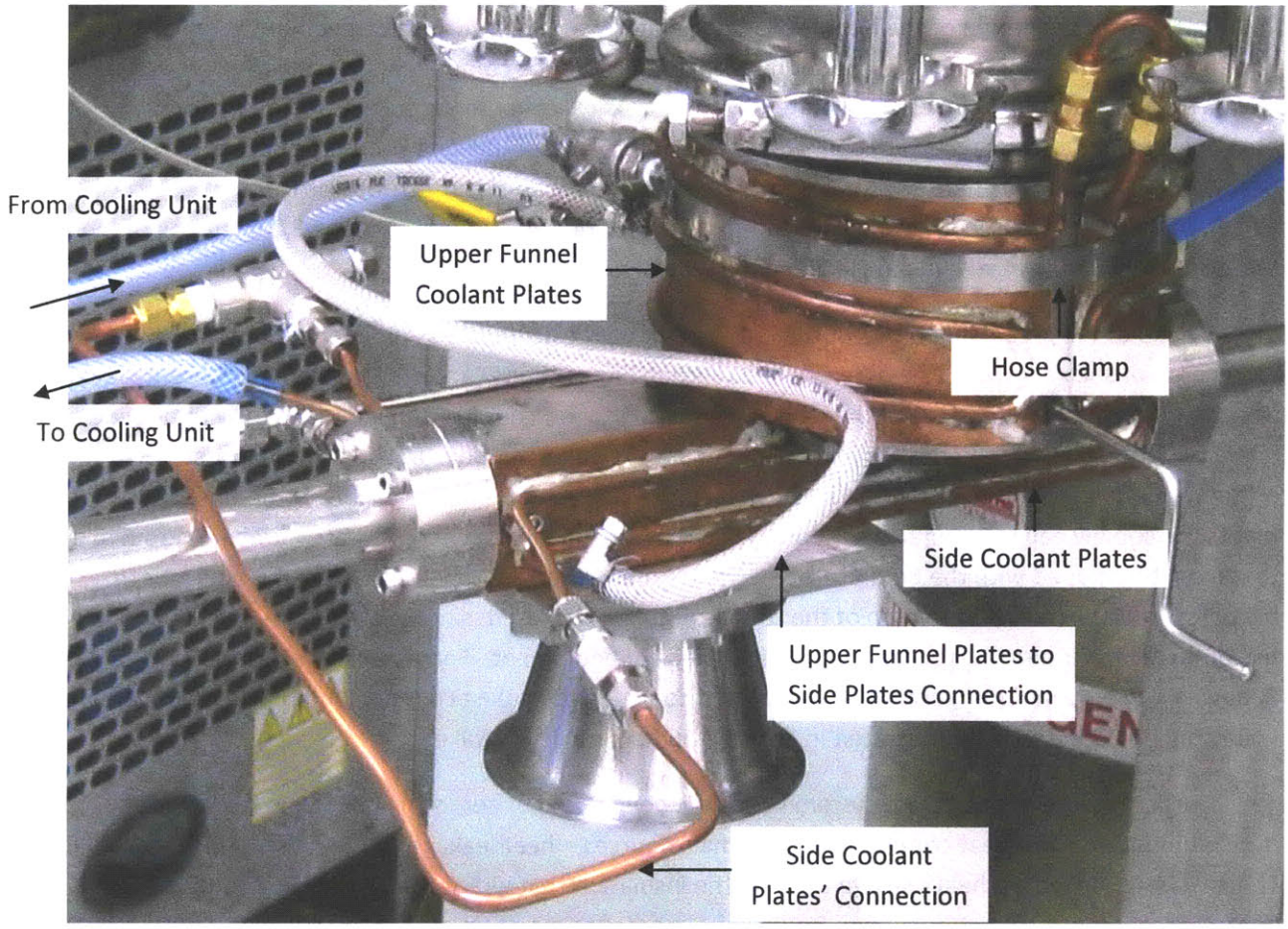

Figure 4-44: Picture of Coolant Loops Installed on the Beta Prototype in PTC Beauvais

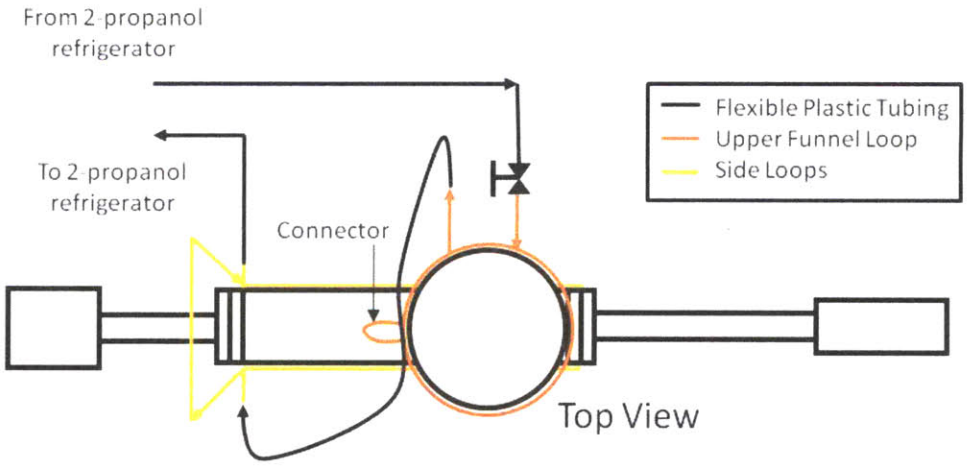

Figure 4-45: Schematic of Cooling System as Installed in PTC Beauvais

The physical design of the heat exchanging plates was largely driven by geometric constraints. The shapes and areas of the plates are set by the geometry of the components that lie beneath them. The paths and sizes of the tubes are dictated by their physical constraints, such as bending radius, physical size, and interference with connectors and other parts of the beta prototype, as well as by a desire to keep them as simple as possible in order to expedite the manufacturing process. Thus, the Upper Funnel loops consist of three back-and-forth passes of 1/4" tubing, while the 3/16" tubing of the side plate loops only make two passes along the plate.

One of the greatest benefits of the inclusion of heat exchangers as independent parts is the modularity of such a layout. The different heat exchanging sections can be connected in different ways depending on the requirements of the device, and each section could be run independently to provide finer control over the temperatures in the Upper Funnel and Main Body. Lacking an integrated refrigeration system, this layout allows the use of any such system that is available at the time and meets the cooling capacity requirement of this device. This flexibility decreases the number of items that must be shipped with the beta prototype. It also decreases the time it takes for the operator to become familiar with the operation of the refrigeration system used, since it will be one that he or she has on-hand and is already a somewhat familiar piece of equipment. For installation and use in PTC Beauvais, a 2-propanol refrigeration unit provided coolant and cooling capacity, and the coolant plates were connected in series as illustrated in Figure 4-46 for simplicity's sake.

The thermal management system keeps the device cool by removing heat from the device during operation. This heat comes from three main sources – heat leakage through the uninsulated Thermal Isolation Tubes, heat leakage through the insulation that wraps the rest of the prototype, and heat generation due to friction within the device. In order to maintain adequate control over the temperature of the prototype, the cooling loops must be matched to a cooling unit with adequate capacity to deal with this amount of heat extraction at a temperature of 233 K (-40°C).

The first heat sources examined are the Thermal Isolation Tubes. A heat transfer model has been built for these tubes and is described in some depth above. The results of this model can be found in Table 2, which has been reproduced here. In order to obtain a conservative estimate of the heat leakage through these tubes, the heat flows given by the Condensation model have been taken for use in determining the cooling capacity requirement. This equates to a heat flow of 73 W.

The next heat source analyzed is the leakage into the device from the outside environment, excluding the Thermal Isolation Tubes, which have been dealt with separately. This heat flow is due to the combined effects of convection and radiation. In calculating this heat flow, it was assumed that all parts

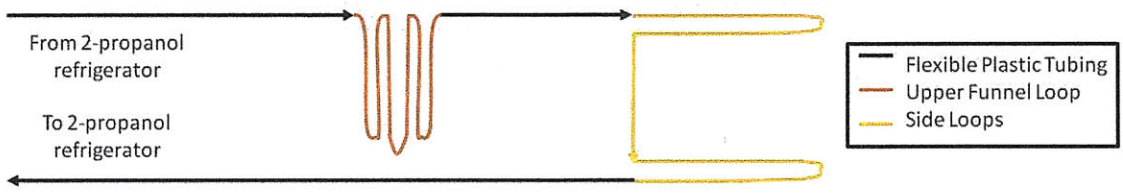

Figure 4-46: Flattened Flow-Path Schematic of Cooling System as Installed in PTC Beauvais

	Small Tube			Large Tube		
	L_{iso} [mm]	L_{tube} [mm]	$\dot{Q}$ [W]	L_{iso} [mm]	L_{tube} [mm]	$\dot{Q}$ [W]
Natural Convection	142	382	2.8	144	216	3.6
Mixed	91	331	24	95	167	36
Condensation	12	252	32	13	85	41
Average	82	322	20	84	156	26

Table 2: Summary of the Results of Thermal Isolation Tube Heat Transfer Models

are covered by an insulating foam, such as expanded polystyrene, and that the temperature of all parts is 253 K (-40°C) just inside this foam. Calculations have been carried out for both 12.7 mm (0.5") and 25.4 mm (1") of foam to give an idea of the marginal improvement of additional insulation. Natural convection was assumed and air properties were evaluated at 263 K, the average temperature between the 233 K part temperature (T_{part}) and the 293 K air temperature (T_a). All heat transfer relations have been taken from Lienhard and Lienhard, 2008.

The heat flow can be solved for by using a simple thermal resistance model. Heat flows from the air into the insulation via radiation and convection and is then conducted through the insulation and into the prototype. All parts of this device can be adequately modeled as either flat plates, cylinders, or a combination thereof. This affects the choice of conduction and convective heat transfer coefficient relations, as shown in Equation *(21b)* for the case of conduction and explained in greater detail below for the more complicated case of convection.

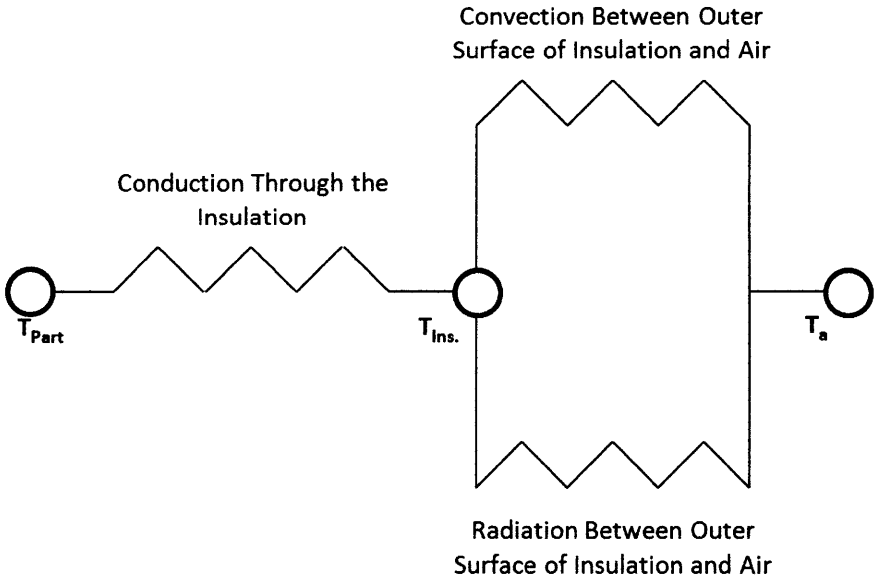

Figure 4-47: Thermal Resistance Model for Heat Transfer between an Insulated Apparatus and the Ambient Environment

$$\dot{Q}_{in} = [R_{cond} + (R_{rad}^{-1} + R_{conv}^{-1})^{-1}]^{-1}(T_a - T_{part}) \quad (21a.)$$

$$R_{cond} = \begin{cases} \dfrac{t_{ins}}{k_{ins}\, A} & plate \\ \dfrac{ln\left(\frac{r_o}{r_i}\right)}{2\,\pi\, k_{ins}\, l} & cylinder \end{cases} \quad (21b.)$$

$$R_{rad} = \frac{1}{4\,\varepsilon\,\sigma\, T_m^3\, A} \quad (21c.)$$

$$R_{conv} = \frac{1}{\bar{h}\, A} \quad (21d.)$$

The device is assumed to be a black-body for the purposes of determining the heat transfer rate due to radiation. As before, the mean temperature (T_m) between the outer surface of the insulation and the air is calculated iteratively, with an initial guess being made at the start and then refined using the model's output. This same initial guess is used in initial calculations of the Rayleigh number of the modeled part, given below as a reference. Again, g is acceleration due to gravity, β is the coefficient of thermal expansion for the air, α is the thermal diffusivity of the air, ν is the kinematic viscosity of the air, ΔT is the difference between the temperature of the outer surface of the insulation and the temperature of the air, and x is a characteristic length dependent on the geometry of the system.

$$Ra_x = \frac{g\,\beta\,\Delta T\, x^3}{\alpha\,\nu}$$

The calculation of heat flow into the prototype due to convection is split up into three separate categories in order to match the three separate geometrical conditions present. These categories – convection off a vertical cooled plate, convection off the top of a cooled plate, and convection off the bottom of a cooled plate – are analyzed separately in order to calculate the heat flow into each respective part. The results of these analyses are then combined in order to provide an estimate of the total heat flow into the device. As with the Thermal Isolation Tubes, the temperature of the room was assumed to be 293 K with a dew point (T_{sat}) of 277 K, the average dew point at Charles de Gaulle airport, roughly 40 miles southeast of Beauvais, during December and January from 1997 to 2007 (Weather Underground). The heat transfer coefficient given by condensation is great enough to pull the temperature up to this saturation in all cases analyzed, so 277 K is taken as a floor for T_{ins} and heat flow is calculated accordingly.

Convection from a cooled vertical plate can be used to model both the flat sides of the Main Body as well as the vertical rounded sides of the cylindrical Upper Funnel and Container. The Lower Funnel, with its sides inclined at an angle of 15° from vertical, can also be modeled using these correlations, but *g* must be replaced by *g cos(θ)* in the Rayleigh number for this case of a non-vertical wall. The Nusselt correlation given below was used to calculated the heat transfer coefficient for this case.

$$\overline{Nu}_L = 0.678\, Ra_L^{1/4} \left(\frac{Pr}{0.952 + Pr}\right)^{1/4} \qquad (22)$$

The exposed flat bottoms of the Main Body, Upper Funnel, and Container can be modeled using correlations describing convection from the bottom of a cold plate. This relation relies on a characteristic length L^* defined as *A/P*, or the area of the surface on which convection is taking place over its perimeter. The Nusselt numbers, calculated as less than ten for these cases, suggest that the boundary layers will be thick. In order to account for this effect, a correction is performed on the calculated Nusselt number, and this corrected number is used to calculate the heat transfer coefficient (Lienhard). Both equations are given below.

$$\overline{Nu}_{L^*} = \frac{0.560\, Ra_{L^*}^{1/4}}{[1 + (0.492/Pr)^{9/16}]^{4/9}} \qquad (23a.)$$

$$\overline{Nu}_{corrected} = \frac{1.4}{\ln\left(1 + 1.4\sqrt{\overline{Nu}_{L^*}}\right)} \qquad (23b.)$$

A correlation for natural convection off the top of a cooled plate will be used to model heat transfer from the exposed upper surface of the Main Body. For this feature, the characteristic length is taken to be the length of the shorter side, or 51 mm (2").

$$\overline{Nu}_L = 0.58\, Ra_L^{1/4} \qquad (24)$$

Using these equations and the iterative method described previously, convection and radiation are found to account for 17 W of heat leakage if 25.4 mm (1") of foam insulation is assumed while accounting for 28 W if the insulation is only 12.7 mm (0.5") thick. The larger rate of heat transfer will be assumed to determine the required cooling capacity of a refrigeration unit. The results of the analyses performed on the three different cases of heat transfer are summarized below in Table 4, separated by case to show the relative importance of each area examined.

The final source of heat is friction. This friction is caused by the rubbing of the pistons and the powder on the inner surface of the bore of the device as they are moved back and forth by the actuators. In order to estimate this heating, a couple simple assumptions are made. The piston is

Insulation Thickness [mm]	12.7	25.4
Sides [W]	24	14
Bottom [W]	3.2	1.8
Top [W]	0.77	0.44
Total [W]	28	17

Table 4: Heat Transfer Rates due to Convection and Radiation
Note: Values may not add to the correct total due to rounding.

assumed to support its entire weight ($m_{pist}\,g$) on the bore through the Main Body. The coefficient of friction between Delrin, the pistons' material, and stainless steel, the Main Body's material, is 0.35 (DuPont). The powder is assumed to present a frictional force of 100 N (F_{powder}) throughout the compression process, a number that was obtained through experiments in which the powder was compressed in a stainless steel cylinder. The cylindrical pellet formed could withstand a force of approximately 100 N before dislodging. Although the powder will not apply a force of this magnitude on the piston during the portions of the stroke before it has been solidly compressed, the use of this value should provide a conservative estimate of the average frictional force exerted by the powder on its surroundings.

$$\dot{Q}_f = \sum_{i}^{small\,,large} \frac{\mu_{d-ss}\, m_{pist\,,i}\, g\, 2s_i}{t} + \frac{F_{powder}\; s_{small}}{t} \qquad (25)$$

In Equation *(25)*, $\mu_{d\text{-}ss}$ is the coefficient of friction between Delrin and stainless steel, m_{pist} is the mass of the piston in question, g is the acceleration due to gravity, s is the stroke of the given piston, and t is the total cycle time, taken as one second in this case. The first term gives the frictional heating due to the pistons rubbing on the inner surface of the bore, which is experienced by the small and the large pistons. The second term gives the heating due to friction between the powder and the bore occurring during the compression and ejection stroke of the small piston. The total heat flow due to friction is 12 W.

The rates of heat transfer from the three major heat sources examined above are summarized below in Table 5. These represent the worst possible cases analyzed and so should provide a conservative figure for cooling unit specification. The calculated heat transfer rate can be used along with known heat exchanger geometry to determine the entrance temperature, mass flow, and coolant pressure required of the refrigerant system.

To determine the heat transfer rate from the refrigerant to the beta prototype, it has been assumed that the copper heat exchanger plates are held at a constant temperature of 233 K (-40°C) at all points on their surface, mirroring the assumption made in calculating the heat leakage into the device from the environment. From this assumption, Equations *(26)* and *(27)* have been derived. Equation *(26)* gives the bulk temperature of the fluid as it travels through the coolant loops assuming a constant heat transfer coefficient, while Equation *(27)* gives the total rate of heat transfer out of the fluid. It is assumed that c_p for the refrigerant does not vary with temperature. The initial temperature of the

Heat Source	Heat Transfer Rate [W]
Thermal Isolation Tubes	73
Convection/Radiation	28
Friction	12
Total	114

Table 5: Summary of Heat Sources
Note: Values may not add to the correct total due to rounding.

refrigerant, T_{in}, is set by the refrigeration unit used with this device, while the wall temperature, T_{wall}, has been set to 233 K (-40°C) by the assumption given above. The outlet temperature, T_{out}, is calculated by evaluating *T(x)* at the end of the refrigerant loop. The mass flow of the refrigerant, $\dot{m}$, is set by the combination of the maximum pumping pressure of the specific refrigeration loop and the pressure loss through the heat exchanger tubes, given by Equation *(18)* above. The average heat transfer coefficient, $\bar{h}$, is calculated through the process described below.

$$T(x) = (T_{in} - T_{wall})\, e^{\frac{\bar{h}\,\pi\, d_{i,tube}}{\dot{m}\, c_p}x} + T_{wall} \qquad (26)$$

$$\dot{Q} = \dot{m}\, c_p\, (T_{in} - T_{out}) \qquad (27)$$

Thermal entry length, given by Equation *(28)* which has been reproduced below, is likely to be long in comparison to the total tubing length for this refrigerant system. On an order of magnitude basis, the Prandtl number for refrigerating liquids ranges from 10^1 for alcohols to 10^3 for the more viscous glycol mixtures. Reynolds numbers will vary in the 10^0 to 10^2 range for the refrigerants being examined. This means that the entry length will be on the order of 10^1 diameters in length. The total length of the system is on the order of 10^2 diameters long, so the entry length will be around 10% of the total length of the system.

$$\frac{x_{el}}{d_{i,tube}} = 0.034\, Re_D\, Pr \qquad (28)$$

Consideration of this entry length is important because heat transfer is enhanced within this region. In order to account for this enhancement, a Nusselt correlation for a constant wall temperature relying on the Graetz number has been chosen. This correlation, as well as that for the Graetz number, is given in Equation *(29)*.

$$\overline{Nu}_D = 3.657 + \frac{0.0668\, Gz^{1/3}}{0.04 + Gz^{-2/3}} \qquad (29a.)$$

$$Gz = \frac{Re_D\, Pr\, d_{i,tube}}{x} \qquad (29b.)$$

	T_{device} [K]	T_{in} [K]	$\dot{Q}$ [W]	$\dot{m}$ [kg/sec]	$\dot{V}$ [L/min]	ΔP [bar]
2-propanol	233	198	114	0.002	0.15	1.8
	253	198	79	0.001	0.04	0.51
	233	213	114	0.007	0.52	2.7
	253	213	79	0.001	0.06	0.33

Table 6: Coolant Model Results for 2-propanol

These relations are all strongly dependent on the properties of the refrigerant used and so must be reexamined for each choice of refrigerating fluid. As an example, the results of this model for a system utilizing 2-propanol (CAS# 67-63-0) as a refrigerant are given in Table 6: Coolant Model Results for 2-propanol for four different cases. The first four of these cases examine performance at the lower and upper limits of the temperature of the device (T_{device}), assuming an inlet refrigerant temperature (T_{in}) of 198 K (-75°C) for the first two and 213 K (-60°C) for the final two cases. Volumetric flow is also provided, as this is generally a value given in the technical data sheets of refrigeration units and so is a more useful quantity in specifying refrigeration units. Equations for the temperature-dependent properties of 2-propanol were obtained from *Chemical Properties Handbook*, 1999 edition (Yaws, 1999).

4.2.Trials and Discussion

The beta prototype has been tested at both MIT and PTC Beauvais. For these trials, the pellet forming device was attached to the Ice Confection Tank and cooled down to approximately 258 K (-15°C) using its Thermal Management system before the normal precooling and pressurization process was undertaken for the main production equipment. After the precooling step, powder production was started after the pellet forming device's coolant temperature stabilized to ensure that it had reached its lowest possible temperature. Once powder production was started, the Agitator was manually operated and the pistons were actuated using a hand-operated pneumatic circuit. After approximately five minutes at MIT or ten minutes at PTC Beauvais, powder production was halted, the production apparatus vented of all pressure, and the Container removed from the prototype in order to examine its contents.

A Thermo Haake DC50-K75 cryostat bath was chosen for use with this device. This circulator can attain refrigerant temperatures down to 198 K (-75°C) and is rated for 280 W of cooling capacity at 293 K (20°C), meeting the 233 K (-40°C) and 114 W temperature and cooling load requirements of the prototype (Thermo Fisher, 2009).

4.2.1. Initial Observations

During the trials, the prototype held pressure up to 11 bar, the maximum attempted, with no leaks. The dynamic seals of the actuators withstood this pressure without any obvious adverse effects. The pistons moved at approximately the same speed with the device under pressure as they had before the tank was pressurized. This suggests that the seal was not causing any marked increase in friction on the piston despite its exposure to a reversed pressure differential close to the quoted 12 bar(g) limit of the seal (Festo).

The decreased weight of the device was immediately noticeable from the start of the trials both at MIT and Beauvais. Its mass is approximately 16 kg less than that of the alpha prototype, falling to approximately 34 kg not including the Collection Container, which is usually mounted to the rest of the prototype after the device has been attached to the tank. The machine could now be moved by hand and could be mounted without the use of the clumsy cart required by the alpha prototype (see Figure 3-7 for a description of this cart). Furthermore, fully half of this mass comes from the 17 kg Upper Funnel, which was taken from the alpha prototype and reused in order to save time. If this part could be redesigned and remade, a large percentage of the beta prototype's weight could be removed with minimal impact on performance and safety.

A separate cooling trial was held for the prototype, in which the coolant system was activated and allowed to run while the device was sitting on a bench. During this trial, the temperature of the inner wall of the Upper Funnel, corresponding to T_{wall} in Equation *(26)* once the system has reached thermal equilibrium, stabilized at a minimum to 258 K (-15°C) after two hours of precooling. The coolant system outlet temperature, equivalent to T_{in} in both Equations *(26)* and *(27)*, reached a limit of 238 K (-35°C).

The inability of the refrigeration system to lower the temperature of the refrigerant below 238 K (-35°C) suggests that the cooling load placed on the refrigeration system outstripped its capacity. This is due to both increased load and depressed cooling capacity compared to the design specifications. The 114 W load from the prototype itself is augmented by additional load coming from an unmodeled portion of the refrigeration loop. The two meter long inlet and outlet hoses attaching the circulation unit's feed and return lines to the inlet and outlet lines of the heat exchangers on the prototype itself were not included in the model because they were expected to be shorter. Unfortunately, space constraints forced the usage of this extended tubing, which were covered in 6.4 mm thick expanded polystyrene foam insulation. The addition of these tubes into the model, using Equation *(29)* to calculate the fluid-tube heat transfer coefficient, assuming a convective heat transfer coefficient of 8 W m^{-2} K^{-1}, and treating radiation as a thermal resistance as described in Equation *(21c)*, yields the following equation for the temperature profile in the tubes:

$$T(x) = (T_{in} - T_a)\, e^{-\frac{R_{total}^{-1}}{\dot{m}\, c_p} x} + T_a \qquad (30a.)$$

$$R_{total} = \frac{1}{h_i\, \pi\, d_i} + \frac{ln\left(d_{o,tube} / d_{i,tube}\right)}{2\, \pi\, k_{tube}} + \frac{ln\left(d_{o,ins} / d_{o,tube}\right)}{2\, \pi\, k_{ins}} + \frac{1}{(h_o + 4\, \varepsilon\, \sigma\, T_m^3)\, \pi\, d_{o,ins}} \qquad (30b.)$$

Equation *(30a.)* gives the temperature profile in the tube. The temperature T_{in} in this equation is equal to the temperature of the refrigerant leaving the circulating unit. The temperature of the coolant at the end of the two meter long tube is given by setting x equal to two meters in Equation *(30a.)*, and this temperature then becomes the inlet temperature of the rest of the cooling circuit as

	T_{device} [K]	T_{in} [K]	$\dot{Q}$ [W]	$\dot{m}$ [kg/sec]	$\dot{V}$ [L/min]	ΔP [bar]
2-propanol	233	198	185	0.003	0.21	1.8
	253	198	136	0.001	0.07	0.33
	233	213	179	0.009	0.61	2.9
	253	213	131	0.001	0.10	0.31
	258	238	112	0.003	0.25	0.34

Table 7: Coolant Model Results for 2-propanol, Extra Tubing Model

before. The outlet temperature of the cooling circuit becomes the inlet temperature for the return tube, and the same analysis is performed on the return tube to determine the outlet temperature of that stretch of tubing. The results of this analysis are shown in Table 7.

The addition of the tubing to the model does add a significant amount of cooling load to the various models. However, the observed case, shown on the last row of Table 7, is still far below the rated 280 W capacity of the circulating unit. It is believed that this capacity was reduced through the use of a plastic sheet to cover the cryostat to protect it from water. Concern was voiced over the possibility of water entering the device through its ventilation holes during a trial, and so these holes were loosely covered by a plastic sheet. This sheet restricted airflow into the machine, effectively raising its environmental temperature. This has a deleterious effect on system performance, greatly limiting the cooling effect it can provide.

During the powder producing trials held with the device mounted to the Ice Confection Tank, the inlet refrigerant temperature fell to between 233 K and 228 K (-40°C and -45°C). This corresponds to cooling circuit wall temperatures of 256 K (-17°C) and 254 K (-19°C), respectively, according to the model above, higher than the 253 K (-20°C) maximum specified prototype temperature. Measurements were unable to be made of the internal temperature of the device during a trial, while temperature readings taken immediately after a trial has been run are skewed by the cooling effects of depressurization.

It is important to note, however, that the interior of the prototype is cooler than the exterior of the prototype once a trial has started due to the 233 K (-40°C) temperature of the precooled Ice Confection Tank. The interior of the prototype, especially the interior surface of the Upper Funnel, will be cooled by a combination of convection to 233 K (-40°C) CO_2 gas and radiation to the 233 K (-40°C) ICT. During precooling trials, it was common to see a several degree temperature difference develop between the outer and inner surfaces of the Upper Funnel during initial stages of the precooling process. It is reasonable to assume that there is a similar temperature gradient occurring due to the cooling effects described above, and so it is likely that the true internal temperature of the prototype is close to or even below its 253 K (-20°C) design value.

The thermal management of the Collection Container was handled differently at MIT and at PTC Beauvais. During trials taking place at MIT, the Collection Container was manually cooled by pouring

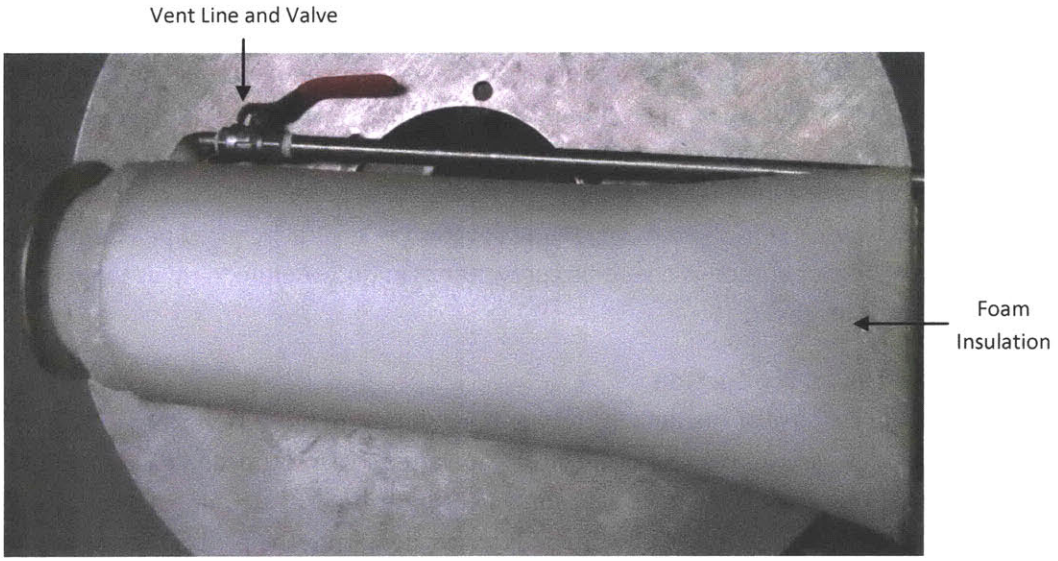

Figure 4-48: Container with Vent Line and Insulation

liquid nitrogen on its exterior. Temperature was monitored using a thermocouple taped to the part's exterior, and the container was held at subzero temperatures throughout the trial to preserve any pellets that were made. Once at Nestlé, however, this method could not be used due to company policies regarding the use of liquid nitrogen, and so an alternate method of cooling had to be devised. The container and its sleeve of foam insulation are separately placed in a freezer set to a temperature of 213 K (-60°C) approximately two hours before the trial was to begin. Just as the trial is about to begin, the container and sleeve are removed from the freezer, the insulating sleeve is slid on to the container, and both are then mounted to the Lower Funnel. The insulating sleeve provides enough thermal resistance on its own to keep the container below 273 K (0°C) for the duration of a 30-minute trial, and the cold gas descending from the prototype above will provide some additional cooling effect. Plans have been made to extend the cooling loop to include the Collection Container to control its temperature more accurately throughout the course of a trial, but this idea has not been implemented yet due to time constraints.

The CO_2 flush line was frequently used during initial trials, but use tapered off during subsequent experiments due to a lack of noticeable degradation of piston speed. Most of the ensuing trials progressed without any issues; however, piston speed noticeably decreased during some of these tests. During these trials, the flush flow was activated, and the pistons then moved more quickly after several cycles. When disassembled after one of these trials, a crust of powder could be seen on the outer diameter of the piston. This crust was partially cleared away from the side of the piston closest to the flush entrance as well as the bottom of the piston, while that on the far side and top of the piston appeared to be largely untouched. There was no trace of this crust in the bore in the Main Body, so it is unlikely that it had simply been scraped off during dismantling. This is consistent with what would be expected if the injected CO_2 had a very high liquid fraction, but it could also simply be a sign that the initial CO_2 injected broke through part of the blockage, opening an unobstructed path for the rest of the injected CO_2 to follow. Despite the partial clearance of the gap, the flush flow system was able to restore the lost performance of the device caused by this powder build up.

This test of the CO_2 flush flow system also showed that the flow could be used to clear this gap of already-accumulated powder, at least on a temporary basis. This result is quite important, suggesting that CO_2 consumption can be decreased by only utilizing the flush lines when needed rather than running this flow continuously as a preventive measure. More trials are needed to determine the behavior of the powder in this gap during the production of several hundred pellets, as it may prove that continuous flush line operation is needed to prevent or limit powder build-up as the number of production cycles increases.

4.2.2. Pellet Production

The main purpose of the beta prototype is, of course, to produce pellets. After the Collection Container is separated from the rest of the prototype after a trial, its contents were poured into a bucket held in a freezer for observation, as shown in Figure 4-49. The contents of the container generally included a fair amount of powder and dry ice along with the pellets that were made. It was thought that the powder entered the container through an open path from the Ice Confection Tank to the container created by desynchronization of the pistons during the production cycle. The presence and amount of dry ice, often filling both the container and the Lower Funnel as a single cohesive chunk, is not as easily explained.

Figure 4-49: Pellets Produced during a Trial at MIT

In order to determine the source of the dry ice, several of its features were examined. Pellets were found mixed throughout the dry ice chunk, suggesting that the dry ice was created either during or after the pellet production process. Finding a large mass of dry ice in the bottom of the ICT is not an uncommon occurrence with this process. Its exact cause is unknown, but the dry ice is believed to form during the venting process, especially when significant amounts of liquid CO_2 are present at the start of depressurization. The container is the lowest component of the production apparatus, including the ICT and the pellet-forming prototype, so it seems likely that any liquid CO_2 in the system would flow down to this location. If the presence of liquid CO_2 is indeed a precursor to dry ice formation during venting, then a pool of liquid CO_2 in the Collection Container could result in the formation of a solid block of dry ice with pellet inclusions inside this part.

The pellets that were formed at MIT were very consistent in every way except length. Their surfaces were very smooth once loose powder was wiped away, and they all were similarly dense, hard, and crunchy. This was as expected, since a pressure-limited compression cycle taking place in a smoothly machined environment is usually going to produce uniformly dense pellets with smooth surfaces. It was encouraging to observe that the pellets did not crack or break upon ejection or impact with the bottom of the 314 mm (12.4") long Collection Container, as this means that it can be assumed that a pellet made at any point during the production run can be a viable product.

The variation in pellet length is of greater concern. Compression is a pressure-limited process with this device so all pellets should have the same density, which is what was observed. Differing powder loads, then, would result in pellets of differing volumes. Since the diameter is set by the geometry of the Main Body, this volume difference would manifest itself through differing lengths of pellets. In the sample shown in Figure 4-49, one can clearly see that some pellets are several times the lengths of others. This is evidence of highly variable powder flow into the filling chamber throughout the production process, despite agitating the powder and control cycle time to try to ensure even loading for each pellet. Although modifications made to the agitator allowed the near-continuous production of dozens of pellets for several minutes in later trials at MIT, attempts to reduce this variance by altering agitation methods and cycle times have thus far been unsuccessful.

Unfortunately, the device was not able to replicate its success seen at MIT while in Beauvais. The prototype did manage to produce a few pellets, but was unable to produce dozens at a time as it had previously. Since the device was able to produce a few pellets before its productivity ceased, the problem is believed to lie with powder flow. When the prototype was dismounted from the Ice Confection Tank, the Upper Funnel was often found to be full of bridged, sintered powder that supported more powder sitting above in the ICT. This behavior had also been seen in the MIT trials, but it had not consistently prevented the formation of multiple pellets as it did in Beauvais. The main difference between the two cases is the geometry of the ICT. The MIT tank is 3.3 L tank made of a 457 mm (18") section of 4" schedule 80 pipe (4.500" [114.3 mm] outer diameter, 3.826" [97.2 mm] inner diameter), while the one at PTC Beauvais is a 25.5 L with a 300 mm inner diameter for most of its height stepping down to a 150 mm diameter for its outlet port. A cross-sectional view of the Ice Confection Tank at PTC Beauvais is provided in Figure 4-50. A funnel has been built and placed in the Beauvais ICT

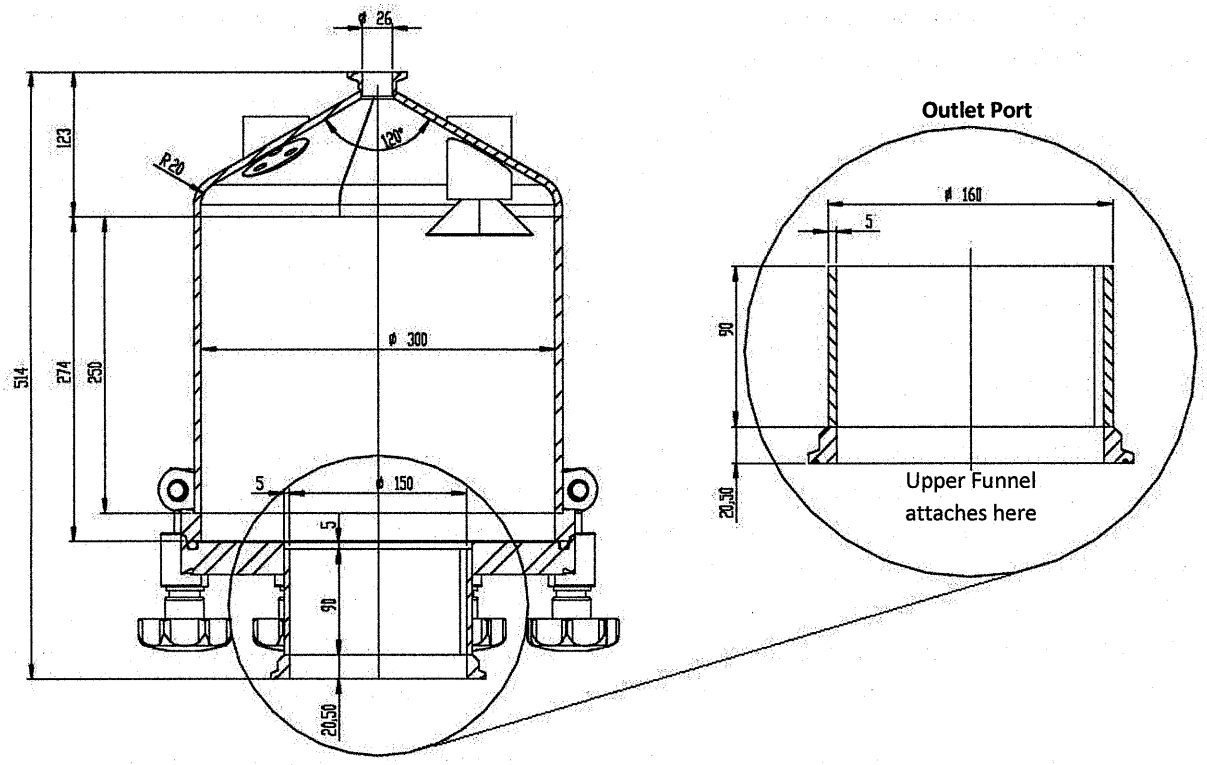

Figure 4-50: Ice Confection Tank of PTC Beauvais

to help guide the powder toward the outlet port and eliminate the step change in diameter, preventing powder from building up on the shelf this creates.

Despite efforts made to control temperature and process parameters to keep conditions as similar to the MIT trials as possible, powder continued to bridge in the Upper Funnel. At MIT, this issue was solved through modification of the agitator paddle to allow it to sweep through a larger volume above the filling chamber. Building on this experience, alteration of the agitator paddle was the next step taken in an attempt to prevent the powder from bridging and sintering over the filling chamber.

4.2.3. Mechanical Agitator Trials

During initial trials held at both MIT and PTC Beauvais, it was clear that the Dual Piston was not always able to form full pellets despite the presence of a significant amount of powder in the Upper Funnel and the ICT. The powder was building up above the filling chamber just as planned, but between actuation cycles it was bridging over the agitator paddle rather than flowing into the compression device. As the powder sat quiescent during an actuation cycle, it loosely adhered to itself and to the walls of the Upper Funnel. It was clear that something must be done to ensure that a proper load of powder is consistently delivered to the filling chamber during each cycle, and it was also clear that the initial agitator paddle, shown below in a reprint of Figure 4-16, was not able to properly ensure powder flow on its own.

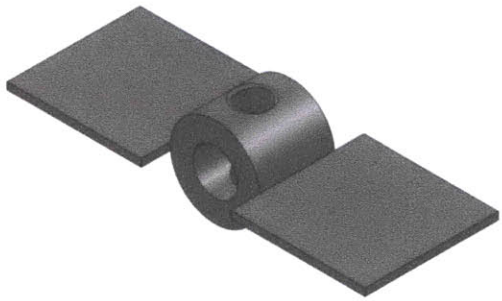

Reproduction of Figure 4-16: Initial Agitator Paddle

The first agitator paddle used was of the simple design shown above in Figure 4-16. This paddle worked well at clearing powder from the area immediately above the inlet port. However, due to its small size and equally small reach, it was only able to clear a small portion of the powder in the Upper Funnel. Powder would then bridge just out of reach of the agitator paddle, halting flow into the device and thereby preventing the formation of any further pellets.

Figure 4-51a shows the dismounting of the prototype after a five-minute long trial in which the powder bridged in the Upper Funnel. Figure 4-51b shows that the agitator was effective in moving the powder that it could reach, but the powder out of its reach simply bridged and blocked further powder flow despite these agitation efforts.

The results of trials such as the one above made it clear that the agitator was beneficial in promoting powder flow, but that its reach needed to be extended if it was to continue ensuring powder flow during longer trials. However, the initial paddle was already as large as it could be without interfering with the movements of the piston below during its rotation (see Figure 4-15 for an illustration of this constraint). In order to improve its reach upwards through the Upper Funnel, it was

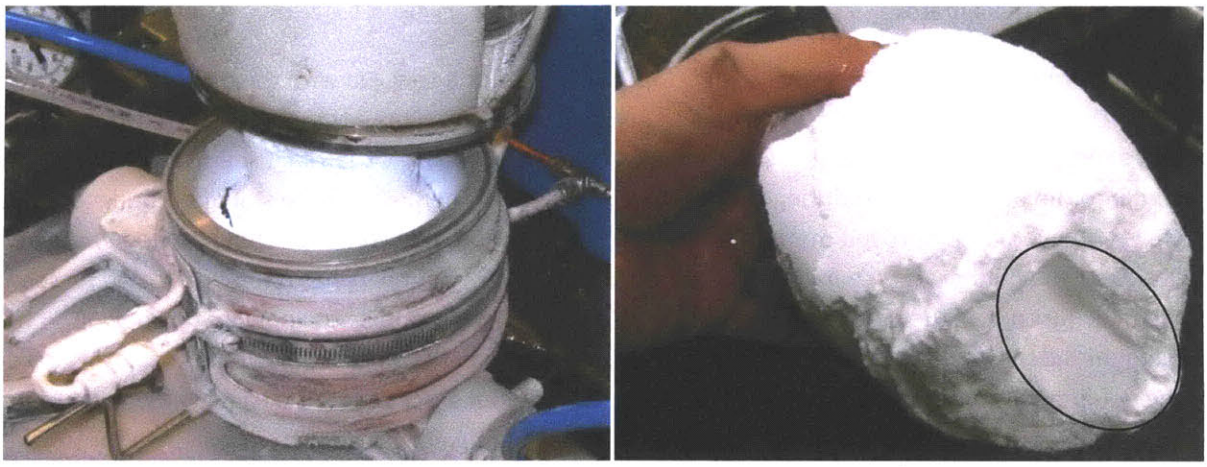

a. b.

Figure 4-51a and b: Mechanical Agitator Trial - Initial Paddle
An example of bridged powder after a five-minute long trial at MIT. The circled feature in Figure 4-51b shows the effect of the agitator paddle on this mass of bridged powder.

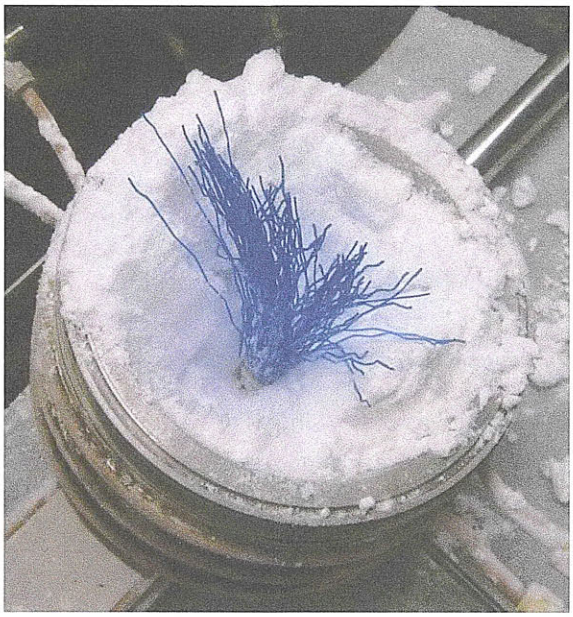

Figure 4-52: Mechanical Agitator Trial at MIT – Initial Paddle with Plastic Brush Bristles

decided to make the agitator paddle asymmetrical, with a long paddle extending upwards to sweep through the powder above and a small paddle that still cleared the piston extending downwards. The agitator paddle could no longer turn a full 360° rotation, but its greatly extended reach was believed to be far more beneficial in reaching its goal.

The initial attempt at implementing such a design utilized plastic bristles taken from a plastic brush. These bristles were tied to one of the paddles of the initial design using stainless steel wire. It was believed that the use of a flexible extension would prevent powder from being too strongly compressed against the wall of the Upper Funnel and adhering there, eventually promoting bridging over the top of the agitator.

Figure 4-52 shows the interior of the Upper Funnel after a trial run with the extended agitator paddle. This design prevented the build up and bridging of powder in the Upper Funnel over the course of a five-minute long trial. Several dozen pellets were made during this trial, so it seems that powder flowed into the filling chamber during the majority of the trial. The pellets were still of differing lengths, however, so even this improved method of agitation does not provide consistent powder flow for every cycle. After the beta prototype had been lowered from the ICT, several inches of powder could be seen in the tank, just out of the reach of the brush bristles of the agitator. It is not known if this powder bridged during the trial or during venting, as there is no easy means of observing what is occurring inside of the equipment during the experiment. However, the general success of this design concept led to its adoption in Beauvais after initial trials showed that powder bridging was a severe problem in those tests.

Once in Beauvais, the brush-agitator had to be dismantled because its construction led to several health and safety concerns. The concerns centered over the possibility of bacteriological contamination in the bristles and the possibility of the mechanical failure of the bristles or stainless steel

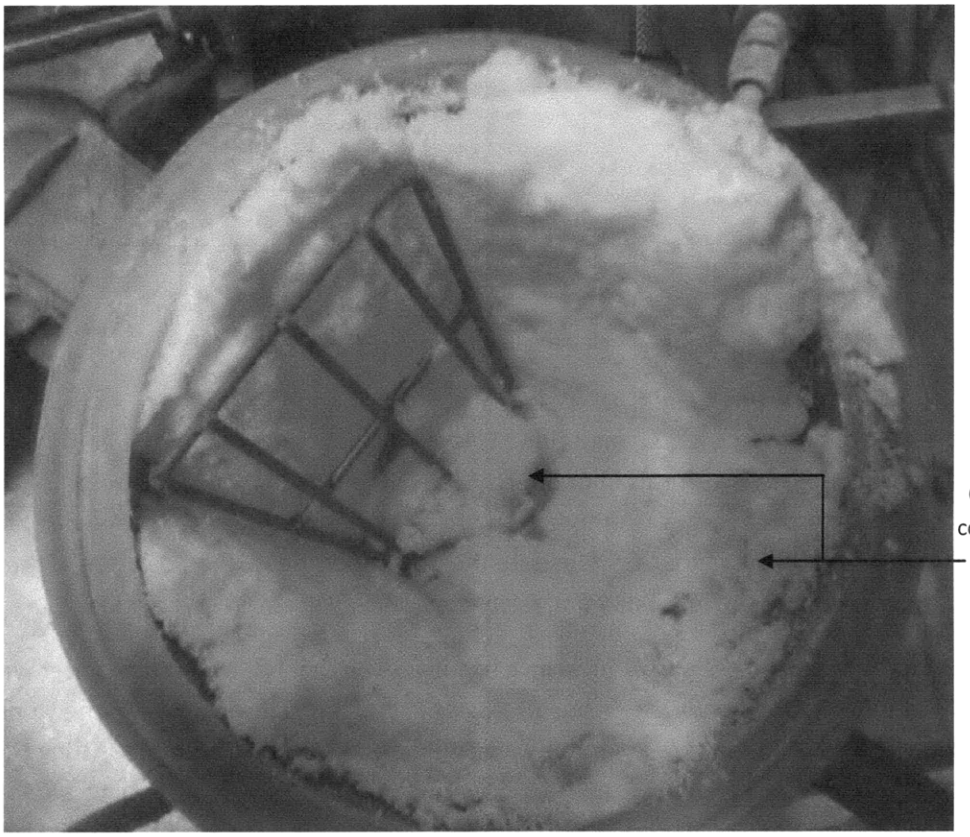

Figure 4-53: Mechanical Agitator Trial in Beauvais - Asymmetric Partial-Rotation Paddle
Chunks of powder can be seen at the base of the upper paddle, blocking sightlines and flow paths into the filling chamber. From correspondence with Haouet and Thomas.

wire leading to inclusions in the product. After the same bridging problems that the powder had experienced at MIT appeared during initial trials, the decision was made to build a new asymmetric paddle. This paddle was made of welded stainless steel rod, trading the flexibility of a plastic or rubber for the durability and short lead-time of stainless steel, which was already on hand. A skeletal structure made of stainless steel rod was chosen over a solid structure made of stainless steel sheet, like the initial agitator paddle shown in Figure 4-16, in an attempt to avoid excessive powder compaction. It was hoped that most of the powder would pass through the paddle rather than being compressed against the inner surface of the Upper Funnel. However, compaction was reportedly severe enough to lead to both bridging and "chunking" behavior, in which pieces of lightly compressed powder would break off and fall to the bottom of the funnel, clogging the inlet port and preventing powder from entering the filling chamber (Haouet, Thomas). Some of this behavior can be seen in Figure 4-53.

Despite these setbacks, the use of the mechanical agitator has a clear positive effect on powder flow into the beta prototype. However, it does not appear that using this simple agitator will be enough on its own to assure steady, predictable powder flow. In order to decrease the variability of the powder flow to an acceptable level and ensure its continual motion during the course of a trial, another method of agitation was developed.

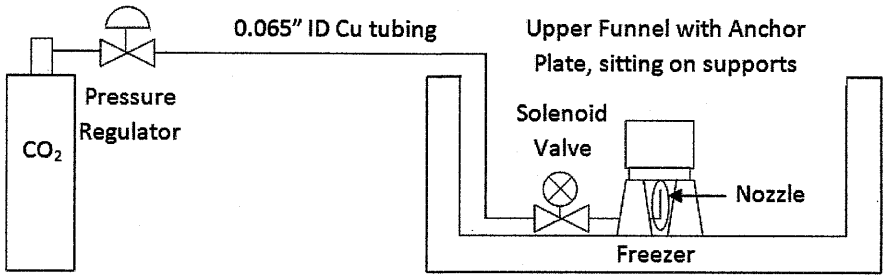

Figure 4-54: CO2 Agitation Proof-of-Concept Test

4.2.4. CO_2 Agitation Trials

The next idea pursued was CO_2 agitation. This method of agitation utilizes short blasts of CO_2 gas to break up any bridging that forms in or directly above the Upper Funnel and helps to fluidize the powder after it sits quiescent during a compression cycle. Carbon dioxide was chosen due to its ready availability and the fact that it cannot contaminate the powder or the CO_2 atmosphere in the production equipment. In order to test the feasibility of this concept, a few short trials were held.

The proof-of-concept tests took place in a top-loading freezer at MIT. The freezer was set to 238 K (-35°C) to simulate the conditions inside of the tank. As shown in Figure 4-54, the Upper Funnel and Upper Funnel Anchor Plate were assembled and then placed on their supports, sitting there overnight to ensure that they cooled to the freezer's temperature. The copper tubing, computer-controlled solenoid valve that controls the CO_2 burst, and the nozzle that directs this burst are placed in the freezer approximately 10 minutes before the trial. There were two nozzles utilized in these experiments – one with an unaltered, round end with a 1.7 mm (0.065") inner diameter, and another whose end had been crushed around a piece of shim stock to make a 0.25 mm (0.010") x 2.4 mm (0.095") rectangular nozzle. The nozzle is placed approximately 19 mm (0.75") beneath the opening in the Anchor Plate, approximately the same distance from the plate as the bottom of the filling chamber, where the CO_2 agitation ports will be located. Powder was then made using the batch process and placed in the Upper Funnel immediately after extraction in an attempt to replicate the build-up of freshly made powder during a trial. When the powder bridged, a short puff of CO_2 was released in order to determine what effect, if any, it would have on the powder above.

Upon actuation of the CO_2 agitation system, the powder began to flow through the gap in the Upper Funnel Anchor Plate, though it did rebridge after a short time. It took seven puffs of CO_2 to flow enough powder out to clear a path through the 89 mm (3.5") of powder in the Upper Funnel. The CO_2 flow punched an approximately 38 mm (1.5") diameter hole through this powder. Higher pressures more energetically agitated the powder, but still resulted in a clear "tunnel" of approximately this same diameter being formed. No difference was seen between the two nozzle designs; they both only cleared powder along a single circular path.

Though the result in each of these experiments was the same, with a circular "tunnel" being bored through the powder in each case, the relevance of this data in describing the behavior of powder present during production is not entirely clear. The powder used in these experiments was fairly lumpy

when extracted, likely contributing to its lack of motion unless directly contacted by the CO_2 stream. It is believed that the powder is much freer flowing and less cohesive when it is first made in the ICT before it has gone through the depressurization process, so it should flow more readily in response to agitation. The powder in the tank has also not had a chance to settle and is much more stable in the sense that its clathrates are not dissociating and it is not absorbing heat radiated from the environment around it. Though the experiments may not show exactly what will occur within the sealed confines of the production equipment, they do show that the basic premise of CO_2 agitation holds merit and suggest that the addition of such a system to the beta prototype may prove quite useful in maintaining proper powder flow.

4.3.Summary

The beta prototype has shown great promise through the course of the trials conducted at both MIT and PTC Beauvais. It improved on almost all of the alpha prototype's major shortcomings, including better seal integrity, improved thermal management, and lighter weight. The apparatus also provided definitive proof that the horizontal compression concept is truly feasible through its production of dozens of pellets in a single trial. The machine does have several weaknesses that could be improved, however, and it has illuminated some of the gaps in knowledge on the product itself.

Agitation is the single largest feature of the beta prototype that can be improved on the existing device. Different mechanical layouts can be tried, such as a series of paddles to reach farther up into the ICT, a sanitary brush to agitate powder while avoiding the compaction of the powder against the inner wall of the Upper Funnel, or a vertical or nearly vertical screw conveyor to pull the powder down from the tank above. The CO_2 agitation system should also be implemented in order to determine its effects on the flow of powder into the filling chamber.

Some important things that can be improved upon are the design choices made in order to save time. For an improved beta or a Gamma prototype, the Upper Funnel should be rebuilt in order to decrease the overall weight of the device. That one part accounts for 50% of the prototype's total weight and is extraordinarily over designed, so there is significant room for improvement. Modifications can be made to the Main Body's design to eliminate the need for the Anchor Plates, thus decreasing part count, decreasing potential leakage sites from the extra seal required by the extra parts, and shortening the powder flow path. If the Upper Funnel, Lower Funnel, and Main Body are all redesigned at the same time, a solution can be found that narrows the required width of the Main Body due to the bolt circles of the current, reused Upper and Lower Funnels. Welding the clamp flanges onto the new Main Body would eliminate four separate parts (both funnels and their anchor plates) and their requisite seals, bolts, and possible interference between the heads of these bolts and other parts of the prototype. It would also reduce the surface area of the device, decreasing the amount of heat flowing into it during a trial and easing the requirements on the thermal management system.

The coolant system should also undergo some modifications to increase its effectiveness. It should be expanded to include the Collection Container, so that its temperature can also be regulated along with that of the Main Body and Upper Funnel. Larger diameter coolant tubes should be used to decrease the pressure loss of the refrigerant being pumped through them, or a refrigeration unit with

pump better matched to the pressure and flow requirements of the current system should be found. If the Upper Funnel is eliminated or incorporated into a new Main Body design, then there is no longer a clearance issue between the tubes on the side plates and the mounting bolts for that part, so they can be expanded with no problems expected.

Improvements should also be made to the observational capabilities of this device. Currently, there is no way to measure the temperature is at any point in the prototype and there is no way to monitor the powder at any point in the CO_2 flash freezing apparatus or the compression device. The former shortcoming can be solved through the placement of ports for temperature probes in several critical locations throughout the device, such as the inlet port and the Collection Container. The latter, however, is slightly more difficult.

Ideally, it would be best to know if the powder is flowing into the filling chamber and if the pellets being made are successfully falling into the Collection Container. This can be done in several different ways. For example, an optional position sensor can be added to the small actuator (Festo). This sensor will give the length of the pellet formed during its compression stroke and thus tell how much powder was in the filling chamber before that stroke, assuming that the last pellet made was successfully ejected. Ejection can be verified by a transparent viewport or camera located in the Collection Chamber.

The most important thing that can be done is to study and quantify the flow properties of the powder produced while it is in the ICT. Even simple observation of the powder while in the ICT and Upper Funnel of the compression device may be enough to better understand the way that this powder interacts with its environment during the production process and gain insight into the best method of agitating it. Current agitation efforts are based on experience with other powders and with this powder after extraction from the tank. The problem with this analysis is that none of these powders behave the same way that the freshly made powder does. Even the extracted samples of the same powder differ, since they have undergone heat shock, are seeing clathrate dissociation, and may have been affected by the presence of liquid and solid CO_2 during the venting process. The physics of the powder are the most mysterious elements of this entire process, and any efforts that can be made to unravel their mysteries can only lead to a better understanding on what will keep it flowing. These added insights will be crucial guidelines in the further development of powder-handling equipment for use with the CO_2 flash freezing process.

Chapter 5: Summary and Future Work

The CO_2 flash freezing process produces a powdery ice confection that imparts a fizzy sensation to the consumer as it is eaten. This fizziness is a result of the dissociation of CO_2 clathrate hydrates contained in the product, which releases the CO_2 contained in this phase. In order to best maintain clathrate hydrates in the product during the transportation and storage processes, it has been decided that compressing the powder into a denser pellet provides a good balance of product stability and attractive presentation. At this point in the development of the product, described in Baker 2006, 2007, and 2009 and in Pizzagalli's two 2008 papers, consumer trials are called for in order to move forward with the development of this fizzy ice confection. These tests will require the production of 250 to 500 pellets for consumption by a panel of consumers, who will then provide feedback helpful in the further refinement of the product.

In order to form clathrate hydrates, a phase of the CO_2-H_2O mixture, the powder must be produced and stored at a combination of pressure and temperatures that allows for the existence of the clathrate hydrates. The production pressure and temperature have been chosen as 10 bar and approximately 233 K (-40°C) for efficiency and safety reasons, while storage takes place at roughly 5 bar and 253 K (-20°C) so as to utilize widely-used refrigeration equipment. Under the current method of production a batch method in which the powder is made, extracted from the production equipment, and then manually compressed into pellets. This leads to large variations of key product characteristics, such as CO_2 content, texture, and density, between batches and within a single batch. In order to obtain useful commentary from the consumer testing panel, the pellets must be as homogenous as possible.

It was decided that the best way to ensure homogenous pellets would be to attach a pellet-forming machine to the Ice Confection Tank, where the powder is produced, and to compress the powder before it is extracted from this tank. Ideally, the compression would be done on a continuous basis, producing all 500 pellets in a single trial. This setup would prevent the exposure of the powder to the higher temperature and lower pressures of the external environment, thus preventing the dissociation of clathrates and settling of the powder. The continuous extraction process would also reduce the effect of transients occurring at the start of a trial, further limiting pellet variation.

In order to function as described above, the compression device would be required to function in the pressurized, low temperature environment of the production equipment. It would need to operate continuously, thus requiring continuous powder flow. Experience has shown that powder is more likely to flow down a path with a small length-to-diameter ratio than a large one, so powder flow paths should be kept as short and wide as possible. Some thought should also be given to the ability of the production method to be adapted to the higher throughput of mass production should the product hit the market.

The concept of a dual piston horizontal compression tablet press was chosen as the most promising idea from a variety of possible options. This design can be easily sealed to hold pressure and

should be able to function in a low temperature environment. Its layout broadens and shortens the powder flow path when compared to a vertical compression device, and it can be attached to the bottom of the existing production equipment with few issues. Its modular design also allows for easy expansion, since several units can be stacked or placed together should higher production rates be desired. A prototype of the concept will be produced and used to further analyze the design.

The alpha prototype showed that the above idea had its merits, but that the specific design utilized for this prototype had some significant shortcomings. This device was able to hold pressure and successfully create a pellet, but the ethylene propylene diene monomer (EPDM) seals around the sliding parts of the device experienced rapid degradation and failure within a few cycles. Tougher polyurethane seals were used to replace the EPDM seals, but were not able to hold pressure during a trial. Due to these seal issues, powder flow characteristics were unable to be examined during a trial, so it is unknown how the powder will flow through the machine during operation. The cooling system of the device was not adequate to keep it cool during trials, potentially leading to powder flow issues. The prototype was also quite heavy and required a separate, unwieldy cart to support its weight during transport and trials. In order to fully realize the potential of the dual piston horizontal compression device, a second prototype that builds on the knowledge gained from this first attempt will be constructed.

The beta prototype improved on many of the shortcomings of the alpha prototype. The seals were moved to room temperature locations at the end of isolation tubes, solving the previous prototype's problems with these parts. Powder flow paths were shortened through the simplification of the design that eliminated a major moving part and its respective seals. The cooling system was completely rebuilt and could now hold the powder flow path's temperature between 253 K (-20°C) and 233 K (-40°C). The weight of the device was greatly diminished when compared to the alpha prototype despite reusing the Upper Funnel, the heaviest single part of the alpha prototype, in order to save time.

This device was able to create dozens of pellets during trials, proving this concept to be wholly viable. However, ensuring consistent, reliable powder flow was difficult despite the use of various mechanical agitators. In order to improve the rate of powder flow, different actuator designs could be tested and implemented, including mechanical agitator paddle designs and the use of gas flow to disrupt powder bridging. However, since the flow properties of the powder are not well understood, these agitator designs are implemented on a trial-and-error basis. The process could be greatly streamlined if more were known about the way in which the powder flows while in an environment similar to that of the Ice Confection Tank and Upper Funnel. The easiest way to accomplish this would be to place a window or camera in the ICT and/or Upper Funnel to allow the direct observation of the powder during these trials.

Though the management of powder flow is the most important aspect of the beta prototype that can be improved, it is not the only possible upgrade that can be made. The geometry of the cooling system could be further optimized to increase its effectiveness. Several other parts, such as the Main Body, both Anchor Plates, and both Funnels, could be redesigned to decrease the weight and complexity of the prototype, changes that were not made on the original device to meet the aggressive time

constraints imposed on its construction. The addition of temperature probes and the enabling of a method to measure the number and size of pellets produced would also be greatly helpful in the use of this device. These changes could be made to the beta prototype itself, or could be incorporated to a newly designed future gamma prototype.

Chapter 6: References

Accoat A/S, DK-3490 Kvistgaard, Denmark. *Technical Data: Accolan Silver.* January, 2008.

AK Steel Corporation. *Product Data Sheet: 304/304L Stainless Steel.* Available http://www.aksteel.com/pdf/markets_products/stainless/austenitic/304_304L_Data_Sheet.pdf. 2007. Accessed 28 July 2008.

AK Steel Corporation. *Product Data Sheet: 316/316L Stainless Steel.* Available http://www.aksteel.com/pdf/markets_products/stainless/austenitic/316_316L_Data_Sheet.pdf. 2007. Accessed 28 July 2008.

AK Steel Corporation. *Product Data Sheet: 420 Stainless Steel.* Available http://www.aksteel.com/pdf/markets_products/stainless/martensitic/420_Data_Sheet.pdf. 2007. Accessed 29 July 2008.

Baker, Teresa. *Carbon Dioxide Flash-Freezing Applied to Ice Cream Production.* Master's Thesis in Mechanical Engineering. Massachusetts Institute of Technology, 2006.

Baker, Teresa. *CO_2 Spray Freezing: an Investigation of Product Characteristics.* Nestlé Internal Document, 2007 (unpublished).

Chattopadhyay, Somnath. *Pressure Vessels – Design and Construction.* Boca Raton, FL:CRC Press, 2005.

Crandall, Stephen H., Dahl, Norman C., and Lardner, Thomas J. *An Introduction to the Mechanics of Solids, Second Edition with SI Units.* Boston, MA:McGraw-Hill Custom Publishing, 1999.

Cravalho, E., Smith Jr, J., Brisson II, J., and McKinley, G. *2.005: Thermal Fluids Engineering I.* Cambridge, MA:CopyTech. Spring 2008.

Cravalho, E., Smith Jr, J., Brisson II, J., and McKinley, G. *2.006: Thermal Fluids Engineering II.* Cambridge, MA:CopyTech. Spring 2008.

DuPont. "Delrin Acetal Resin: Design Guide – Module III." Available http://plastics.dupont.com/plastics/pdflit/americas/delrin/230323c.pdf. Accessed 10 October 2008. Updated 2008.

DuPont. "Technology Profile: Laser Welding." Available http://www2.dupont.com/Plastics/en_US/assets/downloads/processing/H99299.pdf. Accessed 2 June 2009. Updated 2003.

Food and Drug Administration (FDA). *Food Code 2005: Chapter 4 – Equipment, Utensils, and Linens.* Available http://www.fda.gov/downloads/Food/FoodSafety/RetailFoodProtection/FoodCode/FoodCode2005/ucm123980.pdf. Accessed 5 April 2009. Updated 5 October 2007.

Festo, Inc. "Standard Cylinders DNC, to ISO 15552." Available https://xdki.festo.com/xdki/data/doc_engb/PDF/EN/DNC_EN.PDF. Accessed 1 October 2008. Updated October 2007.

Guichard, Stéphane. Sales, ERI-EST, Sainte-Marie-aux-Chênes, France. Personal Communications, January – August, 2008.

Haouet, Houssème. Engineering, Nestlé SA, PTC Beauvais, France. Personal Communications, September 2008 – February 2009.

Lienhard IV, John H. and Lienhard V, John H. *A Heat Transfer Textbook, Third Edition, v1.31*. Cambridge, MA:Phlogiston Press, 2008.

Lopez, David. *Development of a Continuous Process for the CO_2 Spray Freezing Equipment* Nestlé Internal Document, August 2008 (unpublished).

Mazurek, Robert. Head of Engineering, Nestlé SA, PTC Beauvais, France. Personal Communications, 1/2008 to 1/2009.

National Institute of Standards and Technology (NIST). "Thermophysical Properties of Fluid Systems." Available http://webbook.nist.gov/chemistry/fluid/. Accessed 22 April 2008. Updated 2005.

Peters, Teresa Baker. *Clathrate Hydrates in Frozen Confections: Formation by Carbon Dioxide Flash Freezing and Behavior during Distribution and Consumption*. Doctoral Thesis in Mechanical Engineering. Massachusetts Institute of Technology, 2009.

Pizzagalli, Anthony. *Guide d'utilisation du prototype CO2 Spray Freezer*. Nestlé Internal Document, March 2008 (unpublished).

Pizzagalli, Anthony. *CO_2 Spray Freezing scale up and definition of key parameters for fizzy ice cream development*. Nestlé Internal Document, April 2008 (unpublished).

Saïkali, Joumana, Haouet, Houssème, and Thomas, Rémi. "Update on trials and funnel design." 26 February 2009.

Smith, Joseph, Jr. Samuel C. Collins Professor of Mechanical Engineering, Massachusetts Institute of Technology. Personal Communications, 1/2008 – 3/2009.

Slocum, Alexander. *FUNdaMENTALS of Design*. Cambridge, MA:CopyTech. 14 January 2005.

Thermo Fischer Scientific, Inc. "HAAKE DC50-K75 Cryostat." Available http://www.thermo.com/com/cda/product/detail/1,1055,1000000013974,00.html. Accessed 9 April 2008. Updated 2008.

Thermo Haake. *Instruction Manual Circulator DC50 including all Baths*. Available http://www.thermo.com/com/cda/resources/resources_detail/1,2166,112396,00.html. Accessed 9 April 2008. Updated 2008.

Thomas, Rémi. Technical Support, Nestlé SA, PTC Beauvais, France. Personal Communications, September 2008 - February 2009.

Weather Underground. "Trip Planner Weather." Available http://www.wunderground.com/tripplanner/index.asp. Accessed 21 July 2009. Updated 2009.

Yaws, C.L., ed. *Chemical Properties Handbook*. McGraw-Hill, 1999. Available http://knovel.com.libproxy.mit.edu/web/portal/browse/display?_EXT_KNOVEL_DISPLAY_bookid=49&VerticalID=0. Accessed 21 July 2009.

Appendix A: Beta Prototype Part Drawings

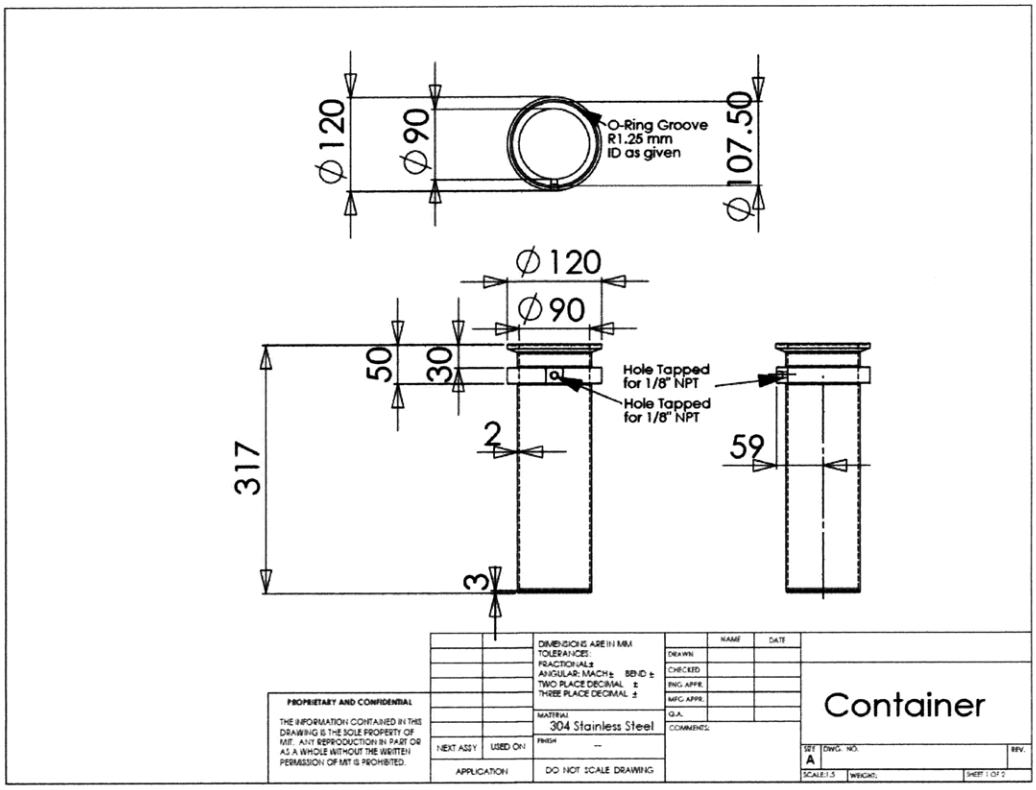

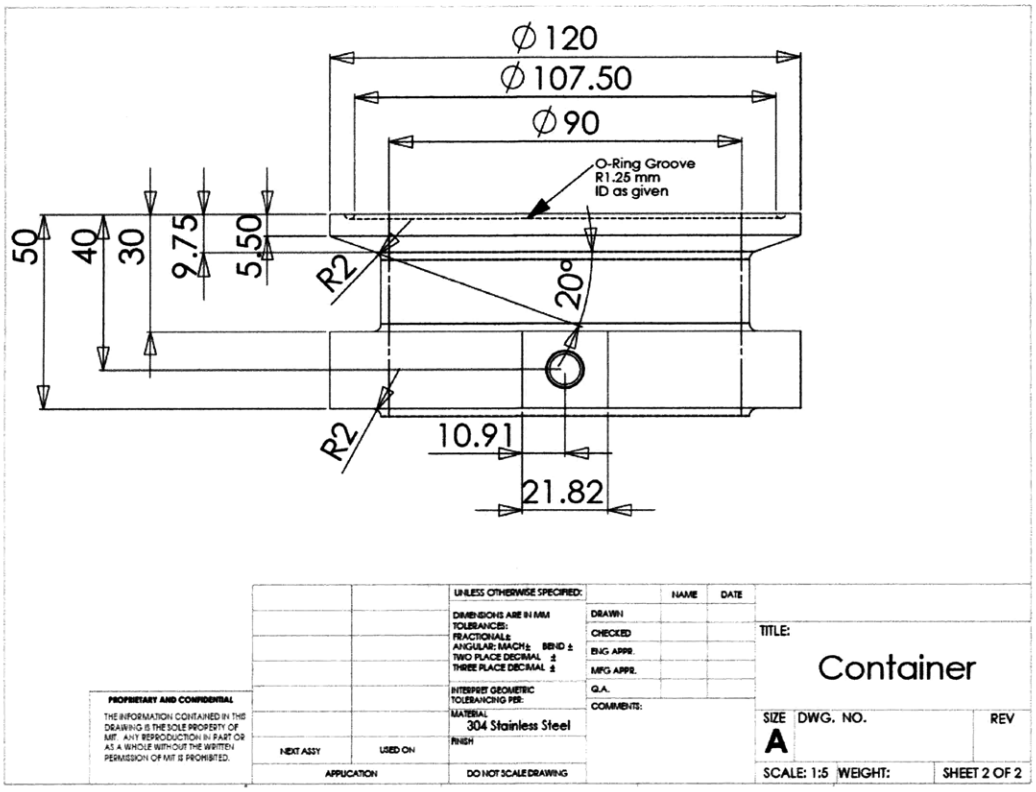

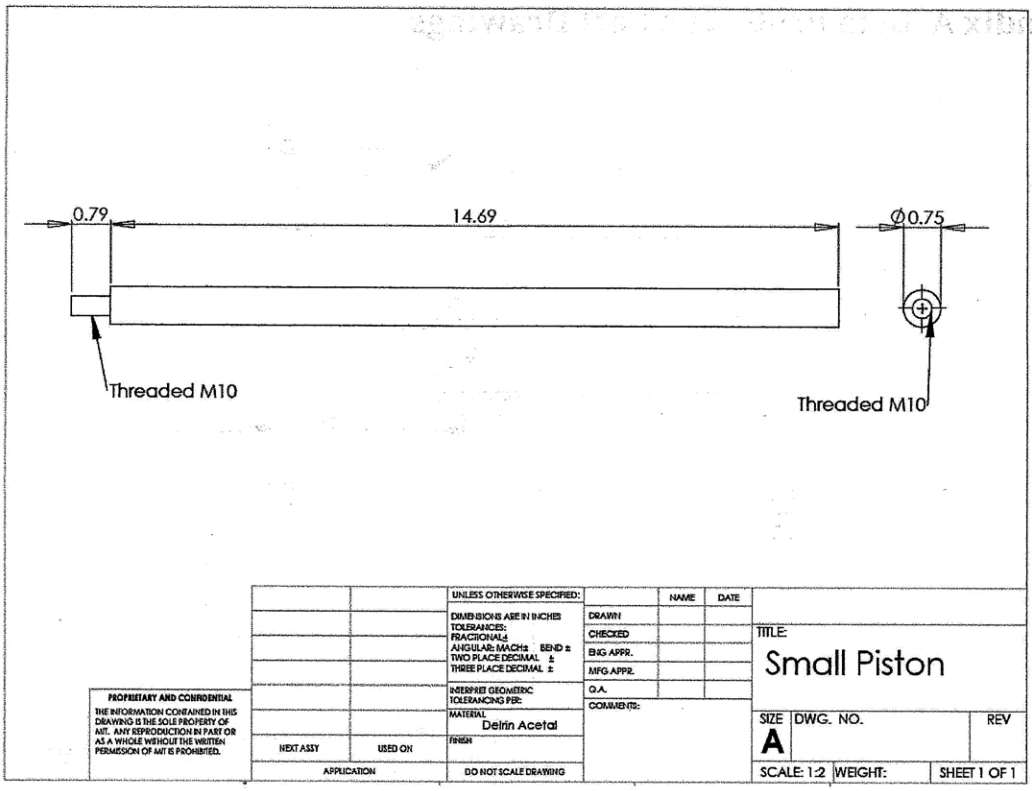
0.79
14.69
Ø0.75
Threaded M10
Threaded M10
UNLESS OTHERWISE SPECIFIED:
DIMENSIONS ARE IN INCHES
TOLERANCES:
FRACTIONAL ±
ANGULAR: MACH ± BEND ±
TWO PLACE DECIMAL ±
THREE PLACE DECIMAL ±
INTERPRET GEOMETRIC TOLERANCING PER:
MATERIAL
Delrin Acetal
FINISH
DO NOT SCALE DRAWING
NAME
DATE
DRAWN
CHECKED
ENG APPR.
MFG APPR.
Q.A.
COMMENTS:
NEXT ASSY
USED ON
APPLICATION
PROPRIETARY AND CONFIDENTIAL
THE INFORMATION CONTAINED IN THIS DRAWING IS THE SOLE PROPERTY OF MIT. ANY REPRODUCTION IN PART OR AS A WHOLE WITHOUT THE WRITTEN PERMISSION OF MIT IS PROHIBITED.
TITLE:
Small Piston
SIZE
A
DWG. NO.
REV
SCALE: 1:2
WEIGHT:
SHEET 1 OF 1

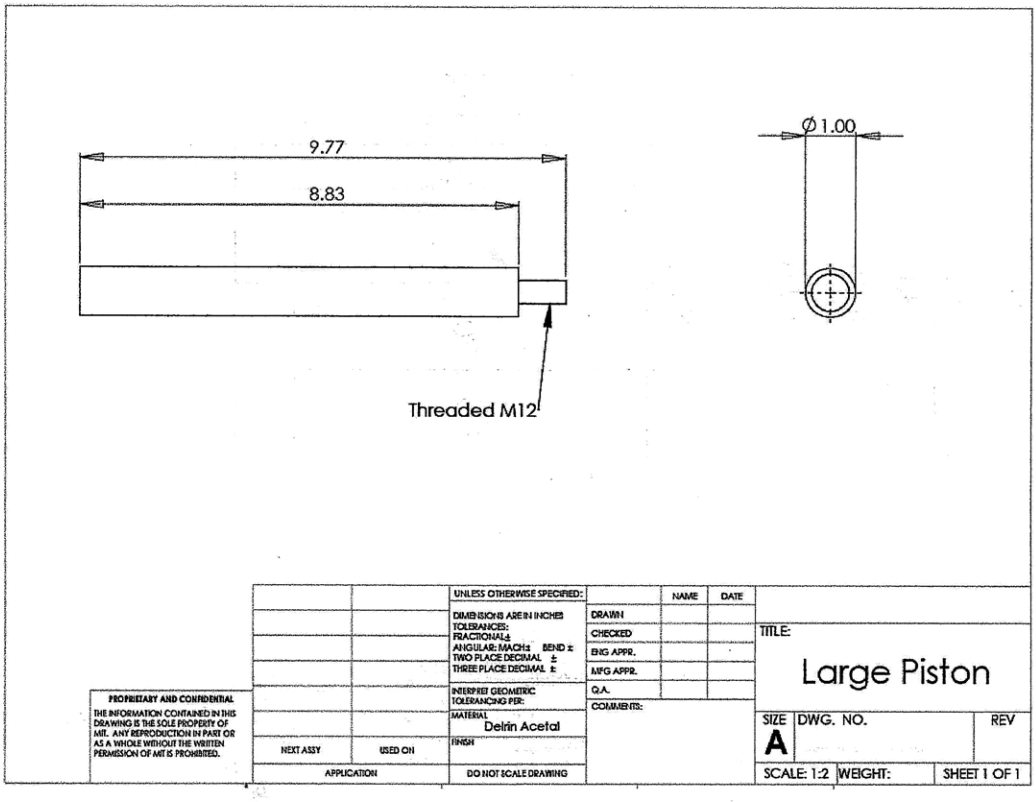
9.77
8.83
Ø1.00
Threaded M12
UNLESS OTHERWISE SPECIFIED:
DIMENSIONS ARE IN INCHES
TOLERANCES:
FRACTIONAL ±
ANGULAR: MACH ± BEND ±
TWO PLACE DECIMAL ±
THREE PLACE DECIMAL ±
INTERPRET GEOMETRIC TOLERANCING PER:
MATERIAL
Delrin Acetal
FINISH
DO NOT SCALE DRAWING
NAME
DATE
DRAWN
CHECKED
ENG APPR.
MFG APPR.
Q.A.
COMMENTS:
NEXT ASSY
USED ON
APPLICATION
PROPRIETARY AND CONFIDENTIAL
THE INFORMATION CONTAINED IN THIS DRAWING IS THE SOLE PROPERTY OF MIT. ANY REPRODUCTION IN PART OR AS A WHOLE WITHOUT THE WRITTEN PERMISSION OF MIT IS PROHIBITED.
TITLE:
Large Piston
SIZE
A
DWG. NO.
REV
SCALE: 1:2
WEIGHT:
SHEET 1 OF 1

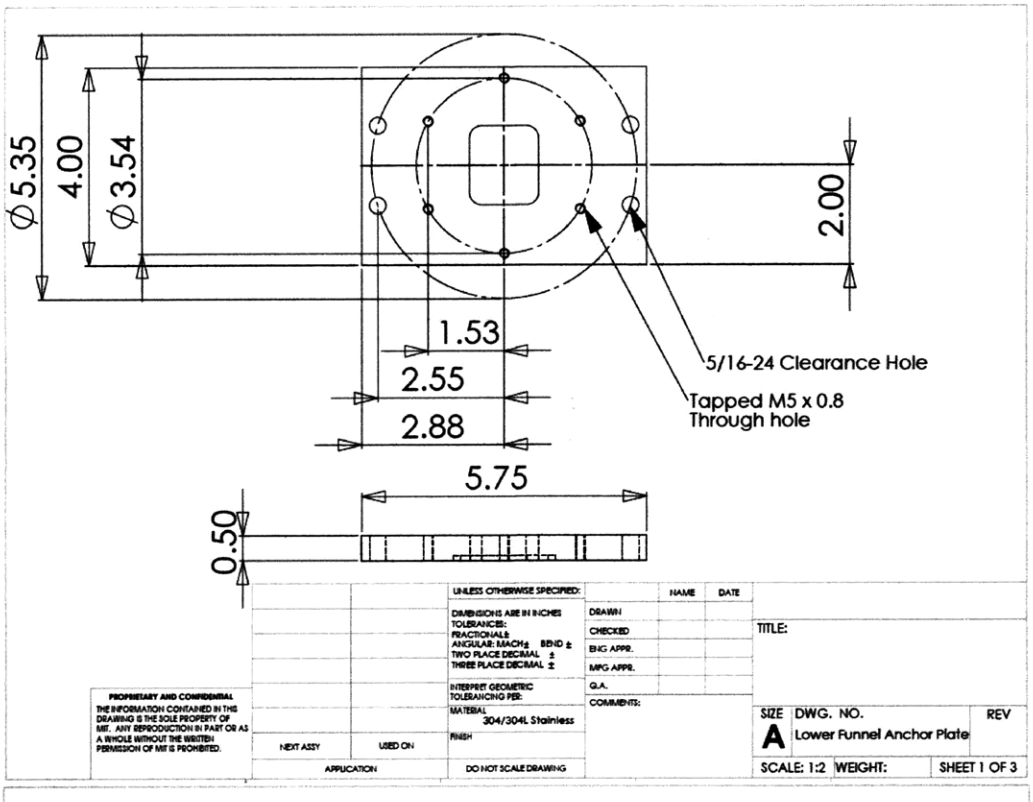

		UNLESS OTHERWISE SPECIFIED:		NAME	DATE
		DIMENSIONS ARE IN INCHES TOLERANCES: FRACTIONAL ± ANGULAR: MACH ± BEND ± TWO PLACE DECIMAL ± THREE PLACE DECIMAL ±	DRAWN		
			CHECKED		
			ENG APPR.		
			MFG APPR.		
		INTERPRET GEOMETRIC TOLERANCING PER:	Q.A.		
		MATERIAL 304/304L Stainless	COMMENTS:		
		FINISH			
NEXT ASSY	USED ON				
APPLICATION		DO NOT SCALE DRAWING			

TITLE:

SIZE	DWG. NO.	REV
A	Lower Funnel Anchor Plate	
SCALE: 1:2	WEIGHT:	SHEET 1 OF 3

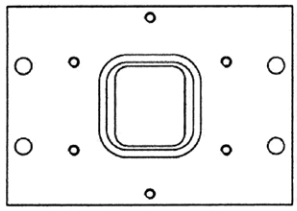

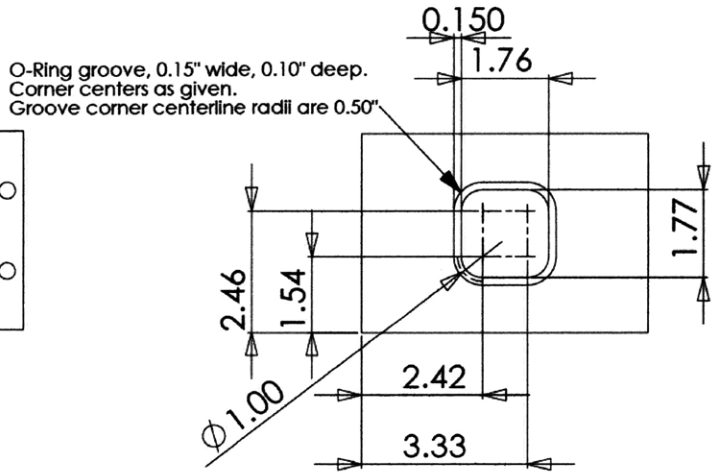

		UNLESS OTHERWISE SPECIFIED:		NAME	DATE
		DIMENSIONS ARE IN INCHES TOLERANCES: FRACTIONAL ± ANGULAR: MACH ± BEND ± TWO PLACE DECIMAL ± THREE PLACE DECIMAL ±	DRAWN		
			CHECKED		
			ENG APPR.		
			MFG APPR.		
		INTERPRET GEOMETRIC TOLERANCING PER:	Q.A.		
		MATERIAL 304/304L Stainless	COMMENTS:		
		FINISH			
NEXT ASSY	USED ON				
APPLICATION		DO NOT SCALE DRAWING			

TITLE:

SIZE	DWG. NO.	REV
A	Lower Funnel Anchor Plate	
SCALE: 1:2	WEIGHT:	SHEET 2 OF 3

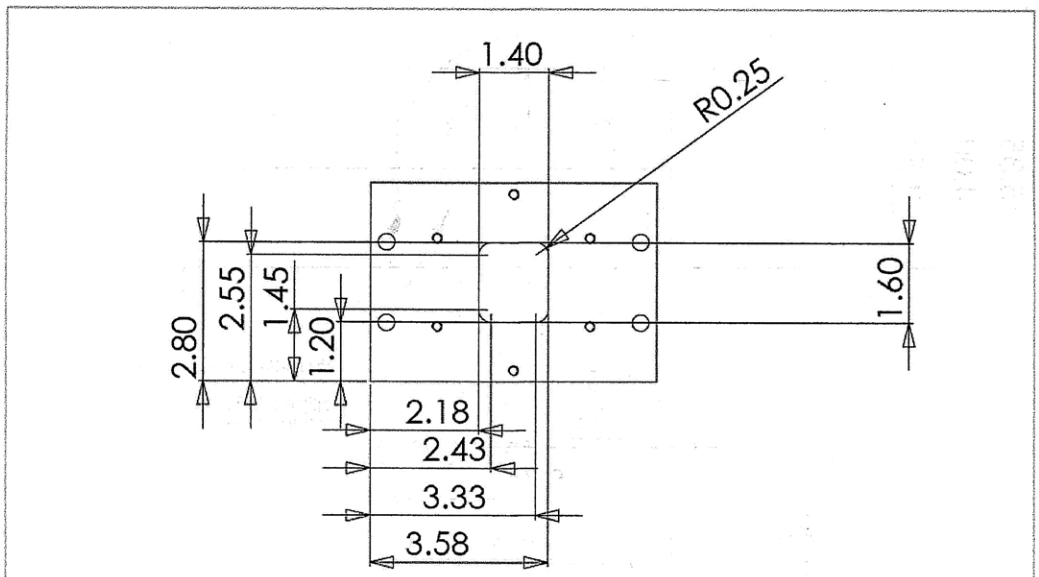

		UNLESS OTHERWISE SPECIFIED:		NAME	DATE
		DIMENSIONS ARE IN INCHES TOLERANCES: FRACTIONAL±	DRAWN		
		ANGULAR: MACH± BEND ±	CHECKED		
		TWO PLACE DECIMAL ±	ENG APPR.		
		THREE PLACE DECIMAL ±	MFG APPR.		
		INTERPRET GEOMETRIC TOLERANCING PER:	Q.A.		
		MATERIAL 304/304L Stainless	COMMENTS:		
NEXT ASSY	USED ON	FINISH			
APPLICATION		DO NOT SCALE DRAWING			

TITLE:

SIZE	DWG. NO.	REV
A	Lower Funnel Anchor Plate	
SCALE: 1:2	WEIGHT:	SHEET 3 OF 3

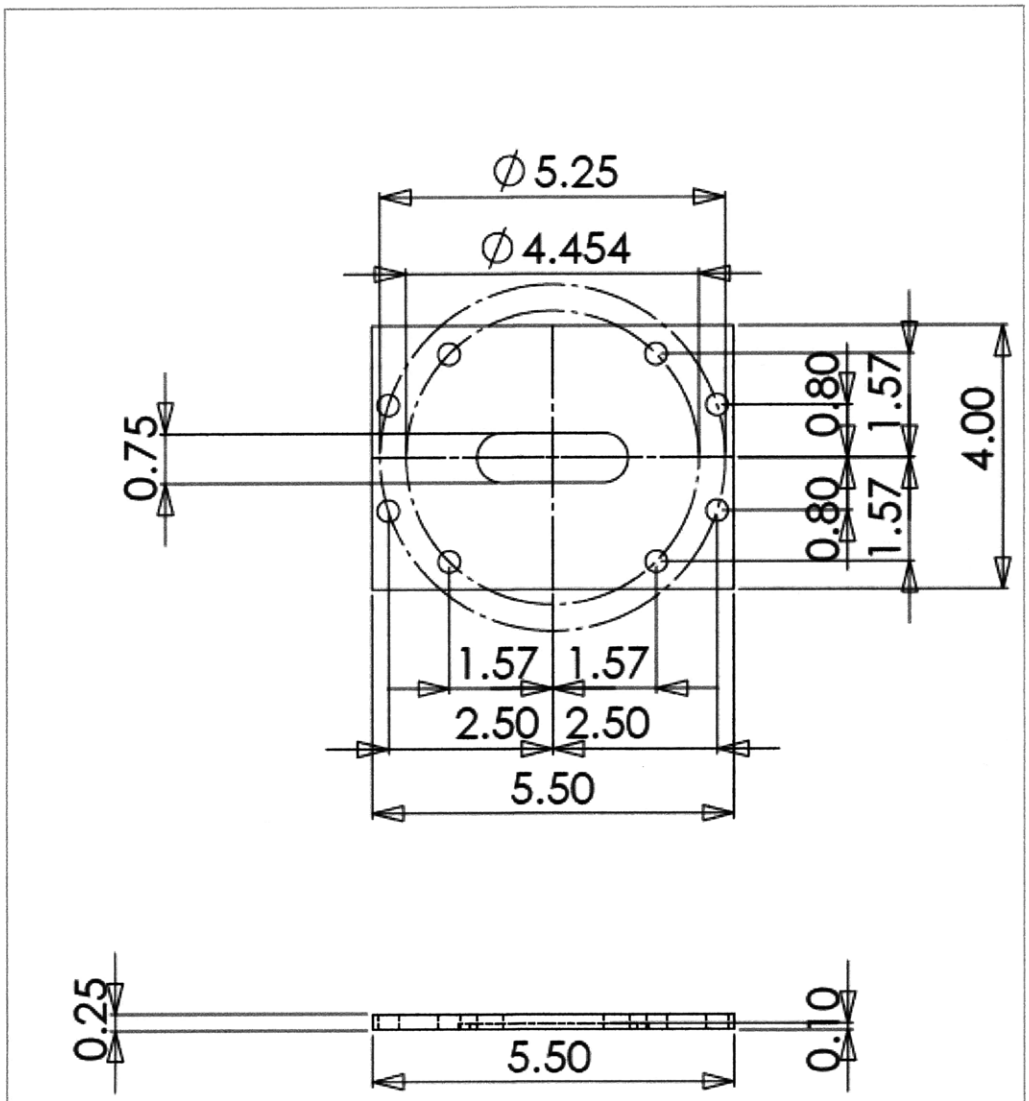

		DIMENSIONS ARE IN INCHES TOLERANCES: FRACTIONAL ± ANGULAR: MACH ± BEND ± TWO PLACE DECIMAL ± THREE PLACE DECIMAL ±		NAME	DATE	
			DRAWN			
			CHECKED			
			ENG APPR.			
			MFG APPR.			
		MATERIAL 304/304L Stainless	Q.A.			
			COMMENTS:			
NEXT ASSY	USED ON	FINISH				
APPLICATION		DO NOT SCALE DRAWING				

SIZE	DWG. NO.	REV.
A	Upper Funnel Anchor Plate	
SCALE:1:2	WEIGHT:	SHEET 1 OF 9

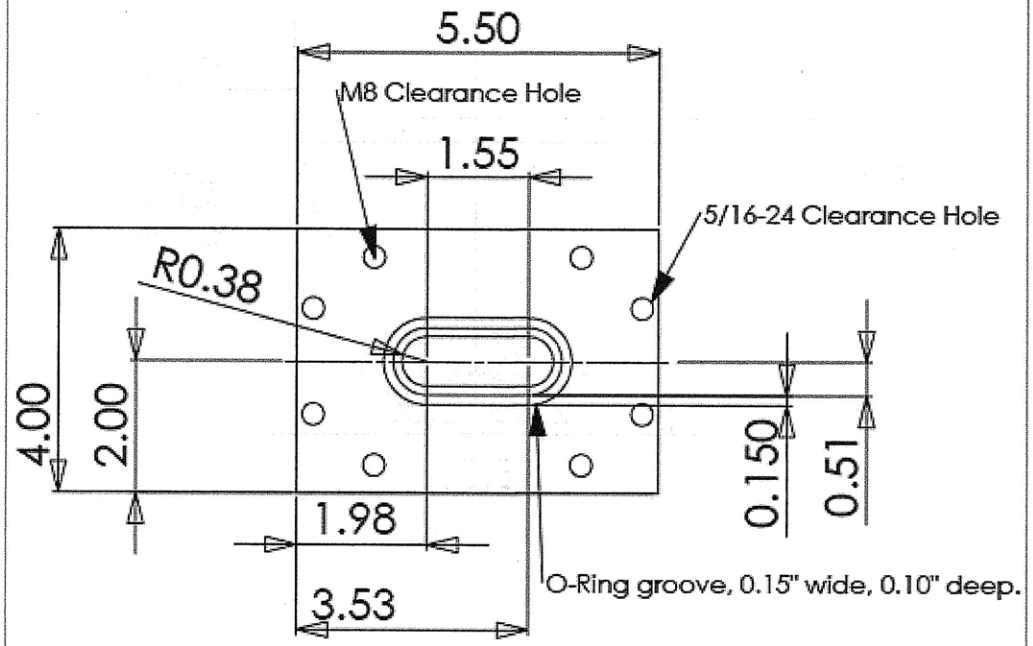

		DIMENSIONS ARE IN INCHES TOLERANCES: FRACTIONAL ± ANGULAR: MACH ± BEND ± TWO PLACE DECIMAL ± THREE PLACE DECIMAL ±		NAME	DATE
			DRAWN		
			CHECKED		
			ENG APPR.		
			MFG APPR.		
			Q.A.		
		MATERIAL 304/304L Stainless	COMMENTS:		
NEXT ASSY	USED ON	FINISH			
APPLICATION		DO NOT SCALE DRAWING			

PROPRIETARY AND CONFIDENTIAL

THE INFORMATION CONTAINED IN THIS DRAWING IS THE SOLE PROPERTY OF MIT. ANY REPRODUCTION IN PART OR AS A WHOLE WITHOUT THE WRITTEN PERMISSION OF MIT IS PROHIBITED.

SIZE	DWG. NO.	REV.
A	Upper Funnel Anchor Plate	
SCALE:1:2	WEIGHT:	SHEET 2 OF 2

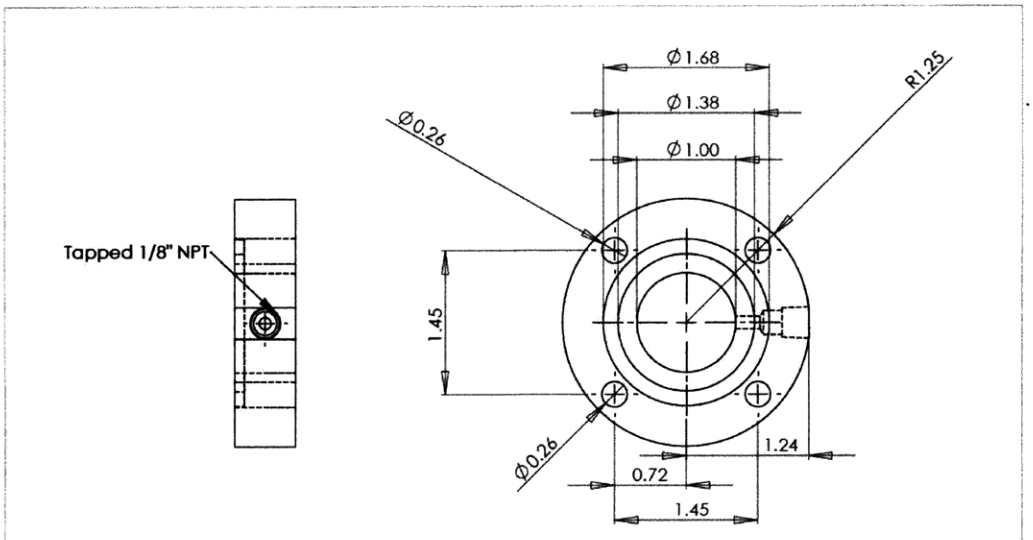

		UNLESS OTHERWISE SPECIFIED:		NAME	DATE
		DIMENSIONS ARE IN INCHES TOLERANCES: FRACTIONAL± ANGULAR: MACH± BEND ± TWO PLACE DECIMAL ± THREE PLACE DECIMAL ±	DRAWN		
			CHECKED		
			ENG APPR.		
			MFG APPR.		
		INTERPRET GEOMETRIC TOLERANCING PER:	Q.A.		
		MATERIAL	COMMENTS:		
		FINISH			
NEXT ASSY	USED ON				
APPLICATION		DO NOT SCALE DRAWING			

TITLE: Large Flush Flange

SIZE	DWG. NO.	REV
A		

SCALE: 1:2 WEIGHT: SHEET 1 OF 1

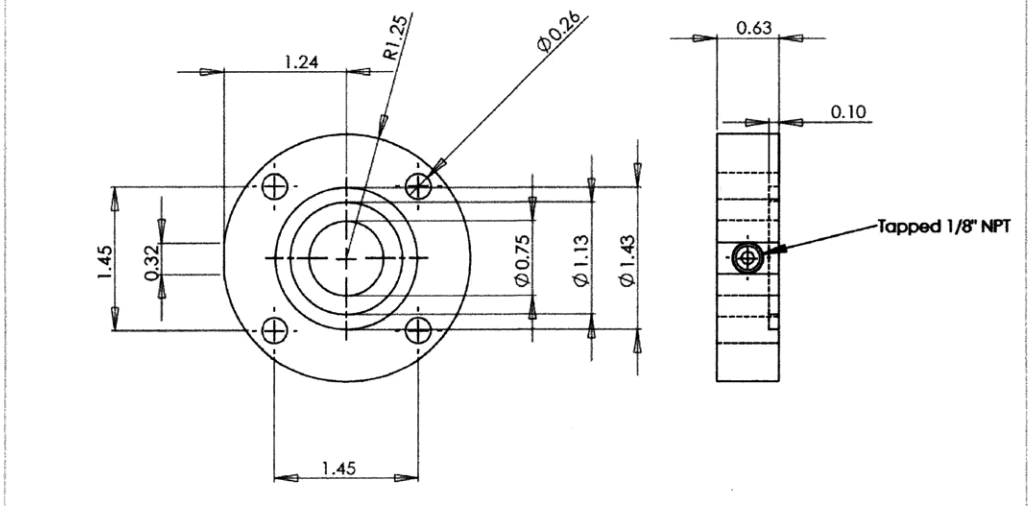

		UNLESS OTHERWISE SPECIFIED:		NAME	DATE
		DIMENSIONS ARE IN INCHES TOLERANCES: FRACTIONAL± ANGULAR: MACH± BEND ± TWO PLACE DECIMAL ± THREE PLACE DECIMAL ±	DRAWN		
			CHECKED		
			ENG APPR.		
			MFG APPR.		
		INTERPRET GEOMETRIC TOLERANCING PER:	Q.A.		
		MATERIAL	COMMENTS:		
		FINISH			
NEXT ASSY	USED ON				
APPLICATION		DO NOT SCALE DRAWING			

TITLE: Small Flush Flange

SIZE	DWG. NO.	REV
A		

SCALE: 1:2 WEIGHT: SHEET 1 OF 1

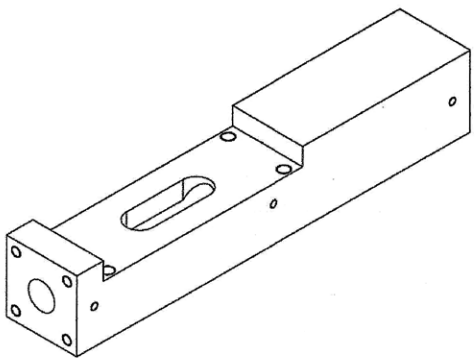

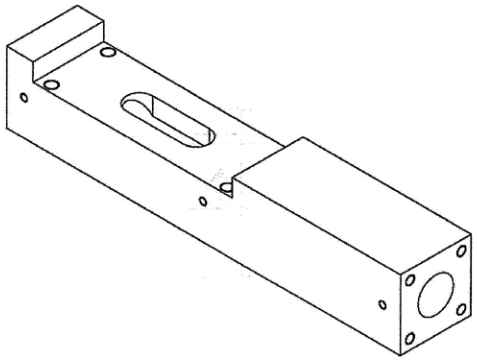

		UNLESS OTHERWISE SPECIFIED:		NAME	DATE
		DIMENSIONS ARE IN INCHES	DRAWN		
		TOLERANCES: FRACTIONAL ±	CHECKED		
		ANGULAR: MACH ± BEND ±	ENG APPR.		
		TWO PLACE DECIMAL ±	MFG APPR.		
		THREE PLACE DECIMAL ±	Q.A.		
		INTERPRET GEOMETRIC TOLERANCING PER:	COMMENTS:		
		MATERIAL 304/304L Stainless			
NEXT ASSY	USED ON	FINISH			
APPLICATION		DO NOT SCALE DRAWING			

TITLE:

SIZE A | DWG. NO. Main Body | REV

SCALE: 1:5 | WEIGHT: | SHEET 1 OF 8

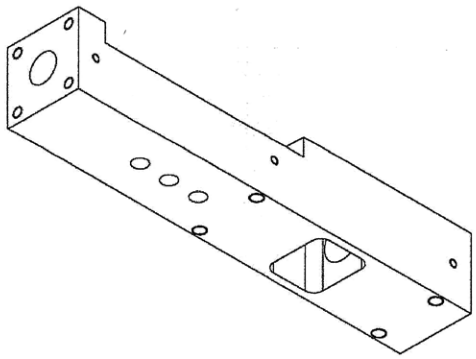

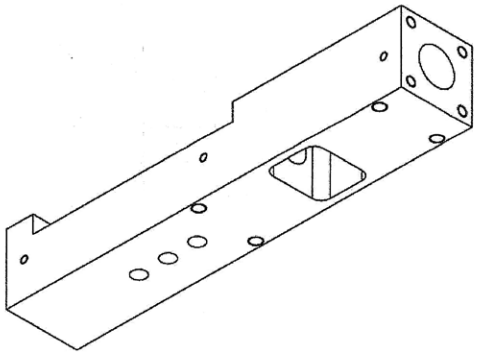

		UNLESS OTHERWISE SPECIFIED:		NAME	DATE
		DIMENSIONS ARE IN INCHES	DRAWN		
		TOLERANCES: FRACTIONAL ±	CHECKED		
		ANGULAR: MACH ± BEND ±	ENG APPR.		
		TWO PLACE DECIMAL ±	MFG APPR.		
		THREE PLACE DECIMAL ±	Q.A.		
		INTERPRET GEOMETRIC TOLERANCING PER:	COMMENTS:		
		MATERIAL 304/304L Stainless			
NEXT ASSY	USED ON	FINISH			
APPLICATION		DO NOT SCALE DRAWING			

TITLE:

SIZE A | DWG. NO. Main Body | REV

SCALE: 1:5 | WEIGHT: | SHEET 2 OF 8

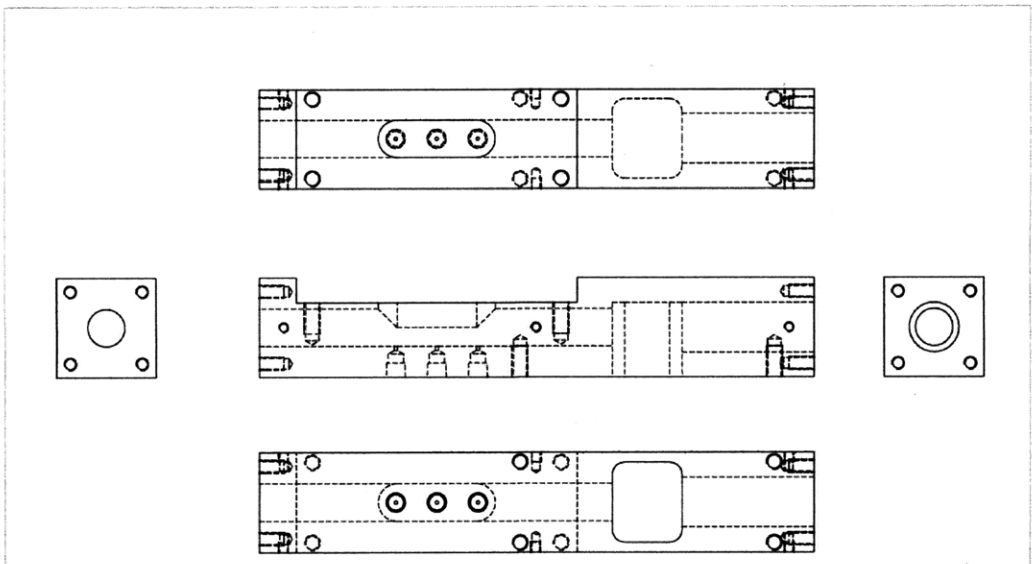

		UNLESS OTHERWISE SPECIFIED:		NAME	DATE
		DIMENSIONS ARE IN INCHES TOLERANCES: FRACTIONAL± ANGULAR: MACH± BEND ± TWO PLACE DECIMAL ± THREE PLACE DECIMAL ±	DRAWN		
			CHECKED		
			ENG APPR.		
			MFG APPR.		
		INTERPRET GEOMETRIC TOLERANCING PER:	Q.A.		
		MATERIAL 304/304L Stainless	COMMENTS:		
		FINISH			
NEXT ASSY	USED ON				
APPLICATION		DO NOT SCALE DRAWING			

TITLE:

SIZE A | DWG. NO. Main Body | REV

SCALE: 1:2 | WEIGHT: | SHEET 3 OF 8

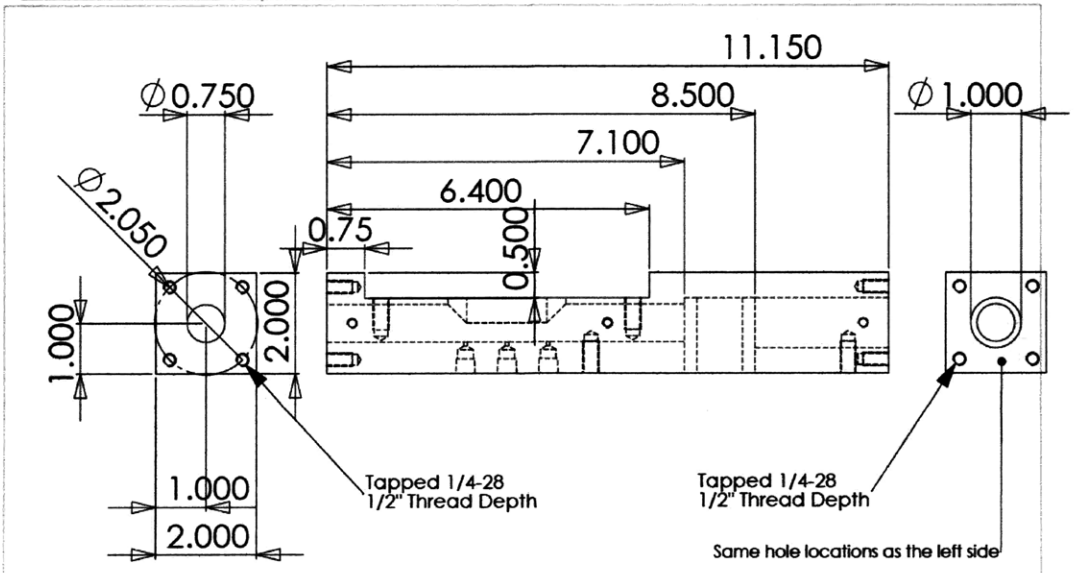

		UNLESS OTHERWISE SPECIFIED:		NAME	DATE
		DIMENSIONS ARE IN INCHES TOLERANCES: FRACTIONAL± ANGULAR: MACH± BEND ± TWO PLACE DECIMAL ± THREE PLACE DECIMAL ±	DRAWN		
			CHECKED		
			ENG APPR.		
			MFG APPR.		
		INTERPRET GEOMETRIC TOLERANCING PER:	Q.A.		
		MATERIAL 304/304L Stainless	COMMENTS:		
		FINISH			
NEXT ASSY	USED ON				
APPLICATION		DO NOT SCALE DRAWING			

TITLE:

SIZE A | DWG. NO. Main Body | REV

SCALE: 1:2 | WEIGHT: | SHEET 4 OF 8

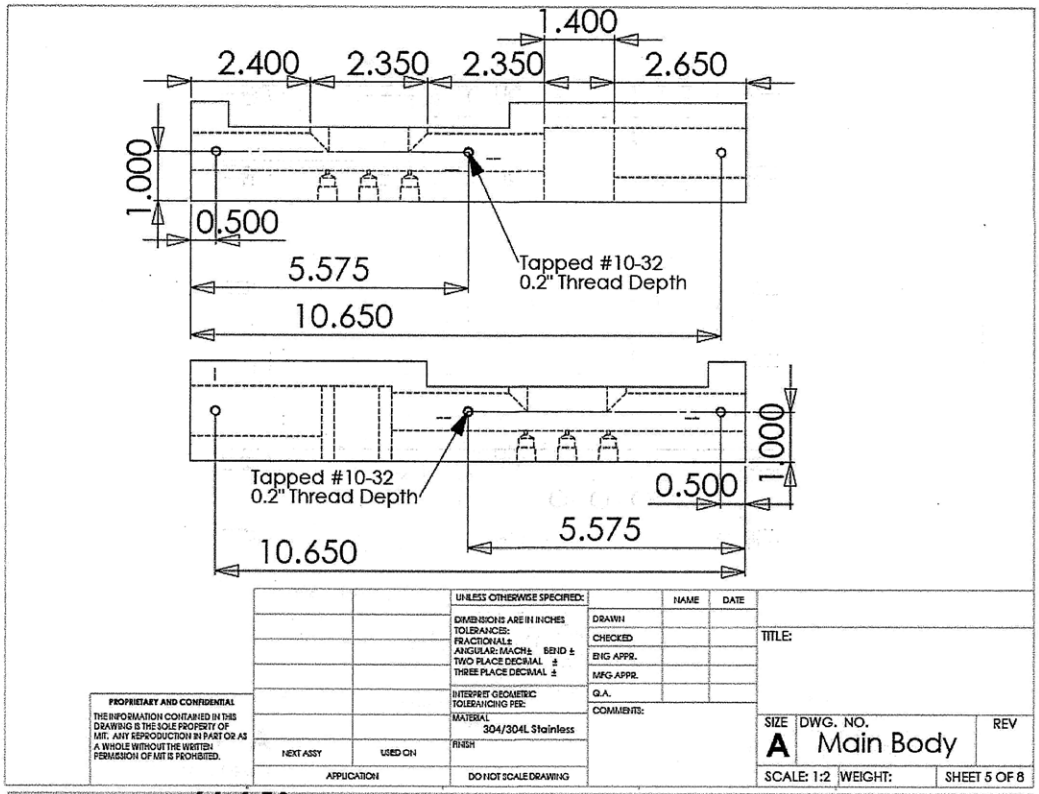

		UNLESS OTHERWISE SPECIFIED:		NAME	DATE
		DIMENSIONS ARE IN INCHES	DRAWN		
		TOLERANCES:	CHECKED		
		FRACTIONAL ±	ENG APPR.		
		ANGULAR: MACH ± BEND ±	MFG APPR.		
		TWO PLACE DECIMAL ±	Q.A.		
		THREE PLACE DECIMAL ±	COMMENTS:		
		INTERPRET GEOMETRIC TOLERANCING PER:			
		MATERIAL 304/304L Stainless			
NEXT ASSY	USED ON	FINISH			
APPLICATION		DO NOT SCALE DRAWING			

PROPRIETARY AND CONFIDENTIAL
THE INFORMATION CONTAINED IN THIS DRAWING IS THE SOLE PROPERTY OF MIT. ANY REPRODUCTION IN PART OR AS A WHOLE WITHOUT THE WRITTEN PERMISSION OF MIT IS PROHIBITED.

TITLE:

SIZE	DWG. NO.	REV
A	Main Body	

SCALE: 1:2 | WEIGHT: | SHEET 5 OF 8

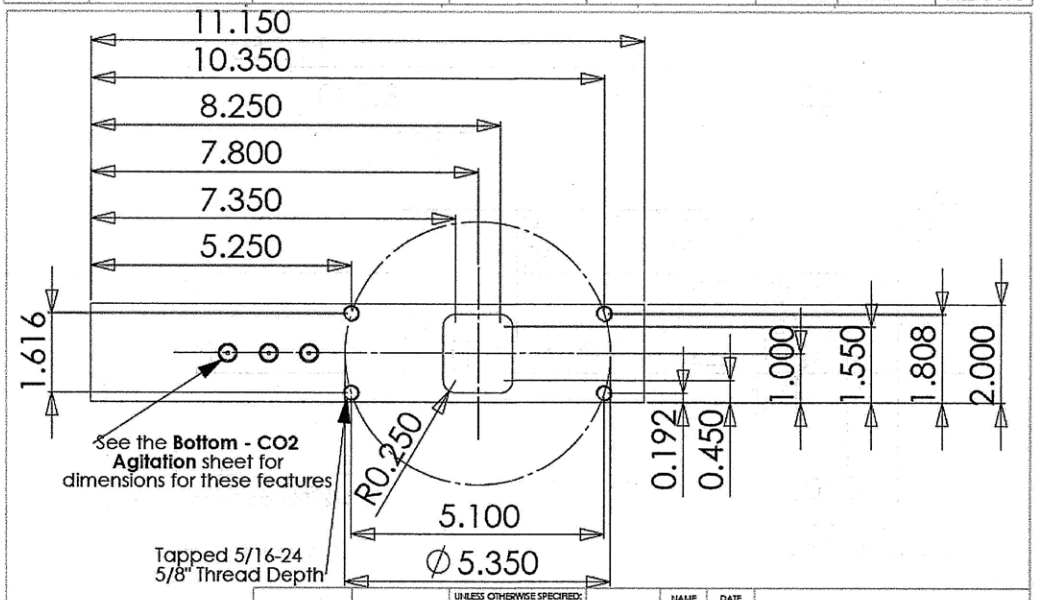

		UNLESS OTHERWISE SPECIFIED:		NAME	DATE
		DIMENSIONS ARE IN INCHES	DRAWN		
		TOLERANCES:	CHECKED		
		FRACTIONAL ±	ENG APPR.		
		ANGULAR: MACH ± BEND ±	MFG APPR.		
		TWO PLACE DECIMAL ±	Q.A.		
		THREE PLACE DECIMAL ±	COMMENTS:		
		INTERPRET GEOMETRIC TOLERANCING PER:			
		MATERIAL 304/304L Stainless			
NEXT ASSY	USED ON	FINISH			
APPLICATION		DO NOT SCALE DRAWING			

PROPRIETARY AND CONFIDENTIAL
THE INFORMATION CONTAINED IN THIS DRAWING IS THE SOLE PROPERTY OF MIT. ANY REPRODUCTION IN PART OR AS A WHOLE WITHOUT THE WRITTEN PERMISSION OF MIT IS PROHIBITED.

TITLE:

SIZE	DWG. NO.	REV
A	Main Body	

SCALE: 1:5 | WEIGHT: | SHEET 6 OF 8

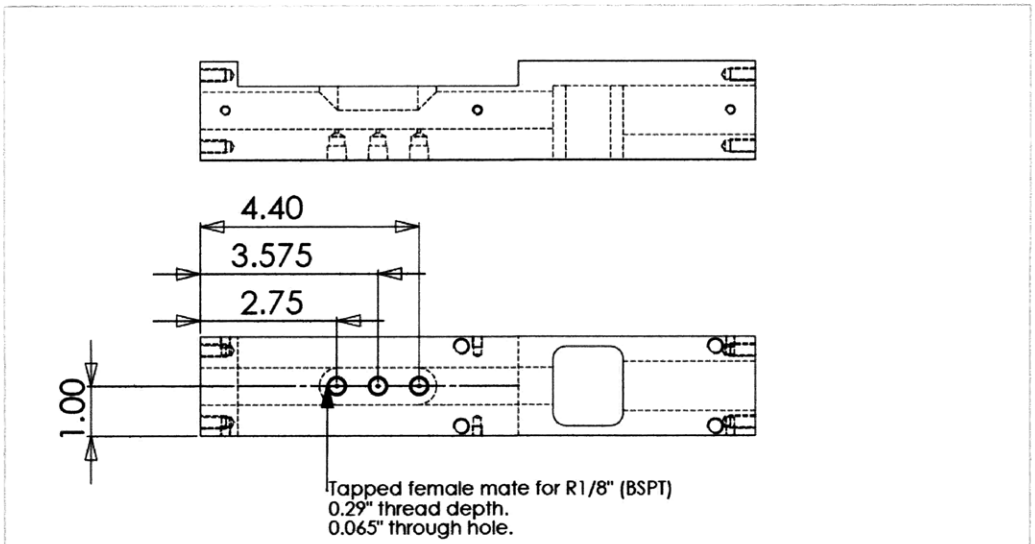

UNLESS OTHERWISE SPECIFIED:		NAME	DATE		
DIMENSIONS ARE IN INCHES TOLERANCES: FRACTIONAL ± ANGULAR: MACH ± BEND ± TWO PLACE DECIMAL ± THREE PLACE DECIMAL ±	DRAWN			TITLE:	
	CHECKED				
	ENG APPR.				
	MFG APPR.				
INTERPRET GEOMETRIC TOLERANCING PER:	Q.A.				
MATERIAL: 304/304L Stainless	COMMENTS:			SIZE A	DWG. NO. Main Body
FINISH					REV
NEXT ASSY / USED ON				SCALE: 1:5	WEIGHT:
APPLICATION	DO NOT SCALE DRAWING				SHEET 7 OF 8

PROPRIETARY AND CONFIDENTIAL
THE INFORMATION CONTAINED IN THIS DRAWING IS THE SOLE PROPERTY OF MIT. ANY REPRODUCTION IN PART OR AS A WHOLE WITHOUT THE WRITTEN PERMISSION OF MIT IS PROHIBITED.

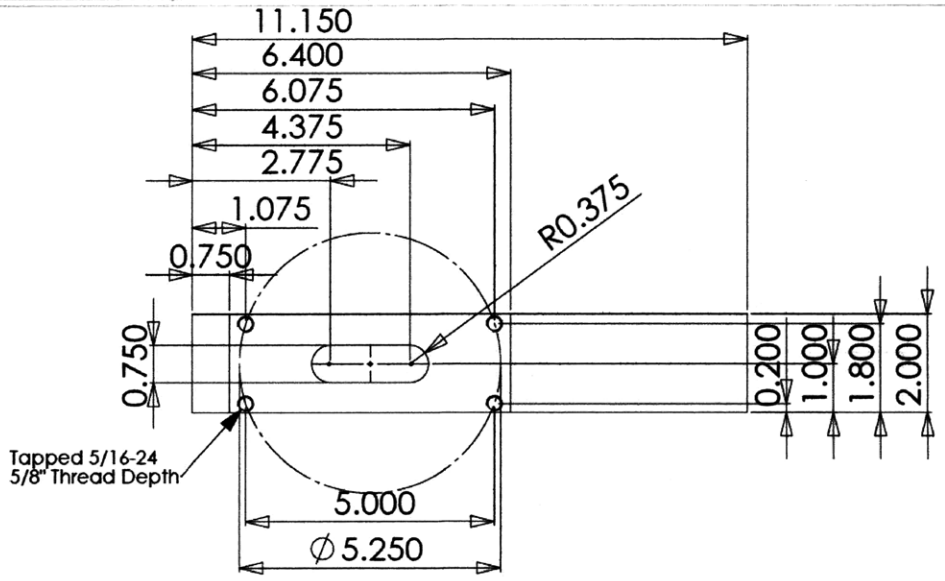

UNLESS OTHERWISE SPECIFIED:		NAME	DATE		
DIMENSIONS ARE IN INCHES TOLERANCES: FRACTIONAL ± ANGULAR: MACH ± BEND ± TWO PLACE DECIMAL ± THREE PLACE DECIMAL ±	DRAWN			TITLE:	
	CHECKED				
	ENG APPR.				
	MFG APPR.				
INTERPRET GEOMETRIC TOLERANCING PER:	Q.A.				
MATERIAL: 304/304L Stainless	COMMENTS:			SIZE A	DWG. NO. Main Body
FINISH					REV
NEXT ASSY / USED ON				SCALE: 1:2	WEIGHT:
APPLICATION	DO NOT SCALE DRAWING				SHEET 8 OF 8

PROPRIETARY AND CONFIDENTIAL
THE INFORMATION CONTAINED IN THIS DRAWING IS THE SOLE PROPERTY OF MIT. ANY REPRODUCTION IN PART OR AS A WHOLE WITHOUT THE WRITTEN PERMISSION OF MIT IS PROHIBITED.

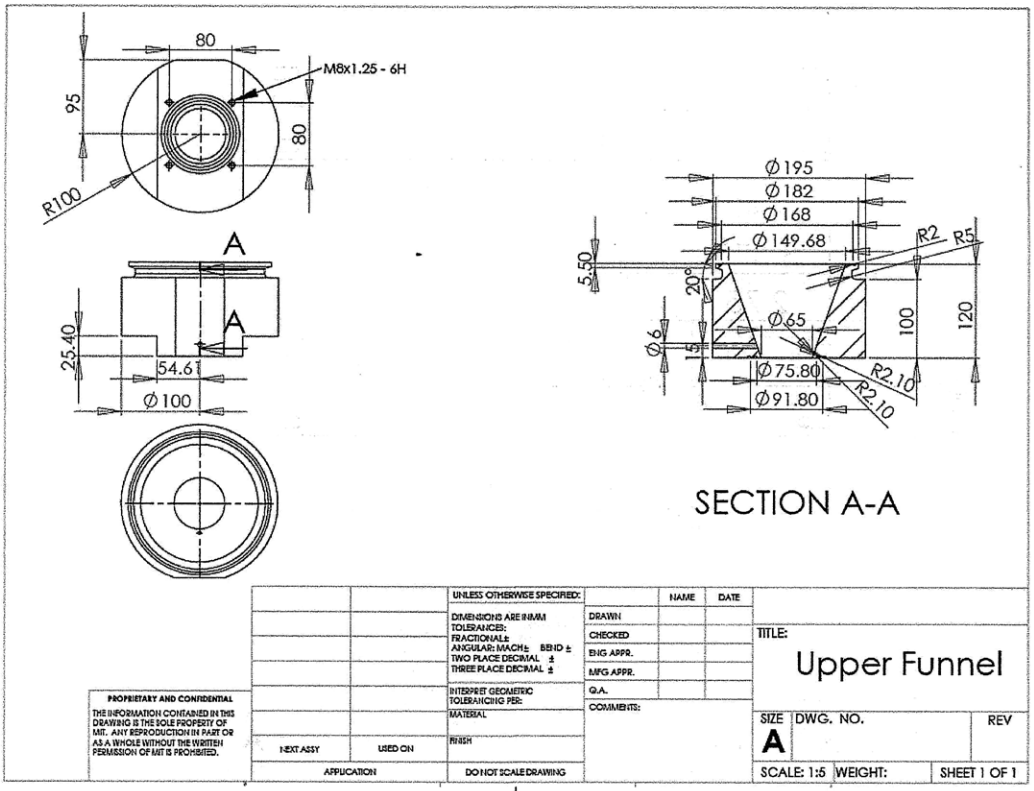

		UNLESS OTHERWISE SPECIFIED:		NAME	DATE
		DIMENSIONS ARE IN MM TOLERANCES: FRACTIONAL ± ANGULAR: MACH ± BEND ± TWO PLACE DECIMAL ± THREE PLACE DECIMAL ±	DRAWN		
			CHECKED		
			ENG APPR.		
			MFG APPR.		
		INTERPRET GEOMETRIC TOLERANCING PER:	Q.A.		
		MATERIAL	COMMENTS:		
NEXT ASSY	USED ON	FINISH			
APPLICATION		DO NOT SCALE DRAWING			

TITLE: Upper Funnel

SIZE	DWG. NO.	REV
A		

SCALE: 1:5 WEIGHT: SHEET 1 OF 1

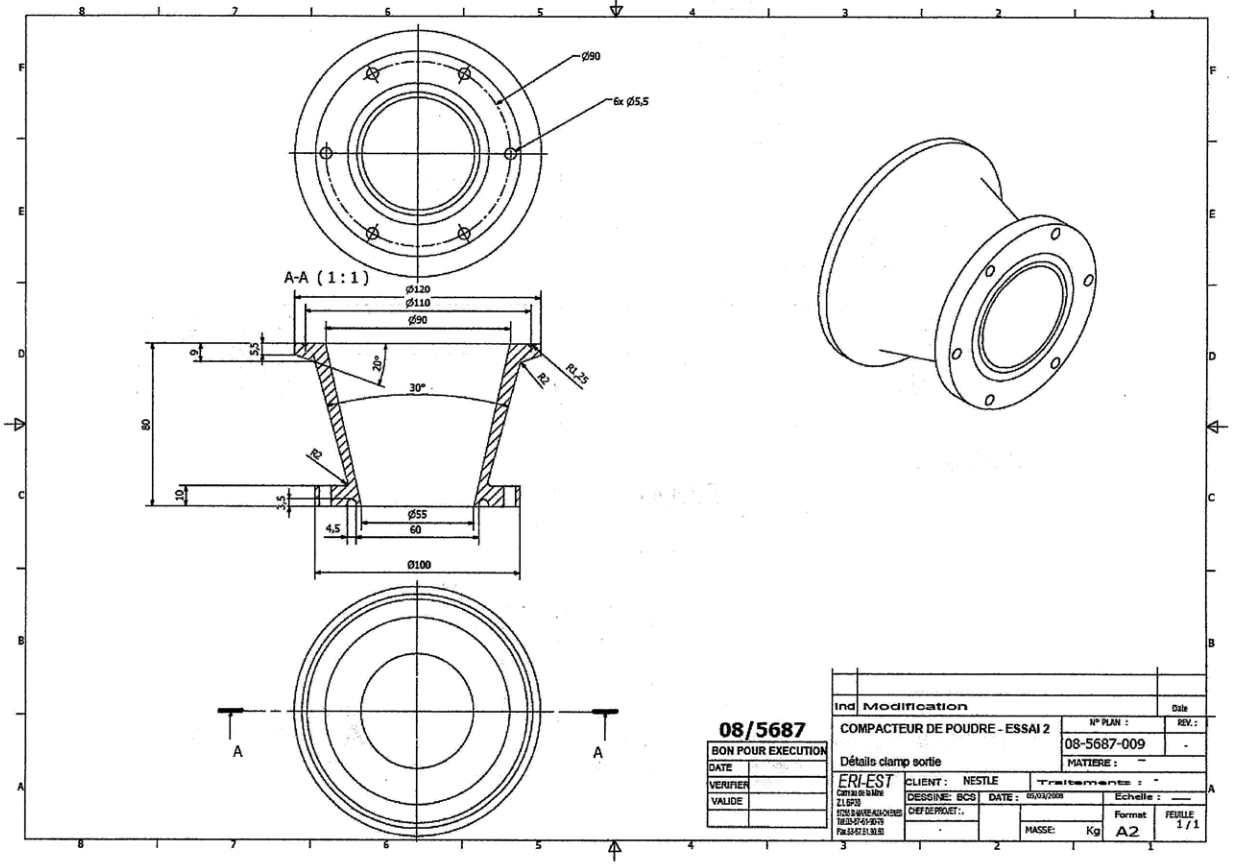

08/5687

BON POUR EXECUTION	
DATE	
VERIFIER	
VALIDE	

Ind	Modification	Date

COMPACTEUR DE POUDRE - ESSAI 2

Détails clamp sortie

N° PLAN :	REV. :
08-5687-009	-

MATIERE : -

ERI-EST

CLIENT : NESTLE Traitements : -

DESSINE: BCS DATE : 05/02/2008 Echelle : —

CHEF DE PROJET : . MASSE: Kg Format A2 FEUILLE 1/1

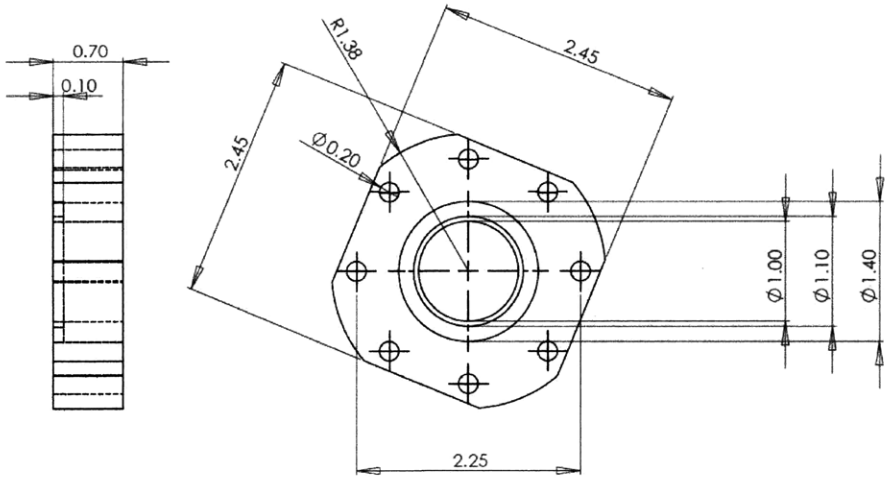

		UNLESS OTHERWISE SPECIFIED:		NAME	DATE
		DIMENSIONS ARE IN INCHES TOLERANCES: FRACTIONAL ± ANGULAR: MACH ± BEND ± TWO PLACE DECIMAL ± THREE PLACE DECIMAL ±	DRAWN		
			CHECKED		
			ENG APPR.		
			MFG APPR.		
		INTERPRET GEOMETRIC TOLERANCING PER:	Q.A.		
		MATERIAL	COMMENTS:		
NEXT ASSY	USED ON	FINISH			
APPLICATION		DO NOT SCALE DRAWING			

PROPRIETARY AND CONFIDENTIAL
THE INFORMATION CONTAINED IN THIS DRAWING IS THE SOLE PROPERTY OF MIT. ANY REPRODUCTION IN PART OR AS A WHOLE WITHOUT THE WRITTEN PERMISSION OF MIT IS PROHIBITED.

TITLE: Small Therm. Iso. Flange, Act

SIZE	DWG. NO.	REV
A		
SCALE: 1:1	WEIGHT:	SHEET 1 OF 1

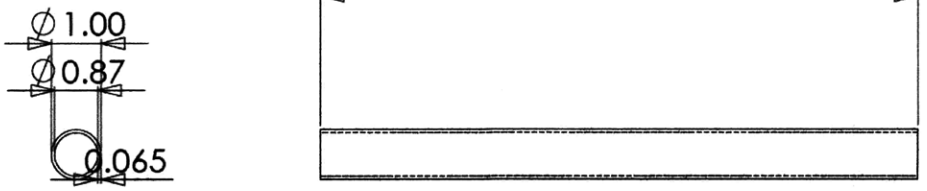

		DIMENSIONS ARE IN INCHES TOLERANCES: FRACTIONAL ± ANGULAR: MACH ± BEND ± TWO PLACE DECIMAL ± THREE PLACE DECIMAL ±		NAME	DATE
			DRAWN		
			CHECKED		
			ENG APPR.		
			MFG APPR.		
		MATERIAL: Stainless Steel	Q.A.		
			COMMENTS:		
NEXT ASSY	USED ON	FINISH: —			
APPLICATION		DO NOT SCALE DRAWING			

PROPRIETARY AND CONFIDENTIAL
THE INFORMATION CONTAINED IN THIS DRAWING IS THE SOLE PROPERTY OF MIT. ANY REPRODUCTION IN PART OR AS A WHOLE WITHOUT THE WRITTEN PERMISSION OF MIT IS PROHIBITED.

Small Therm Iso Tube

SIZE	DWG. NO.	REV.
A		
SCALE: 1:2	WEIGHT:	SHEET 1 OF 1

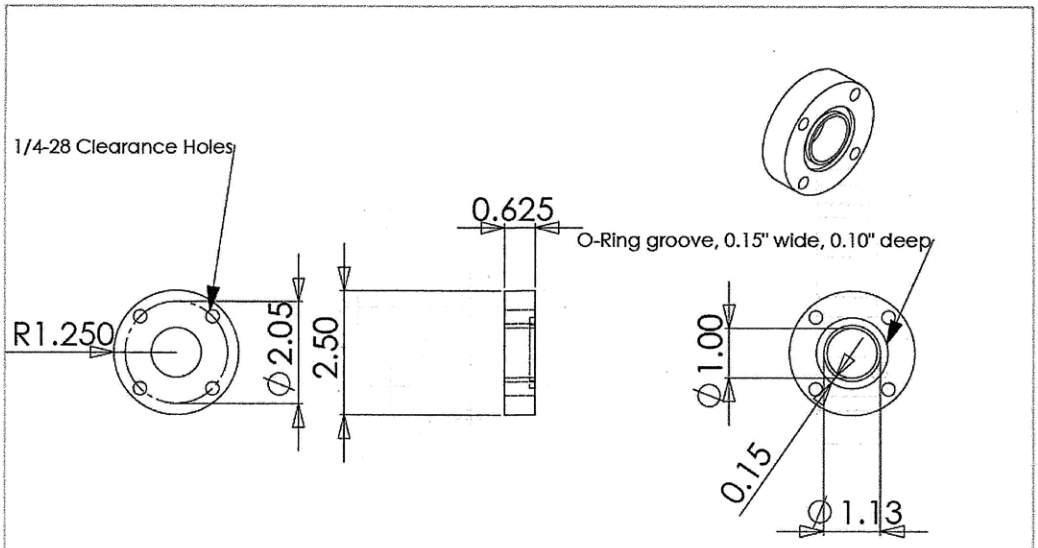

		UNLESS OTHERWISE SPECIFIED:		NAME	DATE
		DIMENSIONS ARE IN INCHES TOLERANCES: FRACTIONAL ± ANGULAR: MACH ± BEND ± TWO PLACE DECIMAL ± THREE PLACE DECIMAL ±	DRAWN		
			CHECKED		
			ENG APPR.		
			MFG APPR.		
		INTERPRET GEOMETRIC TOLERANCING PER:	Q.A.		
		MATERIAL 304/304L Stainless	COMMENTS:		
NEXT ASSY	USED ON	FINISH			
APPLICATION		DO NOT SCALE DRAWING			

PROPRIETARY AND CONFIDENTIAL
THE INFORMATION CONTAINED IN THIS DRAWING IS THE SOLE PROPERTY OF MIT. ANY REPRODUCTION IN PART OR AS A WHOLE WITHOUT THE WRITTEN PERMISSION OF MIT IS PROHIBITED.

TITLE: Small Therm Iso Flange, MB

SIZE	DWG. NO.	REV
A		

SCALE: 1:2 | WEIGHT: | SHEET 1 OF 1

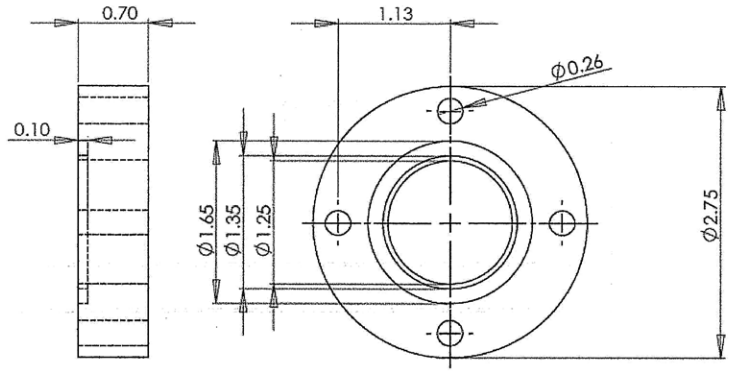

		UNLESS OTHERWISE SPECIFIED:		NAME	DATE
		DIMENSIONS ARE IN INCHES TOLERANCES: FRACTIONAL ± ANGULAR: MACH ± BEND ± TWO PLACE DECIMAL ± THREE PLACE DECIMAL ±	DRAWN		
			CHECKED		
			ENG APPR.		
			MFG APPR.		
		INTERPRET GEOMETRIC TOLERANCING PER:	Q.A.		
		MATERIAL	COMMENTS:		
NEXT ASSY	USED ON	FINISH			
APPLICATION		DO NOT SCALE DRAWING			

PROPRIETARY AND CONFIDENTIAL
THE INFORMATION CONTAINED IN THIS DRAWING IS THE SOLE PROPERTY OF MIT. ANY REPRODUCTION IN PART OR AS A WHOLE WITHOUT THE WRITTEN PERMISSION OF MIT IS PROHIBITED.

TITLE: Large Therm. Iso. Flange, Act

SIZE	DWG. NO.	REV
A		

SCALE: 1:1 | WEIGHT: | SHEET 1 OF 1

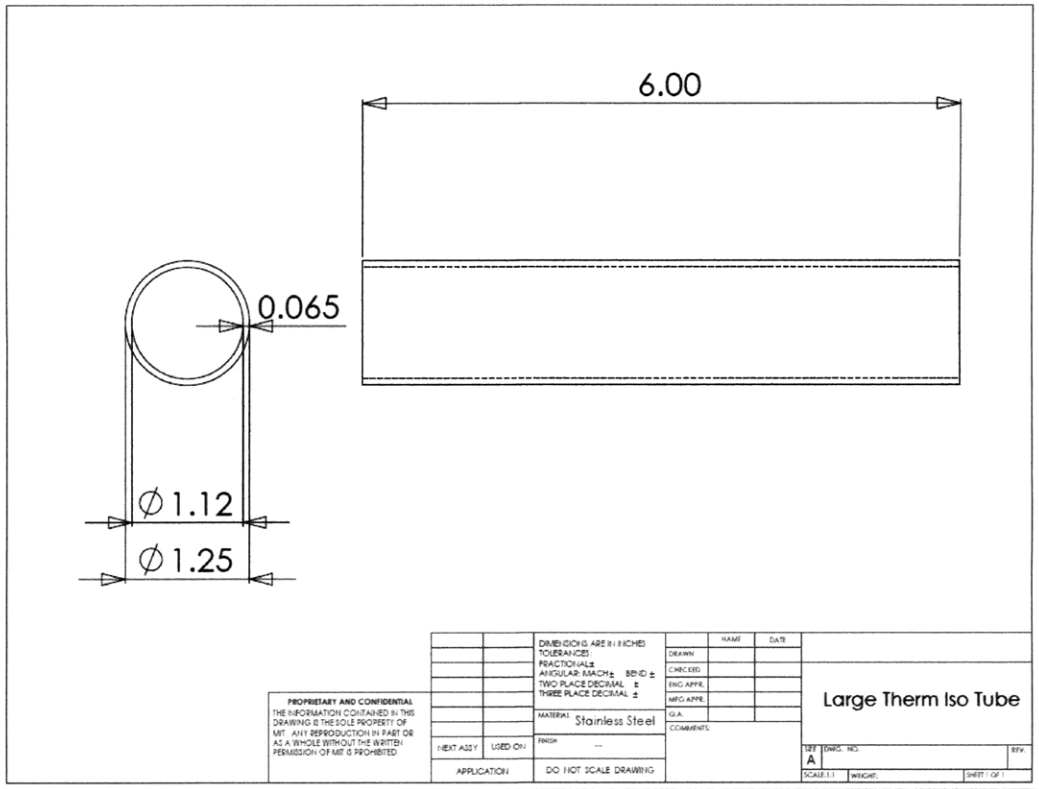
6.00
0.065
Ø1.12
Ø1.25
PROPRIETARY AND CONFIDENTIAL
THE INFORMATION CONTAINED IN THIS DRAWING IS THE SOLE PROPERTY OF MIT. ANY REPRODUCTION IN PART OR AS A WHOLE WITHOUT THE WRITTEN PERMISSION OF MIT IS PROHIBITED.
DIMENSIONS ARE IN INCHES
TOLERANCES:
FRACTIONAL ±
ANGULAR: MACH ± BEND ±
TWO PLACE DECIMAL ±
THREE PLACE DECIMAL ±
MATERIAL Stainless Steel
FINISH --
NEXT ASSY
USED ON
APPLICATION
DO NOT SCALE DRAWING
NAME
DATE
DRAWN
CHECKED
ENG APPR.
MFG APPR.
Q.A.
COMMENTS:
Large Therm Iso Tube
SIZE A
DWG. NO.
REV
SCALE:1:1
WEIGHT:
SHEET 1 OF 1

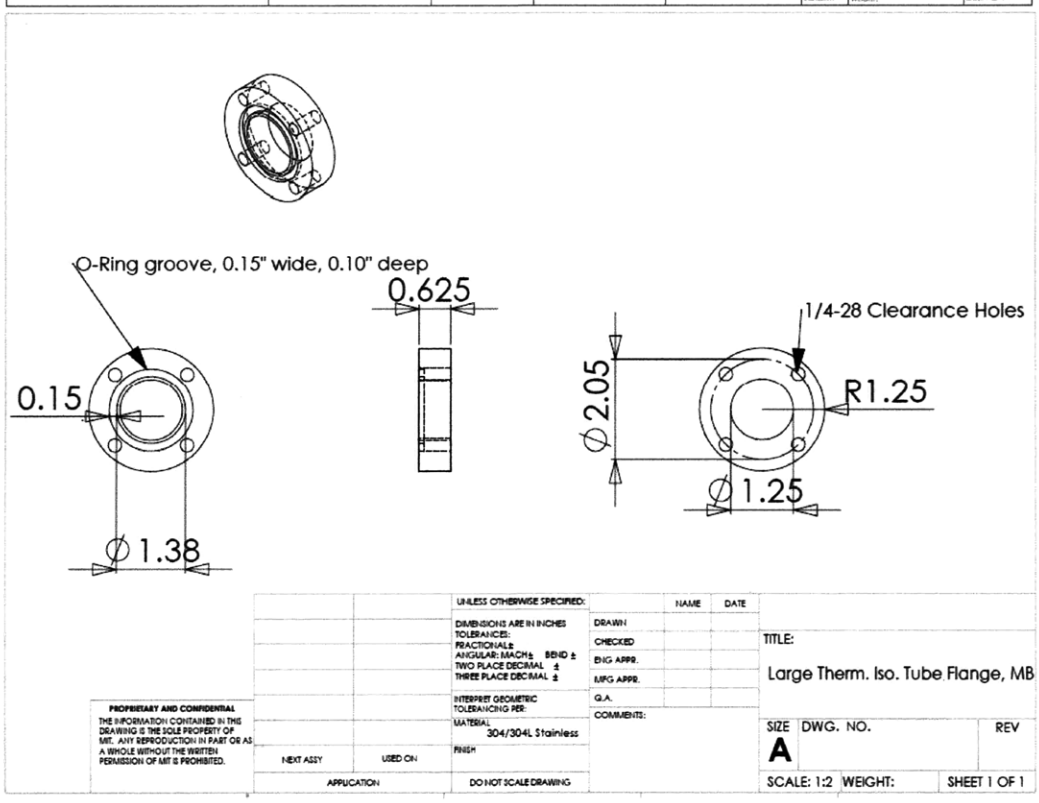
O-Ring groove, 0.15" wide, 0.10" deep
0.625
1/4-28 Clearance Holes
0.15
Ø2.05
R1.25
Ø1.38
Ø1.25
PROPRIETARY AND CONFIDENTIAL
THE INFORMATION CONTAINED IN THIS DRAWING IS THE SOLE PROPERTY OF MIT. ANY REPRODUCTION IN PART OR AS A WHOLE WITHOUT THE WRITTEN PERMISSION OF MIT IS PROHIBITED.
UNLESS OTHERWISE SPECIFIED:
DIMENSIONS ARE IN INCHES
TOLERANCES:
FRACTIONAL ±
ANGULAR: MACH ± BEND ±
TWO PLACE DECIMAL ±
THREE PLACE DECIMAL ±
INTERPRET GEOMETRIC TOLERANCING PER:
MATERIAL 304/304L Stainless
FINISH
NEXT ASSY
USED ON
APPLICATION
DO NOT SCALE DRAWING
NAME
DATE
DRAWN
CHECKED
ENG APPR.
MFG APPR.
Q.A.
COMMENTS:
TITLE:
Large Therm. Iso. Tube Flange, MB
SIZE A
DWG. NO.
REV
SCALE: 1:2
WEIGHT:
SHEET 1 OF 1

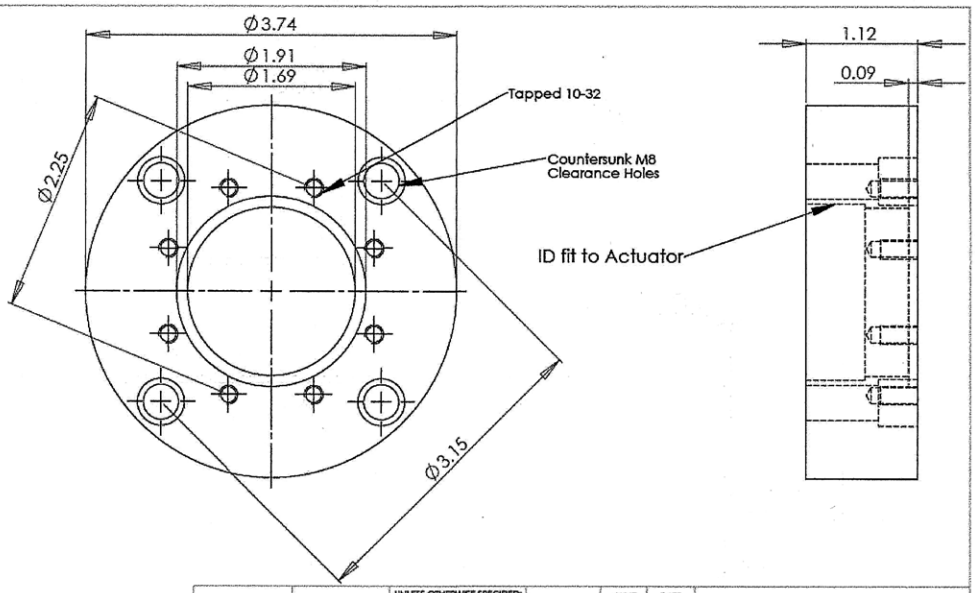

		UNLESS OTHERWISE SPECIFIED:		NAME	DATE
		DIMENSIONS ARE IN INCHES TOLERANCES: FRACTIONAL ± ANGULAR: MACH ± BEND ± TWO PLACE DECIMAL ± THREE PLACE DECIMAL ±	DRAWN		
			CHECKED		
			ENG APPR.		
			MFG APPR.		
		INTERPRET GEOMETRIC TOLERANCING PER:	Q.A.		
		MATERIAL	COMMENTS:		
NEXT ASSY	USED ON	FINISH			
APPLICATION		DO NOT SCALE DRAWING			

PROPRIETARY AND CONFIDENTIAL
THE INFORMATION CONTAINED IN THIS DRAWING IS THE SOLE PROPERTY OF MIT. ANY REPRODUCTION IN PART OR AS A WHOLE WITHOUT THE WRITTEN PERMISSION OF MIT IS PROHIBITED.

TITLE: Small Act Flange

SIZE	DWG. NO.	REV
A		

SCALE: 1:2 | WEIGHT: | SHEET 1 OF 1

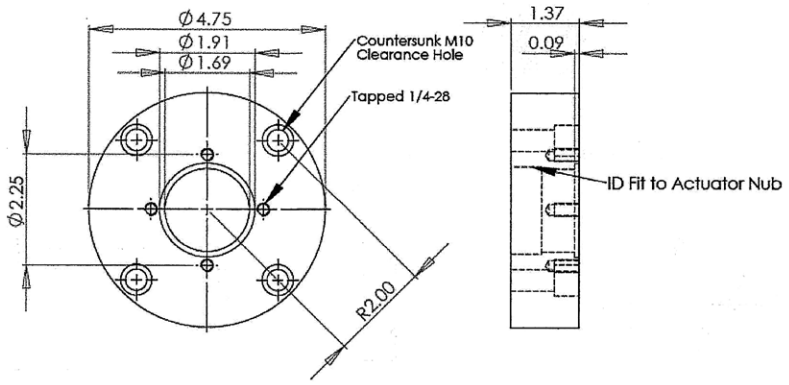

		UNLESS OTHERWISE SPECIFIED:		NAME	DATE
		DIMENSIONS ARE IN INCHES TOLERANCES: FRACTIONAL ± ANGULAR: MACH ± BEND ± TWO PLACE DECIMAL ± THREE PLACE DECIMAL ±	DRAWN		
			CHECKED		
			ENG APPR.		
			MFG APPR.		
		INTERPRET GEOMETRIC TOLERANCING PER:	Q.A.		
		MATERIAL	COMMENTS:		
NEXT ASSY	USED ON	FINISH			
APPLICATION		DO NOT SCALE DRAWING			

PROPRIETARY AND CONFIDENTIAL
THE INFORMATION CONTAINED IN THIS DRAWING IS THE SOLE PROPERTY OF MIT. ANY REPRODUCTION IN PART OR AS A WHOLE WITHOUT THE WRITTEN PERMISSION OF MIT IS PROHIBITED.

TITLE: Large Act Flange

SIZE	DWG. NO.	REV
A		

SCALE: 1:5 | WEIGHT: | SHEET 1 OF 1